CHARACTERIZATION OF THE ELECTRON TRANSFER REACTION MECHANISM OF $TiOSO_4$ AND $MnSO_4$ IN SULFURIC ACID SOLUTION

By

Abdullah Omar O Bahdad

Submitted to the graduate degree program in Chemical and Petroleum Engineering and the Graduate Faculty of the University of Kansas in partial fulfillment of the requirements for the degree of Master of science.

Chair: Prof. Trung Van Nguyen

Dr. Juan Bravo-Suarez

Dr. Lin Liu

Date Defended: December 02, 2020

Acceptance

The thesis committee for Abdullah Omar O Bahdad certifies that
this is the approved version of the following thesis:

CHARACTERIZATION OF THE ELECTRON TRANSFER REACTION MECHANISM OF $TiOSO_4$ AND $MnSO_4$ IN SULFURIC ACID SOLUTION

_____

Chair: Prof. Trung Van Nguyen

_____

Dr. Juan Bravo-Suarez

_____

Dr. Lin Liu

Date Approved: December 10, 2020

ABSTRACT

An electrochemical characteristic evaluation of the Ti-Mn electrolyte system in sulfuric acid aqueous solution is studied in different acid concentrations with and without the mixing of $TiOSO_4$ and $MnSO_4$ electrolyte system for a redox flow battery application. The reaction mechanism of Mn in sulfuric acid electrolyte is studied using the cyclic voltammetry and the anodic voltage hold techniques. The overall anodic behavior of the Mn system can be described by the oxidation reaction of Mn^{2+} to MnO_2 where Mn^{3+} is an intermediate species. As the acid concentration increases, less MnO_2 is formed on the working electrode and more Mn^{3+} is formed in the solution; however, due to the instability of Mn^{3+} in an aqueous solution, Mn^{3+} undergoes a significant hydrolysis reaction to precipitate as MnOOH in the electrolyte solution. The addition of 1M $TiOSO_4$ to the Mn electrolyte is found to lower the H^+ concentration which is believed to increase the amount of MnOOH in the solution and lower the concentration of aqueous Mn^{3+}. The formed MnOOH by the Mn^{3+} hydrolysis reaction is proven to be electrochemically active if it is deposited on the working electrode. The reaction mechanism of Ti in sulfuric acid electrolyte is studied using the cyclic voltammetry technique. Two electro-active species are found to be electrochemically active within the studied voltage window which are Ti^{4+}, and $TiSO_4^{2+}$. In 1M H_2SO_4, Ti^{4+} is found to be the dominant electro-active species, and in 3M H_2SO_4, $TiSO_4^{2+}$ is found to be the dominant electro-active species. The addition of 1M $MnSO_4$ to the 1M $TiOSO_4$+3M H_2SO_4 solution results in a high concentration of undissociated $MnSO_4$, and it is found that the dissociation of $MnSO_4$ to SO_4^{2-} improve the activity of the redox reaction of the Ti(IV)/Ti(III) couple. With the increase of H_2SO_4 and the addition of $MnSO_4$ in the Ti electrolyte, the electrochemical behavior of the Ti(IV)/Ti(III) redox couple tends toward the reversibility.

ACKNOWLEDGMENTS

I would like to express my sincere thanks to my advisor Prof. Trung Van Nguyen for his motivation, his wise advices, and for sharing his experience and his immense knowledge in the field of electrochemical engineering that have provided me with the opportunity to build a strong fundamental knowledge in conducting research in the field. I would also like to thank my committee members Dr. Juan Bravo-Suarez and Dr. Lin Liu for teaching me and for their time and feedback on my thesis.

I would also like to thank Dr. Yuanchao Li for teaching me how to set up and run experiments and for his support and feedback on my research. In addition, I would like to thank all professors and staff of the chemical and petroleum engineering department in the University of Kansas especially Martha Kehr and Dr. Prajnaparmita Dhar.

Ultimately, I would like to thank the government of the Kingdom of Saudi Arabia, the Saudi Arabian Cultural Mission in the United States of America, and King Abdulaziz University for supporting me financially in my graduate study at the University of Kansas.

DEDICATION

To my wonderful beloved wife Reem Khattabi,

to my father, my mother, and my whole family,

to my father in law and my mother in law,

to my friends Hashim, Muhannad, and Mohammed,

and to my beloved country the Kingdom of Saudi Arabia.

Table of Contents

List of Figures

List of Tables

Nomenclature

E: Applied voltage on the working electrode relative to a standard reference working electrode. [V vs. SHE or SCE].

E_{Eq}: Reduction potential of the half-cell rection relative to a standard reference working electrode. [V vs. SHE or SCE].

E^0: The standard reduction potential of the half-cell reaction relative to a standard reference working electrode. [V vs. SHE or SCE].

$E^{0\prime}$: The formal reduction potential of the half-cell rection relative to a standard reference working electrode. [V vs. SHE or SCE].

E^0_{Cell}: The potential difference between two half cells reaction in an electrochemical cell. [V vs. SHE or SCE].

n : number of electron transfer in the half cell reaction.

α: The cathodic transfer coefficient

F: Faraday's constant [96458 C/mole of electron]

R: Gas constant. [8.314 J/K/mole]

T: Temperature. [K]

η : Applied overpotential. [V vs. SHE or SCE].

k^0: Standard rate constant. [cm/s in a simple electron transfer reaction]

k_a: The rate constant of the anodic reaction. [A]

k_c: The rate constant of the cathodic reaction. [A]

k_{el}: The electronic transmission coefficient.

K_{po}: A precursor equilibrium constant of reactant species at a reactive position. [eV]

K: Chemical reaction equilibrium constant for a chemical reaction written from left to right.

ν_n: The frequency of attempts on the energy barrier. [s^{-1}]

A: Light absorption.

$\Delta G^0_{f,i}$: The standard Gibbs free energy of formation of species i. [KJ/mole]

ε: The absorption coefficient of the solute in solution media [dm^2/mole],

Q_i: Amount of charges delivered during the redox reaction, i: anodic, cathodic. [C]

I: current. [A]

I_o: Exchange current. [A]

C_R: Concentration of the reduced species on the working electrode. [mole/L]

C_R^*: Concentration of the reduced species in the solution. [mole/L]

C_O: Concentration of the oxidized species on the working electrode. [mole/L]

C_O^*: Concentration of the oxidized species in the solution. [mole/L]

1. Introduction

1.1. Electrical Energy Demand and Sources

The global demand of electrical energy is increasing as the global population and global economy are growing. [1] Accordance to the data released by International Energy Agency (IEA), the global demand and supply of electrical energy are shown in Figures 1 and 2. [2]

In Figure 1, for stated policies scenario that considered the impact of existing policy frameworks and today's announced policy intentions, the global demand on electric energy in 2020 is nearly 29 TWh in different consuming sectors. [2] The demand on electrical energy is expected to increase by one half in 2040. [2] Stated policies scenario leads to an estimated growth rate in electricity demand of 2.1% per year between 2018 and 2040. [2]

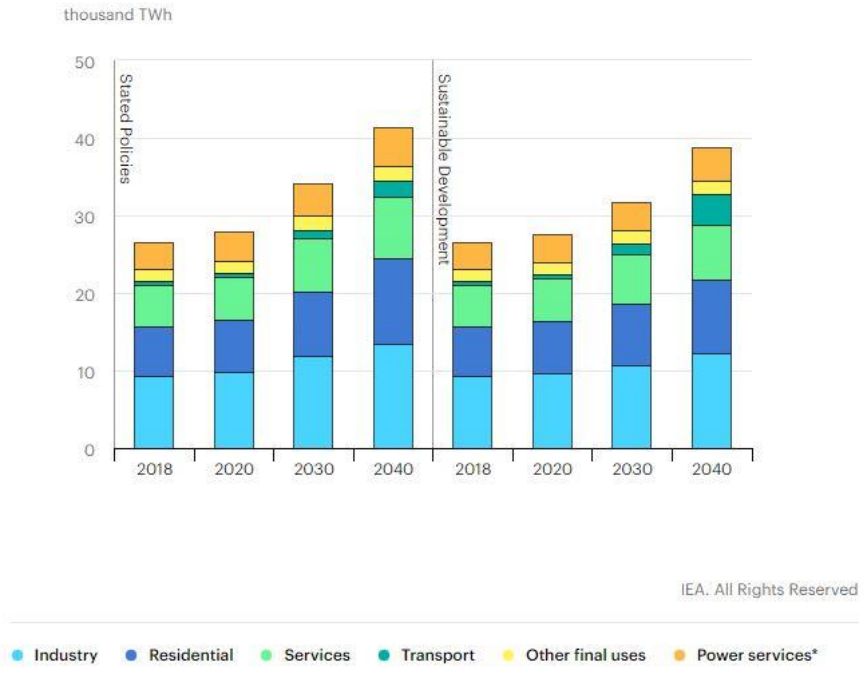

Figure 1. IEA, Electricity demand by sector and scenario, 2018-2040 [2]

In addition to stated policies scenario, IEA considered the projection of electrical energy demand if there was a sustainable development goals scenario. [2] The Sustainable Development Goals (SDGs) accounts for reducing the effect of climate change (reducing CO_2 emission), easiness in universal energy access, and improving air quality (reducing air pollution) when energy is delivered and used. [2] For this scenario, the growth rate of global electric energy demand shows a small increasing rate as opposed to stated policy scenario between 2018 and 2040. [2] These two scenarios for electrical energy demand require increasing the supply of electrical energy to meet the global economic needs. [2]

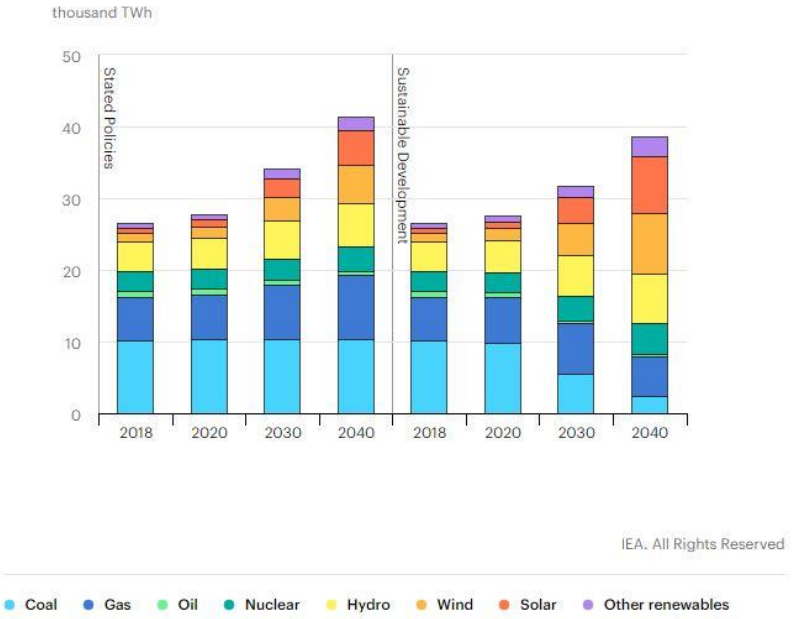

Figure 2. IEA, Electricity generation by fuel and scenario, 2018-2040 [3]

Figure 2 shows two scenarios for the electrical energy generated by different fuel types between 2018 and 2020. [3] In stated policies scenario, generating electricity by using fossil fuel (Coal, Gas, and Oil) makes up almost half of the total electricity generation between 2018 and 2040; although, electricity generation share by using a benign energy source (Hydro, Wind, Solar and other renewables) has increased in the same period. [3] For the projection to 2040 of electrical

energy generation if there was a sustainable development goals scenario, fossil fuel use would be reduced in 2040 and the benign energy sources would make up the supply of electrical energy by more than two thirds. [3] Using benign energy source to generate electricity meets the objective of a sustainable development goals scenario. [3] Eventually, solar energy, wind energy, and hydroelectric energy would make up more than 75% of the means of generating electricity in 2040. [3]

1.2. The Need of Energy Storage Technology

From the previous section, the main source that is used to generate electricity in 2040 would be by using renewable energy that meets the sustainable development goals scenario by IEA. [3] However, one of the major concerns in using renewable energy sources, such as wind and solar, to produce electricity is that it has a variable and unpredictable energy output. [4] Wind energy can be utilized by converting the kinetic energy of wind to electrical energy using wind turbines. [4] This process is strongly depended on wind's speed which is not constant over time. [4] Similarly, solar photovoltaic panels can be used to generate electrical energy by converting sun radiant light to electrical energy. [4] The supply of sunlight can only be processed during daytime; while, electrical energy must be produced during nighttime. [4] This uncontrolled characteristic of using wind energy and solar energy is called intermittent operation where the operation is not sustainable over a long time. [4] As a result, the action to adjust the supply of energy over a long-time operation in a sustainable way is required for any changes in demand when renewable fuel is employed. [4]

Using Electrical Energy Storage is crucial in employing renewable energy sources when generating electricity to operate in a sustainable way and to minimize the intermittent behavior effect. [4] Electrical Energy Storage (EES) refers to processing the electrical energy from a power

network by converting it into a form that can be stored, and then the stored energy form is converted back to electrical energy when needed. [4] EES can be found in three major applications; portable devices, transport vehicles, and stationary energy resources. [4] The focus in this thesis is on the application of Stationary Electrical Energy Storage only. [4] Stationary EES was first used in the 20th century, when power stations used to operate during the daytime time and the residual energy accumulated in Lead-Acid battery. [4] This residual load then discharged to the electrical grid during the night. [4]

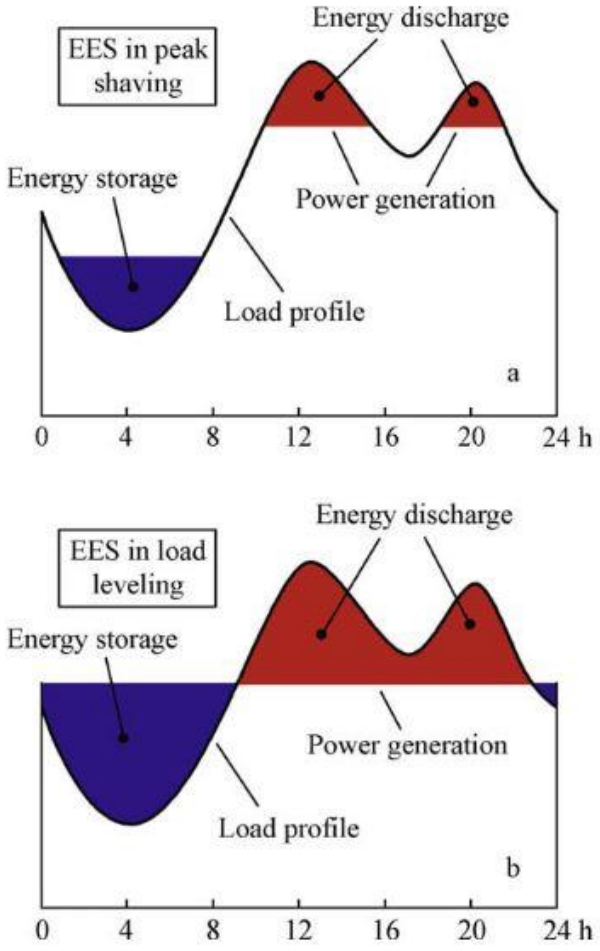

Figure 3. Load profile of a large-scale electricity storage system.
(a) EES for peak shaving (b) EES for load leveling. [4]

These days, some electric power plants use electrical storage technology for grid-level energy storage to adjust the demand fluctuation in seasons for quality management. [4] EES allows them to have large-scale electrical capacity, which can be used at any time during high demand. In this way, the planning of power generation can be based on electricity capacity that can supply the average yearly electricity demand instead of peak demands. [4]

Peak shaving and load leveling are two terms that are widely used in describing the relation of electrical load and stored energy for grid level during a time span. [4] They are both referring to a process of storing energy during low demand and discharging energy during high demand. [4] For peak shaving, energy is stored during low demand and is discharged only to reduce the peak load during high demand. Similarly, load leveling objective is to store energy during low demand, but the aim of the stored energy is to flatten the load as possible instead of reducing the peak load. [4] Figure 3 illustrates the load profile for grid-scale EES for Peak shaving and load leveling scenario. [4] For EES in peak shaving in Figure 3.a, energy is stored during the low demand time, and when the load is high during the high demand time period, energy is discharged to reduce the peak load. [4, 5, 6] In Figure 3.b, EES in load leveling flattens the load profile to get the possible average load between the energy stored and the energy discharge during the whole demand operating time. [4, 5, 6] Ultimately, the use of EES in grid-level allows power plants to reduce the operation cost by functioning below the full capacity during high demand time, and to minimize or postpone the need to build new power plants that are needed to meet new peak demand. [4, 5, 6]

1.3. Electrical Energy Storage Types

Two criteria categorize different types of EES: form and function. [4] The forms of stored energy from electrical energy can be classified in Table 1. [4]:

Table 1. Forms of energy that can be used to store electric energy [4]

Energy Form	System 1	System 2
Electrical energy storage	**Electrostatic energy storage** Ex. (capacitors and supercapacitors, etc.)	**Magnetic/current energy storage** Ex. SMES, etc
Mechanical energy storage	**Kinetic energy storage** Ex. (flywheels, etc.)	**Potential energy storage** Ex. (PHS and CAES).
Chemical energy storage	**Electrochemical energy storage.** Ex. (conventional batteries, flow cells, batteries, and fuel cells)	**Chemical energy storage** Ex. (Hydrogen fuel, molten carbonate, thermal-chemical conversion)
Thermal energy storage	**Low temperature energy Storage.** Ex. (Aquifer cold energy storage, cryogenic energy storage)	**High temperature energy storage** Ex. (sensible heat systems such as steam or hot water.)

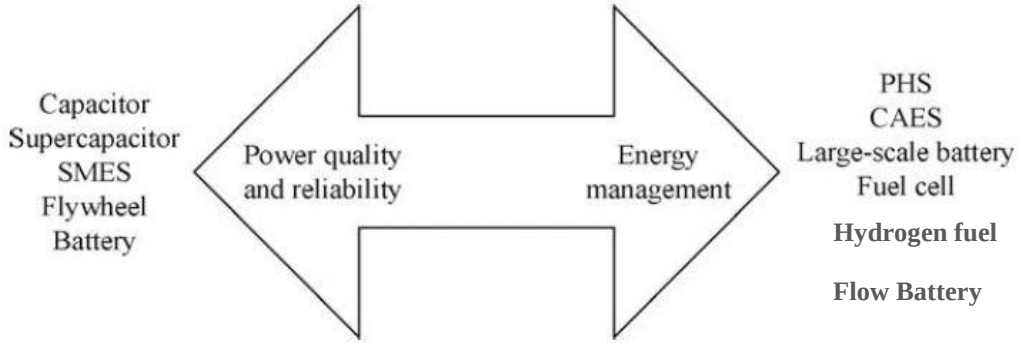

Figure 4. Energy storage classification with respect to function. [4]

In terms of the function, EES technology for high power density and low energy density, such as capacitors, supercapacitor, superconducting magnetic energy storage (SMES), flywheel and battery, is used to store energy and supply it for power quality management because of its high power capacity; while, EES technology such as pumped heat storage (PHS), compressed-air energy storage (CAES), large-scale battery, fuel cell, hydrogen fuel, thermal energy storage (TES), and flow battery is used for energy management because of its high energy density. [4] Figure 4 shows the classification of energy storage system with respect to function. [4] Although PHS and CAES are preferable to be used in large energy storage applications because of their high cost, they are limited by their geographical requirements. [6] The power and energy density characteristics for each EES type are shown in Figure 5 Capacitors which have very high-power density and very low energy density are suitable for power quality management because of their fast response time [7] Batteries, flow batteries, and fuel cells have a high energy density, which makes them suitable for large-scale energy storage applications. [7] The scale-ability and the adaptability of fuel cells and flow batteries allow them to be the most attractive EES technology for large scale storage applications. [8]

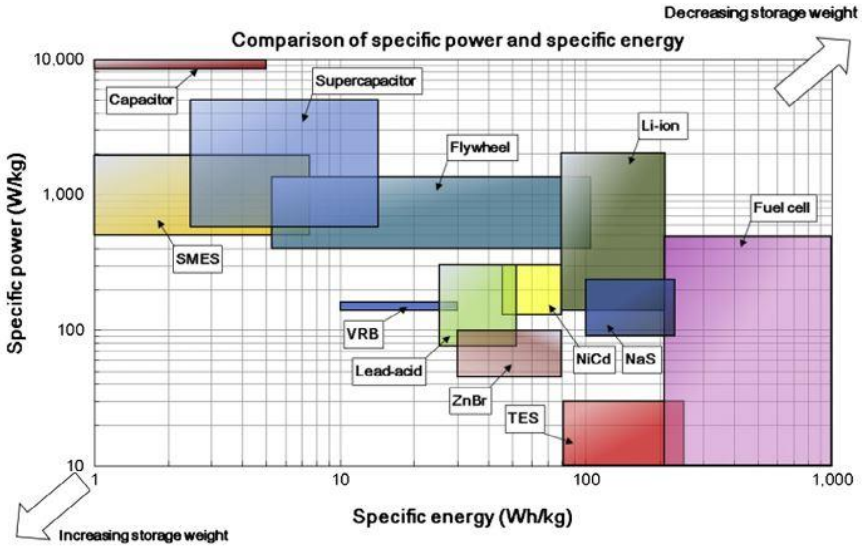

Figure 5. Comparison of specific energy density and specific power density [7]

1.4. Redox Flow Battery

Flow Battery is an electrochemical device that converts the chemical energy in the electro-active materials directly to electrical energy during discharge operation, and during charge operation, electrical energy is converted into chemical energy in the electro-active materials. [8]

The main difference between a flow battery and a conventional battery is that the electro-active materials, that are used to store electrical energy, are stored externally in tanks rather than storing them internally as an electrode in a conventional battery. [8] Then, the stored electro-active materials are introduced in the electrochemical cell when it is needed. When the electro-active material is stored within a liquid system, the system then can be recognized as a redox (for reduction reaction/oxidation reaction) flow batteries (RFB). [8] Also, a RFB is a reversible electrochemical device (secondary battery type) that can store the energy when the energy is not needed and discharge the energy when the energy is needed in a reversible way. [8]

Storing electro-active materials externally allows a RFB to scale-up the energy storage capacity easily and that makes it attractive for large-scale energy storage applications. [8] The energy capacity of a RFB is determined by the size of the volume of the external storage of electro-active materials. [8] The power density of RFB can be designed based on the electrode properties (surface, catalytic, electrical, and transport properties). [8] Note that the electrode does not undergo any chemical reaction or physical change during operation as opposed to conventional batteries where the electrode changes its chemical and physical properties. [8]

Figure 6 shows a typical redox flow battery operation during discharge. [8] A typical RFB during discharge mode consists of positive electrode where the reduction reaction takes place for high positively charged electro-active specie and negative electrode where the oxidation reaction takes place for low positively charged electro-active specie. [8] The two electrodes are separated

by an ion-exchange membrane to allow specific ions that are non-reactive to migrate between the two-electrode section to maintain electroneutrality between negative and positive electrodes. [8] Another role for the ion exchange membrane is that it acts as an ionic selective separator between the two electrode by preventing the crossover of electro-active species between the two electrodes to avoid chemical short-circuit of electro-active materials that leads to losing the charge capacity or reducing the performance of the RFB. [8] The electro-active species are stored externally from the electrochemical cell unit and they pump to the electrochemical cell during operation only.[8] Finally, the membrane serves as an electrical insulator to prevent electrical short circuit of the two electrodes. [8]

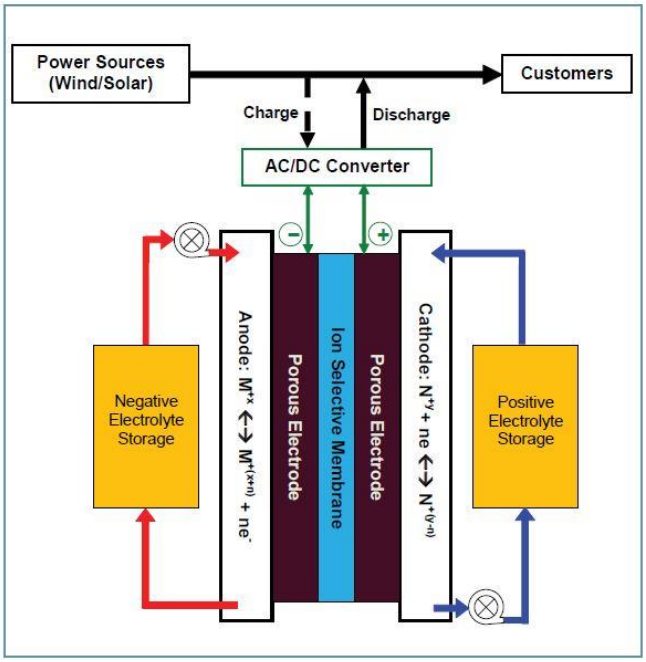

Figure 6. Schematic of a typical redox flow battery system during discharge operation. [8]

During the charge mode, the electrochemical cell converts electrical energy into chemical energy by means of redox reactions.[8] Oxidation reaction takes place at the positive electrode and the reduction reaction takes place at the negative electrode as shown in Eq1.1 and Eq1.2: [8]

At the negative electrode: $A^{+(x+n)} + ne^- \leftrightarrow A^{+x}$ Eq1.1

At the positive electrode: $B^{+(y-n)} \leftrightarrow B^{+y} + ne^-$ Eq1.2

During the discharge mode, the electrochemical reactions are reversed, and electrical energy is generated.[8] The oxidation reaction takes place at the negative electrode and the reduction reaction takes place at the positive electrode as shown Eq1.3 and Eq1.4: [8]

At the negative electrode: $A^{+x} \leftrightarrow A^{+(x+n)} + ne^-$ Eq1.3

At the positive electrode: $B^{+y} + ne^- \leftrightarrow B^{+(y-n)}$ Eq1.4

The theoretical cell voltage for the overall redox reaction can be calculated by summing the reduction potential for the species that undergoes a reduction reaction and the oxidation potential for the species that undergoes an oxidation reaction. [8]

1.5. Types of Redox Flow Battery

Research and development on RFBs have been conducted for more than 40 years in the United States and Japan. [9] The first applicable RFB was based on the Fe (II)/Fe (III) and Cr (III)/Cr (II) as electro-active materials to produce 1KW. [9] Fe/Cr RFB was first made in 1970s by NASA-Lewis Research Center. [9] Since that time, other types of RFBs have been developed using different types of electro-active materials for redox reactions. [8] Generally, the classification of RFBs can be classified based on the solvents employed in the electrolyte and the occurrence of phase transition. [9]

Regarding the solvent used in the electrolyte, RFB can have an aqueous electrolyte system or a non-aqueous electrolyte system. [9] Water and acids are used in aqueous RFBs as supporting electrolytes. [9] Non-aqueous RFBs use organic electrolyte solvent as supporting electrolytes, for

example, acetonitrile. [9] Although non-aqueous RFBs have high potential window >5V, aqueous RFBs are cheaper and safer than non- aqueous RFBs. [9]

RFBs can also be classified into true RFB and hybrid RFB. [9] In true RFBs, the electro-active species are always dissolved in the supporting electrolytes to form a single-phase system. [9] In hybrid RFB systems, at least one of the electro-active species is present in a different phase. [9] Various types of RFBs and hybrid RFB with their reaction information and their standard cell voltages are summarized in Table 2. [8]

Table 2. Characteristics of Some Flow Battery Systems [8]

System	Reactions	E^0_{cell}	Electrolytes
True RFB			**Anode/Cathode**
All Vanadium [10]	(-) terminal: $V^{2+} \underset{\text{charge}}{\overset{\text{Discharge}}{\longleftrightarrow}} V^{3+} + e^-$ (+) terminal: $VO_2^+ + e^- \underset{\text{charge}}{\overset{\text{Discharge}}{\longleftrightarrow}} VO^{2+}$	1.4 V	H_2SO_4/H_2SO_4
Vanadium-Polyhalide [11]	(-) terminal: $V^{2+} \underset{\text{charge}}{\overset{\text{Discharge}}{\longleftrightarrow}} V^{3+} + e^-$ (+) terminal: $\frac{1}{2} Br_2 + e^- \underset{\text{charge}}{\overset{\text{Discharge}}{\longleftrightarrow}} Br^-$	1.3 V	$VCl_3 - HCl \ / NaBr - HCl$
Bromine-Polysulfide [9]	(-) terminal: $2\ S_2^{2-} \underset{\text{charge}}{\overset{\text{Discharge}}{\longleftrightarrow}} S_4^{2-} + 2e^-$ (+) terminal: $Br_2 + 2e^- \underset{\text{charge}}{\overset{\text{Discharge}}{\longleftrightarrow}} 2Br^-$	1.515 V	$Na_2S_2/NaBr$
Iron-Chromium [12]	(-) terminal: $Fe^{2+} \underset{\text{charge}}{\overset{\text{Discharge}}{\longleftrightarrow}} Fe^{3+} + e^-$ (+) terminal: $Cr^{3+} + e^- \underset{\text{charge}}{\overset{\text{Discharge}}{\longleftrightarrow}} Cr^{2+}$	1.2 V	HCl/HCl
H_2-Br_2 [13]	(-) terminal: $H_2 \underset{\text{charge}}{\overset{\text{Discharge}}{\longleftrightarrow}} 2H^+ + 2e^-$ (+) terminal: $Br_2 + 2e^- \underset{\text{charge}}{\overset{\text{Discharge}}{\longleftrightarrow}} 2Br^-$	1.1 V	PEM^*/HBr *proton Exchange Membrane
Hybrid RFB			**Anode/Cathode**
Zinc-Bromine [8]	(-) terminal: $Zn \underset{\text{charge}}{\overset{\text{Discharge}}{\longleftrightarrow}} Zn^{2+} + 2e^-$ (+) terminal: $Br_2 + 2e^- \underset{\text{charge}}{\overset{\text{Discharge}}{\longleftrightarrow}} 2Br^-$	1.8 V	$ZnBr_2/ZnBr_2$
Zinc-Cerium [8]	(-) terminal: $Zn \underset{\text{charge}}{\overset{\text{Discharge}}{\longleftrightarrow}} Zn^{2+} + 2e^-$ (+) terminal: $2Ce^{4+} + 2e^- \underset{\text{charge}}{\overset{\text{Discharge}}{\longleftrightarrow}} 2Ce^{3+}$	2.4 V	CH_3SO_3H/CH_3SO_3H

Most of RFBs that are used commercially are based on aqueous solvents because of their low cost and safety. [9] These days, only the all-vanadium RFB and Zn–Br RFB are commercialized and used in EES applications. [14] Typical RFB energy density is between 20-50 Wh/L depending on the RFB's cell voltage and the solubility of electro-active species. [14] RFB is considered a technology underdevelopment and not well established. [8]

Since the increase of vanadium price in 2018, there has been a challenge to find a new RFB system that can have low materials cost, sustainable chemistry for electro-active species, high solubility for electro-active materials, and high cell voltage. [15] Figure 7 shows the price of vanadium prices between 2000 and 2019. From Figure 7, there was a rapid increase in vanadium price in 2005 from nearly 2 $/lb to almost 30 $/lb. Vanadium price has been stabilized to be near 5 $/lbs between 2009 and the end of 2017. [15] In 2018, vanadium price increased rapidly to more than 33 $/lb. [15] This fluctuation trend profile and an unexpected increase in vanadium price have a negative impact on the RFB industries. Thus, the need to find an alternative to the vanadium RFB is crucial in term of cost. [15]

Figure 7. Market Vanadium price in $/lb between 2000 and 2018. [15]

1.6. Titanium-Manganese Redox Flow Battery System

In 2017, Sumitomo Electric Industries introduced a new RFB based on a Titanium-Manganese electrolyte for a redox reaction. [16] Titanium-Manganese electrolyte system was selected based on the high potential and the low cost of electro-active materials because they are present abundantly in nature and the high theoretical cell voltage (1.41 V in a sulfuric acid solution) based on their standard reduction potentials. [16] A schematic for the Titanium-Manganese RFB is shown in Figure 8.

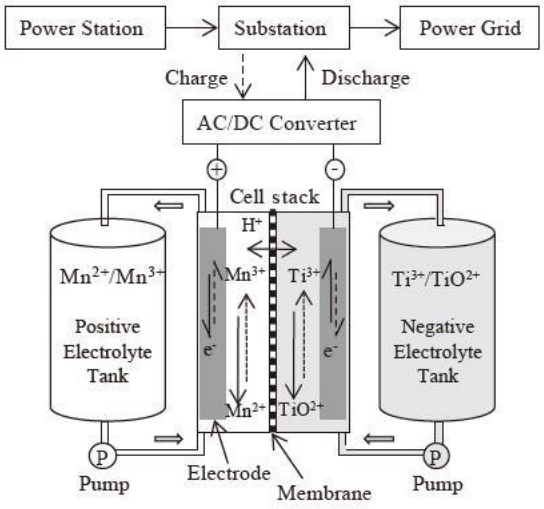

Figure 8. Schematic of Titanium-Manganese Redox Flow Battery [16]

From Figure 8, sulfuric acid is used as a supporting electrolyte in both the positive electrolyte tank and the negative electrolyte tank. [16] A proton exchange membrane is used to maintain electroneutrality between the two sides in the cell stack where the proton is allowed to migrate between the two electrode sides. [16]

During the charge mode, the electrochemical cell charges the electrolytes using the voltage and current from the power source by means of redox reactions. [16] Oxidation reaction takes

place at the positive electrode and the reduction reaction takes place at the negative electrode as shown Eq1.7 and Eq1.8 [16]:

At the negative electrode: $TiO^{2+} + H^{+} + e^{-} \leftrightarrow H_2O + Ti^{3+}$, $E^{o} = 0.1\ V\ vs.\ SHE$ Eq1.7

At the positive electrode: $Mn^{2+} \leftrightarrow Mn^{3+} + e^{-}$, $E^{o} = 1.51\ V\ vs.\ SHE$ Eq1.8

And during the discharge mode, the electrochemical cell discharges the electrolyte and generates electricity for the consumers. Oxidation reaction takes place at the negative electrode and the reduction reaction takes place at the positive electrode as shown Eq1.9 and Eq1.10 [16]:

At the negative electrode: $H_2O + Ti^{3+} \leftrightarrow TiO^{2+} + H^{+} + e^{-}$, $E^{o} = 0.1\ V\ vs.\ SHE$ Eq1.9

At the positive electrode: $Mn^{3+} + e^{-} \leftrightarrow Mn^{2+}$, $E^{o} = 1.51\ V\ vs.\ SHE$ Eq1.10

During charge operation, disproportionation reaction of Mn^{3+} to MnO_2 and Mn^{2+} in the electrolyte solution was reported as shown in Eq1.11. [16]

$$2Mn^{3+} + 2H_2O \leftrightarrow Mn^{2+} + MnO_2 + 4H^{+} \quad \text{Eq1.11}$$

The effect of disproportionation reaction results in losing charge capacity and forming solid MnO_2 that can affect the flow of the electrolytes into the cell during operation. In order to stabilize Mn^{3+} and to suppress the disproportionation reaction of Mn^{3+}, $TiOSO_4$ was used and tested in the positive electrolyte solution in high sulfuric acid concentration and high Mn^{2+} concentration. [16, 17]

The application of Mn electrolyte was studied extensively for primary alkaline manganese batteries where the electrolytic manganese dioxide (EMD) is the major Mn electro-active material and Mn(III)/Mn(II) redox couple was viewed to be an intermediate step of forming EMD. [18] The low cost of Mn stock materials and the high reduction potential of Mn(III)/Mn(II) redox

couple attract the use of Mn materials as a positive electrolyte in RFB. Although the system was reported to be stabilized by the addition of TiOSO4 in Mn electrolyte solution, there is still no clear study about the mechanism and the speciation of the Mn electrolyte system in sulfuric acid aqueous solution. Ti electrolyte has not been commercialized or used in any RFBs which makes it a new negative electrolyte for RFBs. The chemistry of Ti(IV)/Ti(III) is well identified; however, its electrochemical behavior has not been completely evaluated.

1.7. Objective of This Work

In this work, electrochemical characteristic of the Ti-Mn electrolyte system in sulfuric acid aqueous solution is studied in different sulfuric acid concentrations with and without the mixing of $TiOSO_4$ and $MnSO_4$ electrolyte system. First, solubility measurements are conducted to find the solubility of Ti-Mn electrolyte system in different sulfuric acid concentrations at different temperatures. Then, a theoretical study on the Ti-Mn electrolytes is evaluated to study the speciation of Ti-Mn electrolyte in sulfuric acid solution. The electron reaction mechanisms of Mn electrolyte and Ti electrolyte are studied using the cyclic voltammetry technique for Mn electrolyte and Ti electrolyte, and the anodic voltage hold technique for Mn electrolyte. The evaluation of the electron transfer reaction mechanism for Mn-electrolyte and Ti-electrolyte systems in sulfuric acid solution is based on the experimental observation from the electrochemical characterization results and the theoretical study of the speciation of Ti-Mn electrolytes in sulfuric acid solution to find the possible route for the electron transfer reaction in both systems.

2. Ti- Mn Electrolyte System Literature Survey

2.1. Manganese Electrolyte in Sulfuric Acid

Manganese element has various oxidation states ranging from -1 to 7. [18] The electro-active materials in a Ti-Mn RFB positive electrolyte is manganese in oxidation states from 2 to 4. [16] In this section an overview of the apparent form and the chemical and electrochemical behavior of Mn(II), Mn(III), and Mn(IV) in sulfuric acid aqueous solution is reviewed.

2.1.1. Mn(II) in Sulfuric Acid Solution

Mn(II) is the starting positive electro-active material in a Ti-Mn RFB before it is charged. [16] Mn(II) species is the most stable manganese oxidation state in aqueous acidic solution among all manganese oxidation states. [18] In sulfuric acid solution (for pH<1), Mn(II) is present in the form of Mn^{2+} with an octahedral coordination structure with water molecules that is stable over a wide range of potential. [19] However, with the presence of SO_4^{2-} in acidic media, Mn^{2+} forms $MnSO_{4\,(Aq)}$ complex in the solution. [20, 21]

2.1.2. Mn(III) and Mn(IV) in Sulfuric Acid Solution

On the other hand, Mn(III) and Mn(IV) are less stable in sulfuric acid solution because they hydrolyze quickly in aqueous solution. [19] Mn(III) is present in sulfuric acid solution as Mn^{3+} with an octahedral coordination with water molecules; however, it is hydrolyzed in aqueous solution to form $Mn(OH)_x^{+(3-x)}$ ions and non-stochiometric solid MnOOH and it is disproportionated to Mn^{2+} and MnO_2 in acidic solution. [18, 19, 22, 23, 24]. The stability of Mn(III) in acidic solution depends on its concentration and the pH of the solution. [24] Mn(III) can be stabilized in acidic solution by increasing the acidity of the solution and by introducing a complexing agent . [16, 25] Mn(IV) is found in sulfuric acid solution as solid MnO_2. [18, 22]

MnO_2 can form different phases in sulfuric acid solution depending on the solution pH, temperature, and the presence of foreign ions in the solutions. [18, 22] The most stable phase of MnO_2 in aqueous acidic solution is the β-phase. [18] Meta stable phases of MnO_2 are formed prior to β-phase and they have long life-time before they are converted into β-phase at room temperature. [26] These meta stable phases of MnO_2 have a polymorph crystal structure in which foreign cation can be hosted inside the lattice structure. [27] In sulfuric acid solution, it was reported that the phase of MnO_2 that is resulted from the electrochemical oxidation of $MnSO_4$ is the non-stochiometric γ-MnO_2 ,while the MnO_2 formed via disproportionation reaction of Mn^{3+} in sulfuric acid media was reported as a combination of the non-stochiometric γ-MnO_2 and α-MnO_2. [23, 25] Generally, γ-MnO_2 is the dominant phase of the solid MnO_2 in sulfuric acid media. [19, 23, 27] γ-MnO_2 polymorph structure is hexagonal close packed as shown in Figure 9. The manganese atoms occupy half of the octahedral voids in this matrix, as in Pyrolusite β- MnO_2 or Ramsdellite R-MnO_2. The chemical formula of γ-MnO_2 was proposed by Ruetschi as: [28]

$$Mn^{4+}_{1-x-y} . Mn^{3+}_{y} . O^{2-}_{2-4x-y} . OH^{-}_{4x+y}$$

Typical values of x and y in unreduced state are 0.06 and 0.075, respectively. [28]

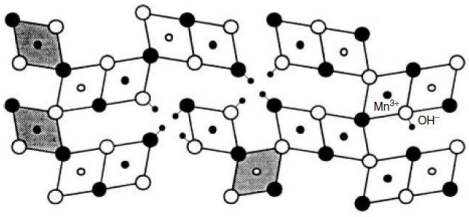

Figure 9. Vacancy (Ruetschi) model for the crystal structure of MnO_2 [7]

2.1.3. The Standard Reduction Potentials of Mn(II), Mn(III), and Mn(IV)

The standard reduction potentials in acidic media between the three manganese oxidation states (Mn(II), Mn(III), and Mn(IV)) were reported in literature. [18]

- Mn(III)/Mn(II)

$$Mn^{3+} + e^- \leftrightarrow Mn^{2+} \qquad E^0 = 1.5 \text{ V vs SHE} \qquad \text{Eq.2.1}$$

- Mn(IV)/Mn(II)

$$MnO_2 + 4H^+ + 2e^- \leftrightarrow Mn^{2+} + 2H_2O \qquad E^0 = 1.23 \text{ V vs SHE} \qquad \text{Eq.2.2}$$

- Mn(IV)/Mn(III)

$$MnO_2 + 4H^+ + e^- \leftrightarrow Mn^{3+} + 2H_2O \qquad E^0 = 0.952 \text{ V vs SHE} \qquad \text{Eq.2.3}$$

The low standard reduction potential of Mn(IV) / Mn(III) as opposed to the standard reduction potential of Mn(IV) / Mn(II) indicates that Mn(III) is unstable and it has to disproportionate to Mn^{2+} and MnO_2 to allow the system to be stable. [18] Disproportionation reaction happens when a species is oxidized to species with a higher oxidation state and reduced to species with a lower oxidation state simultaneously. [29] In this case, the disproportionation of Mn^{3+} is the reduction of Mn^{3+} to Mn^{2+} and the oxidation of Mn^{3+} to MnO_2 simultaneously as shown below:

$$2Mn^{3+} + 2H_2O \leftrightarrow Mn^{2+} + MnO_2 + 4H^+ \qquad E^0_{Cell} = 0.548 \text{ V vs SHE}$$

From E^0_{Cell}, the reaction equilibrium constant at standard condition can be calculated to be is $K=1.85 \times 10^9$. The large value of equilibrium reaction constant shows that the Mn^{3+} disproportionation is a highly favorable reaction.

2.1.4. Solubility of $MnSO_4$ in Sulfuric Acid Solution

The solubility of $MnSO_4.H_2O$ material in H_2O-H_2SO_4 solvent was thermodynamically studied and compared with experimental values by Petri Kobylin in 2013. [30] Petri used various thermodynamic models such as Gibbs energy minimization model, Pitzer model, and CALPHAD method in order to find the solubility of $MnSO_4$ at different temperatures and at different acid concentrations. [30] Petri ‘s theorical study generated data for the solubility of $MnSO_4$ in sulfuric acid solution up to 10 mol/Kg H_2SO_4 concentration and temperature up to 90 ^oC, and the results were in a good agreement with the experimental measurements. [30] The results that were obtained by Petri are shown in Figure 10 to Figure 13. [30]

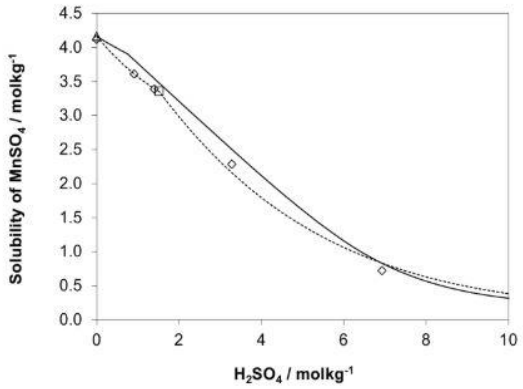

Figure 10. Solubility of $MnSO_4$ in sulfuric acid solution with different acidic concentrations at 20 ^oC. ___ Petri work, ---- and Other symbols are the experimental results. [30]

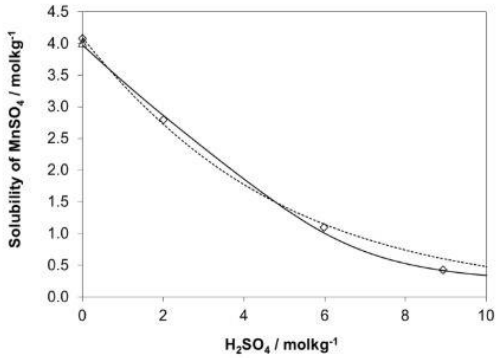

Figure 11. Solubility of $MnSO_4$ in sulfuric acid solution with different acidic concentrations at 40 ^oC. ____Petri work, ---- and Other symbols are the experimental results. [30]

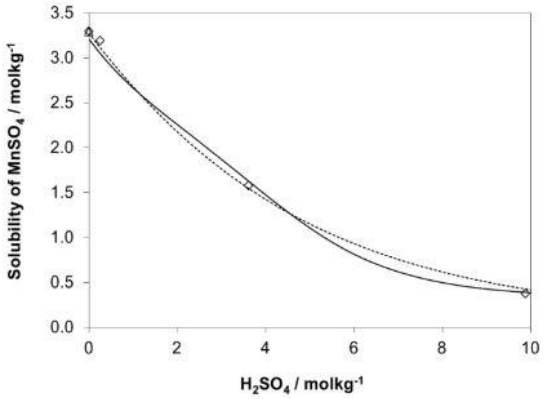

Figure 12. Solubility of $MnSO_4$ in sulfuric acid solution with different acidic concentrations at 70 ^oC. ___Petri work, ---- and Other symbols are the experimental results. [30]

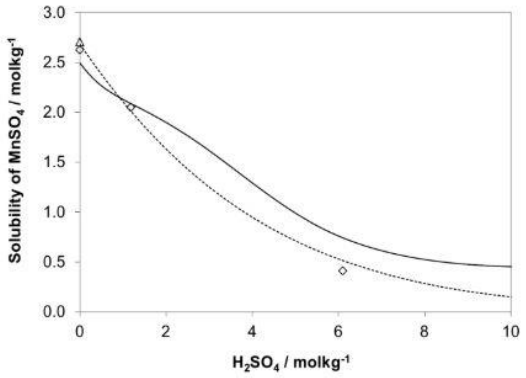

Figure 13. Solubility of $MnSO_4$ in sulfuric acid solution with different acidic concentrations at 90 ^oC. ___Petri work, ---- and Other symbols are the experimental results. [30]

The results in Figure 10 to Figure 13 show that the solubility of $MnSO_4$ in sulfuric acid decreases with increasing temperature, and the solubility of $MnSO_4$ decreases with increasing the sulfuric acid concentration. [30]

2.1.5. Speciation Study of Mn(II), Mn(III), and Mn(IV) in Sulfuric Acid Media

Mn(II), Mn(III), and Mn(IV) were reported to exist as an octahedral coordination framework, albeit somewhat distorted. [31]

2.1.5.1. Speciation Study of Mn(II)

Mn(II) in sulfuric acid solution exists in the form of Mn^{2+} with an octahedral coordination structure with water molecules and aqueous undissociated $MnSO_4$. [18, 20] However, with the presence of SO_4^{2-} in acidic media, Mn^{2+} forms $MnSO_{4\,(Aq)}$ complex in the solution as shown in Eq. 2.4. [20, 21, 32]

$$MnSO_{4_{Aq}} \leftrightarrow Mn^{2+} + SO_4^{-2}\,, \qquad K = 0.00158 \qquad \text{Eq. 2.4}$$

Mn(II) hydrolyzes in aqueous solution in low acid concentration (pH ~5.3). [31] Hydrolysis reaction of Mn(II) in acidic solution is shown in Eq. 2.5 with its reported equilibrium reaction constant. [31]

$$Mn^{2+} + H_2O \leftrightarrow MnOH^{+} + H^{+}\,, \qquad K = 2.57x10^{-11} \qquad \text{Eq. 2.5}$$

The hydrolysis of Mn(II) would lead to $Mn(OH)_2$ solid formation in low acid concentration (pH approximately > 5.3). [31]

2.1.5.2. Speciation Study of Mn(III)

Mn(III) exists in sulfuric acid solution as Mn^{3+} with an octahedral coordination with water molecules; however, it is readily hydrolyzed in aqueous solution to form $Mn\,(OH)_x^{+(3-x)}$ ions and non-stochiometric solid MnOOH. [31] Hydrolysis of Mn(III) in acidic solution was studied by Biedermann in 1978. [33] He studied the equilibria of Mn^{3+} in an acidic media that consisted of H^+, Li^+, and ClO_4^- at 25 ^oC by using potentiometric method. The resulted equilibrium reaction constants of Mn(III) hydrolysis obtained by Biedermann are shown in Eq. 2.6 and Eq. 2.7 [33]

$$Mn^{3+} + H_2O \leftrightarrow MnOH^{+2} + H^{+}\,, \qquad K = 10^{0.4\pm0.1} \qquad \text{Eq. 2.6}$$

$$Mn^{3+} + 2H_2O \leftrightarrow Mn(OH)_2{}^{+} + 2H^{+}\,, \qquad K = 10^{0.1\pm0.1} \qquad \text{Eq. 2.7}$$

Beside Mn(III) hydrolysis in aqueous solution, Mn(III) tends to disproportionate to Mn(II) and Mn(IV) in acidic solution if no stabilizing complexing agent is present in the system. [16, 18,

19, 31] Various materials have been found to complex with Mn(III) and to stabilize the Mn(III) species from disproportionation reaction. EDTA, pyrophosphate, and citrate complexation in acidic medium were suggested by Klewicki in 1988 to stabilize Mn(III). [34] Various organic complex agents were also reported in the literature that can suppress Mn(III) disproportionation reaction. [35] However, using organic materials to stabilize Mn(III) in aqueous solution would increase the ohmic resistance in the electrolyte and it can also introduce other side electrochemical reactions of hydrocarbon species. Therefore, inorganic materials are preferable as a complex agent to stabilize Mn(III) in aqueous solution. Recently, ions such as TiO^{2+}, and Ti^{4+} with Mn^{3+} in aqueous sulfuric acid solution were suggested to help in stabilizing Mn(III). [25, 36] It was found that Mn(III) stability increased the most with the presence of Ti^{4+} in sulfuric acid solution. [36] A prior study was conducted by Sumitomo Electric Industries in 2016 to study the stability of Mn(III) with the presence of $TiOSO_4$ in 3M sulfuric acid solution for Ti/Mn RFB. [25] In their study, they found that TiO^{2+} slowed down the disproportionation reaction of Mn(III) in sulfuric acid solution and the stability of Mn(III) increases with TiO^{2+} concentration in sulfuric acid solution. [25] They believed that the TiO^{2+} stabilized Mn(III) in sulfuric acid solution by forming a complex ligand with Mn^{3+} in sulfuric acid solution. [25]

2.1.5.3. Speciation Study of Mn(IV)

Mn(IV) ions were found to be not stable in aqueous acidic solution because it hydrolyzes very rapidly to MnO_2. [22, 31] They may exist in acidic solution in a negligible amount in equilibrium with other species in the system. [22, 31] Finally, the standard Gibbs free energy of formation of all possible manganese species in acidic solution are listed in Table 3.

Table 3. Reported standard Gibbs free energy of formation $\Delta G^0_{f,i}$ [KJ/mole], for Manganese species from different sources

Species	[18]	[37]	[22]	[24]	[38]	[39]	[40]	[41]	[42]
H_2O	-237.18	-	-	-	-	-	-	-	-
SO_4^{2-}	-744.63	-	-	-	-	-	-	-	-
HSO_4^-	-756.01	-	-	-	-	-	-	-	-
Mn^{2+}	-228.1	-227.61	-	-	-	-228.11	-	-	-
$MnSO_{4_{Aq}}$	-	-	-	-	-	-	-	-	-982.4
$Mn(OH)^+$	-	-	-404.9	-	-	-405.01	-	-	-
$Mn(OH)_2$	-615.0	-	-	-	-	-615.01	-615.7	-	-
Mn^{3+}	-83	-81.92	-	-	-	-	-	-	-
$Mn(OH)^{2+}$	-		-324.4	-322.46	-	-	-	-	-
$Mn(OH)_2^+$	-	-	-	-557.93	-	-	-	-	-
$Mn(OH)_3$	-	-	-	-	-757.73	-757.3			-
$MnO_2(\gamma)$	-448.5	-	-	-	-	-456.47	-461.9	-461.88	-
$MnO_2(\alpha)$	-	-	-	-	-	-453.13	-	-	-
$MnOOH(\alpha)$	-557.7	-	-	-	-		-556.045	-554.8	-
$MnOOH(\gamma)$	-563.2	-	-	-	-	-557.73	-557.69	-557.7	-
$MnOOH(\delta)$	-	-553.54	-	-	-	-	-	-	-
$MnOOH(\beta)$	-	-	-	-	-	-	-547.07	-	-
$Mn(OH)_2^{+2}$	-	-	-	-	-431.93	-	-	-	-
Mn^{4+}	-	74.85	-	-	-	-	-	-	-

2.1.6. Electrochemical Study of $MnSO_4$ Redox Mechanism in Sulfuric Acid Solution

Several electrochemical studies of $MnSO_4$ electrolyte in sulfuric acid solution were conducted using cyclic voltammetry technique, chronoamperometry technique, and linear sweep voltammetry technique with different working electrodes materials such as Platinum-based working electrode, solid carbon-based working electrode, and porous carbon-based working electrode to study the mechanism of redox reaction of $MnSO_4$ in aqueous sulfuric acid solution. [16, 19, 25, 43, 44, 45, 46] Most of the mechanism studies of $MnSO_4$ redox reaction were made to explain to the formation of MnO_2 electrodeposition in acidic solution. [19, 43, 44, 45, 46, 47]

2.1.6.1. Platinum-Based Working Electrode

In 1992, Kao and Weibel studied the electrochemical oxidation of $MnSO_4$ to form electrolytic manganese dioxide (EMD) in sulfuric acid aqueous solution using a platinum Rotating-Ring-Disc working electrode. [43] The electrolyte solution used by Kao was 10mM $MnSO_4$ in 0.5M H_2SO_4 solution. Based on their work on the electrodeposition of EMD on Pt electrode, they concluded that the nucleation of EMD was controlled by an equilibrium reaction of an unknown Mn(III) intermediate that was undergone a disproportionation reaction on the Pt electrode and the growth of EMD involved the reduction of the already formed MnO_2 surfaces by Mn^{2+} in the solution to form MnOOH followed by MnOOH oxidation and proton releasing from MnOOH structure to form MnO_2. [43] They also believed that at high Mn^{2+} concentration, the MnOOH layer was built up and the controlling step of EMD electrodeposition was the proton insertion into MnOOH solid. On the other hand, when low Mn^{2+} concentration was used, the controlling step of EMD electrodeposition was controlled by the rate of diffusion of Mn^{2+} from the bulk electrolyte to the electrode surface. [43]

In 1994, Bodoardo investigated the reduction of the electrodeposited MnO_2 in sulfuric acid solution with considering the effect of temperature, pH, and Mn^{2+} concentration using linear sweep voltammetry and cyclic voltammetry technique. [23] He conducted his electrochemical experiments using a Pt working electrode and 0.5M $MnSO_4$ in 0.5M H_2SO_4 electrolyte solution and the resulted cyclic voltammogram is shown in Figure 14. In addition, XRD measurement of the electrodeposited MnO_2 that resulted from oxidizing $MnSO_4$ in sulfuric acid solution at room temperature and at 90 ^oC showed the phase of MnO_2 to be γ-phase as shown in Figure 15. Bodoardo conclusion differs from what Kao and Weibel found regarding the formed MnOOH. Bodoardo believed that a thin insulated layer of MnOOH was formed on the surface of MnO_2 during the first

reduction peak, its thickness depending on the solution pH and the Mn^{2+} concentration in the solution electrolyte. This MnOOH layer was believed to limit the reduction reaction of MnO_2 leading to a limited current measured after the first reduction peak, and at low applied voltage during cathodic scan, the cathodic current intensity increased again. He concluded that when MnO_2 was electrodeposited on a non-stationary working electrode at room temperature, the surface oxide layer was destroyed during the first reduction peak to form MnOOH and a second peak appeared during the reduction scan of cyclic voltammetry. [23]

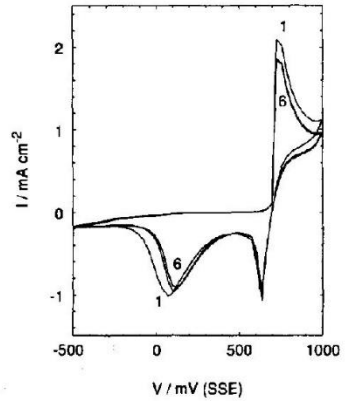

Figure 14. Cyclic voltammetry on platinum for 0.5M $MnSO_4$ in 0.5M H_2SO_4 at 25°C and at scan rate of 0.5mV/s [23]

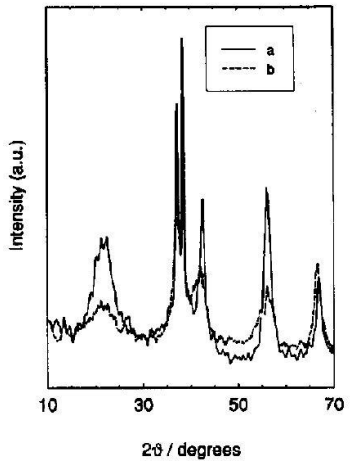

Figure 15. X-ray diffraction patterns for γ-MnO_2 electrodeposited resulted from oxidizing $MnSO_4$ in sulfuric acid solution at (a) room temperature. (b) at 90 °C [23]

Bodoardo's explanation for the reduction of γMnO_2 to MnOOH agreed with the theoretical basis of the polymorph γMnO_2 that was first introduced by Ruetschi in 1988. [47] Ruetschi explained the electrochemical reduction of γMnO_2 to be proceeded via proton insertion into the solid phase to form a mixture of polymorph solid of γMnO_2 and $\alpha MnOOH$. The partial reduced γMnO_2 leads to the insulated $\alpha MnOOH$ solid. The process that leads to $\alpha MnOOH$ is produced by a topotactic reduction of γMnO_2 [47]. The electrochemical reactivity of γMnO_2 is largely determined by the rate of proton diffusion in the solid phase of MnO_2. The structure of $\alpha MnOOH$ is shown below:

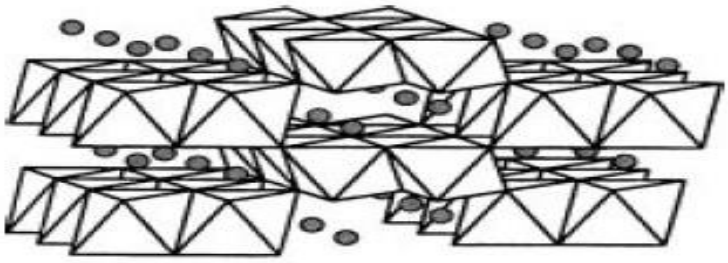

Figure 16. Crystal structure of α-MnOOH that was proposed by Ruetschi model [27]

The chemical formula of $\alpha MnOOH$ that was proposed by Ruetschi is [28]

$$Mn_{1-x}^{3+}.\, O_{1-3x}^{2-}\, .\, OH_{1+3x}^{-}$$

It is well accepted that the electrochemical reduction of γMnO_2 can be written without considering the nonstoichiometric γMnO_2 for sake of simplicity as shown in Eq. 2.8. [23]

$$MnO_2 + H^+ + e^- \leftrightarrow MnOOH \qquad \text{Eq. 2.8}$$

Nijjer studied the electrochemical oxidation of $MnSO_4$ and the electrochemical reduction of MnO_2 in sulfuric acid solution by cyclic voltammetry on Pt working electrode at different temperatures, $MnSO_4$ concentration, and sulfuric acid concentration, with and without convection in 2000. [45] In his study, the $MnSO_4$ electrolyte that was used in cyclic voltammetry was in the range of 0.018M-0.73M $MnSO_4$ in different sulfuric acid concentrations ranging from 0.5M-6M

H_2SO_4 and at a 22 ºC and 35 ºC. [45] Nijjer conclusion about the electrochemical oxidation of Mn(II) to Mn(III) was that the electrochemical reaction was limited by mass transport and the oxidation of Mn(II) to MnO_2 was proceed via the ECE mechanism (electron transfer reaction-chemical reaction- electron transfer reaction) where the chemical reaction step was the controlling step for the EMD electrodeposition. [45] He observed that at high temperature and convection, the oxidation of Mn(II) to MnO_2 was enhanced; at low acid concentration, the electrodeposition of MnO_2 was favored; and at high acid concentration, MnO_2 formation was inhibited [45]. The ECE mechanism for the oxidation of Mn^{2+} to Mn^{3+} and MnO_2 that was described by Nijjer is shown in Eq.2.9 to Eq.2.12 [45]

$$Mn^{3+} + e^{-} \leftrightarrow Mn^{2+} \qquad \text{Eq.2.9}$$

At low acid concentration: Mn^{3+} is disproportionated as shown in Eq.2.10 or it may hydrolyze to form MnOOH as in Eq. 2.11 [45]

$$2Mn^{3+} \leftrightarrow Mn^{4+} + Mn^{2+} \qquad \text{Eq.2.10}$$

$$Mn^{3+} + 2H_2O \leftrightarrow MnOOH + 3H^{+} \qquad \text{Eq.2.11}$$

The intermediates products such as Mn^{4+} and MnOOH are oxidized to form MnO_2 on the electrode surface. [45] Nijjer suggested that the overall oxidation reaction of Mn^{2+} during the cyclic voltammetry oxidation scan was from Mn^{2+} to MnO_2 as shown in Eq. 2.12. [45]

$$Mn^{2+} + 2H_2O \leftrightarrow MnO_2 + 4H^{+} \qquad \text{Eq.2.12}$$

Regarding the electrochemical reduction of MnO_2 to Mn^{2+}, Nijjer suggested that the deposited MnO_2 was partially reduced at the electrode interface between the electrode and MnO_2 interface

depending on the acid concentration and Mn^{2+} concentration where the electrodeposited MnO_2 was affected by a chemical reaction with Mn^{2+}. [45]

In 2006, Clarke studied the mechanism of MnO_2 electrodeposition using Pt-RDE and Pt-RRDE voltammetry for 0.1M-1M $MnSO_4$ concentration range, 0.1M-5M H_2SO_4 concentration range, at a rotation rate of 1000-4000 rpm, and at 22 ^oC and 98 ^oC temperature range. [19] Based on his experimental results, the current response of the voltammetry showed a peak. He believed that peak was due to a decrease on the catalytic activity of the electrode due to MnO_2 deposition on the electrode surface. [19] From the effect of varying Mn(II) concentration in both dilute H_2SO_4 solution and concentrated H_2SO_4 solution, Clarke concluded that the solid precipitated in concentrated acid solution was only MnO_2 and the solid precipitated in dilute acid solution was initially MnOOH. [19] Based on Levich plot analysis, Clarke suggested that the limited current observed during voltammetry oxidation scan was attributed to the activation instead of the mass transport limitation of Mn(II) to the electrode surface. Regarding Mn(III) stability after oxidizing Mn(II) in dilute and concentrated acid media, Clarke concluded that based on his voltammetry results, small amount of Mn(III) was formed in dilute acid concentration, while in concentrated acid solution almost all of Mn(III) was presented in the solution and it disproportionated into MnO_2 and Mn(II) in the solution. [19] He suggested that in dilute acid concentration the electrogenerated Mn(III) hydrolyzed and precipitated to form solid MnOOH which eventually oxidized to form MnO_2 on the electrode surface. Ultimately, a mechanism for the oxidation of $MnSO_4$ in dilute and concentrated sulfuric acid solution was proposed by Clarke as shown below [19]:

- Dilute sulfuric acid solution (<1M) [19]

$$[Mn(H_2O)_6]^{2+} \leftrightarrow [Mn(H_2O)_6]_{ads}{}^{2+}$$

$$[Mn(H_2O)_6]_{ads}{}^{2+} \leftrightarrow [Mn(H_2O)_6]_{ads}{}^{3+} + e^-$$

$$[Mn(H_2O)_6]_{ads}^{3+} \leftrightarrow [Mn(H_2O)_5(OH)]_{ads}^{2+} + H^+$$

$$[Mn(H_2O)_5(OH)]_{ads}^{2+} \leftrightarrow MnOOH.(H_2O)_4 + 2H^+ \text{ (Fast)}$$

$$MnOOH \leftrightarrow MnO_2 + H^+ + e^- \text{(slow)}$$

- Concentrated sulfuric acid solution (>1M) [19]

$$[Mn(H_2O)_6]^{2+} \leftrightarrow [Mn(H_2O)_6]_{ads}^{2+}$$

$$[Mn(H_2O)_6]_{ads}^{2+} \leftrightarrow [Mn(H_2O)_6]_{ads}^{3+} + e^-$$

$$[Mn(H_2O)_6]_{ads}^{3+} \leftrightarrow [Mn(H_2O)_6]^{3+}$$

$$2[Mn(H_2O)_6]^{3+} \leftrightarrow [Mn(H_2O)_6]^{2+} + [Mn(H_2O)_6]^{4+} \text{ (slow)}$$

$$[Mn(H_2O)_6]^{4+} \rightarrow\rightarrow MnO_2 \text{ (fast)}$$

2.1.6.2. Solid Carbon-Based Working Electrode

Xue investigated the electrochemical behavior of Mn(II)/Mn(III) couple using steady state polarization curve, electrochemical impedance spectroscopy, transient potential-step experiment, X-ray diffraction, charge–discharge experiments, and cyclic voltammetry on spectral pure graphite working electrode at room temperature for 0.01M-0.3M $MnSO_4$ concentration range in 0.5M-5M H_2SO_4 solution. [46] The result obtained by Xue for the cyclic voltammetry for 0.3M $MnSO_4$ in 0.5M-5M H_2SO_4 solution on pure graphite electrode at room temperature is shown in Figure 17. Xue concluded that during anodic scan in cyclic voltammetry, Mn^{2+} was oxidized to Mn^{3+} and then Mn^{3+} was disproportionated to MnO_2. During cathodic scan, the main reduction reaction was the reduction from MnO_2 to Mn^{2+}. [46] He believed that disproportionation reaction of Mn(III) was weak on graphite electrode as opposed to carbon felt electrode due to graphite electrode's fewer active sites. [46] Based on his cyclic voltammetry on graphite electrode, Xue concluded that, the reversibility of Mn(II)/Mn(III) redox reaction was best when sulfuric acid concentration was 5M. [46]

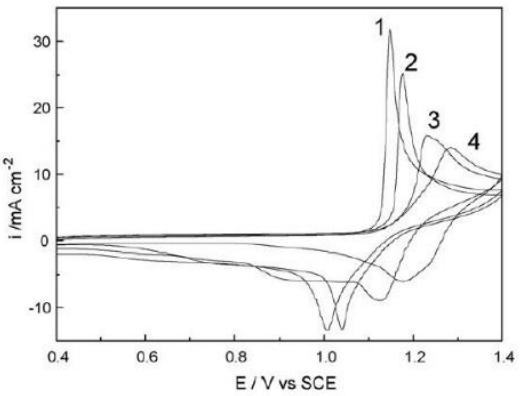

Figure 17. Cyclic voltammograms for 0.3M $MnSO_4$ in sulfuric acid with different sulfuric acid concentrations at scan rate of $5mVs^{-1}$ on graphite rod electrodes. Concentrations of the sulfuric acid, (1) 0.5M; (2) 1M; (3) 3M; (4) 5M [46]

2.1.6.3. Porous Carbon-Based Working Electrode

Xue also conducted cyclic voltammetry using carbon felt working electrode. The result of cyclic voltammetry obtained by xue for 0.3M MnSO4 in 1M-5M H_2SO_4 solution on carbon felt electrode at room temperature is shown in Figure 18. [46] Xue suggested that using carbon felt for Mn(III)/Mn(II) redox couple in sulfuric acid solution for RFB application was not suitable because Mn(III) disproportionation reaction became highly active on carbon felt working electrode. [46]

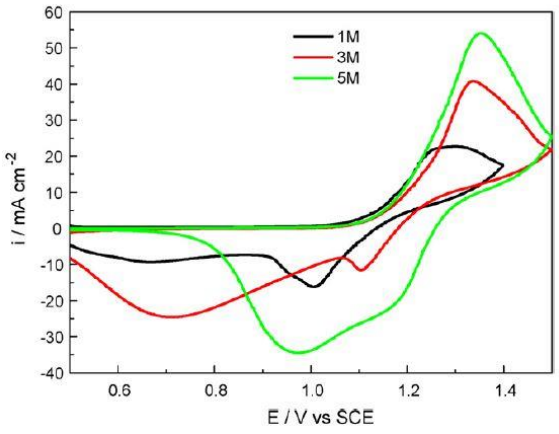

Figure 18. Cyclic voltammograms for 0.3M $MnSO_4$ in sulfuric acid with different concentrations at scan rate of $5mVs^{-1}$ on carbon felt electrodes. [46]

In 2017, Sumitomo Electric Industries (SEI), in their study of the characteristic of Ti-Mn RFB, studied the electrochemical behavior of Mn(III)/Mn(II) redox couple using cyclic voltammetry on carbon felt working electrode. [16] SE used 1M of $MnSO_4$ in 3M H_2SO_4 electrolyte solution with and without the addition of 1M $TiOSO_4$ as a stabilizer for Mn(III) in aqueous solution in their cyclic voltammetry experiment on carbon felt electrode at room temperature. [16] They used a small flow cell with a carbon felt as a working electrode and as a counter electrode. The working electrode area was 0.785 cm^2. [16] During the cyclic voltammetry, the tested electrolyte was kept still on the working electrode and the electrolyte on counter electrode was flowed. [16] The cyclic voltammogram of 1M of $MnSO_4$ in 3M H_2SO_4 electrolyte solution with and without the addition of 1M $TiOSO_4$ obtained by SEI is shown in Figure 19. [16]

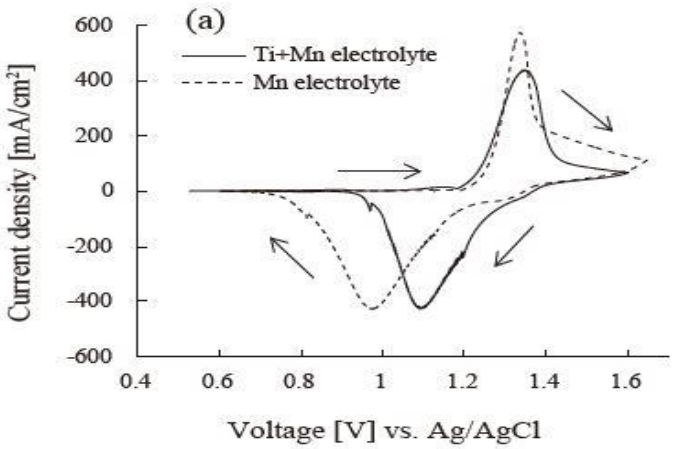

Figure 19. Voltammogram of 1M $MnSO_4$ in 3M H_2SO_4 __ with 1M $TiOSO_4$ addition; ---without 1M $TiOSO_4$ addition [16]

SEI assumed that the observed oxidation peak of cyclic voltammetry in both Mn electrolyte with and without the addition of $TiOSO_4$ attributed to the oxidation reaction of the entire Mn active material at the working electrode. [16] For the cyclic voltammetry of Mn electrolyte during the negative scan, two reduction peaks were detected at 1.3V vs. Ag/AgCl and at 0.97 V vs. Ag/AgCl.

These two reduction peaks were assumed to be attributed to the reduction reaction of Mn^{3+} to Mn^{2+} and MnO_2 to Mn^{2+}. [16] SEI observed that with the addition of 1M $TiOSO_4$ in 1M $MnSO_4$ electrolyte the oxidation peak decreased which indicated that the oxidation reaction of Mn electroactive species was suppressed. [16] In addition, the reduction peak of MnO_2 to Mn^{2+} during the cathodic scan was shifted from 0.97V to 1.1V vs. Ag/AgCl. [16] From the shifted peak, SEI concluded that the reduction reaction activity of MnO_2 to Mn^{2+} was increased when $TiOSO_4$ was added to Mn electrolyte. [16] The total number of the reactive electron from Mn electrolyte was 1.5 or more. [16]

SEI also found based on their FE-SEM images of the Mn electrolyte with a 90% SOC that the addition of $TiOSO_4$ to the Mn electrolyte led to the formation of smaller MnO_2 solids from the disproportionation reaction compared to the case where $TiOSO_4$ was not added as shown in Figure 20. [16] They found that with addition of Ti in the Mn electrolyte, the size of the solid precipitates in the solution was changed from 2,000 nm to 5 nm. [16]

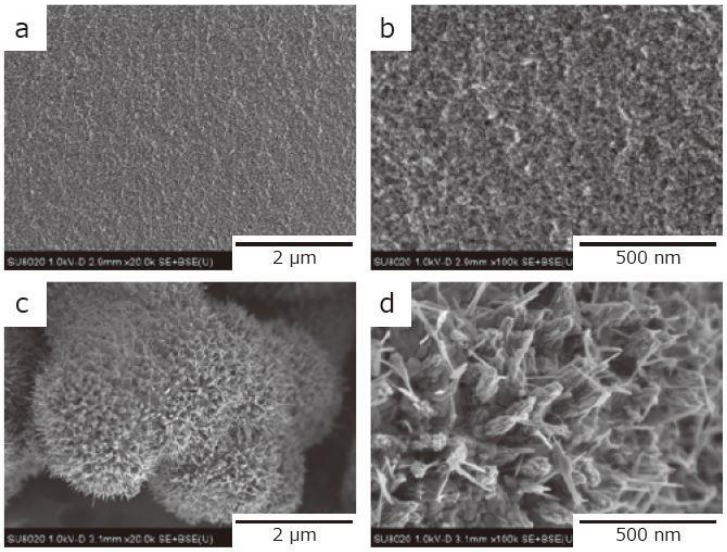

Figure 20 FE-SEM images of MnO_2 precipitates derived from (a,b) Ti+Mn electrolyte and (c,d) Mn electrolyte [16]

2.1.7. Stability of Manganese Electrolyte in Sulfuric Acid solution after being Charged

The stability of Mn electrolyte in sulfuric acid solution after being charged was studied by SEI with and without the addition of Ti(IV) species in Mn electrolyte system in 2016. [25] SEI found that after charging the positive Mn electrolyte material in Ti/Mn RFB by oxidizing Mn(II), Mn(III) was formed in the electrolyte; however, Mn(III) can readily disproportionate in the aqueous solution to form Mn(II) and MnO_2. [25] SEI suggested that Ti(IV) species can be used to stabilize Mn(III) after the positive electrolyte was charged. [25] They suggested that by mixing Ti(IV) in the positive electrolyte, Mn(III) disproportionation reaction was suppressed and the morphology of the precipitated MnO_2 was only γMnO_2 in smaller size that had less effect on the flow of the positive electrolyte to the electrochemical cell during discharge mode. [25] They also noted that by adding more $TiOSO_4$ to the Mn electrolyte, the redox of Mn electrolyte became more reversible in cyclic voltammetry. [25] The cyclic voltammetry on carbon felt working electrode for Mn electrolyte with different $TiOSO_4$ concentrations in 3M H_2SO_4 solution is shown in Figure 21. [25]

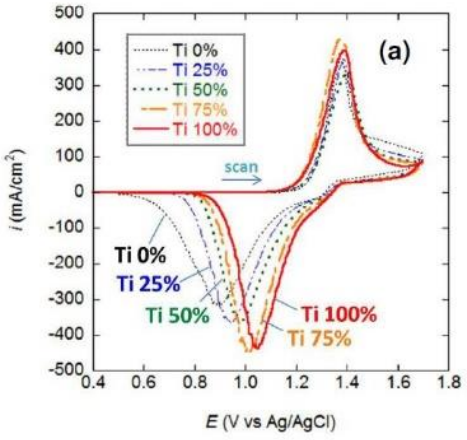

Figure 21. Cyclic voltammetry results for 1M $MnSO_4$ in 3M H_2SO_4 with different $TiOSO_4$ addition in % mol of $TiOSO_4$. [25]

From Figure 22, SEI observed that, the reduction peak during cyclic voltammetry was shifted to the right with the addition of TiOSO4 which indicated higher reversibility of charged species. [25] SEI suggested that Mn^{3+} formed a complex with the added Ti(IV) species based on their UV-vis spectroscopic study. [25] The spectra of 1M Mn SO_4+3M H_2SO_4 with and without the addition of 1M $TiOSO_4$ in different charging conditions in Figure 24. [25]

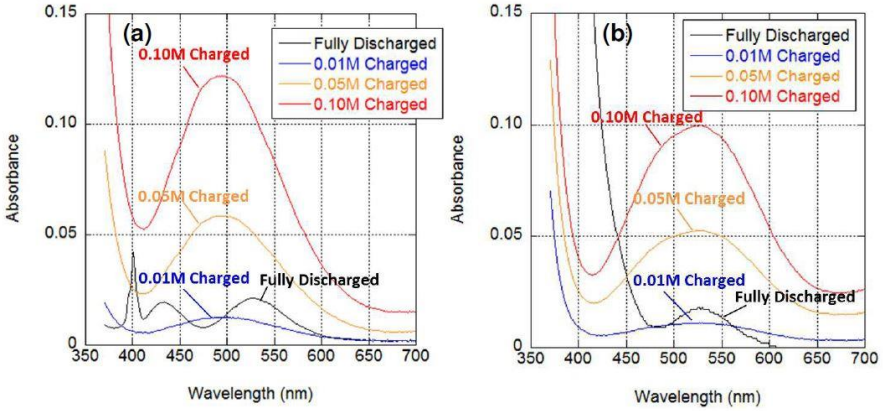

Figure 22. UV-visible spectra of (a) Ti 0% electrolyte, (b) Ti 100% electrolyte. Fully discharged, charged to 0.01, 0.05, 0.1 mol dm^{-3} as Mn^{3+} concentration. [25]

SE attributed the wavelength of Mn^{3+} to be at 520 nm. [25] The interpretation of the UV-vis spectra on the basis of the wavelength location was assumed to be the reason of the assumed interaction of Ti(IV) species and Mn(III) species by SE; However, the observation between the intensity of the absorbance with and without the addition of Ti shows a higher absorbance in the case of Mn electrolyte Ti-free the intensity which may indicates that the concentration of Mn^{3+} is high in Ti-free solution. [25]

However, solid material was observed in the electrolyte one week after the Mn electrolyte with and without the addition of $TiOSO_4$ system was charged up to 90%SOC using XRD as shown in Figure 23 . [25]

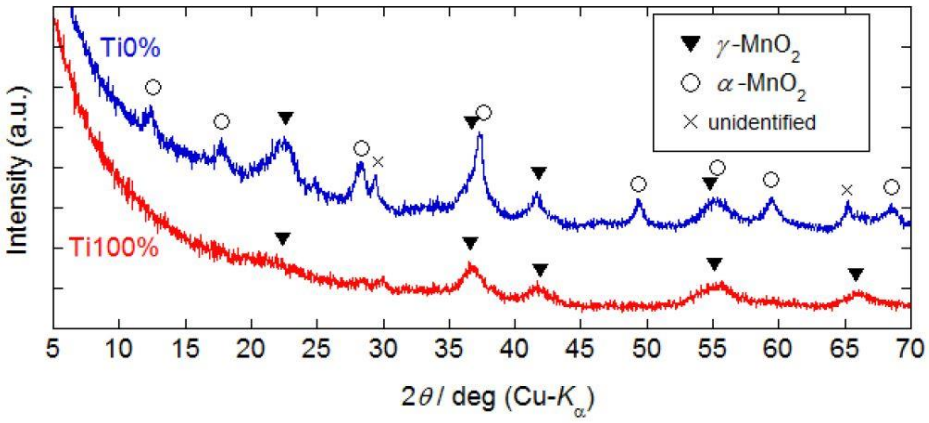

Figure 23. XRD patterns of the precipitates collected from the bottom of the vials of Ti 0% and Ti 100% electrolytes. [25]

From the XRD of SE of the Mn solid without Ti addition in the electrolyte, the solid observed by SE indicates the formation of α-MnO_2, γ-MnO_2 with undefined peaks. With the addition of Ti in the electrolyte, the peaks in the XRD were weak due to the small particle size formed in the solution <100nm, and based on the SE analysis, those weak peaks were only attributed to γ-MnO_2. [25] The γ-MnO_2 solid was suggested to be reactive, so that it can be reduced to Mn^{2+} and small enough to be flowed to the electrochemical cell during discharge operation. [25] The analysis of XRD by SE did not account for the formation of Mn(III) solid such as MnOOH, and the reason of forming α-MnO_2 in the Ti-free Mn electrolyte was not discussed.

In 2019, Garcia studied the speciation and the mechanism of the complexation between Mn(III) and Ti(IV) species using K-edge XANES technique for 0.2M $MnSO_4$+3M H_2SO_4 with and without the addition of 0.2 M $TiOSO_4$ after oxidizing the tested solution at 100 mA/cm^2 on 9 cm^2 until a voltage of 1.7V vs. Ag/AgCl was measured as shown in Figure 24. [36]

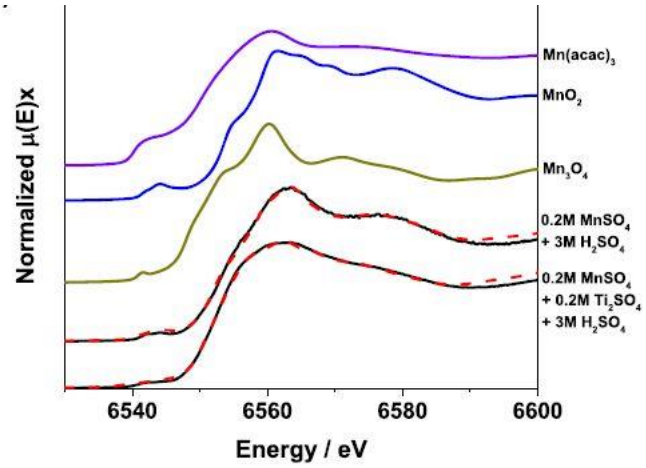

Figure 24. Mn K-edge XANES measurements for Mn(III) solutions formed through the electrochemical oxidation of $MnSO_4$ in 3 M H_2SO_4 in the presence and absence of 0.2 M $Ti(SO_4)_2$. [36]

Garcia compared the tested solutions spectra with $Mn(acac)_3$, Mn_3O_4 and MnO_2 powder spectra. [36] Garcia attributed the decrease of the spectra of the Mn-Ti electrolyte to the decrease of the formation of Mn(IV) via disproportionation reaction. [36] He hypothesized that this decreased pattern of Mn(IV) species in Mn-Ti electrolyte may due to the formation of a weak interaction between Mn(III) and Ti(IV) species through oxo bridge ligand that can stabilize the Mn(III) in sulfuric acid. [36] In his study, Garcia did not account for the decrease of the solid particle size for the charged species in Mn-Ti electrolyte as was suggested by SE.

2.2. Titanium Electrolyte in Sulfuric Acid

Titanium element has various oxidation states ranging from 0 to 4. [18] The Ti-Mn RFB negative electrolyte deals with Titanium of oxidation states from 3 to 4 which are the most stable oxidation state in aqueous solution among all Titanium oxidation states . [16, 22] In this section an overview of the apparent form and the chemical and electrochemical behavior of Ti(IV), and Ti(III) in sulfuric acid aqueous solution is reviewed.

2.2.1. Ti(IV) in Sulfuric Acid Solution

Ti(IV) is used as a starting negative electro-active material in the Ti-Mn RFB before it is charged. [16] Ti(IV) salts have many forms in nature such as TiO_2, $TiSO_4$, and $TiOSO_4$ etc. In high sulfuric acid concentration solution (for pH<1), Ti(IV) is present in the form of $[Ti(OH)_2]^{2+}$and $[Ti(OH)_3]^{+}$. [48] In addition to the formation of $[Ti(OH)_2]^{2+}$and $[Ti(OH)_3]^{+}$, recent studies conducted by Fabien Baillon, and Alexandre Pichavant indicated that Ti(IV) complexes with SO_4^{2-} in sulfuric acid solution to form $[Ti(OH)_2SO_4]^0_{Aq}$ and $[Ti(OH)_2 (SO_4)_2]^{2-}_{Aq}$. [49, 50]

2.2.2. Ti(III) in Sulfuric Acid Solution

Ti(III) hydrolyzes in aqueous solution to form $Ti(OH)^{2+}$. [51] In the presence of sulfuric acid in the solution, Ti(III) is present in the form of Ti^{3+} and it reacts with SO_4^{2-} to form $Ti (SO4)_x^{2-x}$, which is considered to be most stable form of Ti(III) in a sulfuric acid solution. [52]

2.2.3. The Standard Reduction Potentials of Ti(IV)/Ti(III)

The standard reduction potentials of the Ti(IV)/Ti(III) couple in acidic media ,where Ti(IV) is in the form of TiO^{2+} and Ti(III) is in the form of Ti^{3+}, was reported in literature as shown in Eq2.13. [16, 18]

- Ti(IV)/Ti(III):

$$TiO^{2+} + 2H^{+} + e^{-} \leftrightarrow Ti^{3+} + H_2O \qquad E^0 = 0.1V \text{ vs SHE} \qquad \text{Eq.2.13}$$

The standard reduction of Ti(IV)/Ti(III) was also reported in chloride media, where Ti(IV) and Ti(III) are in the form of $Ti(OH)_2^{2+}$, Ti^{4+}, and Ti^{3+}, as shown in Eq2.14 and Eq2.15. [53]

- Ti(IV)/Ti(III):

$$Ti(OH)_2^{2+} + 2H^{+} + e^{-} \leftrightarrow Ti^{3+} + 2H_2O \qquad E^0 = 0.007(+/-)0.006V \text{ vs SHE} \qquad \text{Eq.2.14}$$

$$Ti^{4+} + e^{-} \leftrightarrow Ti^{3+} \qquad E^0 = 0.202(+/-)0.002V \text{ vs SHE} \qquad \text{Eq.2.15}$$

2.2.4. Solubility of $TiOSO_4$ in Sulfuric Acid Solution

No data can be found for $TiOSO_4$ solubility in aqueous sulfuric acid solution in the literatures.

2.2.5. Speciation Study of Ti(IV) and Ti(III) in Sulfuric Acid Media

Ti(III) was reported to exist as an octahedral coordination framework in most aqueous solution. Ti(IV) may not exist as a free tetra-valent oxidation state species in the form of octahedral structure. Rather, in acidic aqueous solution, Ti(IV) exists in the form of oxo species. [31, 48] Ti(IV) was reported to be readily hydrolyzed in acidic solution to form different titanium (IV) hydroxide species and precipitated out as TiO_2 in low to moderate acidic solution. [22, 31, 48]

2.2.5.1. Speciation Study of Ti(IV) and Ti(III)

Collected values of standard Gibbs free energy of formation of all possible species of Ti(IV) in acidic aqueous solution are shown in Table 4. In addition, experimental values of the equilibrium chemical reactions that were reported in the literature for Ti(IV) and Ti(III) species are listed in Table 5.

Table 4. Values of standard Gibbs free energy of formation, $\Delta G^0_{f,i}$ [KJ/mole], of Ti(IV) and Ti(III) species in [KJ/mol] from different sources

Species	[54]	[55]	[56]	[18]	[57]
H_2O	-237.178408	-237.190	-	-237.18	-
SO_4^{2-}	-744.62648	-744.459	-	-744.63	-
HSO_4^-	-	-755.756	-	-756.01	-
TiO^{2+}	-	-	-	-577.4	-610 (+/-) 17
Ti^{4+}	-	-	-354.18	-	-349 (+/-) 9
$Ti(SO_4)^{+2}$	-	-1082.400	-	-	-
$Ti(OH)^{3+}$			-614.00		-611 (+/-) 2.3
$Ti(OH)_2^{2+}$			-869.56		-866 .4(+/-) 2.3
$Ti(OH)_3^+$	-	-	-1092.5	-	-1091.4 (+/-)2.3
$Ti(OH)_4$	-	-1320.310	-	-	-1314.1 (+/-)2.3
H_2SO_4	-690.06712	-	-	-690.101	-

Table 5. Reported equilibrium reaction constants, K, for Ti(IV) and Ti(III) chemical reactions in an acidic aqueous solution

Reactions	[58], [59]	[60]	[53]	[49], [50]	[61], [62]	[63]	[64]
$H_2SO4 + H_2O \leftrightarrow H_3O^+ + HSO_4^-$	10^8	-	-	-	-	-	-
$HSO_4^- + H_2O \leftrightarrow H_3O^+ + SO_4^{2-}$	0.012	-	-	-	-	-	-
$Ti(OH)_2^{2+} + H^+ \leftrightarrow Ti(OH)^{3+} + H_2O$	-	4.47 E-3	0.083	-	-	-	-
$TiOH^{3+} + H^+ \leftrightarrow Ti^{4+} + H_2O$	-	1.62 E-3	0.49	-	-	-	-
$Ti(OH)_2^{2+} + H_2O \leftrightarrow Ti(OH)_3^+ + H^+$	-	7.94 E-3	-	0.0195	-	-	-
$Ti(OH)_3^+ + H_2O \leftrightarrow Ti(OH)_4 + H^+$	-	4.27E-4	-	-	-	-	-
$Ti(OH)_2^{2+} + SO_4^{-2} \leftrightarrow [Ti(OH)_2SO_4]^0_{aq}$	-	-	-	3.4	-	-	-
$Ti(OH)_2^{2+} + 2SO_4^{-2} \leftrightarrow [Ti(OH)_2(SO_4)_2]^{-2}_{aq}$	-	-	-	12.02	-	-	-
$Ti^{3+} + H_2O \leftrightarrow Ti(OH)^{2+} + H^+$	-	-	-	-	-	0.0028	0.072
$Ti(OH)^{2+} + H_2O \leftrightarrow Ti(OH)_2{}^+ + H^+$	-	-	-	-	-	-	0.032
$Ti^{3+} + SO_4^{-2} \leftrightarrow Ti(SO_4)^+$	-	-	-	-	24.3	-	-

2.2.6. Electrochemical Study of $TiOSO_4$ Redox Mechanism in Sulfuric Acid Solution

Several electrochemical studies of $TiOSO_4$ electrolyte in sulfuric acid solution were conducted using cyclic voltammetry and square voltammetry techniques with different working electrode materials such as a solid carbon-based working electrode and porous carbon-based working electrode to study the mechanism of redox reaction of Ti(III)/Ti(IV) couple in aqueous sulfuric acid solution. [16, 65, 66]

2.2.6.1. Solid Carbon-Based Working Electrode

In 1981, Kiekens studied the electrochemical behavior of Ti(IV)/Ti(III) redox couple on a rotating glassy carbon electrode in sulfuric acid media. He conducted his experiment using 2mM Ti(IV) in the form of $TiOSO_4$ salt in a concentrated sulfuric acid solution (>5M H_2SO_4 solution) at room temperature. [66] During the cyclic voltammetry reduction scan of Ti(IV) on glassy carbon electrode, Kiekens did not observe a reduction wave of Ti(IV) below 5M H_2SO_4 solvent, while at

higher sulfuric acid concentration the reduction wave of Ti(IV) was obvious with no observed limited current. [66] He suggested that a limited current was not observed because of other non-Ti species in the solution was reduced such as hydrated sulfate complexes, or because of the interference of hydrogen reduction current in the low voltage range used in the voltage scan window from 1.2V vs SCE to -0.8V vs SCE. [66] The voltammogram during reduction scan of Ti(IV) on glassy carbon electrode obtained by Kiekens is shown in Figure 25. [66]

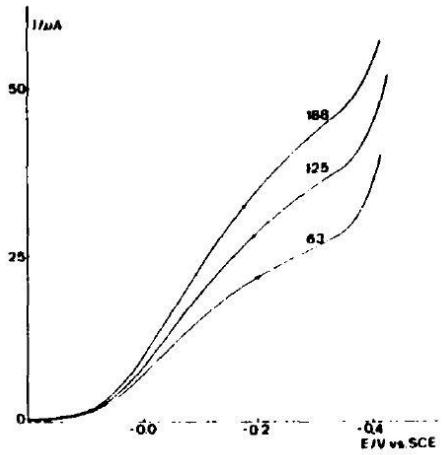

Figure 25. Current-Voltage curve of the reduction of 2mM $TiOSO_4$ in 10M H_2SO_4 solution on glassy carbon electrode with different rotation speed in (rad/s) [66]

During the cyclic voltammetry oxidation scan of Ti(III) on glassy carbon electrode, single wave was observed by Kiekens for the oxidation of Ti(III) to Ti(IV) in 4M H_2SO_4 solution with a limited current. [66] When Kiekens increased the concentration of H_2SO_4, he noticed that the oxidation wave was shifted to a more negative potential and the limited current decreased. [66] He concluded that the reversibility of the oxidation of Ti(III) was increased with increasing the acid concentration and viscosity of the solution was increased with increasing the acid concentration that was led to a low limited current. [66] The voltammogram during oxidation scan of Ti(III) on glassy carbon electrode that was obtained by Kiekens is shown in Figure 26. [66]

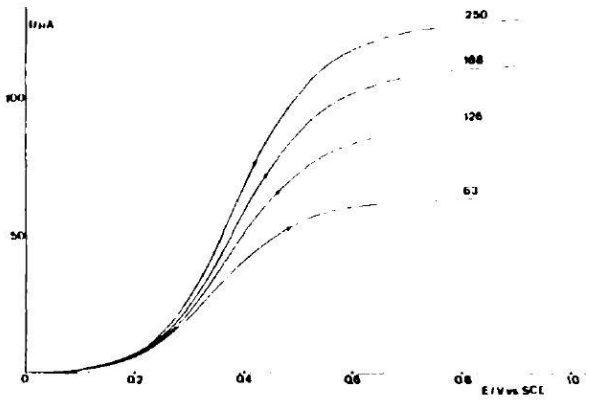

Figure 26. Current-Voltage curve of the reduction of 1.5mM Ti(III) in 4M H_2SO_4 solution on glassy carbon electrode with different rotation speed in (rad/s) [66]

In 1987, Noel and Anantharaman studied the voltammetry behavior of Ti(IV)/Ti(III) redox system in H_2SO_4 solution on glassy carbon electrode. [65] The electrolyte used in their study was 124.7 mM $TiOSO_4$ in 2M H_2SO_4. [65] The result obtained by Noel and Anantharaman is shown in Figure 27. [65] The same observation of unlimited Ti(IV) reduction current reported by Kiekens was also noticed in Noel and Anantharaman Ti(IV)/Ti(III) voltammogram shown in Figure 27. [65]

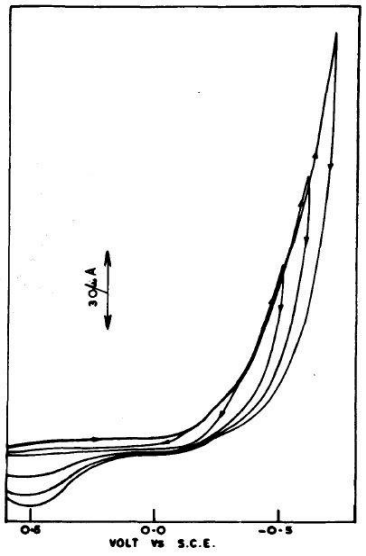

Figure 27. Cyclic voltammogram of 124.7 mM $TiOSO_4$ in 2M H_2SO_4 on glassy carbon with scan rate 20mV/s at room temperature. [65]

Noel and Anantharaman concluded that the cause of the unlimited cathodic current was attributed to the uncomplex Ti(IV) species in 2M sulfuric acid solution, and the supporting electrolyte reduction reaction during the cathodic scan was not the cause of the unlimited cathodic current because Noel and Anantharaman suggested that hydrogen reduction on a glassy carbon electrode should occur at a potential that is more negative than the voltage windows that they used which was from 0.7V vs. SCE to -0.8 V vs. SCE. [65] They believed that if a high Ti(IV) concentration was used with a high sulfuric acid concentration, Ti(IV) could complex with the sulfate in the solution to form a more electrochemically active Ti(IV) that is easily reducible. [65] During the anodic scan, Noel and Anantharaman observed an oxidation peak and they attributed it to the oxidation of Ti(III) species to Ti(IV) species. [65] They believed that Ti(III) species formed a stable complex form with the sulfate anion species in the solution that could be easily oxidized back to Ti(IV) when needed. [65]

2.2.6.2. Porous Carbon-Based Working Electrode

In 2017, Sumitomo Electric Industries (SEI), in their study of the characteristic of Ti-Mn RFB, studied the electrochemical behavior of Ti(IV)/Ti(III) redox couple using cyclic voltammetry on carbon felt working electrode. [16] They used 1M $TiOSO_4$ in 3M H_2SO_4 electrolyte solution with and without the addition of 1M $MnSO_4$ to study the interference effect of $MnSO_4$ on the Ti(IV)/Ti(III) redox couple in aqueous solution in their cyclic voltammetry experiment on carbon felt electrode at room temperature. [16] They used a small flow cell with a carbon felt as a working electrode and as a counter electrode. The working electrode area was 0.785 cm^2. [16] During the cyclic voltammetry, the tested electrolyte was kept still on the working electrode and the electrolyte on counter electrode was flowed continuously. [16] The cyclic voltammogram of 1M

of $TiOSO_4$ in 3M H_2SO_4 electrolyte solution with and without the addition of 1M $MnSO_4$ that was obtained by SEI is shown in Figure 28. [16]

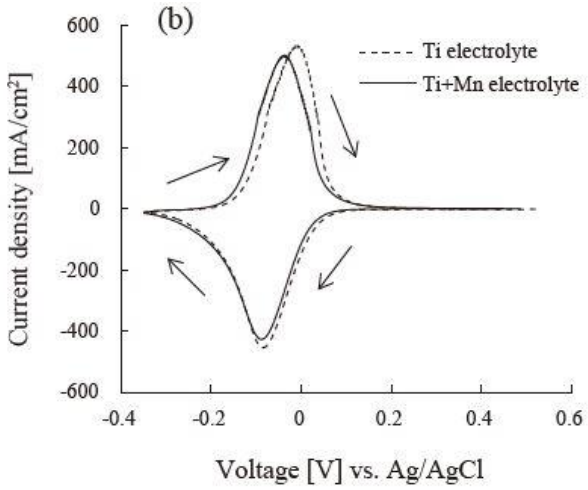

Figure 28. Voltammogram of 1M $TiOSO_4$ in 3M H_2SO_4 __ without 1M $MnSO_4$ addition; ---with 1M $MnSO_4$ addition [16]

SEI assumed that the observed reduction peak of cyclic voltammetry during the cathodic scan in both Ti electrolyte with and without the addition of 1M $MnSO_4$ to be due to the reduction reaction of TiO^{2+} to Ti^{3+} and the oxidation peak during the anodic scan to the oxidation reaction of Ti^{3+} to TiO^{2+}. [16] SEI observed that with the addition of 1M $MnSO_4$ in 1M $TiOSO_4$ electrolyte, there was almost no effect on the redox reaction of TiO^{2+}/Ti^{3+} couple and concluded that there was no issue in using $TiOSO_4$ as negative materials for Ti-Mn RFB. [16]

3. Theoretical and Experimental Study

In this chapter, an introduction to the fundamental of the cyclic voltammetry in electrochemical system is briefly described with the microscopic theory of electron transfer reaction for single and multiple reactions cases. Next, a thermodynamic calculation for Ti-Mn system in sulfuric acid is performed to help give an overall evaluation for the stability of electrolyte in aqueous sulfuric acid solution. Finally, the preparation and procedure of all conducted experiments for Ti-Mn redox electrochemical characterization and the Ti-Mn electrolyte solubility in sulfuric acid solution are discussed in detail.

3.1. Overview of Cyclic Voltammetry Experiment

Cyclic voltammetry (CV) is a qualitative electrochemical technique that is used to investigate the redox reaction process of molecular species. [67, 68] In general, CV is the initial electrochemical study of new electrochemical systems because it can give information about complicated electrode reactions. [68] CV experiment constructs a plot of the measured current flowing through the working electrode with respect to the applied voltage on the working electrode as function of time which can be called a voltammogram. [67, 69] The working electrode's potential starts at a potential E_1 which is usually selected so that the electro-active species that are under study are not oxidized or reduced. [69] The potential is then swept linearly to a voltage E_2 where E_2 is selected so that the potential difference between E_1 and E_2 includes reduction reaction or oxidation reaction of interest. [69] The applied voltage reverses the sweep direction from E_2 to the starting potential E_1. During the forward scan from E_1 to E_2, if $E_2 > E_1$, the swept voltage process is called an anodic scan where oxidation reaction takes place on the working electrode. [69] In contrast, during the reverse scan, the swept voltage is called a cathodic scan where reduction reaction takes place on the working electrode. [69] A typical profile of the wave form of

the voltage applied on the working electrode during CV experiment is shown in Figure 29. [69] From Figure 25, the applied potential on the working electrode during the CV experiment sweeps from E_1 initially to E_2 at t_{switch}, then the potential sweeps from E_2 at t_{switch} to E_1. [69] The slope of the applied potential between t=0 to t= t_{switch} indicates the scan rate of the applied voltage during the CV experiment. [69]

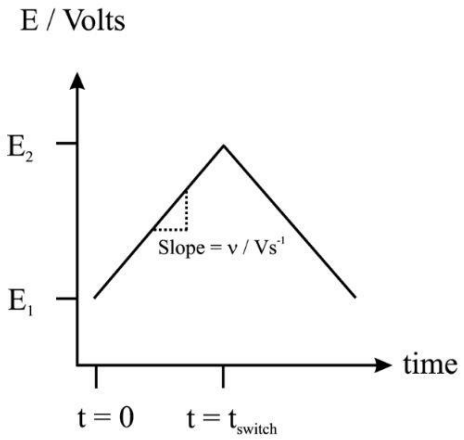

Figure 29. Typical applied voltage wave shape as function of time in cyclic voltamettry experimnet. [69]

For simple reversible one-electron reaction, two peak currents are expected on the voltammogram during a CV experiment and they reveal that the electrochemical reaction process of the electro-active species is under mass transport control mode. [68, 69] The first peak current is observed during anodic scan and it indicates the mass transport limitation in delivering electro-active species from the bulk solution to the working electrode surface for an oxidation reaction. [68, 69] The second current peak current is attributed to the mass transport limitation in delivering electro-active species from the bulk solution to the working electrode surface for a reduction reaction. [68, 69] More often the behavior of the electrochemical system during CV experiment depend on the kinetics of the heterogenous redox reaction, the equilibria of the chemical reactions

associated with the redox reaction, the mass transport of electro-active species near the electrode surface, and the voltage scan rate during CV experiment. [68, 69]

An electrochemical reversible system of one electron transfer reaction can be characterized from the voltammogram when two current peak ratio, that can be observed during the anodic scan and the cathodic scan, is equal to unity and the voltage peak separation is equal to 59 mV at 25 ^{o}C for one-electron transfer reaction. [68, 69] An electrochemical reversible system (or a Nernstian system) is often said if the system follows the Nernst equation as shown in Eq 3.1 and Eq 3.2 or an equation derived from it. [68]

$$O + ne^{-} \leftrightarrow R \qquad \text{Eq3.1}$$

$$E = E^{0\prime} + \frac{RT}{nF} \ln\left(\frac{C_O}{C_R}\right) \qquad \text{Eq3.2}$$

From Eq3.1, O is the oxidized species and R is the reduced species. Eq3.2 shows the relation of the equilibrium potential of the cell, E (V vs. SHE), to the formal reduction potential, $E^{0'}$ (V vs. SHE), and the concentration of the electro-active species on the electrode surface. [68] The formal potential measures the potential of the half-cell (in V vis SHE) when the concentration of species O and the concentration of species R are equal on the electrode surface in a giving medium electrolyte at a given temperature and pressure in an electrolyte. [68] In general, the formal potential is used to avoid dealing with the activity coefficients of electro-active species in the electrolyte solution because they are almost always unknown. [68] Often, the formal potential contains the standard reduction potential of the half-cell reaction, the activity coefficient of electro-active species and terms involving chemical reaction equilibrium constants in different electrolyte media. [68]

3.2. Overview of the Theory of Electron Transfer Reaction

If an electrochemical cell has a defined equilibrium potential, the departure of the cell potential from the equilibrium value upon passage of a faradic current is called polarization. [68] The extent of polarization is the driving force of electron transfer reaction and it is measured by the overpotential η. [68]

$$\eta = E - E_{eq} \qquad \text{Eq3.3}$$

For simple one electron transfer reaction that is shown in Eq3.1, the current-overpotential equation is shown in Eq3.4 [68]

$$I = I_0 \left[\frac{C_R(0,t)}{C_R^*} e^{\frac{(1-\alpha)F}{RT}\eta} - \frac{C_O(0,t)}{C_O^*} e^{\frac{-\alpha F}{RT}\eta} \right] \qquad \text{Eq3.4}$$

and,

$$E_{eq} = E^{0\prime} + \frac{RT}{F} \ln\left(\frac{C_0^*}{C_R^*}\right) \qquad \text{Eq3.5}$$

Note that the first term describes the anodic component current and the second term describes the cathodic component current based on the convention that positive current due to the net oxidation current. [68] C_R^* and C_O^* are the concentrations of the electro-active species in the bulk solution. [68] The exchange current I_0 is the measure of any system's ability to deliver a net current without an appreciable lost due to activation. [68] Exchange current I_0 is expressed in Eq3.6 as function of the bulk electrolyte concentration and the standard rate constant K^0 which measures the kinetic facility of a redox couple. [68] The cathodic transfer coefficient α value is near 0.5 for simple one electron transfer reaction. [68]

$$I_0 = FAK^0 C_o^{*(1-\alpha)} C_R^{*\alpha} \qquad \text{Eq3.6}$$

A straightforward definition of the standard rate constant K^0 is that it measures the electrochemical kinetic facility of a redox couple. [68] The larger the value of K^0, the faster the equilibrium is achieved. [68] The largest measured value of K^0 was reported to be in the range of 1 to 10 cm/s in a simple electron transfer reaction and the lowest value was reported to be less than 10^{-9} cm/s when a significant molecular rearrangement is associated with the electron transfer reaction. [68] Another way to express the current-overpotential equation is by using the form of the rate constant of the anodic reaction k_a and the rate constant of the cathodic reaction k_c as shown in Eq3.7. [67, 69]

$$I = \frac{C_R(0,t)}{C_R^*} k_a - \frac{C_O(0,t)}{C_O^*} k_c \qquad \text{Eq3.7}$$

where,

$$k_a = I_0 \left[e^{\frac{(1-\alpha)F}{RT}\eta} \right] \text{ and } k_c = I_0 \left[e^{\frac{-\alpha F}{RT}\eta} \right]$$

3.3. Microscopic Theory of Electron Transfer

The microscopic theory of electron transfer reaction considers two aspects during the heterogenous electron transfer reaction. [68] For an outer sphere, single electron transfer reaction from an electrode to a species O to form a reduced species R as shown in Eq3.1, the electron transfer reaction is proceeded by an electronic rearrangement of the reacting species radiationlessly. [68] Due to the radiationless electron transfer, the electron must transfer from an initial state on the electrode to a receiving state that is species O on the electrode surface where the receiving state has the same energy level of the initial state. [68, 69] Second, During the action of electron transfer, the reactants and the products resulted from the electron transfer reaction do not change their nuclear configuration, such as nuclear momenta and position, on the time scale of

electronic transition. This theory is based on the Franck-Condon principle. [67, 69] As a result, the reactant O and product R have a similar nuclear configuration during the moment of electron transfer. [67, 69] Based on Marcus microscopic model of electron transfer, the rate constant of reduction reaction can be written as a function of the activation energy of reduction of O species $\Delta G_f^{\ddagger}$, a precursor equilibrium constant of reactant species at a reactive position on the electrode $K_{P,O}$, the frequency of attempts on the energy barrier (associated with bond vibration and solvent motion) v_n, and the electronic transmission coefficient k_{el} as shown in Eq3.8. [68]

$$k_c = K_{P,O} v_n k_{el} \left[e^{\frac{-\Delta G_f^{\ddagger}}{RT}} \right] \qquad \text{Eq3.8}$$

The activation energy of reduction of O species $\Delta G_f^{\ddagger}$ was evaluated based on Marcus model to be a function of the reorganization energy and the difference between the applied potential to the standard reduction potential as shown in Eq3.9. [68]

$$\Delta G_f^{\ddagger} = \frac{\lambda}{4} \left(1 + \frac{F(E - E^0)}{\lambda} \right)^2 \qquad \text{Eq3.9}$$

λ is the reorganization energy which represents the energy required to transform the nuclear configuration in the reactant and the solvent to those of the product state. [68] It can be divided into inner component λ_i that is for the contribution of reactant O and outer component λ_o that is for the contribution of the solvent as shown in Eq3.10. [68]

$$\lambda = \lambda_i + \lambda_o \qquad \text{Eq3.10}$$

Typical values of λ are in the range of 0.5 to 1 eV. [68]

3.3.1. Multiple Electron Transfer Reactions Case

A general concept in electrochemistry of multiple electron transfer reactions is that an overall process involving a change of n electrons must involve n distinct electron transfer steps where it may also involve other chemical reaction elementary steps. [68] In most cases of multiple electron transfer, one elementary step is more sluggish than all the others, so that it controls the overall reaction. A true elementary electron transfer reaction is always involving the exchange of one electron. [68]

3.4. Chemistry of Manganese in Sulfuric Acid Solution

3.4.1. Selected Thermodynamic Values of Mn System

Due to the variety of reported thermodynamic values of the Mn system, the selected thermodynamic values of the standard Gibbs free energy of formation of all possible Manganese species in sulfuric acid solution are shown in Table 6. Those values were chosen based on the reproducibility from different source and how closely they are from experimental data. Some of the Gibbs free energy of formation of Mn species could not be found in literature, and their Gibbs free energy of formation were assumed to be in linear fitting with the addition of the complex ion such as OH^-.

Table 6. Selected values of Standard Gibbs free energy of formation $\Delta G^0_{f,i}$, in [KJ/mol] from Table 3 for Manganese species in sulfuric acid solution from different sources.

Species	Assumed value	Selected values
H_2O	-	-237.178
H_2SO_4		-690.101
SO_4^{2-}	-	-744.63
HSO_4^-	-	-756.01
Mn^{2+}	-	-228.1
$Mn(OH)^+$	-	-405.0112
$Mn(OH)_2$	-	615.0
Mn^{3+}	-	-83
$Mn(OH)^{2+}$	-	-324.4
$Mn(OH)_2^+$	-	-557.93
$Mn(OH)_3$	-	-757.727
$MnO_2(\gamma)$	-	-456.4744
$MnO_2(\alpha)$	-	-453.1272
$MnO_2(\beta)$	-	-465.14
$MnOOH(\alpha)$	-	-556.045
$MnOOH(\gamma)$	-	-557.6851
$MnOOH(\delta)$	-	-553.543
$MnOOH(\beta)$	-	-547.072
$Mn(OH)_4$	-925.79	-925.79
$Mn(OH)_3^+$	-680.36	-680.36
$Mn(OH)_2^{+2}$	-	-431.93
$Mn(OH)^{3+}$	-180.5	-180.5
Mn^{4+}	-	74.852

Due to few reported chemical reactions for Mn system in literature, the equilibrium constants for unreported chemical reaction was estimated by evaluating the chemical reaction constants of

those proposed chemical reactions using the reported values of Gibbs free energy of formations from Table 6. All possible chemical reactions, where some chemical reactions were proposed in this thesis to study their effect with experiments, that may occur for Mn(II), Mn(III) and Mn(IV) in aqueous sulfuric acid solution are shown in Table 7.

Table 7. Calculated equilibrium reaction constants for all Mn(II), Mn(III), and Mn(IV) in an acidic aqueous solution.

No.	Reactions	Calculated K	Experimental K	Selected K
Eq3.11	$MnSO_4 \leftrightarrow Mn^{2+} + SO_4^{-2}$	0.02	0.0052	0.02
Eq3.12	$Mn^{2+} + H_2O \leftrightarrow Mn(OH)^+ + H^+$	2.725 E-11	2.57 E-11	2.57 E-11
Eq3.13	$Mn(OH)^+ + H_2O \leftrightarrow Mn(OH)_2 + H^+$	1.7E-5	-	1.7E-5
Eq3.14	$Mn^{3+} + H_2O \leftrightarrow Mn(OH)^{2+} + H^+$	5.5	2.5	2.5
Eq3.15	$Mn(OH)^{2+} + H_2O \leftrightarrow Mn(OH)_2^+ + H^+$	0.23	0.5	0.5
Eq3.16	$Mn(OH)_2{}^+ + H_2O \leftrightarrow Mn(OH)_3 + H^+$	2.8 E-7	-	2.8 E-7
Eq3.17	$Mn(OH)_2{}^+ \leftrightarrow (\gamma)MnOOH + H^+$	0.9059	-	0.9059
Eq3.18	$Mn(OH)_2{}^+ \leftrightarrow (\alpha)MnOOH + H^+$	0.467	-	0.467
Eq3.19	$Mn(OH)_2{}^+ \leftrightarrow (\delta)MnOOH + H^+$	0.17	-	0.17
Eq3.20	$Mn(OH)_2{}^+ \leftrightarrow (\beta)MnOOH + H^+$	0.0125	-	0.0125
Eq3.21	$Mn^{4+} + H_2O \leftrightarrow Mn(OH)^{3+} + H^+$	1532.4	-	1532.4
Eq3.22	$Mn(OH)^{3+} + H_2O \leftrightarrow Mn(OH)_2{}^{2+} + H^+$	122.87	-	122.87
Eq3.23	$Mn(OH)_2{}^{2+} + H_2O \leftrightarrow Mn(OH)_3^+ + H^+$	240	-	240
Eq3.24	$Mn(OH)_3{}^+ + H_2O \leftrightarrow Mn(OH)_4 + H^+$	27.9	-	27.9
Eq3.25	$Mn(OH)_2{}^{2+} \leftrightarrow \alpha MnO_2 + 2H^+$	5.2 E+3	-	5.2 E+3
Eq.3.26	$Mn(OH)_2{}^{2+} \leftrightarrow \gamma MnO_2 + 2H^+$	2E+4	-	2E+4
Eq3.27	$Mn(OH)^{3+} + H_2O \leftrightarrow \alpha MnO_2 + 3H^+$	1.6E+6	-	1.6E+6
Eq3.28	$Mn(OH)^{3+} + H_2O \leftrightarrow \gamma MnO_2 + 3H^+$	6.3E+6	-	6.3E+6
Eq3.29	$H_2SO4 + H_2O \leftrightarrow H_3O^+ + HSO_4^-$	3.6E+11	10^8	10^8
Eq3.30	$HSO_4^- + H_2O \leftrightarrow H_3O^+ + SO_4^{2-}$	0.012	0.012	0.012

3.4.1.1. Manganese Speciation Study in 1-3 M Sulfuric Acid Solution

3.4.1.1.1. Mn(II) Species in 1-3 M Sulfuric Acid Solution

Mn(II) was reported to hydrolyze in low acidic solution to form $Mn(OH)^+$ and $Mn(OH)_2$ based on Eq3.12, and Eq3.13 in Table 7; however, in 1-3M H_2SO_4, the dominant Mn(II) species is in the form of Mn^{2+} free cation. However, with the presence of SO_4^{2-} in acidic media, Mn^{2+} forms $MnSO_{4(Aq)}$ complex in the solution. [20, 21, 32]

$$MnSO_{4_{Aq}} \leftrightarrow Mn^{2+} + SO_4^{-2}, \qquad K = 0.00158 \qquad \text{Eq3.11}$$

$$Mn^{2+} + H_2O \leftrightarrow Mn(OH)^{+} + H^{+} \qquad K=2.725\ E\text{-}11 \qquad Eq3.12$$

$$HSO_4^{-} \leftrightarrow H^{+} + SO_4^{2-} \qquad K=0.012 \qquad Eq3.30$$

Assume we have 1M $MnSO_{4\ Aq}$ in 1-3M H_2SO_4. All possible reactions that may occur for Mn(II) in 1-3M H_2SO_4 are based on reactions Eq.3.11, Eq3.12, and Eq.3.30. H_2SO_4 was assumed to be fully dissociate into HSO_4^- and H_3O^+ based on Eq3.29 in Table 7. Sample modeling equations of the equilibrium concentration of species in the solution are shown in Appendix A.

Table 8. Equilibrium concentrations of Mn(II) species in 1-3M sulfuric acid solution.

	[M] H_2SO_4 Concentration			
Species	**1**	**2**	**3**	**Trend**
$C_{HSO_4^-}$ [M]	1.085587	2.093852	3.097058	Increase
C_{H^+}[M]	0.914413	1.906148	2.902942	Increase
$C_{Mn^{2+}}$ [M]	0.099834	0.107034	0.10986	Same
$C_{SO_4^{-2}}$[M]	0.014246	0.013182	0.012802	Decreased
$C_{Mn(OH)^+}$[M]	3.00E-12	1.54E-12	5.63E-12	Peaked
$C_{MnSO_{4\ Aq}}$[M]	0.900167	0.892966	0.89014	Decreased

From Table 8, as the acid concentration increases, the dissociation of $MnSO_4$ increases; however, Mn^{2+} concentration in all three sulfuric acid solutions seems to be almost the same.

3.4.1.1.2. Mn(III) Species in 1-3 M Sulfuric Acid Solution

Assume we have 1M Mn^{3+}, 1.5M SO_4^{-2} in 1-3M H_2SO_4. All possible reactions that may occur for Mn(III) in 1-3M H_2SO_4 without considering Mn(III) disproportionation reaction are shown below. H_2SO_4 was assumed to fully dissociate into HSO_4^- and H_3O^+ based on Eq3.29 in Table 7.

$$Mn^{3+} + H_2O \leftrightarrow Mn(OH)^{2+} + H^{+} \qquad K=2.5 \qquad Eq3.13$$

$$Mn(OH)^{2+} + H_2O \leftrightarrow Mn(OH)_2^{+} + H^{+} \qquad K=0.5 \qquad Eq3.14$$

$$HSO_4^{-} \leftrightarrow H^{+} + SO_4^{2-} \qquad K=0.012 \qquad Eq3.30$$

The equilibrium concentration of all Mn(III) species in Eq3.30, Eq3.13, and Eq3.14 were estimated, and their values are shown in Table 9.

Table 9. Equilibrium concentrations of Mn(III) species without considering disproportionation reaction in 1-3M sulfuric acid solution.

	[M] H_2SO_4 Concentration			
Species	**1**	**2**	**3**	**Trend**
$C_{HSO_4^-}$ [M]	2.46	3.47	4.48	Increase
C_{H^+}[M]	0.735	1.418	2.21	Increase
$C_{Mn^{3+}}$ [M]	0.149	0.295	0.42	Increase
$C_{SO_4^{-2}}$[M]	0.04	0.0293	0.024	Decreased
$C_{Mn(OH)^{2+}}$[M]	0.507	0.521	0.474	Peaked
$C_{Mn(OH)_2^+}$[M]	0.344	0.184	0.107	Decreased

From Table 9, the concentrations of HSO_4^-, H^+, and Mn^{3+} increased with increasing the acid concentration from 1M to 3M H_2SO_4. $Mn(OH)_2^+$ concentration decreases as the acid concentration increases from 1M to 3M H_2SO_4.

3.4.1.1.3. Mn(IV) Species in 1-3 M Sulfuric Acid Solution

Assume we have 1M Mn^{4+}, 2M SO_4^{-2} in 1-3M H_2SO_4. All possible reactions that may occur for Mn(IV) in 1-3 H_2SO_4 without considering Mn(III) disproportionation reaction are shown below. H_2SO_4 was assumed to be fully dissociate into HSO_4^- and H_3O^+ based on E3q.29.

$$HSO_4^- \leftrightarrow H^+ + SO_4^{2-} \qquad K=0.012 \qquad \text{Eq3.30}$$

$$Mn^{4+} + H_2O \leftrightarrow Mn(OH)^{3+} + H^+ \qquad K=1532.4 \qquad \text{Eq3.21}$$

$$Mn(OH)^{3+} + H_2O \leftrightarrow Mn(OH)_2{}^{2+} + H^+ \qquad K=122.87 \qquad \text{Eq3.22}$$

$$Mn(OH)^{3+} + H_2O \leftrightarrow \gamma MnO_{2(S)} + 3H^+ \qquad K= 6.3E6 \qquad \text{Eq3.28}$$

The equilibrium concentration of all Mn(IV) species in Eq3.30, Eq3.21, Eq3.22, and Eq3.28 were estimated, and they are shown in Table 10.

Table 10. Equilibrium concentrations of Mn(IV) species reaction in 1-3M sulfuric acid solution.

	[M] H_2SO_4 Concentration			
Species	**1**	**2**	**3**	**Trend**
$C_{HSO_4^-}$ [M]	2.98809	3.98807	4.98805	Increase
C_{H^+}[M]	3.011544	4.011272	5.010912	Increase
$C_{Mn^{4+}}$ [M]	0	0	0	-
$C_{SO_4^{-2}}$[M]	0.01191	0.01193	0.01195	Increase
$C_{Mn(OH)^{3+}}$[M]	4.22E-06	1.04E-05	1.96E-05	Increase
$C_{Mn(OH)_2^{2+}}$[M]	1.77 E-4	3.14 E-4	4.89 E-4	Increase

From Table 10, the concentrations of HSO_4^-, and H^+ increased with increasing the acid concentration for 1M to 3M H_2SO_4. The dominant form of Mn(IV) in 1M to 3M H_2SO_4 was in the form of MnO_2 because of the significant hydrolysis reaction of Mn(IV) in sulfuric acid solution. $Mn(OH)^{3+}$ and $Mn(OH)_2^{+2}$ concentrations were negligibly small in 1M to 3M H_2SO_4. Based on this theoretical calculation, Mn^{4+} was not stable in sulfuric acid solution and it hydrolyzed significantly to MnO_2.

3.4.2. Possible Electron Transfer Reactions of $MnSO_4$ in Sulfuric Acid Solution

Based on the theoretical study of the Mn system in sulfuric acid solution in the previous sections, all possible reduction reactions of Mn species in a sulfuric acid solution that may possibly occur with their standard reduction potential against standard Saturated Calomel Electrode (SCE) are shown below.

- Mn(III)/ Mn(II):

$$Mn^{3+} + e^- \leftrightarrow Mn^{2+}, \quad E^0 = 1.26 \text{ V vs SCE, [18]} \qquad \text{Eq3.31}$$

$$Mn(OH)^{2+} + e^- \leftrightarrow Mn(OH)^{+}, \quad E^0 = 0.59 \text{ V vs SCE} \qquad \text{Eq3.32}$$

$$Mn(OH)_2^{+} + e^- \leftrightarrow Mn(OH)_2, \quad E^0 = 0.347 \text{ V vs SCE} \qquad \text{Eq3.33}$$

- Mn(IV)/ Mn(III):

$$Mn^{4+} + e^- \leftrightarrow Mn^{3+}, \quad E^0 = 1.392 \text{ V vs SCE} \qquad \text{Eq3.34}$$

$$Mn(OH)^{3+} + e^- \leftrightarrow Mn(OH)^{2+}, \quad E^0 = 1.247 \text{ V vs SCE} \qquad \text{Eq3.35}$$

$$Mn(OH)_2^{2+} + e^- \leftrightarrow Mn(OH)_2^{+}, \quad E^0 = 1.06 \text{ V vs SCE} \qquad \text{Eq3.36}$$

$$Mn(OH)_3^{+} + e^- \leftrightarrow Mn(OH)_3, \quad E^0 = 0.557\text{V vs SCE} \qquad \text{Eq3.37}$$

- $yMnO_2$/ xMnOOH:

$$** H^+ + (\gamma)MnO_2 + e^- \leftrightarrow (\alpha)MnOOH, \quad E^0 = 0.788 \text{ V vs SCE, [18]} \qquad \text{Eq3.38}$$

$$** H^+ + (\alpha)MnO_2 + e^- \leftrightarrow (\gamma)MnOOH, \quad E^0 = 0.839 \text{ V vs SCE, [18]} \qquad \text{Eq3.39}$$

$$H^+ + (\alpha)MnO_2 + e^- \leftrightarrow (\delta)MnOOH, \quad E^0 = 0.797 \text{ V vs SCE} \qquad \text{Eq3.40}$$

$$H^+ + (\alpha)MnO_2 + e^- \leftrightarrow (\alpha)MnOOH, \quad E^0 = 0.823 \text{ V vs SCE} \qquad \text{Eq3.41}$$

$$H^+ + (\alpha)MnO_2 + e^- \leftrightarrow (\beta)MnOOH, \quad E^0 = 0.73 \text{ V vs SCE} \qquad \text{Eq3.42}$$

**It was reported that $(\gamma)MnO_2$ is formed by oxidizing $(\alpha)MnOOH$ and $(\alpha)MnO_2$ is formed by oxidizing $(\gamma)MnOOH$. [18]

3.4.2.1. MnO_2 Morphology in Sulfuric Acid Solution

Disproportionation reaction of Mn(III) species in a system consist of $MnSO_4$ and H_2SO_4 was studied theoretically to predict the possible route for disproportionation reaction in the electrolyte system. Based on the study of Mn system in sulfuric acid solution, SEI found that Mn(III) can readily disproportionate in the aqueous solution to Mn(II) and MnO_2. [25] Their characterization measurement for the solid formed in Mn-sulfuric acid aqueous solution using XRD indicated that the morphology of MnO_2 was a mixture of γ-MnO_2 and α-MnO_2 with relatively high dominant

phase of γ-MnO_2. [25] Based on SEI results, a proposed hypothetical route for the formation of γ-MnO_2 and α-MnO_2 is that γ-MnO_2 is the phase that is favored to form by the electrochemical pathway since it is more thermodynamically favorable in sulfuric acid solution. If Mn^{3+} was assumed to hydrolyze all the way to MnOOH solid species, the more favorable pathway for Mn^{3+} may be the formation of γ-MnOOH and the oxidation of γ-MnOOH to α-MnO_2.

Speciation of Mn(III) should be considered to find the possible pathway of the disproportion reaction in aqueous sulfuric acid solution. The possible scenario for the disproportionation reaction is by considering two types of Mn(III) species where one may be the solid MnOOH. As Mn(III) diffuses away from the electrode surface after being generated electrochemically in a very high acid concentration, the most apparent form of Mn(III) is the free cation Mn^{3+}. Some of this free Mn(III) cation hydrolyze in water to form many hydrolyzed Mn(III) species and metastable solids such as MnOOH. $(\gamma)MnOOH$ was found to be oxidized to produce $(\alpha)MnO_2$. [27] $(\alpha)MnOOH$ was reported to be oxidized to form $(\gamma)MnO_2$. [18, 27] The generated electron is taken by Mn^{3+} to form Mn^{2+}. The whole process should be spontaneous as shown in the reaction sequence below.

$$Mn^{3+} + H_2O \leftrightarrow Mn(OH)^{2+} + H^+, \text{ K=2.5} \qquad \text{Eq3.14}$$

$$Mn(OH)^{2+} + H_2O \leftrightarrow Mn(OH)_2^+ + H^+, \text{ K=0.5} \qquad \text{Eq3.15}$$

$$Mn(OH)_2{}^+ \leftrightarrow (\gamma)MnOOH + H^+, \text{ K=0.9059} \qquad \text{Eq3.17}$$

$$(\gamma)MnOOH \leftrightarrow H^+ + (\alpha)MnO_2 + e^-, \quad E^0 = 0.839 \text{ V vs SCE} \qquad \text{Eq3.38}$$

$$Mn^{3+} + e^- \leftrightarrow Mn^{2+}, \quad E^0 = 1.26 \text{ V vs SCE} \qquad \text{Eq3.30}$$

Overall: $$2Mn^{3+} + 2H_2O \leftrightarrow Mn^{2+} + (\alpha)MnO_2 + 4H^+ \qquad \text{Eq3.43}$$

The key reaction for the disproportion reaction is the sum of reaction Eq3.38 and Eq3.30 to give Eq3.44.

$$(\gamma)\mathrm{MnOOH} + \mathrm{Mn^{3+}} \leftrightarrow \mathrm{Mn^{2+}} + \mathrm{H^{+}} + (\alpha)\mathrm{MnO_2},\ \text{K=1.3 E+7} \qquad \text{Eq3.44}$$

Similarly, for $(\gamma)\mathrm{MnO_2}$ formed by disproportionation reaction

$$\mathrm{Mn^{3+}} + \mathrm{H_2O} \leftrightarrow \mathrm{Mn(OH)^{2+}} + \mathrm{H^{+}},\ \text{K=2.5} \qquad \text{Eq3.14}$$

$$\mathrm{Mn(OH)^{2+}} + \mathrm{H_2O} \leftrightarrow \mathrm{Mn(OH)_2^{+}} + \mathrm{H^{+}},\ \text{K=0.5} \qquad \text{Eq3.15}$$

$$\mathrm{Mn(OH)_2^{+}} \leftrightarrow (\alpha)\mathrm{MnOOH} + \mathrm{H^{+}},\ \text{K=0.467} \qquad \text{Eq3.18}$$

$$(\alpha)\mathrm{MnOOH} \leftrightarrow \mathrm{H^{+}} + (\gamma)\mathrm{MnO_2} + \mathrm{e^{-}},\ \mathrm{E^0} = 0.788\ \text{V vs SCE} \qquad \text{Eq3.39}$$

$$\mathrm{Mn^{3+}} + \mathrm{e^{-}} \leftrightarrow \mathrm{Mn^{2+}},\ \mathrm{E^0} = 1.26\ \text{V vs SCE} \qquad \text{Eq3.30}$$

Overall: $$2\mathrm{Mn^{3+}} + 2\mathrm{H_2O} \leftrightarrow \mathrm{Mn^{2+}} + (\gamma)\mathrm{MnO_2} + 4\mathrm{H^{+}} \qquad \text{Eq3.45}$$

The key reaction for the disproportion reaction is the sum of reaction Eq3.39 and Eq3.30 to give Eq3.46.

$$(\alpha)\mathrm{MnOOH} + \mathrm{Mn^{3+}} \leftrightarrow \mathrm{Mn^{2+}} + \mathrm{H^{+}} + (\gamma)\mathrm{MnO_2},\ \text{K=2.5E+7} \qquad \text{Eq3.46}$$

According to the reaction constants of $\mathrm{Mn^{3+}}$ hydrolysis to MnOOH species, $\mathrm{Mn^{3+}}$ is more likely to hydrolyze to $(\gamma)\mathrm{MnOOH}$. Therefore, Mn(III) disproportionation reaction in aqueous solution may more likely form $(\alpha)\mathrm{MnO_2}$.

3.5. Chemistry of Titanium in Sulfuric Acid Solution

3.5.1. Selected Thermodynamic Values of Ti System

Similar to the selected Mn thermodynamic data, the selected thermodynamic values of the Standard Gibbs free energy of formation of all possible Titanium species in sulfuric acid solution and the reported equilibrium constants of all possible reactions of Ti in sulfuric acid solution are shown in Tables 11 and 12. Those values were chosen based on the reproducibility from different sources and how closely they are from experimental data.

Table 11. Selected values of Standard Gibbs free energy of formation $\Delta G^0_{f,i}$ [KJ/mol], from Table 4 for Titanium species in sulfuric acid solution from different sources.

Species	Reported $\Delta G^0_{f,i}$[KJ/mole]	Estimated $\Delta G^0_{f,i}$[KJ/mole]	Selected $\Delta G^0_{f,i}$[KJ/mole]
TiO^{2+}	-577.4		-577.4
Ti^{4+}	-340		-340
$Ti(SO_4)^{+2}$	-1082.4		-1082.4
$Ti(OH)^{3+}$	-611		-611
$Ti(OH)_2^{2+}$	-866 .4		-866 .4
$Ti(OH)_3^{+}$	-1093.7		-1093.7
Ti^{3+}		-359.682, [53]	-359.682
$Ti(OH)^{2+}$		-590.161 [64]	-590.161
$Ti(OH)_2{}^{+}$		-818.813 [64]	-818.813
$Ti(SO_4)^{+}$		-1112.216 [[61], [62]]	-1112.216

Table 12. Selected equilibrium reaction constants for all possible Ti(III), and Ti(IV) species in an acidic aqueous solution.

No.	Reactions	Selected K
Eq3.47	$TiO^{2+} + H_2O \leftrightarrow Ti(OH)_2^{2+}$	1.2E+9 *
Eq3.48	$Ti(OH)_2^{2+} + H^+ \leftrightarrow Ti(OH)^{3+} + H_2O$	0.083
Eq3.49	$TiOH^{3+} + H^+ \leftrightarrow Ti^{4+} + H_2O$	0.49
Eq3.50	$Ti^{4+} + SO_4^{-2} \leftrightarrow Ti(SO_4)^{+2}$	0.4065*
Eq3.51	$Ti(OH)_2^{2+} + H_2O \leftrightarrow Ti(OH)_3^{+} + H^+$	1.95 E-2
Eq3.52	$Ti(OH)_3^{+} + H_2O \leftrightarrow Ti(OH)_4 + H^+$	8.5 E-4
Eq3.53	$Ti(OH)_2^{2+} + SO_4^{-2} \leftrightarrow [Ti(OH)_2SO_4]^0_{aq}$	3.4
Eq3.54	$Ti(OH)_2^{2+} + 2SO_4^{-2} \leftrightarrow [Ti(OH)_2(SO_4)_2]^{-2}_{aq}$	12.02
Eq3.55	$Ti^{3+} + H_2O \leftrightarrow Ti(OH)^{2+} + H^+$	0.072
Eq3.56	$Ti(OH)^{2+} + H_2O \leftrightarrow Ti(OH)_2{}^{+} + H^+$	0.0323
Eq3.57	$Ti^{3+} + SO_4^{-2} \leftrightarrow Ti(SO_4)^{+}$	24.3

* Calculated K based on the selected values of Gibbs free energy of formation

3.5.1.1. Titanium Speciation in 1-3 M Sulfuric Acid Solution

3.5.1.1.1. Ti(IV) Species in 1-3 M Sulfuric Acid solution

Assume we have 1M TiO^{2+}, 1M SO_4^{-2} in 1-3M H_2SO_4. All possible reactions that may occur for Ti(IV) in aqueous phase in 1-3M H_2SO_4 are shown below. H_2SO_4 was assumed to be fully dissociate into HSO_4^- and H_3O^+ based on Eq3.29 and TiO^{2+} was assumed to be fully converted to $Ti(OH)_2^{2+}$ according to Eq3.47. Equilibrium concentrations of Ti(IV) species are shown in Table 13.

$$HSO_4^- \leftrightarrow H^+ + SO_4^{2-} \qquad K=0.012 \qquad Eq3.30$$

$$Ti(OH)_2^{2+} + H^+ \leftrightarrow Ti(OH)^{3+} + H_2O \qquad K=0.083 \qquad Eq3.48$$

$$Ti(OH)^{3+} + H^+ \leftrightarrow Ti^{4+} + H_2O \qquad K=0.49 \qquad Eq3.49$$

$$Ti^{4+} + SO_4^{-2} \leftrightarrow Ti(SO_4)^{+2} \qquad K=0.4065 \qquad Eq3.50$$

$$Ti(OH)_2^{2+} + H_2O \leftrightarrow Ti(OH)_3^+ + H^+ \qquad K=1.95E\text{-}2 \qquad Eq3.51$$

$$Ti(OH)_2^{2+} + SO_4^{-2} \leftrightarrow [Ti(OH)_2SO_4]^0_{aq} \qquad K=3.4 \qquad Eq3.53$$

$$Ti(OH)_2^{2+} + 2SO_4^{-2} \leftrightarrow [Ti(OH)_2(SO_4)_2]^{-2}_{aq} \qquad K=12.02 \qquad Eq3.55$$

Table 13. Equilibrium concentrations of Ti(IV) species in 1-3M sulfuric acid solution

	[M] H_2SO_4 Concentration			
Species	**1**	**2**	**3**	**Trend**
$C_{HSO_4^-}$ [M]	1.68	2.85	3.90	Increase
C_{H^+}[M]	0.3	1.01	1.80	Increase
$C_{Ti(OH)_2^{+2}}$ [M]	7.60E-01	7.95E-01	7.24E-01	Peaked
$C_{SO_4^{-2}}$[M]	6.69E-02	3.38E-02	2.60E-02	Decreased
$C_{Ti(OH)^{+3}}$ [M]	1.90E-02	6.71E-02	1.09E-01	Increased
$C_{Ti^{4+}}$ [M]	2.81E-03	3.33E-02	9.58E-02	Increased
$C_{Ti(OH)_3^+}$[M]	4.92E-03	1.53E-03	7.84E-04	Decreased
$C_{TiSO_4^{2+}}$[M]	7.64E-05	4.58E-04	1.01E-03	Increased
$C_{(Ti(OH)_2(SO_4))^0}$ [M]	1.73E-01	9.13E-02	6.39E-02	Decreased
$C_{(Ti(OH)_2(SO_4)_2)^{-2}}$ [M]	4.10E-02	1.09E-02	5.87E-03	Decreased

From Table 13, the most dominant Ti(IV) species formed in sulfuric acid solution is $Ti(OH)_2^{+2}$ at acid concentration from 1M to 3M H_2SO_4. The concentrations of various species of Ti(IV) with increasing the sulfuric acid concentration are shown in Table 13.

3.5.1.1.2. Ti(IV) and Mn(II) Species in 1-3 M Sulfuric Acid solution

Based on all chemical reactions for Mn(II) and Ti(IV) that were discussed in **3.4.1.1.1** and **3.5.1.1.1**, the speciation of compounded Ti(IV) and Mn(II) can be studied in 1-3M H_2SO_4 by assuming that the same chemical reactions that were proposed in sections **3.4.1.1.1** and **3.5.1.1.1** are occurred.

If one dissolve 1M $TiOSO_4$ salt with 1M $MnSO_4$ salt in in 1-3 M H_2SO_4, the dissociation of 1M $TiOSO_4$ salt yields 1M TiO^{2+} and 1M SO_4^{-2} and the dissociation of 1M $MnSO_4$ salt yields 1M $MnSO_{4\,(Aq).}$ All possible reactions that may occur for Ti(IV) and Mn(II) species in aqueous phase in 1-3 H_2SO_4 are shown below. H_2SO_4 was assumed to be fully dissociate into HSO_4^- and H^+ based on Eq3.29, and TiO^{2+} was assumed to be fully converted to $Ti(OH)_2^{2+}$ according to Eq3.47. Equilibrium concentrations of Ti(IV) and Mn(II) species are shown in Table 14.

$HSO_4^- \leftrightarrow H^+ + SO_4^{2-}$	K=0.012	Eq3.30
$MnSO_{4_{Aq}} \leftrightarrow Mn^{2+} + SO_4^{-2}$,	$K = 0.00158$	Eq3.11
$Ti(OH)_2^{2+} + H^+ \leftrightarrow Ti(OH)^{3+} + H_2O$	K=0.083	Eq3.48
$Ti(OH)^{3+} + H^+ \leftrightarrow Ti^{4+} + H_2O$	K=0.49	Eq3.49
$Ti^{4+} + SO_4^{-2} \leftrightarrow Ti(SO_4)^{+2}$	K=0.4065	Eq3.50
$Ti(OH)_2^{2+} + H_2O \leftrightarrow Ti(OH)_3^+ + H^+$	K=1.95E-2	Eq3.51
$Ti(OH)_2^{2+} + SO_4^{-2} \leftrightarrow [Ti(OH)_2SO_4]^0_{aq}$	K=3.4	Eq3.53
$Ti(OH)_2^{2+} + 2SO_4^{-2} \leftrightarrow [Ti(OH)_2(SO_4)_2]^{-2}_{aq}$	K=12.02	Eq3.55

Table 14. Equilibrium concentrations of Ti(IV)/Mn(II) species in 1-3M sulfuric acid solution

	[M] H_2SO_4 Concentration			
Species	**1**	**2**	**3**	**Trend**
$C_{HSO_4^-}$ [M]	1.71	2.89	3.95	Increase
C_{H^+}[M]	0.308	0.995	1.77	Increase
$C_{Ti(OH)_2^{+2}}$ [M]	7.28E-01	7.84E-01	7.22E-01	Peaked
$C_{SO_4^{-2}}$[M]	6.67E-02	3.49E-02	2.68E-02	Decreased
$C_{Ti(OH)^{+3}}$ [M]	1.86E-02	6.47E-02	1.06E-01	Increased
$C_{Ti^{4+}}$ [M]	2.82E-03	3.15E-02	9.17E-02	Increased
$C_{Ti(OH)_3^+}$[M]	4.61E-02	1.54E-02	7.96E-03	Decreased
$C_{TiSO_4^{2+}}$[M]	7.63E-05	4.47E-04	9.99E-04	Increased
$C_{(Ti(OH)_2(SO_4))^0}$ [M]	1.65E-01	9.30E-02	6.58E-02	Decreased
$C_{(Ti(OH)_2(SO_4)_2)^{-2}}$ [M]	3.89E-02	1.15E-02	6.24E-03	Decreased
C_{MnSO_4} [M]	9.77E-01	9.57E-01	9.44E-01	Decreased
$C_{Mn^{2+}}$ [M]	2.31E-02	4.33E-02	5.56E-02	Increased

From Table 14, the most dominant Ti(IV) species formed in sulfuric acid solution is $Ti(OH)_2^{+2}$ at acid concentration from 1M to 3M H_2SO_4. The dissociation of $MnSO_{4(Aq)}$ into Mn^{2+} is less compared to the case when there is no Ti from Table 8. The concentrations of the species of Ti(IV) with increasing the sulfuric acid concentration are shown in Table 13.

3.5.1.1.3. Ti(III) Species in 1-3 M Sulfuric Acid solution

Ti(III) was reported to hydrolyze in low acidic solution to form $Ti(OH)^{+2}$ and $Ti(OH)_2$ based on Eq3.55 and Eq3.56; however, in 1-3M H_2SO_4, the dominant Ti(IV) species is in the form of $TiSO_4^+$ as shown in Eq3.57.

$$Ti^{3+} + SO_4^{-2} \leftrightarrow Ti(SO_4)^+ \qquad K=24.3 \qquad \text{Eq3.57}$$

3.5.2. Possible Electron Transfer Reactions of $TiOSO_4$ in Sulfuric Acid Solution

Based on the theoretical study of the Ti system in sulfuric acid solution in the previous sections, all possible reduction reactions of Ti species in a sulfuric acid solution that may possibly occur with their standard reduction potential against standard Saturated Calomel Electrode (SCE) are shown below.

- Reported standard reduction potential, E^0 in [V vs. SCE] of Ti(IV)/Ti(III) redox couple from literature: [53]

$$Ti(OH)_2^{2+} + 2H^+ + e^- \leftrightarrow Ti^{3+} + 2H_2O \qquad E^0 = -0.235 \text{ V vs SCE} \qquad \text{Eq.2.13}$$

$$Ti^{4+} + e^- \leftrightarrow Ti^{3+} \qquad E^0 = -0.04 \text{ V vs SCE} \qquad \text{Eq.2.14}$$

- Proposed additional redox reactions in sulfuric acid media that was estimated based on the Standard Gibbs free energy of formation from Table 5.

$$Ti(SO_4)^{+2} + e^- \leftrightarrow Ti(SO_4)^+ \qquad E^0 = 0.065 \text{ V vs SCE} \qquad \text{Eq3.58}$$

$$Ti(OH)^{3+} + e^- \leftrightarrow Ti(OH)^{2+} \qquad E^0 = -0.46 \text{ V vs SCE} \qquad \text{Eq3.59}$$

$$Ti(OH)_2{}^{2+} + e^- \leftrightarrow Ti(OH)_2{}^{+} \qquad E^0 = -0.735 \text{ V vs SCE} \qquad \text{Eq3.60}$$

3.6. Experimental Study for Ti-Mn System in Sulfuric Acid Solution

In this section, several experiments used to investigate the Ti-Mn electrolyte system in sulfuric acid solution media are discussed. The method of measuring the solubility of $MnSO_4$ salt in 1-3M sulfuric acid solution at different temperatures ranging from 20^oC to 45^oC was conducted by using the UV-vis spectroscopy characterization technique. For $TiOSO_4$ salt solubility in 1-3M sulfuric acid solution, there was no characteristic peak of Ti(IV) species that can be measured from the UV-vis spectrometer. This might be explained by that $TiOSO_4$ salt hydrolyzes into different hydrolyzed species and $TiOSO_4$ salt forms different types of complexes in the sulfuric acid solution. Therefore, the solubility of $TiOSO_4$ salt in 1-3M sulfuric acid solution at different temperatures ranging from 20^oC to 45^oC was suggested by using mass addition into the solvent until it was saturated with $TiOSO_4$. Then, the electrochemical behavior of Ti-Mn electrolyte system in sulfuric acid solution media was studied using the cyclic voltammetry and anodic voltage hold techniques. Cyclic voltammetry was employed to study the electrochemical behavior for $MnSO_4$ in 1-3M sulfuric acid solution, $TiOSO_4$ in 1-3M sulfuric acid solution, and $MnSO_4$+ $TiOSO_4$ in 1-3M sulfuric acid solution. The anodic voltage hold technique was used for $MnSO_4$+ $TiOSO_4$ in 3M sulfuric acid solution to study the anodic product formation by reduction scan. Detailed descriptions of the experimental procedure and the setup are shown in this section.

3.6.1. Method of Preparation the Solution of $MnSO_4$ or $TiOSO_4$

During all proposed experiments, the ultimate goal is to study the chemical and the electrochemical behavior of Ti/Mn system in a free oxygen condition. In addition, the electrochemical state of Ti/Mn system is not affected by the added acid. During the solution preparation, both oxygen and concentrated sulfuric acid can oxidize Mn(II) and Ti(IV) and that may alter the experimental results of the Ti/Mn system. Thus, caution should be considered when one prepares $MnSO_4$ or $TiOSO_4$ in sulfuric acid solution. A procedure of preparation Ti/Mn electrolyte in sulfuric acid solution was developed as shown below where the physical amount of 1M $MnSO_4$ in 3M H_2SO_4 is taken as an example.

1) Use two cleaned 250 ml volumetric flask.
2) For the first volumetric flask, fill it with DI water and deoxygenate the DI water using a N_2 gas for 20 min.
3) Fill half of the second volumetric flask with 127.6 ml DI water and use N_2 gas for 20 min to deoxygenate it.
4) Add 122.4 ml of 98% concentrated sulfuric acid solution using a volumetric pipette to prepare a 9M sulfuric acid solution in the second volumetric flask and then deoxygenate the whole solution using N_2 gas for 20 min.
5) Stir the 9M sulfuric acid solution until it cools down to the room temperature while keeping the N_2 gas to deoxygenate the solution.
6) Use wax paper to seal the two volumetric flasks.
7) Use a cleaned 10 ml volumetric flask and fill it with 5ml deoxygenated DI water.
8) For 1M $MnSO_4$ solution, take 1.609g from the stock salt bottle of $MnSO_4.H_2O$ and add it to the 10 ml volumetric flask.

9) Add a magnetic bar to stir the solution and N_2 gas for 10 min to 15min to remove oxygen while stirring.
10) While the solution is stirred and deoxygenated, use a clean volumetric pipette and withdraw 3.33 ml from the 9M deoxygenated sulfuric acid flask and add to the 10 ml volumetric flask that contains the salt to make a 3M sulfuric acid solution.
11) Stir the 10ml volumetric flask until it cools down to the room temperature while keeping the N_2 gas to deoxygenate the solution and then make up the remaining volume by the deoxygenated DI water up to the calibration line on the volumetric flask to have exactly 10ml solution.

The salt that was used to prepare Mn electrolyte and Ti electrolyte solution was purchased from Sigma Aldrich. Table 15 shows the specification of the used Ti and Mn salts in experiments.

Table 15. Stock materials used in experiments

Materials name	Molecular weight [g/mol]
Manganese(II) sulfate monohydrate	169.02
Titanium(IV) oxysulfate monohydrate	177.93

3.6.2. Measuring the Solubility of $MnSO_4$ at Different Temperatures in 1-3 M Sulfuric Acid Solution by UV-Vis Spectroscopy

3.6.2.1. UV-Vis Spectroscopy Technique Overview

UV-Vis spectroscopic method directs a light beam through the solution containing the soluble species of interest. [70] Then, some of the light beam is absorbed by the electrons in the species. When an electron absorbs a visible and ultraviolet photon, it changes its energy level. [70] The absorbance spectra are like fingerprints. [70] Each compound has its own unique spectrum. In some cases, the spectrum can be used to identify the presence of certain compounds in a sample.

[70] More often, it is used to determine the amount of a compound present. [70] The wavelength of UV-vis spectroscopic range from 100nm to 700nm. [70]

The UV-Vis spectrometer used in this study is GENESYS™ 10S UV-Vis Spectrophotometer as shown in Figure 30 [71]

Figure 30. GENESYS™ 10S UV-Vis Spectrophotometer [71]

The mechanism of a typical spectrophotometer in measuring the light absorbed by the sample solution is shown in Figure 31. [72] A typical spectrophotometer consists of a light source, a collimator, a monochromator, a wavelength selector, a cuvette for sample solution, a photoelectric detector, and a digital display. [72] The measurement of light absorbed starts with supplying the desired wavelength of light from a light source. [72] Then, the collimator directs a beam of light to a monochromator to be spitted into different wavelengths. The wavelength selector allows only the desired spectrum to pass it. [72] Then, the desired range of spectrum of light passes through

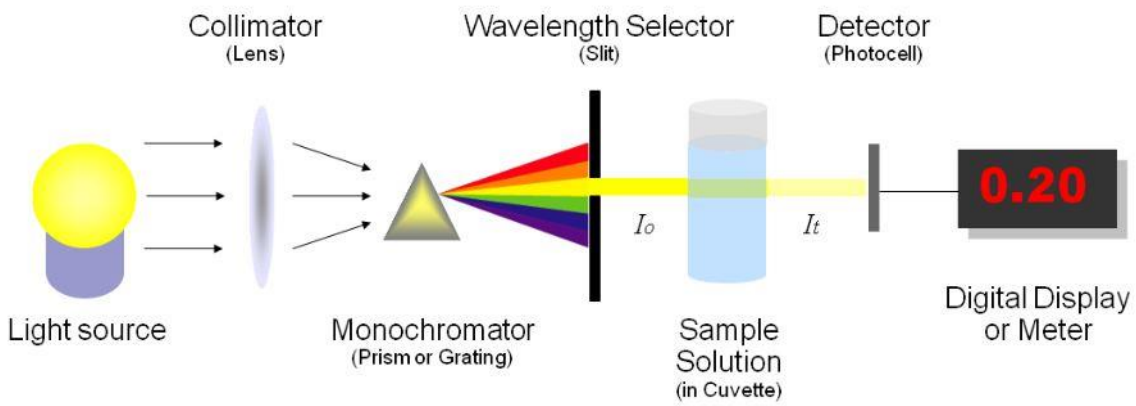

Figure 31. Basic structure of spectrophotometer [72]

the sample solution in the cuvette. [72] The photometer measures the adsorbed light by the sample solution and then sends a signal to the digital display. [72]

3.6.2.2. Beer-Lambert Law

Beer-Lambert law states that the amount of energy absorbed by passing a light beam through a homogeneous solution is directly proportional to the concentration of absorbing solute and the path length of light. [48]

The mathematical expression of Beer-Lombard law is shown in Eq3.61. [48]

$$A = \varepsilon \, l \, C \qquad \text{Eq3.61}$$

Where ε is the absorption coefficient of the solute in solution media [dm^2/mole], l is the optical path length in [dm], and C is the concentration of the solute [mole/L] in the solution.

The UV-Vis spectroscopy technique allows one to measure the concentration of an unknown solute sample concentration based on the light absorbed by the sample if one has a calibration curve between the light absorbed in different solute concentrations.

3.6.2.3. $MnSO_4$-H_2SO_4 Calibration Curve

Seven sample solutions of known concentration of $MnSO_4$ in either solvent DI water or 3M H_2SO_4 were used as shown in Table 16 as standard solutions for the calibration curve of $MnSO_4$. The ranges of H_2SO_4 and $MnSO_4$ concentrations measured in this study are reported below in Table 16.

Table 16. $MnSO_4$ solution used for UV-Vis spectroscopy calibration

	M $MnSO_4$						
Solvent	0.75 M	0.9 M	1 M	1.1 M	1.25 M	1.35 M	1.5 M
M H_2SO_4	0 M	0 M	0 M	0 M	0 M	0 M	0 M
M H_2SO_4	3 M	3 M	3 M	3 M	3 M	3 M	3 M

Several concerns, such as the solvent, the cuvette, and the temperature during the UV-vis measurements, need to be studied to get a reliable calibration measurement. First, Mn(II) solution absorbance was measured for 1M $MnSO_4$ in 3M H_2SO_4,1.25M MnSO4 in 3M H_2SO_4, and 1.5M $MnSO_4$ in 3M H_2SO_4 to search for the characteristic wavelength of Mn(II). The UV-Vis spectroscopy was scanned using a light wavelength ranging from 300 nm to 450 nm at 23^oC with DI water blank sample. The resulted spectra for all three Mn(II) concentrations are shown in Figure 32. The spectra of all three $MnSO_4$ concentrations show that at 401.1nm wavelength the resulted absorbance is directly proportional to the $MnSO_4$ concentration in the solution. Thus, the 401.1nm wavelength was assumed as the characteristic wavelength of Mn(II) species in the form of Mn^{2+} free cation in the sulfuric acid solution.

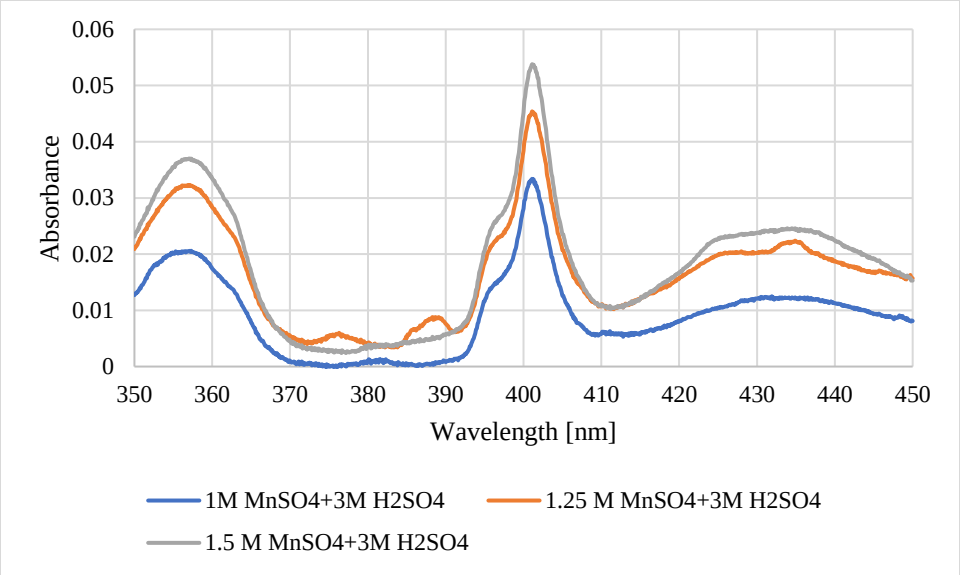

Figure 32. UV-vis spectrum of 1M, 1.25M, and 1.5M $MnSO_4$ in 3M H_2SO_4

Second, the absorbance of all solutions in Table 16 were measured at 401.1nm wavelength as shown in Tables 17 and 18. All measurements were repeated three times and the average value was calculated with the standard deviation of the measured values. From Table 17, the relative error of absorbance of $MnSO_4$ in DI water standard solution was calculated relative to the absorbance of the same $MnSO_4$ concentration when 3M H_2SO_4 was the solvent. The relative error of absorbance of $MnSO_4$ shows that at 401.1nm wavelength the light absorption is independent of the used solvent. Therefore, $MnSO_4$ standard solutions in DI water solvent were selected to be used to make the UV-Vis calibration curve of $MnSO_4$.

Table 17. UV-Vis absorbance at 401.1 nm wavelength of $MnSO_4$ in 3M H_2SO_4 standard solutions at 23 ^oC

Solution	(1) Intensity	(2) Intensity	(3) Intensity	(Avg.) Intensity	SD
0.75M MnSO4+3MH2SO4	0.026	0.027	0.026	0.026	0.001
0.9M MnSO4+3MH2SO4	0.034	0.033	0.033	0.033	0.001
1M MnSO4+3MH2SO4	0.036	0.036	0.035	0.036	0.001
1.1M MnSO4+3MH2SO4	0.037	0.040	0.041	0.039	0.002
1.25M MnSO4+3MH2SO4	0.045	0.046	0.048	0.046	0.002
1.35M MnSO4+3MH2SO4	0.049	0.049	0.049	0.049	0.000
1.5M MnSO4+3MH2SO4	0.054	0.054	0.055	0.054	0.001

Table 18. UV-Vis absorbance at 401.1 nm wavelength of $MnSO_4$ in DI water standard solutions at 23 ^oC

Solution	(1) Intensity	(2) Intensity	(3) Intensity	(Avg.) Intensity	%Relative error	SD
0.75M MnSO4+DIW	0.027	0.027	0.027	0.027	1.25	0.0E+00
0.9M MnSO4+DIW	0.032	0.032	0.032	0.032	-2.04	0.0E+00
1M MnSO4+DIW	0.034	0.033	0.039	0.035	-0.47	3.2E-03
1.1M MnSO4+DIW	0.037	0.037	0.044	0.039	0.00	4.0E-03
1.25M MnSO4+DIW	0.045	0.045	0.045	0.045	-1.46	8.5E-18
1.35M MnSO4+DIW	0.049	0.049	0.049	0.049	0.00	8.5E-18
1.5M MnSO4+DIW	0.052	0.056	0.055	0.054	0.00	2.1E-03

During the UV-Vis spectroscopy measurements, the cuvette condition was found to affect the measured spectrum. It was observed that using the same cuvette for different solution multiple times gave different absorbance readings. Thus, it was suggested to use a new cuvette for each solution to get an accurate absorbance measurement.

Regarding the temperature effect on UV-Vis spectroscopy measurements, two measurements of 0.9 M $MnSO_4$ standard solution absorbance at 401.1 nm wavelength were conducted at 23 ^oC and 35 ^oC. The measured absorbance of the standard solution at 23 ^oC was 7.7% higher than the one that was measured at 35 ^oC, so the temperature had an effect on the measurement. The resulted absorbance of 0.9 M $MnSO_4$ standard solution at 401.1 nm wavelength at 23 ^oC and 35 ^oC are shown in Table 19. Therefore, all the measured values of Mn(II) absorbance in UV-vis spectroscopy device are conducted at 23 ^oC.

Table 19. UV-Vis absorbance at 401.1 nm wavelength of 0.9 M $MnSO_4$ in DI water standard solutions at 23^oC and 35^oC

Solution	Measured absorbance
0.9M MnSO4+DIW at 23 ^oC	0.032
0.9M MnSO4+DIW at 35 oC	0.03

The generated calibration of $MnSO_4$ standard solution is shown in Figure 33. The data points of the calibration curve were fitted in a linear equation form with a zero intercept in order to get

the Beer-Lombard mathematical relation form of the calibrated data points of $MnSO_4$ standard solutions as shown in Eq3.62.

$$A = 0.036\ C_{Mn^{2+}} \qquad \text{Eq3.62}$$

The slope in Eq3.62 represents the cuvette optical pathway l which is 0.1dm multiplied by the solute absorptivity ε which is 0.36 dm^2/mole. Thus, the calibration curve of Mn^{2+} solute shows that the solute concentration of Mn^{2+} is directly proportional to the measured absorbance.

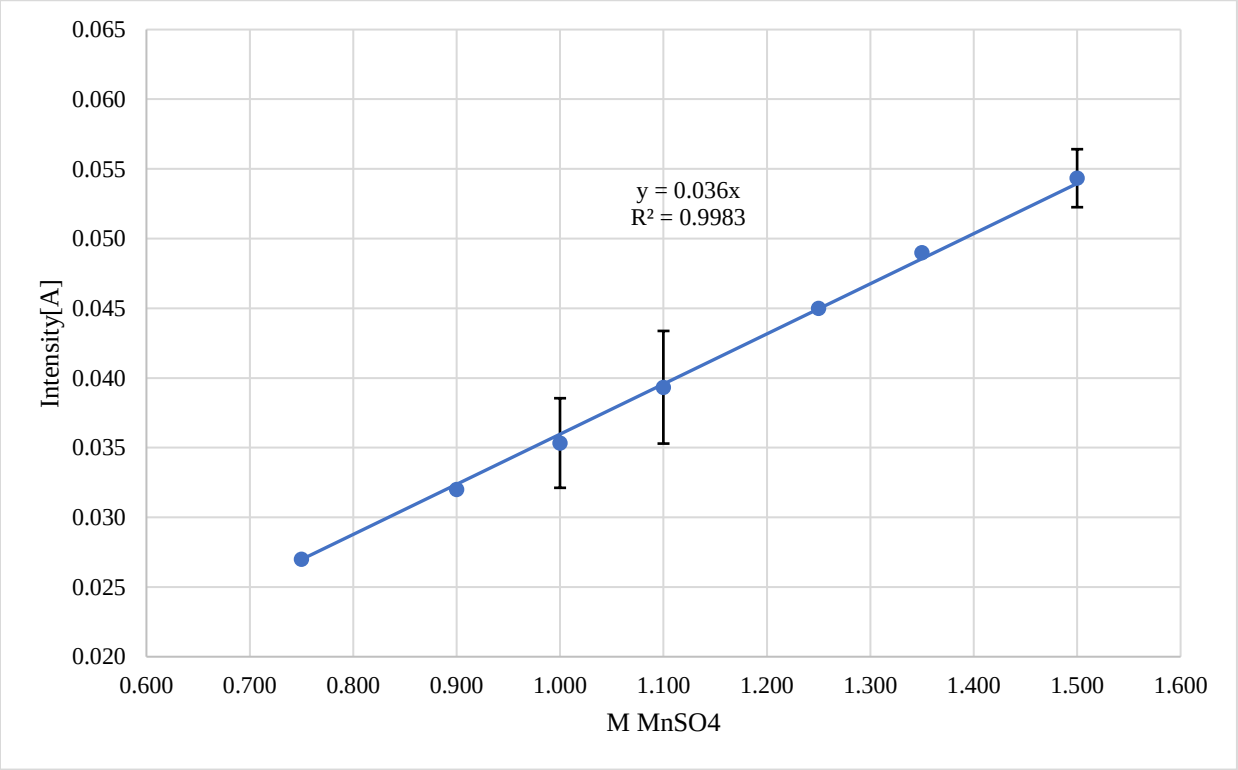

Figure 33. UV-Vis spectroscopy calibration curve of $MnSO_4$ standard solutions at 23 ^oC

3.6.2.4. Experimental Procedure for Measuring Solubility of $MnSO_4$ in 1-3 M Sulfuric Acid Solution at Different Temperatures

The goal of this experiment is to find the solubility of $MnSO_4$ in different sulfuric acid concentrations at different temperatures. In doing that, the solubility of $MnSO_4$ salt is measured in 1M, 2M, and 3M sulfuric acid solution at 20°C, 25°C, 30°C, 40°C, and 45°C. A controlled temperature water bath is used to maintain a constant temperature. The schematic of the controlled temperature water bath is shown in Figure 34.

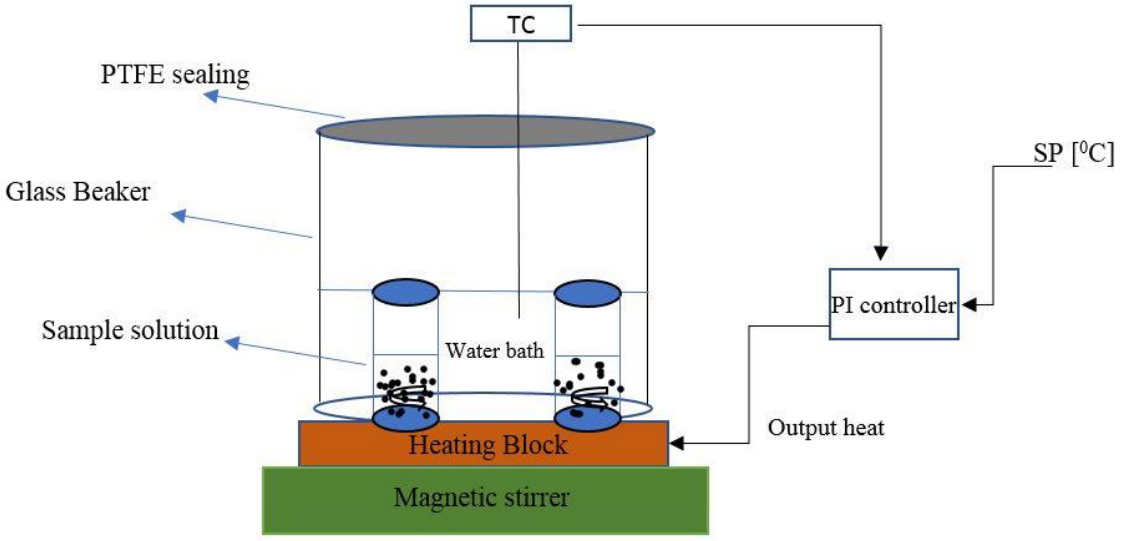

Figure 34. Schematic of a controlled temperature water bath with magnetic stirring

In Figure 34, the sample supersaturated solution of $MnSO_4$ is placed in a 10 ml volumetric flask sealed with a double wax paper. PI temperature controller is installed as shown in Figure 30 to control the water temperature in the glass beaker by heating the metal heating block that is placed under the glass beaker. The water bath temperature is measured by a thermocouple that is immersed in the water bath. The thermocouple would send a signal to the PI controller to adjust the water bath temperature to be equivalent to the set point (SP) temperature. A magnetic stirring device is placed under the heating block to stir the magnetic bar inside the sample solution flask.

The glass beaker is sealed at the top by a wax sealing paper to avoid water evaporation. The procedure of measuring the solubility of $MnSO_4$ in different sulfuric acid solution at a given temperature is shown below:

1. Prepare a standard solution of $MnSO_4$ that is fully dissolved in the given standard solution in a 10 ml volumetric flask at lab temperature.
2. After the $MnSO_4$ standard solution is fully dissolved at lab temperature, immerse the volumetric flask into the controlled temperature water bath with stirring.
3. Leave the solution for one day to reach to the equilibrium state.
4. After one day, if the solution still homogenous, take the sample solution out the water bath and add more of $MnSO_4$ salt into the flask and put it back again in the water bath and leave it for another day.
5. Repeat step 4 until you get a saturated $MnSO_4$ solution in a given sulfuric acid solvent.

After getting a saturated $MnSO_4$ solution at a given sulfuric acid concentration, the procedure in measuring the concentration in the UV-Vis spectroscopy device is shown below:

1. Take a new cuvette and wash it with DI water three times.
2. Dry the cuvette by using N_2 gas.
3. Take a clean 1mm pipette and wash it with the sample solution by withdrawing the sample solution into the pipette and let it move inside the pipette to avoid any dilution of the sample solution and dispose it out into a separate beaker.
4. Next, withdraw the sample solution into the pipette slowly and pour it into a cuvette by gravity.
5. Then, use a new 1mm pipette to withdraw DI water and discharge the DI water into the cuvette that contains the sample solution.

6. Repeat step 5 one more time, so the sample solution is diluted it by three times its original concentration.
7. Close the cuvette and shake it gently for 30 min.
8. Take a new cleaned cuvette and fill it with DI as a blank sample to be used in the UV-Vis device.
9. Before putting the cuvette in the UV-Vis device, measure the temperature of the solution by inserting a clean thermostat inside the cuvette to make sure the UV-Vis measurement is done at 23 ^{o}C.
10. Insert the cuvette inside the UV-Vis device and do UV-Vis scanning of the sample solution at 401.1 nm three times.
11. After measuring the absorbance at 401.1 nm wavelength, use the calibration curve to determine the concentration of Mn^{2+} in the sample solution.

The raw data of $MnSO_4$ solubility are shown in Appendix B.

3.6.3. Measuring the Solubility of $TiOSO_4$ by Mass Addition at Different Temperatures in 1-3M Sulfuric Acid Solution

The goal of this experiment is to find the solubility of $TiOSO_4$ in different sulfuric acid concentrations at different temperatures. In doing that, the solubility of $TiOSO_4$ salt is measured in 1M, 2M, and 3M sulfuric acid solution at 20 ^{o}C, 25^{o}C, 30 ^{o}C, 40 ^{o}C, and 45^{o}C. A controlled temperature water bath is used to maintain a constant temperature. The schematic of the controlled temperature water bath is shown in Figure 30. $TiOSO_4$ salt is added manually to the sample solution with a known amount until the sample solution is saturated with the salt. This method was used in the study for $TiOSO_4$ because no suitable UV-vis wavelength was found.

3.6.3.1. Experimental Setup and Procedure

The procedure of measuring the solubility of $TiOSO_4$ in different sulfuric acid solution at a given temperature is shown below:

1. Prepare a standard solution of $TiOSO_4$ that is fully dissolved in the given standard solution in a 10 ml volumetric flask at lab temperature.
2. After the $TiOSO_4$ standard solution is fully dissolved at lab temperature, immerse the volumetric flask into a controlled temperature water bath with stirring.
3. Leave the solution for one day to reach to the equilibrium state.
4. After one day, if the solution still homogenous, take the sample solution out the water bath and add 0.1 M of $TiOSO_4$ salt into the flask and put it back again in the water bath and leave it for another day.
5. Record the added amount of $TiOSO_4$ salt in the solution.
6. Repeat step 4 and 5 until you get a saturated $TiOSO_4$ solution in a given sulfuric acid solvent.
7. Repeat all the steps at a different water bath temperature.

The raw data of $TiOSO_4$ solubility are shown in Appendix B.

3.7. Cyclic Voltammetry Experiment for $MnSO_4$ and $TiOSO_4$ in Sulfuric Acid Solution

In this section, the cyclic voltammetry and the anodic voltage hold test setup and procedure are explained in detail. The cyclic voltammetry technique is employed to study the electrochemical behavior of $MnSO_4$ and $TiOSO_4$ in different sulfuric acid concentration solution concentrations. The electrochemical behavior of $MnSO_4$ and $TiOSO_4$ electrolyte are studied individually and when they are mixed in the same solution using the cyclic voltammetry technique. The anodic voltage hold test is used to analyze the anodic products of $MnSO_4$ electrolyte with and without the addition of $TiOSO_4$ by reducing the anodic products in different solutions. The cyclic voltammetry and anodic voltage hold tests are conducted using Interface 5000E™ potentiostat that is made by GAMRY Instruments as shown in Figure 35.

Figure 35. Interface 5000E™ potentiostat GAMRY INSTRUMENTS

3.7.1. Electrochemical Cell Setup

A three-electrode electrochemical cell is used for the cyclic voltammetry and anodic voltage hold tests. The electrochemical cell consists of a working electrode (WE), a Saturated Calomel Reference electrode (SCE), and a counter electrode (CE). The WE and the RE are placed in the tested electrolyte solution in which the WE is placed close to the RE to minimize the solution resistance. The CE is placed in a separate compartment that contains the solvent solution only and the two compartments are separated by a proton-exchange membrane separator made of NAFION 117 material. A schematic of the three-electrode electrochemical cell setup is shown in Figure 36.

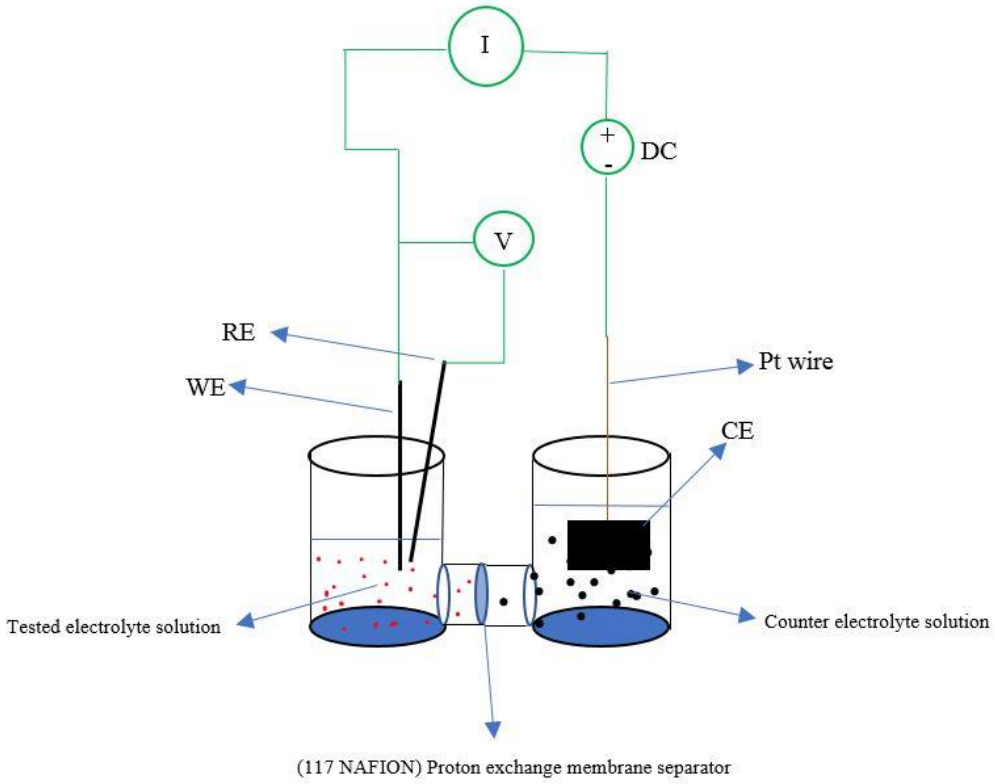

Figure 36. Schematic diagram of the three-electrode electrochemical cell setup

The setup of the electrochemical cell when the WE, CE, and RE are connected to a potentiostat is represented in Figure 33. The current flow through the WE is measured with an I/E converter and the potential difference between the WE and the RE is measured by an electrometer. To control the applied potential on the electrochemical cell, the potentiostat passes the needed current through the control amplifier between the WE and the CE until the measured potential between the WE and the RE matches the set potential by the user. If the applied potential is higher than the equilibrium potential of the tested electrolyte solution relative to the RE potential, an anodic current is generated on the WE due to an oxidation reaction on the WE. In contrast, if the applied potential is lower than the equilibrium potential of the tested electrolyte solution relative to the RE potential, a cathodic current is generated on the WE due to a reduction reaction on the WE.

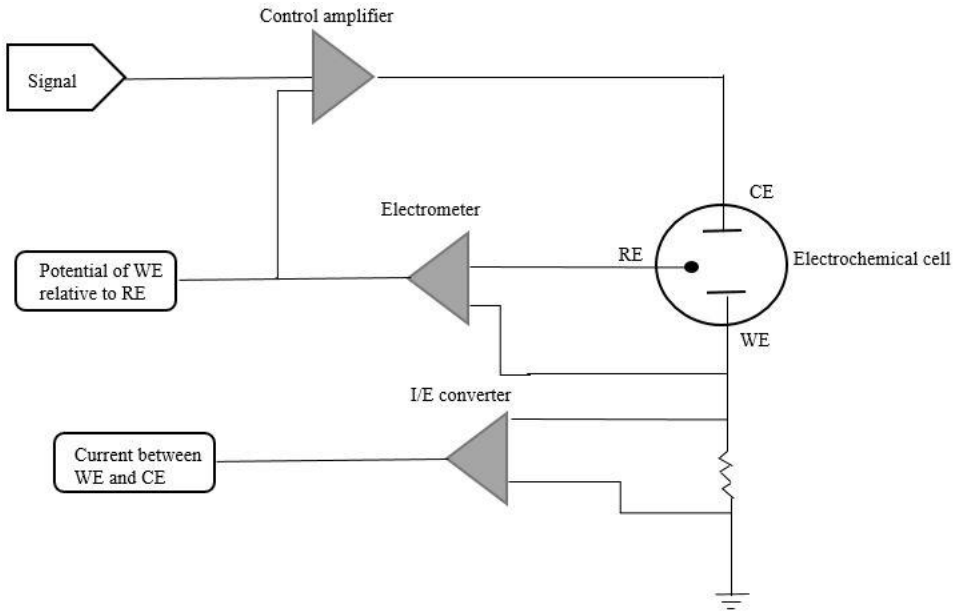

Figure 37. Setup and operation of a potentiostat connect to a three-electrode electrochemical cell

3.7.2. Experimental Details

Two working electrode materials were used to conduct the cyclic voltammetry scan of $TiOSO_4$ in H_2SO_4 solution and $MnSO_4$ in H_2SO_4 solution with and without the addition of $TiOSO_4$. A graphite rod working electrode is used in the first cell and a carbon felt working electrode is used in the second cell. The counter electrode material is 3cm x 3cm carbon felt that is attached to Pt wire to increase the counter electrode electrical conductivity and to ensure that the overall electrochemical behavior of the electrochemical cell is not limited by the counter electrode. The same solution free of tested electroactive species ($MnSO_4$ or $TiOSO_4$) is used in the counter electrode compartment. The expected redox reactions on the counter electrode are oxygen evolution reaction at high applied potential above 1.2 V vs. SHE, hydrogen evolution reaction at a potential lower than 0 V vs. SHE, and carbon oxidation reaction. The specifications of electrochemical cell that is used in cyclic voltammetry are shown below:

- **Cell (1) specifications**

Working Electrode: ~0.8cm^2 graphite rod

Reference Electrode: Saturated Calomel Electrode

Counter Electrode: 9cm^2 carbon felt

Ion exchange separator: NAFION 117 membrane

Working electrode compartment solution volume: 10ml

Counter electrode compartment solution volume: 20ml

Temperature: Lab temperature ~ 23 ^oC

- **Cell (2) specifications**

Working Electrode: ~1cm^2 carbon felt

Reference Electrode: Saturated Calomel Electrode

Counter Electrode: 9cm^2 carbon felt

Ion exchange separator: NAFION 117 membrane

Working electrode compartment solution volume: 10ml

Counter electrode compartment solution volume: 20ml

Temperature: Lab temperature ~ 23 ^oC

The electrolyte solutions that were studied using the cyclic voltammetry are shown in Tables 20 and 21.

- **$MnSO_4$ tested electrolyte**

Table 20. $MnSO_4$ electrolyte solutions used in cyclic voltammetry

Solution no.	1	2	3	4	5	6
M $MnSO_4$	1	1	1	1	1	1
M H_2SO_4	1	2	3	1	2	3
M $TiOSO_4$	0	0	0	1	1	1

- **$TiOSO_4$ tested electrolyte**

Table 21. $TiOSO_4$ electrolyte solutions used in cyclic voltammetry

Solution no.	7	8	9	10	11	12
M $MnSO_4$	0	0	0	1	1	1
M H_2SO_4	1	2	3	1	2	3
M $TiOSO_4$	1	1	1	1	1	1

Before the cyclic voltammetry scan, the open circuit potential (OCP) is measured for 10min for each solution to study the effect of increasing the acid concentration in the electrolyte solution on the electro-active species stability. The open circuit potential (OCP) is the potential measured between the reference electrode (RE) and the working electrode WE. [68, 73] The OCP measurement is a passive experiment where the counter electrode circuitry of the potentiostat is bypassed, so the measured potential is only between the reference electrode and the working electrode. [73] Although a true equilibrium of the electrochemical system is not obtained during the OCP measurement because the measured OCP is measured with one ion type such as Mn^{2+} ion and without Mn^{3+} counter ion. However, negligible impurities of the Mn^{3+} counter ion may coexist with Mn^{2+} salt. Thus, the system may not be considered electrochemically at equilibrium and the measured OCP value may attributed to the electrometer internal circuit and the electrolyte solution ability to conduct current. A small change of the OCP over a long period of time (±5 mV/min or less) reveals that the chemical system is stable enough chemically. [68, 73] This experiment was conducted using Cell 1. The OCV results are shown in Appendix C.

All the electrolyte solutions that are shown in Tables 20 and 21 are prepared by following the procedure in section **3.6.1**. In addition to the OCP measurements, the potential loss due to the solution resistance is measured using the Electrochemical Impedance Spectroscopy (EIS) for all electrolyte solutions in Tables 20 and 21.

3.7.3. Test Setting Selections

- **Electrochemical Impedance Spectroscopy Setting**

The voltage loss due to the electrolyte resistance of each $MnSO_4$ and $TiOSO_4$ electrolyte solution is measured by using the EIS spectroscopy tools in the potentiostat. The resistance

measurements are done in the frequency ranging from 500 Hz to 20,000 Hz. This experiment was conducted using Cell 1. The IR results are shown in Appendix C.

- **Cyclic voltammetry scan Settings**

1) Cyclic voltammetry for the solvent
   - The cyclic voltammetry sets and settings for solvent electrolyte solutions (1M, 2M, and 3M H_2SO_4) in $MnSO_4$ voltage window are shown below:

     Voltage Scan window: -0.244 V to1.506 V vs. SCE

     Scan rate: 2 mV/s

     Number of cycles: 3
   - The cyclic voltammetry sets and settings for solvent electrolyte solutions (1M, 2M, and 3M H_2SO_4) in $TiOSO_4$ voltage window are shown below:

     Voltage Scan window: 0.358 V to -0.442 V vs. SCE

     Scan rate: 2 mV/s

     Number of cycles: 3
2) Cyclic voltammetry for $MnSO_4$ electrolyte solution without the addition of $TiOSO_4$
   - The cyclic voltammetry sets and settings for $MnSO_4$ electrolyte solution ranging from solution 1 to solution 3 in Table 20 are shown below:

     Voltage Scan window: -0.244 V to1.506 V vs. SCE

     Scan rate: 2 mV/s

     Number of cycles: 3

- For solution number 3, different end applied potential during anodic scan is selected to study the effect of end potential on the reduction scan of Mn electrolyte.

  Voltage Scan window: -0.244 V to (1.2, 1.25, 1.3, 1.35, 1.4, and 1.6) V vs. SCE

  Scan rate: 2 mV/s

  Number of cycles: 3

3) Cyclic voltammetry for $MnSO_4$ electrolyte solution with the addition of $TiOSO_4$

- The cyclic voltammetry sets and settings for $MnSO_4$ electrolyte solution ranging from solution 4 to solution 6 in Table 20 are shown below:

  Voltage Scan window: 0.2 V vs. SCE to1.506 V vs. SCE

  Scan rate: 2 mV/s

  Number of cycles: 3

4) Cyclic voltammetry for $TiOSO_4$ electrolyte solution without the addition of $MnSO_4$

- The cyclic voltammetry sets and settings for $TiOSO_4$ electrolyte solution ranging from solution 7 to solution 9 in Table 21 are shown below:

  Voltage Scan window: 0.358 V vs. SCE to -0.442 V vs. SCE

  Scan rate: 2 mV/s

  Number of cycles: 3

- The voltage scan rate is varied for solution 9 to study the effect of associated chemical reactions of Ti electrolytes during the cyclic voltammetry.

  Voltage Scan window: 0.358 V vs. SCE to -0.442 V vs. SCE

  Scan rate: 10 mV/s, 20 mV/s, and 50 mV/s

  Number of cycles: 3

5) Cyclic voltammetry for $TiOSO_4$ electrolyte solution with the addition of $MnSO_4$

- The cyclic voltammetry sets and settings for $TiOSO_4$ electrolyte solution ranging from solution 10 to solution 12 in Table 21 are shown below:

  Voltage Scan window: 0.358 V vs. SCE to -0.442 V vs. SCE

  Scan rate: 2 mV/s

  Number of cycles: 3

- The voltage scan rate is varied for solution 12 to study the effect of associated chemical reactions of Ti electrolytes during the cyclic voltammetry.

  Voltage Scan window: 0.358 V vs. SCE to -0.442 V vs. SCE

  Scan rate: 10 mV/s, 20 mV/s, and 50 mV/s

  Number of cycles: 3

The third cycle is selected for the analysis; while, the first and second cyclic voltammetry scans are shown in Appendix C.

3.8. Anodic Voltage Hold Experiment Setup for $MnSO_4$ in Sulfuric Acid Solution

3.8.1. Qualitative Experimental Details

The anodic voltage hold experiment is used to study the anodic products formation during the anodic voltage hold by studying the voltage-current responses during the cathodic scan in a new electrolyte solution. This experiment was proposed mainly to study whether MnO_2 solid would be formed on the working electrode when $MnSO_4$ in 3M H_2SO_4 with and without $TiOSO_4$ addition is held at an anodic voltage. First, an anodic voltage hold at 1.5V vs. SCE for 15 min is conducted for 1M $MnSO_4$+3M H_2SO_4 and for 1M $MnSO_4$+1M $TiOSO_4$+3M H_2SO_4 on a graphite rod working electrode to study whether the anodic products are formed on the working electrode or in the electrolyte solution. To do this, the working electrode that is used for the anodic voltage hold is removed from the electrolyte after the anodic voltage hold. The working electrode is washed with a 10 ml of 3M H_2SO_4 and is held for 15 min to be completely dried. Then, a new electrolyte solution of 3M H_2SO_4 is used with the washed and dried electrode for the cathodic linear voltage scan down to -0.242V vs. SCE for the anodic products on the working electrode resulted from Mn electrolyte and down to 0.2V vs. SCE for the anodic products on the working electrode resulted from Mn+Ti electrolyte after holding the OCV for 10 min.

If the ratio of the cathodic charges to the anodic charges is greater than half, then the anodic products from Mn electrolyte oxidation reactions during the anodic voltage hold experiment are assumed to be mostly generated as a solid deposited on the working electrode. Otherwise, it can be used that the anodic charge went to create soluble products.

To confirm the findings of the previous experiment, the solution is stirred after the anodic voltage hold experiment for 2 min. Then, the working electrode is replaced by a new working electrode to measure the OCV of the electro-active species in the solution. From the measured

OCV, one may use Nernst equation relation, Eq.3.5, for Mn^{3+}/Mn^{2+} redox couple to estimate the concentrations of the aqueous Mn^{3+} species generated from the anodic voltage hold experiment in the electrolyte solution. From the estimated Mn^{3+} concentration, the anodic charges generated during the anodic voltage hold from the Mn^{3+} ions in the solution can be estimated by using Faraday's law as shown in Eq.3.63:

$$Q_{anodic} = C_i \, V \, n \, F \qquad \text{Eq. 3.63}$$

Where,

Q_{anodic}: Amount of charges delivered during the oxidation reaction. [C]

C_i: The concentration of species i in the solution. [mol/L]

V: Solution volume. [L]

n: Number of electrons delivered during the oxidation reaction. [mole e^-/mole of i]

F: Faraday constant, 96485. [C/mole e^-]

If the anodic products are found to be formed on the working electrode as a deposited solid, the formed anodic solid materials are investigated in different solution conditions, in different working electrodes types, and in different mass transport conditions.

3.8.2. Anodic Voltage Hold Experiment Details

3.8.2.1. Study the Effect of Mn^{2+} on the Anodic Products Resulted from 1M $MnSO_4$-3M H_2SO_4 Anodic Voltage at 1.5 V vs. SCE During the Cathodic Scan

Two anodic voltage holds at 1.5 V vs. SCE for 15min for 1M $MnSO_4$+3M H_2SO_4 were conducted on a graphite rod working electrode. A pre-step anodic voltage hold at 0.6V was

conducted for 5min, where there is no faradaic process, followed by applying a 1.5V step voltage for 15min. After the anodic voltage hold experiment, the working electrode was rinsed with a 3M H_2SO_4 solution for 3min and then was dried for 15 min. Then, a cathodic linear voltage sweep scan at 2mV/s was conducted after measuring the OCV for 10 min from the OCV down to -0.242V vs. SCE in:

1- 1M $MnSO_4$+3M H_2SO_4 electrolyte solution

2- 3M H_2SO_4 electrolyte solution

The observation of this experiment is expected to show the effect of Mn^{2+} species on the anodic products.

3.8.2.2. Study the Effect of H^+ on the Anodic Products Resulted from 1M $MnSO_4$-3M H_2SO_4 Anodic Voltage Hold at 1.5 V vs. SCE with a Different Holding OCV Time Prior the Cathodic Scan

In this experiment, the anodic voltage hold is repeated three times with the same amount of anodic charge for 1M $MnSO_4$+3M H_2SO_4 solution on a graphite rod working electrode, and the working electrode is washed using a 3M H_2SO_4 solution and is dried after the anodic voltage hold experiment. The dried electrode is then placed in a new solution for the cathodic scan study. The time of holding the working electrode OCV in 3M H_2SO_4 is varied, in which the OCV is held for 5 sec, 10 min, and 2hrs, before the cathodic linear voltage sweep in 3M H_2SO_4 solution from OCV down to -0.242V vs. SCE. The observation of this experiment is expected to show the effect of H^+ species interaction with the anodic products.

3.8.2.3. Study the Effect of $TiOSO_4$ on the Anodic Products Resulted from 1M $MnSO_4$-3M H_2SO_4 Anodic Voltage Hold at 1.5 V vs. SCE

Two anodic voltage holds at 1.5 V vs. SCE for 15min for 1M $MnSO_4$+3M H_2SO_4 are conducted on a graphite rod working electrode. A pre-step anodic voltage hold at 0.6V, where there is no any faradic process, followed by a applying a 1.5V step voltage for 15min. After the anodic voltage hold experiment, the working electrode is rinsed with a 3M H_2SO_4 solution for 3min and then is dried for 15 min. Then, it is studied in a new solution and a cathodic linear voltage sweep scan at 2mV/s is conducted after measuring the OCV for 10 min from the OCV down to 0.2 V vs. SCE in:

1- 1M $MnSO_4$+1M $TiOSO_4$+ 3M H_2SO_4 electrolyte solution

2- 1M $TiOSO_4$+3M H_2SO_4 electrolyte solution

The observation of this experiment is expected to show the effect of TiO^{2+} species interaction with the anodic products during the cathodic scan.

3.8.2.4. Study the Effect of $TiOSO_4$ on the Anodic Products Resulted from 1M $MnSO_4$-1M $TiOSO_4$-3M H_2SO_4 Anodic Voltage Hold at 1.5 V vs. SCE

Four anodic voltage holds at 1.5 V vs. SCE for 15min for 1M $MnSO_4$+3M H_2SO_4 are conducted on a graphite rod working electrode. A pre-step anodic voltage hold at 0.6V for 5min, where there is no any faradic process, followed by applying a 1.5V step voltage for 15min. After the anodic voltage hold experiment, the working electrode is rinsed with a 3M H_2SO_4 solution for 3min and then is dried for 15 min. Then, it is placed in a new solution and a cathodic linear voltage sweep scan at 2mV/s is conducted after measuring the OCV for 10 min from the OCV down to 0.242V vs. SCE in:

1- 1M $MnSO_4$+1M $TiOSO_4$+ 3M H_2SO_4 electrolyte solution

2- 1M $TiOSO_4$+ 3M H_2SO_4 electrolyte solution

3- 1M $MnSO_4$+3M H_2SO_4 electrolyte solution

4- 3M H_2SO_4 electrolyte solution

The observation of this experiment is expected to show the effect of TiO^{2+} species interaction with the anodic products during the anodic voltage hold.

3.8.2.5. Study the Effect of Using a Porous Working Electrode (Carbon Felt) on the Anodic Products Resulted from 1M $MnSO_4$-1M $TiOSO_4$-3M H_2SO_4 and 1M $MnSO_4$-3M H_2SO_4 Anodic Voltage Hold at 1.5 V vs. SCE

Two anodic voltage holds at 1.5 V vs. SCE for 15min for 1M $MnSO_4$+3M H_2SO_4 with and without the addition of $TiOSO_4$ are conducted on a carbon felt working electrode. A pre-step anodic voltage hold at 0.6V for 5min, where there is no any faradic process, followed by a applying a 1.5V step voltage for 15min. After the anodic voltage hold experiment, the working electrode is rinsed with a 3M H_2SO_4 solution for 3min and then is dried for 15 min. Then, it is placed in a new solution and a cathodic linear voltage sweep scan at 2mV/s is conducted after measuring the OCV for 10 min from the OCV down to -0.242V vs. SCE for the case without $TiOSO_4$ and from the OCV down to 0.2V vs. SCE for the case with $TiOSO_4$ in 3M H_2SO_4 solution. The observation of this experiment is expected to show that if the reduced species from the reduction of the anodic product during the cathodic scan falls from the working electrode, the falling reduced species would fall within the carbon felt material and not in the solution. Based on this assumption, the cathodic behavior of the fallen reduced species can be studied from the cathodic linear voltage scan.

3.8.2.6. Study the Effect of Convection on the Anodic Products Resulted from 1M MnSO4-1M TiOSO4-3M H2SO4 and 1M MnSO4-3M H2SO4 Anodic Voltage Hold at 1.5 V vs. SCE on a Flat Working Electrode (Graphite Rod) and on a Porous Working Electrode (Carbon Felt)

Two anodic voltage holds at 1.5 V vs. SCE for 15min for 1M $MnSO_4$+3M H_2SO_4 with and without the addition of $TiOSO_4$ are conducted on a carbon felt working electrode and, on a graphite rod working electrode with convection at 600 rpm. A pre-step anodic voltage hold at 0.6V for 5min, where there is no any faradic process, followed by a applying a 1.5V step voltage for 15min. An 8mm PTFE magnetic stirrer bar is inserted in the working electrode electrolyte compartment and the stirring rate is set at 600rpm in using a magnetic stirrer made by Thermo Scientific during the anodic hold experiment.

After the anodic voltage hold experiment, the working electrode is rinsed with a 3M H_2SO_4 solution for 3min and then is dried for 15 min. Then, the dried electrode is placed in a new solution and a cathodic linear voltage sweep scan at 2mV/s is conducted after measuring the OCV for 10 min from the OCV down to -0.242V vs. SCE for the case without $TiOSO_4$ and from the OCV down to 0.2V vs. SCE for the case with $TiOSO_4$ in 3M H_2SO_4 solution. The observation of this experiment can be used to study the effect of convection on the anodic voltage hold intermediate electro-active species during the anodic voltage hold. The resulted anodic products can be studied by the cathodic linear voltage sweep in 3M H_2SO_4 solution and a comparison is made between the case of convection condition and the case of stagnant condition anodic products cathodic scan.

4. Results and Discussions

4.1. $MnSO_4$ and $TiOSO_4$ Electrolyte Solubility in Sulfuric Acid Solution

- $MnSO_4$ electrolyte solubility in 1-3M H_2SO_4 aqueous solution at 20 ^oC, 25 ^oC, 30 ^oC, 40 ^oC, and 45 ^oC.

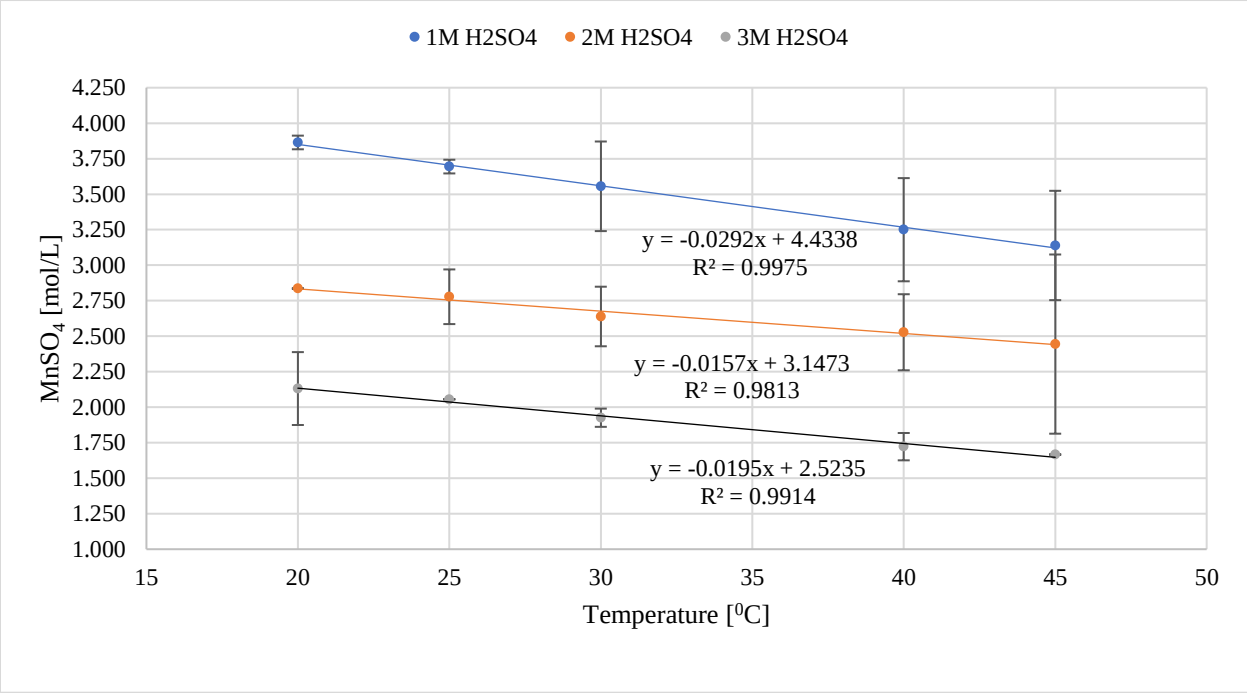

Figure 38. $MnSO_4$ electrolyte solubility in 1-3M H_2SO_4 aqueous solution at 20 ^oC, 25 ^oC, 30 ^oC, 40 ^oC, and 45 ^oC

From Figure 38, the solubility of $MnSO_4$ salt decreases as the concentration of H_2SO_4 in the solution increase. The solubility of $MnSO_4$ negatively depends on the electrolyte temperature. As the temperature of the electrolyte increases from 20^oC up to 45^oC, the solubility of $MnSO_4$ salt decreases in the solution. The results show a good agreement with the work done by Petri Kobylin in 2013 as his results show that the solubility of $MnSO_4$ in sulfuric acid decreases with increasing temperature and decreases with increasing the sulfuric acid concentration. [30]

The experimental data points for each acid concentrations were fitted in a linear function by using the least square method and the solubility of $MnSO_4$ salt is found to be linearly proportional

to the temperature of the solution. From the fitted line equation for each acid concentrations, the absolute value of the slope of $MnSO_4$ solubility with increasing the temperature is the highest for the case when the H_2SO_4 concentration in the solution is 1M H_2SO_4 and the absolute value of the slope is the lowest in the case when H_2SO_4 concentration is 3M H_2SO_4. The highest solubility of $MnSO_4$ was measured at 20^{o}C in 1M H_2SO_4 and it is 3.86 ±0.048M $MnSO_4$, and the lowest was measured at 45^{o}C in 3M H_2SO_4 at 1.667±0.000M $MnSO_4$. Table 22 shows the numerical values of $MnSO_4$ solubility in 1-3M H_2SO_4 at 20^{o}C, 25^{o}C, 30^{o}C, 40^{o}C, and 45^{o}C

Table 22. $MnSO_4$ electrolyte solubility [M] in 1-3M H_2SO_4 aqueous solution at 20 ^{o}C, 25 ^{o}C, 30 ^{o}C, 40 ^{o}C, and 45 ^{o}C

	H_2SO_4 concentration		
Temperature [^{o}C]	**1M**	**2M**	**3M**
20±0.1	3.864±0.048	2.836±000	2.131±0.257
25±0.1	3.694±0.048	2.778±0.192	2.056±000
30±0.1	3.556±0.315	2.639±0.21	1.926±0.064
40±0.1	3.250±0.363	2.528±0.268	1.722±0.096
45±0.1	3.139±0.385	2.444±0.631	1.667±000

- $TiOSO_4$ electrolyte solubility in 1-3M H_2SO_4 aqueous solution at 20 ^oC, 25 ^oC, 30 ^oC, 40 ^oC, and 45 ^oC

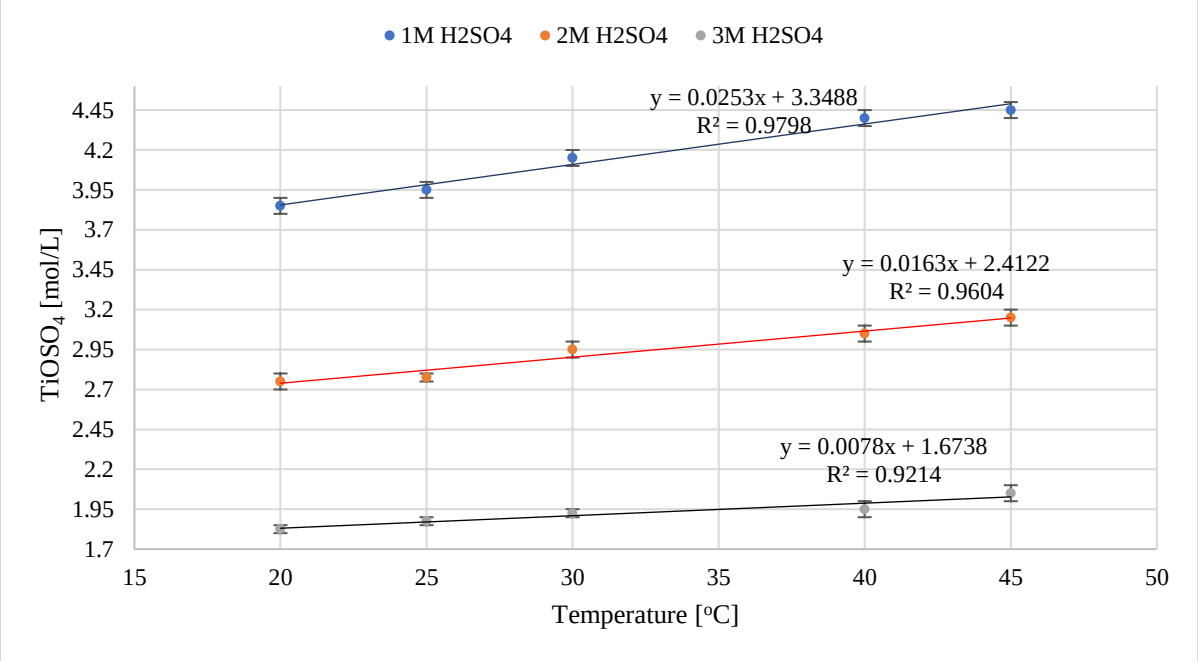

Figure 39. $TiOSO_4$ electrolyte solubility in 1-3M H_2SO_4 aqueous solution at 20 ^oC, 25 ^oC, 30 ^oC, 40 ^oC, and 45 ^oC

From Figure 39, the solubility of $TiOSO_4$ salt decreases as the concentration of H_2SO_4 in the solution increase. The solubility of $TiOSO_4$ positively depends on the electrolyte temperature. As the temperature of the electrolyte solution increases from 20^oC up to 45^oC, the solubility of $TiOSO_4$ salt increases.

The experimental data points for each acid concentrations were fitted in a linear function by using the least square method and the solubility of $TiOSO_4$ is found to be linearly proportional to the temperature of the solution. From the fitted line equation for each acid concentrations, the slope of $TiOSO_4$ solubility with increasing the temperature is the highest for the case when the H_2SO_4 concentration in the solution is 1M H_2SO_4 and the slope is the lowest in the case when H_2SO_4 concentration is 3M H_2SO_4. The highest solubility of $TiOSO_4$ was measured at 45^oC in 1M H_2SO_4 and it is 4.45 ±0.05 M $TiOSO_4$, and the lowest was measured at 20^oC in 3M H_2SO_4 at

1.825±0.025 M $TiOSO_4$. Table 23 shows the numerical values of $MnSO_4$ solubility in 1-3M H_2SO_4 at 20 ^oC, 25 ^oC, 30 ^oC, 40 ^oC, and 45 ^oC.

Table 23. $TiOSO_4$ electrolyte solubility [M] in 1-3M H_2SO_4 aqueous solution at 20 ^oC, 25 ^oC, 30 ^oC, 40 ^oC, and 45 ^oC

	H_2SO_4 concentration		
Temperature [^oC]	**1M**	**2M**	**3M**
20±0.1	3.85±0.05	2.75±0.05	1.825±0.025
25±0.1	3.95±0.05	2.775±0.025	1.875±0.025
30±0.1	4.15±0.05	2.95±0.05	1.925±0.025
40±0.1	4.4±0.05	3.05±0.05	1.95±0.05
45±0.1	4.45±0.05	3.15±0.05	2.05±0.05

4.2. Cyclic Voltammetry Scans for Solvent Electrolyte Solutions

4.2.1. Cyclic voltammetry of solvents within $MnSO_4$ voltage scan window

The third cyclic voltammetry scans of 1M, 2M, and 3M H_2SO_4 solutions on graphite rod working electrode and on carbon felt working electrode at a 2mV/s voltage scan rate as shown in Figures 40 and 41. An anodic current wave is observed starting after 1V vs SCE during the positive scan and a cathodic current wave is observed below 0.16V during the negative scan.

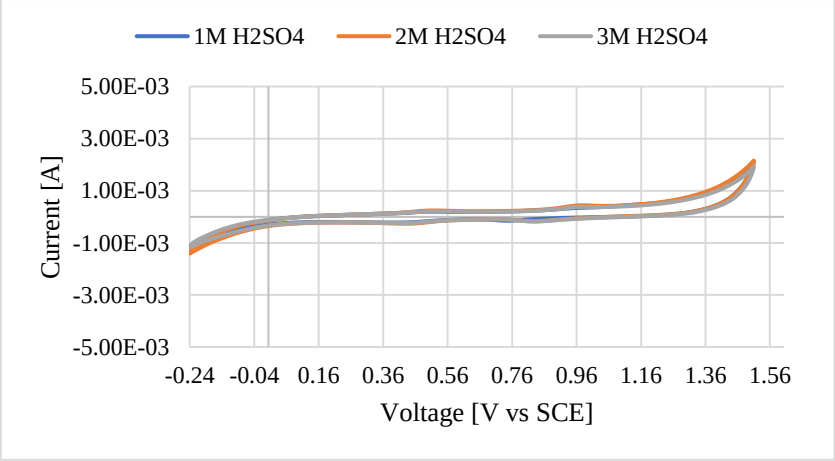

Figure 40. Third cyclic voltammetry scan of 1M H_2SO_4, 2M H_2SO_4, and 3M H_2SO_4 on graphite rod working electrode at 2minV/s voltage scan rate in $MnSO_4$ voltage scan window

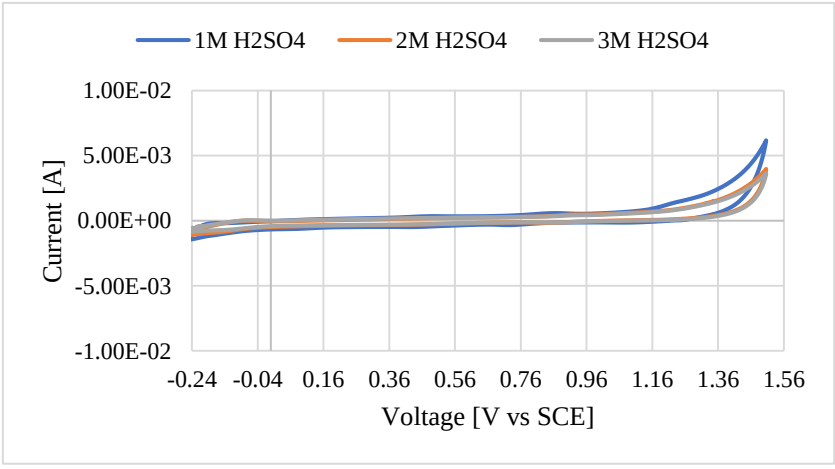

Figure 41. Third cyclic voltammetry scan of 1M H_2SO_4, 2M H_2SO_4, and 3M H_2SO_4 on carbon felt working electrode at 2minV/s voltage scan rate in $MnSO_4$ voltage scan window

The anodic current wave after 1V can be attributed to both carbon oxidation and oxygen evolution reaction in which the oxygen evolution reaction is the dominant oxidation reaction. As the working electrode area increases when a carbon felt working electrode is used, the anodic current increases. Although the acid concentration was increased for the cyclic voltammetry scan for 2M and 3M sulfuric acid solutions in which the reduction potential of oxygen evolution reaction and the reduction potential of hydrogen evolution reaction are expected to shift to a more positive value, the observed currents for those solutions seem to be not influenced by the shifting of the reduction potentials and almost similar current behavior is observed among all the three tested solutions. This may suggest that the graphite rod working electrode has a low electrochemical reaction activity for OER and HER reactions. However, the anodic wave after 1V on carbon felt working electrode for 1M sulfuric acid solution is influenced by the shifted reduction potential of OER as shown in Figure 41. Nevertheless, the anodic current waves of 2M and 3M sulfuric acid solutions are almost the same. Regarding the observed cathodic wave below 0.16 V, the reduction wave is attributed to the hydrogen evolution reaction on the working electrode and the observed cathodic current does not exceed 1.5 mA in the cyclic voltammetry scans on graphite rod and carbon felt working electrodes for all tested solutions. Within the region between the anodic wave lower than 1V and the cathodic wave higher than 0.16, two anodic peak currents at 0.5 V and 0.96V, three reduction pecks current 0.84V, 0.76V, and 0.436V are detected in all three solutions scanned. The current intensity of those peaks does not exceed 500 µA. Those observed peak currents are attributed to carbon materials redox reactions and their current intensity is low which indicates their low reactivity during the cyclic voltammetry scan.

4.2.2. Cyclic voltammetry of solvents within $TiOSO_4$ voltage scan window

Figures 42 and 43 show the third cyclic voltammetry scan of 1M, 2M, and 3M H_2SO_4 solutions on graphite rod working electrode and on carbon felt working electrode in the $TiOSO_4$ voltage scan window at a 2mV/s voltage scan rate.

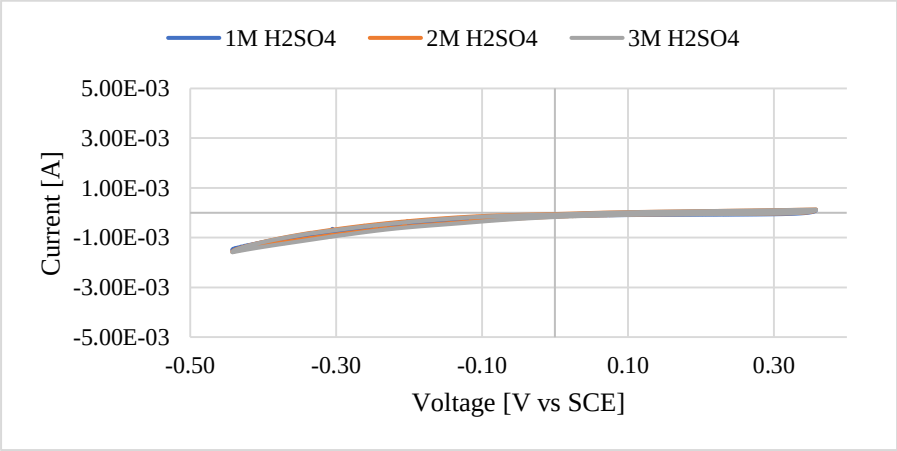

Figure 42. Third cyclic voltammetry scan of 1M H_2SO_4, 2M H_2SO_4, and 3M H_2SO_4 on graphite rod working electrode at 2minV/s voltage scan rate in $TiOSO_4$ voltage scan window

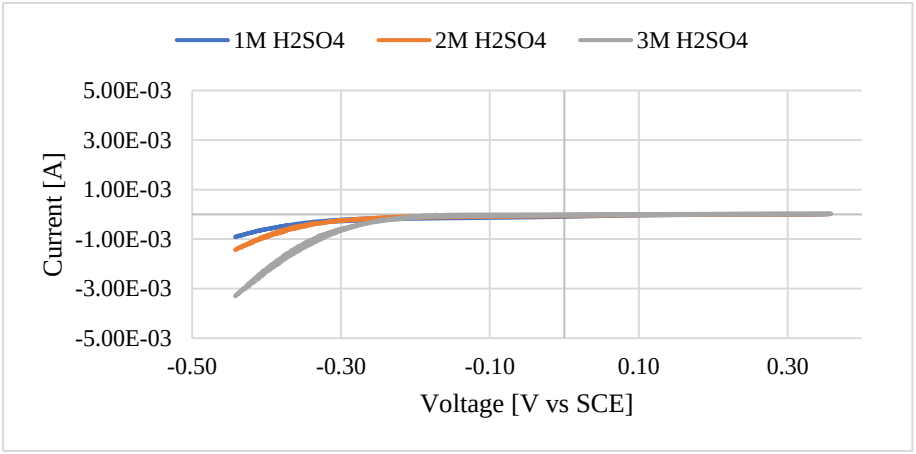

Figure 43. Third cyclic voltammetry scan of 1M H_2SO_4, 2M H_2SO_4, and 3M H_2SO_4 on carbon felt working electrode at 2minV/s voltage scan rate in $TiOSO_4$ voltage scan window

One cathodic current wave below 0.3 V vs SCE is observed during cyclic voltammetry scan of all tested solution. This current wave is attributed to the hydrogen evolution reaction on the working electrode. In Figure 42, Some sparks in current during the negative scan are observed between

0.1V and -0.3V during the cathodic scan. This observation may due to the ripping effect of the formed hydrogen atoms on the working electrode at low overpotential. Although the acid concentration was increased for the cyclic voltammetry scan for 2M and 3M sulfuric acid solutions in which the reduction potential of hydrogen evolution reaction is expected to shift to a more positive value, the observed currents for those solution seem to be not influence by the thermodynamic potential shifting of the HER reduction potential and almost similar current behavior is observed among all the three tested solutions. This may suggest that the graphite rod working electrode has a low electrochemical reaction activity for HER reactions. However, the cathodic wave below 0.3 V on carbon felt working electrode for 1M, 2M, and 3M sulfuric acid solution is clearly influenced by the shifted reduction potential of HER where the cathodic current increases with increasing the sulfuric acid concentration as shown in Figure 43. Nevertheless, the cathodic current wave is still low on the carbon felt working electrode.

4.3. Mn Electrolyte Characterization Results

4.3.1. Cyclic Voltammetry of Mn Electrolyte Results

The third cyclic voltammetry scans of 1M Mn in 1-3M H_2SO_4 solution on a graphite rod working electrode and on a carbon felt working electrode at 2mV/s scan rate are shown in Figures 44 and 45. The obtained cyclic voltammograms are different from the cyclic voltammograms by Xue due to the low $MnSO_4$ concentration used in their work. [46]

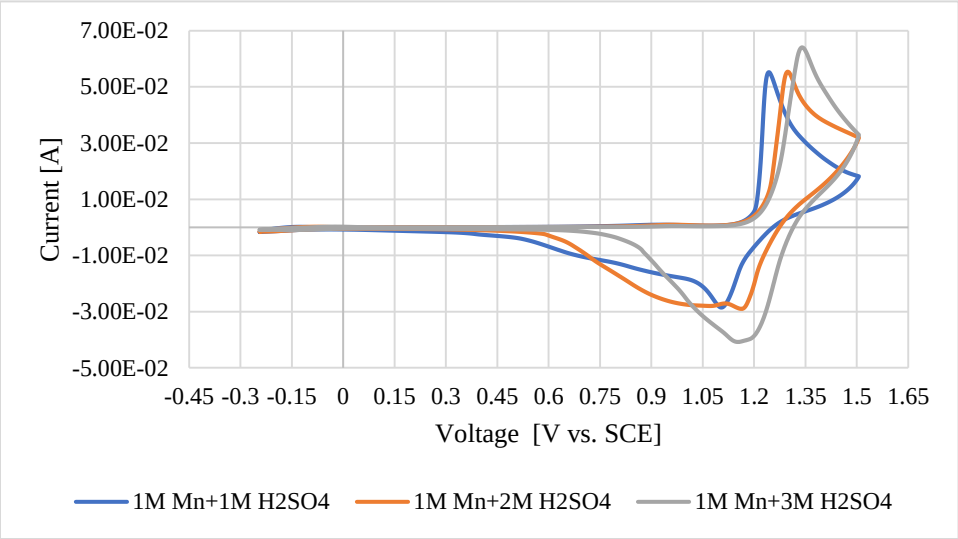

Figure 44. Third cyclic voltammetry scan of 1M $MnSO_4$ in 1M H_2SO_4, 2M H_2SO_4, and 3M M H_2SO_4 on a graphite rod working electrode with 2mV/s scan rate

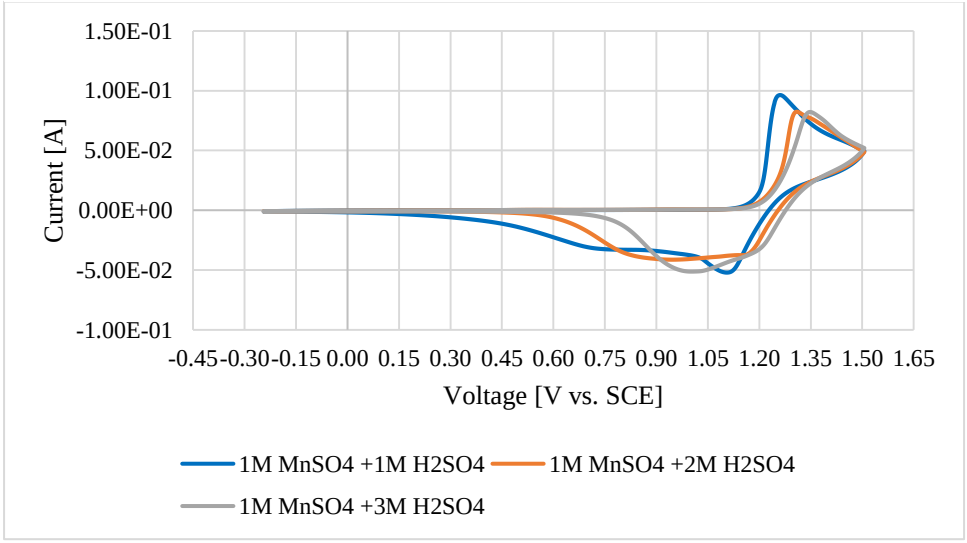

Figure 45. Third cyclic voltammetry scan of 1M $MnSO_4$ in 1M H_2SO_4, 2M H_2SO_4, and 3M M H_2SO_4 on a carbon felt working electrode with 2mV/s scan rate

- **Observations from Figures 44 and 45 during the positive scan:**

- During the anodic scan, only one single peak is observed in all three tested solutions on a graphite rod working electrode, and on a carbon felt working electrode.
- An anodic current starts to show up after 1.1 V vs SCE for all tested solutions.
- The slope during the anodic scan after 1.1V increases at 1.21V for 1M Mn+1M H_2SO_4 case, 1.25V for 1M Mn+2M H_2SO_4, and 1.27V for 1M Mn+ 3M H_2SO_4 case on both working electrodes.
- The anodic peak currents are observed at 1.23V for 1M Mn+1M H_2SO_4 case, at 1.29V for 1M Mn+2M H_2SO_4, and at 1.33V for 1M Mn+3M H_2SO_4.
- From Figure 44, the peak currents intensity is the same for 1M Mn+1M H_2SO_4 and 1M Mn+2M H_2SO_4 cases and higher in 1M Mn+3M H_2SO_4 case by 14.4% on a graphite rod working electrode.
- From Figure 45, the peak currents intensity is the same for 1M Mn+2M H_2SO_4 and 1M Mn+3M H_2SO_4 cases and higher in the 1M Mn+1M H_2SO_4 O4 case by 16.5% on a carbon felt working electrode.

- **Observations from Figures 40 and 41 during the negative scan:**

- For the 1M Mn+1M H_2SO_4 case, the first cathodic peak current is measured at 1.11V when using both the graphite rod and the carbon felt working electrode. After the first cathodic peak current, a limited current is measured during the negative scan on both used working electrodes where the cathodic current decreases to zero current faster in the case when the graphite rod working electrode is used.
- For the 1M Mn+2M H_2SO_4 case, the first peak current is measured at 1.17V when either the graphite rod or the carbon felt working electrode is used. After the first cathodic peak

current, a limited current is observed during the negative scan on both electrodes with the cathodic current decreases to zero faster when the graphite rod working electrode.

- For the 1M Mn+3M H_2SO_4 case, the first peak current is measured at 1.20V for both the graphite rod and the carbon felt working electrodes. After the first cathodic current peak, a smaller limited current is observed during the negative scan on a graphite rod electrode, while for the carbon felt electrode a second cathodic peak current at 1V was observed before it decreases to zero current. The cathodic current decreases zero current earlier in the case of the graphite rod working electrode.
- From Figure 44, the intensity of the first cathodic peak current with a graphite rod electrode in 1M Mn+3M H_2SO_4 is higher than the cathodic peak currents intensity of 1M Mn in 1M H_2SO_4 and 2M H_2SO_4 cases where their peak currents are almost equal in magnitude.
- From Figure 45, the intensity of the first cathodic peak current for the carbon felt electrode in 1M Mn+1M H_2SO_4 is higher than the cathodic peak currents intensity of 1M Mn in 2M H_2SO_4 and 3M H_2SO_4 cases where their peak currents are almost equal in magnitude.

- **1M Mn+3M H_2SO_4 after the cyclic voltammetry experiment on a graphite rod working electrode**

Figure 46. 1M Mn-3M H_2SO_4 solution after the cyclic voltammetry experiment on graphite rod working electrode.

A Black solid material was observed in the tested electrolyte after the cyclic voltammetry test. The electrolyte color was changed to red color after the cyclic voltammetry in which the darker the red color was observed in the case of 1M $MnSO_4$ in 3M H_2SO_4 tested solution. The red color

may due to the presence of Mn^{3+} species in the solution, and the black solid material at the bottom of the cell may due to the hydrolysis of Mn^{3+} species to form MnOOH solid in the solution.

- **Observation of the graphite working electrode after the cyclic voltammetry of 1M Mn+3M H_2SO_4 solution**

A black solid deposit was found on the graphite rod electrode surface after the cyclic voltammetry test of 1M Mn+3M H_2SO_4. This black material may be due to the reduction of MnO_2 solid (in Eq3.38) to form MnOOH.

Figure 47. Graphite working electrode after the cyclic voltammetry of 1M Mn-3M H2SO4 solution

- **Possible oxidation pathway of $MnSO_4$ electrolyte in H_2SO_4**

During the positive scan, Mn(II) electro-active species is present in the form of Mn^{2+} in 1-3M H_2SO_4 solutions. According to Table 8, Mn^{2+} equilibrium concentration can be assumed to be the same in 1-3M H_2SO_4 solutions. Mn^{2+} is more likely oxidized during the positive scan on the working electrode after 1.1V to form Mn^{3+} species based on Eq3.31 and not directly to Mn(IV) species because Mn^{2+} has to go through two elementary electron transfer reaction steps to form Mn(IV) species. The change on the anodic current slope after 1.1V may attribute to the Mn(III) oxidation reaction to form Mn(IV) where the oxidation reaction of Mn(III) species to Mn(IV) species may be influenced by the Mn^{3+} hydrolysis reactions to form the electro-active Mn(III) species that undergoes the oxidation reaction in which the concertation of the Mn(III) electro-active species decreases as the acid concentration increases. The oxidized

Mn(IV) species may undergo significant hydrolysis on the working electrode surface to form MnO_2 deposit on the electrode surface. The MnO_2 formed by the oxidation of Mn^{2+} in sulfuric acid is assumed to be $(\gamma)MnO_2$ as it was reported. [44] The overall process during the positive scan can be expressed by Eq.2.2:

$$Mn^{2+} + 2H_2O \leftrightarrow MnO_2 + 4H^+ + 2e^- \qquad E^0 = 0.988 \text{ V vs SCE} \qquad \text{Eq.2.2}$$

To support the proposed Mn oxidation pathway, based on the listed observations during the positive scan of the cyclic voltammetry, the anodic current during the positive scan seems to be limited in 1M Mn+1M H_2SO_4 and 1M Mn+2M H_2SO_4 cases on the graphite rod electrode, shown in Figure 44, by the formed anodic products which seem to have a direct effect on the course of the overall Mn(II) oxidation process. From Figure 45, once the electrode surface area is increased when using a carbon felt working electrode, the effect observed above on the overall Mn(II) oxidation reaction, in 1M Mn+1M H_2SO_4 and 1M Mn+2M H_2SO_4 cases disappears in which the anodic peak current of 1M Mn+1M H_2SO_4 becomes the highest among all the tested electrolyte. A possible explanation of this observation is that during the positive scan, the oxidation of Mn^{2+} is expected to form Mn^{3+} first on the electrode surface as shown in Eq.3.31:

$$Mn^{2+} \leftrightarrow Mn^{3+} + e^- \qquad E^0 = 1.26 \text{ V vs SCE} \qquad \text{Eq3.31}$$

A direct oxidation of Mn^{3+} species to Mn^{4+} species is not likely occurred on the electrode because the high reduction potential of the Mn^{4+}/ Mn^{3+} redox couple as shown in Eq.34 and that Mn^{4+} is not a stable Mn(IV) species. In addition, the first hydrolyzed Mn(III) species may not be the one that is oxidized to Mn(IV) due to the close standard reduction potential of $Mn(OH)^{3+}$/ $Mn(OH)^{2+}$ to the Mn^{3+}/ Mn^{2+} standard reduction potential, and that the estimated

equilibrium concentration of $Mn(OH)^{2+}$ in 1-3M sulfuric acid solutions from Table 9 does not decrease with increasing acid concentration.

$$Mn^{3+} \leftrightarrow Mn^{4+} + e^{-}, \quad E^{0} = 1.392 \text{ V vs SCE} \qquad \text{Eq3.34}$$

$$Mn(OH)^{2+} \leftrightarrow Mn(OH)^{3+} + e^{-}, \quad E^{0} = 1.247 \text{ V vs SCE} \qquad \text{Eq3.35}$$

More likely $Mn(OH)_2^{+}$ may be the Mn(III) electro-active species that undergoes oxidation reaction to form $Mn(OH)_2^{2+}$, as shown in Eq.3.36, which has a lower standard reduction potential:

$$Mn(OH)_2^{+} \leftrightarrow Mn(OH)_2^{2+} + e^{-}, \quad E^{0} = 1.06 \text{ V vs SCE} \qquad \text{Eq3.36}$$

Mn^{3+} hydrolysis reactions near the electrode surface to form $Mn(OH)^{2+}$ and $Mn(OH)_2^{+}$ are described in Eq.3.14 and Eq.3.15:

$$Mn^{3+} + H_2O \leftrightarrow Mn(OH)^{2+} + H^{+} \quad K=2.5 \qquad \text{Eq3.14}$$

$$Mn(OH)^{2+} + H_2O \leftrightarrow Mn(OH)_2^{+} + H^{+} \quad K=0.5 \qquad \text{Eq3.15}$$

From Eq.3.14 and Eq.3.15, as the H^{+} concentration increases, according to Le Châtelet's principle, the equilibrium reactions in Eq.3.14 and Eq.3.15 are expected to shift from right to left and less $Mn(OH)_2^{+}$ species are formed. Thus, the reduction potential of Eq3.36 is expected to increase with the low concentration of $Mn(OH)_2^{+}$, so that less $Mn(OH)_2^{2+}$ is formed by Eq.3.36. The formed $Mn(OH)_2^{2+}$ is then hydrolyzed rapidly to γMnO_2 based on Eq.3.26:

$$Mn(OH)_2^{2+} \leftrightarrow (\gamma)MnO_2 + 2H^{+} \qquad K=2E+4 \qquad \text{Eq.3.26}$$

The electrode electronic activity may be reduced when γ-MnO_2 is deposited on the electrode surface due to its lower electronic conductivity compared to the carbon-based

working electrode. As the MnO_2 covers the working electrode, Mn^{2+} may be oxidized on γ-MnO_2 substrate to form Mn^{3+}. The formed Mn^{3+} may not oxidize further to Mn(IV) species due to the low electronic conductivity of the substrate, rather Mn^{3+} may diffuse away from the electrode or hydrolyze on the MnO_2 substrate to form MnOOH solid. More likely the MnOOH phase resulted from Mn(III) hydrolysis is γ-MnOOH because of the high equilibrium reaction constant of Eq.3.17 compared to α-MnOOH in Eq3.18.

$$Mn(OH)_2^{+} \leftrightarrow (\gamma)MnOOH + H^{+}, \text{ K=0.9059} \qquad \text{Eq3.17}$$

$$Mn(OH)_2^{+} \leftrightarrow (\alpha)MnOOH + H^{+}, \text{ K=0.467} \qquad \text{Eq3.18}$$

The resulted γ-MnOOH and α -MnOOH solids may disproportionate with the present of Mn^{3+} in the solution to form α-MnO_2 and γ-MnO_2, as shown in Eq.3.44and Eq.3.46:

$$(\gamma)MnOOH + Mn^{3+} \leftrightarrow Mn^{2+} + H^{+} + (\alpha)MnO_2, \text{ K=1.3 E+7} \qquad \text{Eq3.44}$$

$$(\alpha)MnOOH + Mn^{3+} \leftrightarrow Mn^{2+} + H^{+} + (\gamma)MnO_2, \text{ K=2.5E+7} \qquad \text{Eq3.46}$$

The MnO_2 coverage phenomenon may explain that the similar anodic peak currents are observed in Figure 44 for 1M Mn+1M H_2SO_4 and 1M Mn+2M H_2SO_4 because of the fast MnO_2 build up deposit on the working electrode that limits the overall anodic process. From Figure 44, the significant drop of the anodic current of 1M Mn+1M H_2SO_4 solution by the end of the positive scan may reveal that the large thick MnO_2 deposit significantly increases the working electrode electronic resistance. However, in the case of 1M Mn+3M H_2SO_4 the high anodic peak current on the graphite rod working electrode indicates that the reduction potential of Eq3.36 is shifted to more positive voltage due to the low hydrolysis of Mn^{3+} that decreases the formation of $Mn(OH)_2^{+}$. In this case MnO_2 build up on the working electrode may be slow compared to the oxidation of Mn^{2+} in Eq3.34 and more Mn^{3+} is formed, so that more anodic

current is measured because of the high available Mn^{3+} that is slowly hydrolyzed and oxidized to build up the MnO_2 deposit on the working electrode until it is limited by the MnO_2 coverage.

As the working electrode area increases in Figure 45, the large available surface area on the carbon felt working electrode reveals that MnO_2 deposit is greater in 1M Mn+1M H_2SO_4 solution than in 1M Mn in 2-3M H_2SO_4 solutions as it can be seen from the anodic peak current of each tested solutions. As the working electrode area increases, the consumption rate of Eq3.31 is increased and more Mn^{3+} is formed during the positive scan. In this case, the limited anodic current for the case of 1M H_2SO_4 may still due to the MnO_2 substrate that reduces the electronic conductivity of the electrode. For 2M H_2SO_4 and 3M H_2SO_4 cases, the limited current may due to the diffusion limitation of Mn^{2+} species from the bulk to the electrode surface.

- A proposed oxidation reaction mechanism of Eq.2.2 during the positive scan of the cyclic voltammetry of $MnSO_4$ in sulfuric acid solution before the peak current is described below:

$$Mn^{2+} \leftrightarrow Mn^{3+} + e^- \qquad E^0 = 1.26\ \text{V vs SCE} \qquad \text{Eq3.31}$$

$$Mn^{3+} + H_2O \leftrightarrow Mn(OH)^{2+} + H^+,\ \text{K=2.5} \qquad \text{Eq3.14}$$

$$Mn(OH)^{2+} + H_2O \leftrightarrow Mn(OH)_2^+ + H^+,\ \text{K=0.5} \qquad \text{Eq3.15}$$

$$Mn(OH)_2^+ \leftrightarrow Mn(OH)_2^{2+} + e^-,\ \ E^0 = 1.06\ \text{V vs SCE} \qquad \text{Eq3.36}$$

$$Mn(OH)_2{}^{2+} \leftrightarrow (\gamma)MnO_2 + 2H^+,\ \text{K=2E+4} \qquad \text{Eq3.26}$$

$$\text{Overall:} \qquad Mn^{2+} + 2H_2O \leftrightarrow (\gamma)MnO_2 + 4H^+ + 2e^-$$

- A proposed oxidation reaction mechanism during the positive scan of the cyclic voltammetry of $MnSO_4$ in sulfuric acid solution after the peak current is described below:

After $(\gamma)MnO_2$ is fully covered the working electrode area, the working electrode electronic resistance may increase and the anodic current may only be described by the Mn^{2+} diffusion to the substrate and the oxidation of Mn^{2+} into Mn^{3+} only as shown below:

$$Mn^{2+} \leftrightarrow Mn^{3+} + e^- \qquad E^0 = 1.26\ V \text{ vs SCE} \qquad \text{Eq3.31}$$

$$Mn^{3+} + H_2O \leftrightarrow Mn(OH)^{2+} + H^+, \quad K=2.5 \qquad \text{Eq3.14}$$

$$Mn(OH)^{2+} + H_2O \leftrightarrow Mn(OH)_2^+ + H^+, \ K=0.5 \qquad \text{Eq3.15}$$

$$Mn(OH)_2{}^+ \leftrightarrow (\gamma)MnOOH + H^+, \ K=0.9059 \qquad \text{Eq3.17}$$

- **Possible reduction pathway of the anodic products of $MnSO_4$ electrolyte in H_2SO_4**

It is difficult to interpret the cathodic scan behavior from the cyclic voltammetry results in Figures 44 and 45 alone where there is MnO_2 on the electrode surface and Mn(III) species may present in the solution as a Mn^{3+} and MnOOH or on the electrode as MnOOH. During the negative scan, mainly two cathodic wave currents can be noticed in all tested solutions. The first cathodic peak current during the negative scan in Figure 44 increases and shifts to more positive voltage with the increase of the acid concentration. However, from Figure 45, when using a carbon felt working electrode, the first cathodic peak current decreases and shifts to more positive voltage with the increase of the acid concentration. For the region below 1.05V in Figure 44, the second cathodic wave current has irregular pattern where it increases in 2M H_2SO_4 and decrease in 3M H_2SO_4. However, the second cathodic wave shifts to more positive voltage with the increase of the acid concentration. In Figure 45, the second cathodic current wave decreases and shifts to the right with the increase of the acid concentration. The irregular pattern of the second cathodic wave current that is observed in Figure 44 is due to solids fallen from the working electrode surface after the first cathodic peak current. This phenomenon is

supported by a video recording. When using a carbon felt working electrode, the porous structure of the working electrode retains the fallen solids after the first cathodic peak current, and a regular pattern is shown for the second cathodic current wave in Figure 45 when this solid is reduced.

These two observed cathodic waves are initially investigated by conducting a new cyclic voltammetry scan for 1M Mn+3M H_2SO_4 with varying the end voltage during the positive scan to study the effect of end potential on the two cathodic waves during the negative scan. as shown in Figure 48.

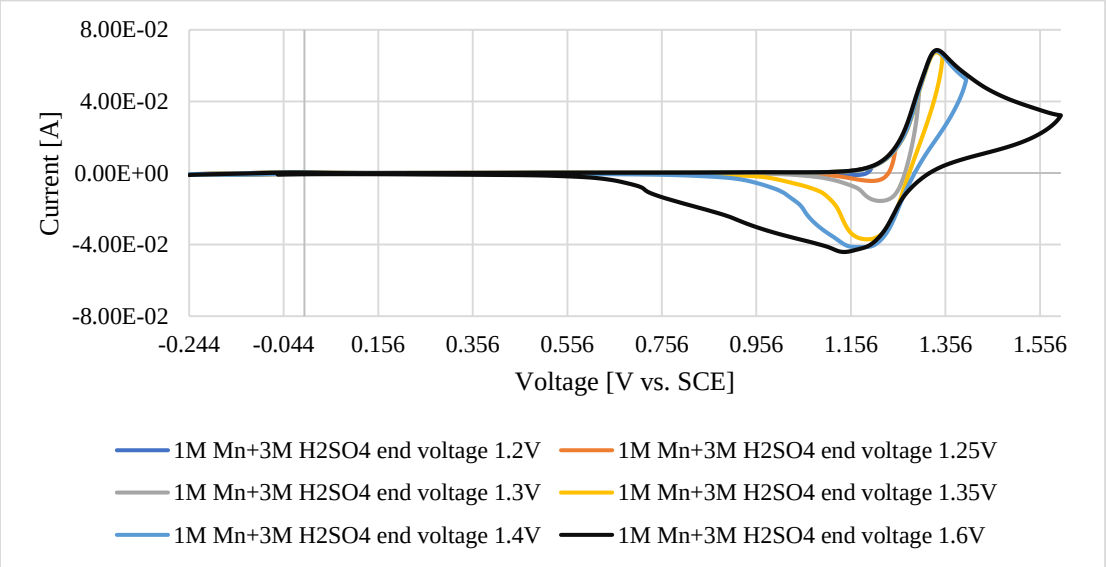

Figure 48. Third cyclic voltammetry scan of 1M $MnSO_4$ in 3M M H_2SO_4 on graphite rod working electrode with 2mV/s scan rate, and with varying the end voltage during the positive scan

From Figure 48, as the end applied voltage increases, the first cathodic peak current becomes almost fixed and the second cathodic wave current grows. At low cut off (E<1.25 V vs. SCE) voltage only a small amount of Mn^{3+} is formed and is reduced during the cathodic scan. At high cut off voltage when more Mn^{3+} is formed, more MnO_2 and MnOOH is created, which results in a more complex cathodic peak. Based on the proposed oxidation pathway, the overall oxidation

reaction of Mn(II) leads to the formation of MnO_2 deposit on the working electrode until the MnO_2 is fully covered the electrode area and limits the anodic process.

A cathodic route of the Mn anodic products is proposed to explain the observations in Figure 48. During the negative scan, the first cathodic wave is assumed to be attributed to the reduction reaction of $(\gamma)MnO_2$ solid to (α)MnOOH solid on the working electrode as shown in Eq.3.38, where the electrochemical reduction of $(\gamma)MnO_2$ proceeds via proton insertion into the solid phase as it was suggested by Bedoardo, and the second cathodic wave is assumed to be attributed to the reduction reaction of (α)MnOOH and (γ)MnOOH to Mn^{2+} as shown in Eq.3.18, Eq.3.17, Eq.3.15, Eq.14, and Eq3.31. [28, 47] (α)MnOOH was reported to be an electronically insulating material. [28, 47] (γ)MnOOH is assumed to be formed on the $(\gamma)MnO_2$ solid structure after the positive scan in Figure 48 becomes limited by the $(\gamma)MnO_2$ solid deposits on the electrode surface where the oxidation process on the $(\gamma)MnO_2$ substrate is assumed to be only for the oxidation of Mn^{2+} to Mn^{3+} due to the high electronic resistance of the substrate. Regarding Mn^{3+} species, if Mn^{3+} species was allowed to diffuse away from the electrode surface, it may hydrolyze into (γ)MnOOH and (α)MnOOH solid in the solution. Thus, the proposed reduction pathway of Mn anodic products is shown below:

$$H^+ + (\gamma)MnO_2 + e^- \leftrightarrow (\alpha)MnOOH \ , \ E^0 = 0.788 \text{ V vs SCE} \qquad \text{Eq3.38}$$

$$(\alpha)MnOOH + H^+ \leftrightarrow Mn(OH)_2{}^+ \qquad \text{K=2.14} \qquad \text{Eq3.18}$$

$$(\gamma)MnOOH + H^+ \leftrightarrow Mn(OH)_2{}^+ \qquad \text{K=1.1} \qquad \text{Eq3.17}$$

$$Mn(OH)_2^+ + H^+ \leftrightarrow Mn(OH)^{2+} + H_2O, \qquad \text{K=2} \qquad \text{Eq3.15}$$

$$Mn(OH)^{2+} + H^+ \leftrightarrow Mn^{3+} + H_2O, \qquad \text{K=0.4} \qquad \text{Eq3.14}$$

$$Mn^{3+} + e^{-} \leftrightarrow Mn^{2+} \qquad E^{0} = 1.26\ V\ vs\ SCE \qquad Eq3.31$$

Based on the proposed cathodic route of the Mn anodic products, the behavior of the negative scan by varying the end voltage of the positive scan indicates that the oxidation process that takes place after the anodic peak may not be attributed to the oxidation reaction of Mn^{2+} to $(\gamma)MnO_2$. Instead, as the working electrode resistance increases by the deposited $(\gamma)MnO_2$, Mn^{2+} may only be able to oxidize to Mn^{3+}. This can be seen from the intensity of the first cathodic peak current where the first cathodic peak stops increasing as the applied voltage increases further beyond the anodic peak current voltage as in the last two scans. The formed Mn^{3+} on the $(\gamma)MnO_2$ may hydrolyze to (γ)MnOOH or (α) MnOOH instead of being oxidizing further oxidize to Mn(IV) species.

From Figure 45, with a carbon felt working electrode where the anodic process is not limited by the small area of the electrode, as the concentration of H^+ increases, less MnO_2 is formed on the working electrode, so that the first cathodic peak current is less in magnitude. The reduction reaction of MnO_2 on the working electrode surface as described by Eq.3.38 seems to be influenced by the H^+ concentration where the first cathodic wave shifts to the right with increasing the H^+ concentration due to the positive shifting of the reduction potential of Eq.3.38 with increasing the H^+ concentration. Another reaction that may also interfere with the first cathodic wave is that the interaction of Mn^{2+} with MnO_2 substrate when Mn^{3+} is present in a negligible concentration as shown in Eq.3.46:

$$Mn^{2+} + H^{+} + (\gamma)MnO_2 \leftrightarrow (\alpha)MnOOH + Mn^{3+},\ K=4E\text{-}8 \qquad Eq3.46$$

From Figure 45, the second cathodic wave may be attributed to the reduction reaction of MnOOH based on Eq.3.18, Eq.3.17, Eq.3.15, Eq.14, and Eq3.31. As the acid concentration of the

electrolyte increases, less MnOOH is formed on the electrode surface due to the positive potential shift and the resulting slower deposition of MnO_2 on the electrode surface. The overall reduction reaction of MnOOH to Mn^{2+} is enhanced by increasing the H^+ concentration based on Eq.3.46 where the second cathodic wave current shifts to the right with increasing the H^+ concentration allowing the reaction to start early and have more time to be consumed. However, the large generated Mn^{3+} from the oxidation of Eq.3.31 in 3M H_2SO_4 may increase the ratio of MnOOH to MnO_2 on the electrode surface as it can be seen in Figure 45 for the first cathodic peak current and the second cathodic peak current.

- **Cyclic voltammetry of $MnSO_4$+$TiOSO_4$ in H_2SO_4 solution on a graphite rod and on a carbon felt working electrode**

The third cyclic voltammetry scan of 1M Mn+1M Ti in 1-3M H_2SO_4 solution on a graphite rod working electrode and on a carbon felt working electrode with 2mV/s scan rate are shown in Figures 49 and 50.

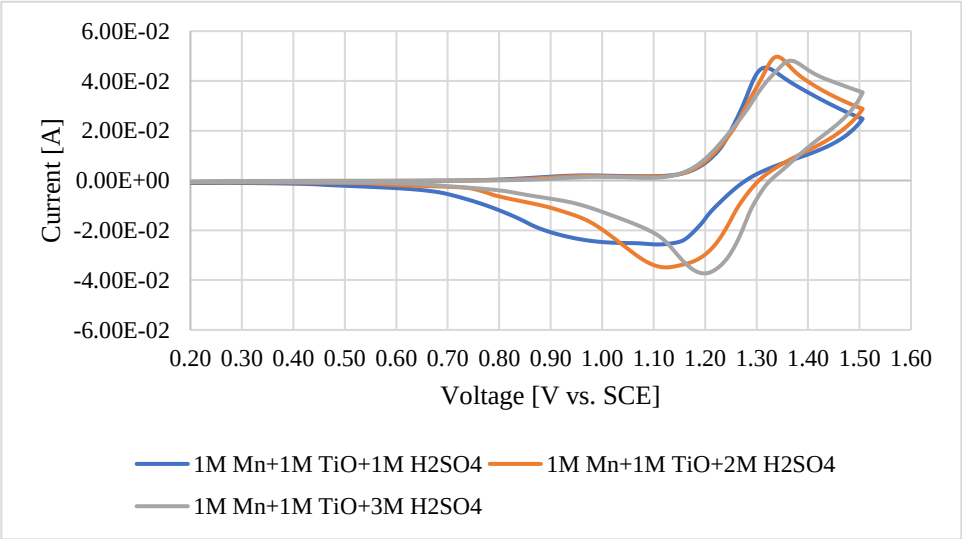

Figure 49. Third cyclic voltammetry scan of 1M $MnSO_4$-1M $TiOSO_4$ in 1M H_2SO_4, 2M H_2SO_4, and 3M M H_2SO_4 on graphite rod working electrode with 2mV/s scan rate

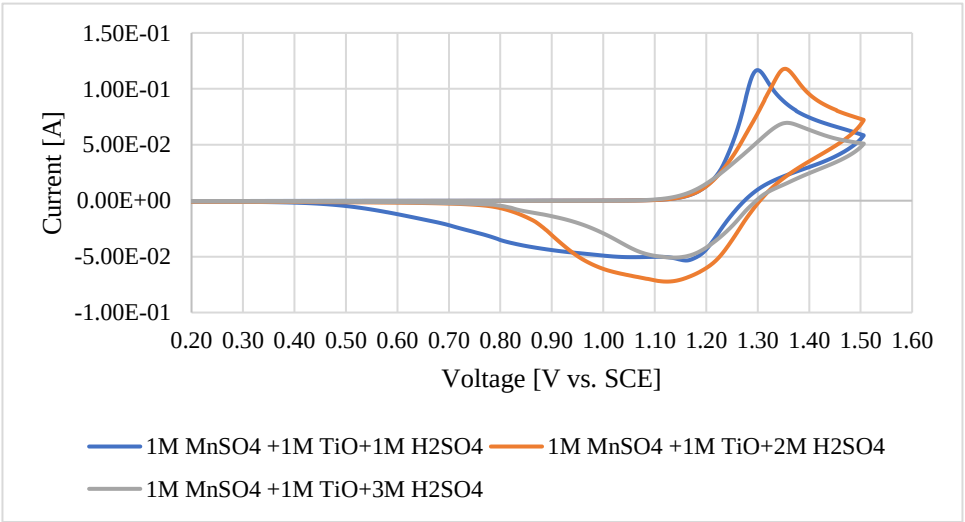

Figure 50. Third cyclic voltammetry scan of 1M $MnSO_4$-1M $TiOSO_4$ in 1M H_2SO_4, 2M H_2SO_4, and 3M M H_2SO_4 on carbon felt working electrode with 2mV/s scan rate

- **Observations from Figures 49 and 50 during the positive scan:**

- During the positive scan, only one single peak is observed in all three tested solutions on a graphite rod working electrode, and on a carbon felt working electrode.
- An anodic current is started to show up after 1.1 V vs SCE for all tested solutions.
- The anodic slope during the anodic scan after 1.2V decreases as the acid concentration increases when using a carbon felt working electrode; while, the anodic slope is almost the same for all tested solution on graphite working electrode.
- The anodic peak currents are observed at 1.31V for 1M H_2SO_4 case, at 1.35V for 2M H_2SO_4, and at 1.36V for 3M H_2SO_4.
- From Figure 49, the peak currents intensity is almost the same for all tested solutions on a graphite rod working electrode.
- From Figure 50, the peak currents intensity is the same for 1M H_2SO_4 and 2M H_2SO_4 cases and lower in the 3M H_2SO_4 case by 37% on a carbon felt working electrode.

- **Observations from Figures 45 and 46 during the negative scan:**

- For 1M H_2SO_4 case, the first peak current is measured at 1.15V when using both the graphite rod and the carbon felt working electrodes. After the first cathodic peak current, a limited current is observed during the negative scan on both working electrodes where the cathodic current decreases to zero current faster in the case with the graphite rod working electrode.
- For 2M H_2SO_4 case, a broad peak current is measured at 1.13V when using both the graphite rod and the carbon felt working electrodes. After the cathodic peak current, a limited current is measured during the negative scan on both working electrodes where the

cathodic current decreases to zero current faster in the case with the graphite rod working electrode.

- For 3M H_2SO_4 case, the first peak current is measured at 1.20V with the graphite rod and at 1.16V with the carbon felt working electrode. After the first cathodic current peak, a smaller limited current is measured during the negative scan on graphite working electrode compared to the carbon felt working electrode. The cathodic current decreases to zero current faster in the case when using the graphite rod working electrode.
- From Figure 49, as the acid concentration increases, the intensity of the first cathodic peak current increases and shifts to the right.
- From Figure 50, the intensity of the first cathodic peak current for 2M H_2SO_4 is higher than the cathodic peak currents intensity of 1M H_2SO_4 and 3M H_2SO_4 cases where their peak currents intensity is similar.

- **Discussion of the effect of the addition of $TiOSO_4$ on $MnSO_4$+H_2SO_4 cyclic voltammetry**

The current-voltage behavior of Figures 49 and 50 is quite similar to the cyclic voltammetry of Mn electrolyte without the addition of $TiOSO_4$ salt in terms of the single anodic peak current and the broadness of the cathodic peak current in different acid concentrations. Based on the theoretical calculation of the Mn^{2+} and H^+ in Mn+Ti electrolyte in Table 14, the addition of $TiOSO_4$ to the $MnSO_4$+H_2SO_4 solutions significantly reduces the H^+ concentration and the Mn^{2+} concentration in the electrolyte compared to Mn solution without Ti.

Based on the observations during the positive scan, the same proposed oxidation mechanism for Mn electrolyte without the addition of Ti may still hold for the Mn electrolyte with the addition of Ti as shown below:

- A proposed oxidation reaction mechanism during the positive scan of the cyclic voltammetry of $MnSO_4$+$TiOSO_4$ in sulfuric acid solution before the peak current is described below.

$$Mn^{2+} \leftrightarrow Mn^{3+} + e^- \qquad E^0 = 1.26\ \text{V vs SCE} \qquad \text{Eq3.31}$$

$$Mn^{3+} + H_2O \leftrightarrow Mn(OH)^{2+} + H^+, \quad \text{K=2.5} \qquad \text{Eq3.14}$$

$$Mn(OH)^{2+} + H_2O \leftrightarrow Mn(OH)_2^+ + H^+, \text{K=0.5} \qquad \text{Eq3.15}$$

$$Mn(OH)_2^+ \leftrightarrow Mn(OH)_2^{2+} + e^-, \quad E^0 = 1.06\ \text{V vs SCE} \qquad \text{Eq3.36}$$

$$Mn(OH)_2{}^{2+} \leftrightarrow (\gamma)MnO_2 + 2H^+ \qquad \text{K=2E+4} \qquad \text{Eq3.26}$$

Overall: $Mn^{2+} + 2H_2O \leftrightarrow (\gamma)MnO_2 + 4H^+ + 2e^-$

- A proposed oxidation reaction mechanism during the positive scan of the cyclic voltammetry of $MnSO_4$+$TiOSO_4$ in sulfuric acid solution after the peak current is described below:

$$Mn^{2+} \leftrightarrow Mn^{3+} + e^- \qquad E^0 = 1.26\ \text{V vs SCE} \qquad \text{Eq3.31}$$

$$Mn^{3+} + H_2O \leftrightarrow Mn(OH)^{2+} + H^+, \quad K=2.5 \qquad \text{Eq3.14}$$

$$Mn(OH)^{2+} + H_2O \leftrightarrow Mn(OH)_2^+ + H^+, \ K=0.5 \qquad \text{Eq3.15}$$

$$Mn(OH)_2{}^+ \leftrightarrow (\gamma)MnOOH + H^+, \ K=0.9059 \qquad \text{Eq3.17}$$

From Figure 49, the anodic peak current intensity of all tested solutions is almost the same with a slight shifting of the anodic peak voltage with increasing the acid concentration. The same intensity of the anodic peak current may due to the low consumption rate of Mn^{2+} by Eq3.31 and the fast MnO_2 build up on the working electrode by Eq3.36. Based on Table 14, as the acid concentration of the electrolyte increases, the Mn^{2+} concentration increases and more Mn^{3+} is generated by Eq3.31, so the oxidation reaction rate of Mn^{2+} to Mn^{3+} is increased with increasing the acid concentration. With the effect of the small area of the graphite rod, the generated Mn^{3+} may hydrolyze to $Mn(OH)_2{}^+$ fast in low acid concentration to be further oxidized to $Mn(OH)_2{}^{2+}$ based on Eq3.36. The fast build of MnO_2 on the graphite rod based on Eq3.14, Eq3.15, and Eq.3.36 compared to the slow oxidation reaction of Mn^{2+} to Mn^{3+} in Eq.3.31 in the case of 1M H_2SO_4 may limit the anodic process and less MnO_2 is formed on the graphite rod for the case 1M H_2SO_4. As the acid concentration increases in the electrolyte solution, the slow accumulation of MnO_2 on the graphite rod based on Eq3.14, Eq3.15, and Eq.3.36 may increase the oxidation reaction of Mn^{2+} to Mn^{3+} in Eq.3.31, so that more Mn^{3+} is formed. As the Mn^{3+} concentration increases, more MnO_2 is built up on the graphite rod by Eq3.14, Eq3.15, and Eq.3.36. However, MnO_2 is built up

on the graphite rod may still be fast in 3M H_2SO_4, so that the anodic process may be still limited by the MnO_2 covering the electrode.

From the negative scan in Figure 49, The first cathodic current wave describes the reduction of MnO_2 deposit to MnOOH based on Eq3.38, and as the acid concentration of the electrolyte solution increases, the first cathodic peak current gets higher which is consistent with the description of the anodic behavior during the positive scan. The second cathodic current wave below 1.15V indicates that the reduction of MnOOH to Mn^{2+} is enhanced by increasing the acid concentration. During the second cathodic peak, a black solid was observed to fall from the graphite rod working electrode which is assumed to be MnOOH that is less adhesive to the MnO_2 substrate. This phenomenon was captured in a video recording during the experiment.

As the electrode area increases in Figure 50, the consumption rate of Mn^{2+} in Eq3.31 is increased and more Mn^{3+} is generated during the anodic scan. The same anodic peak current intensity for 1M H_2SO_4 and 2M H_2SO_4 cases with the low anodic current after the anodic peak current in 1M H_2SO_4 reveals the low concentration of Mn^{2+} which may result in less MnO_2 and MnOOH in the 1M H_2SO_4 case compared to the 2M H_2SO_4 case. In the 2M H_2SO_4 case, as the Mn^{2+} concentration increases, more MnO_2 and MnOOH are formed compared to the 1M H_2SO_4 case where the H^+ concentration is still low based on Table 14, so that the hydrolysis of Mn^{3+} is still fast. This hypothesis can be supported by the magnitude of the cathodic peak current of 1M H_2SO_4 and 2M H_2SO_4 cases where the cathodic peak current during the negative scan of 2M H_2SO_4 is higher than the cathodic peak current of the 1M H_2SO_4 case. For the 3M H_2SO_4 case during the positive scan, the high concentration of H^+ slows the oxidation reaction of Mn(III) to Mn(IV) in Eq3.36 due to the low hydrolysis of Mn^{3+}. This may form less MnO_2 deposit on the electrode surface compared to 1M H_2SO_4 and 2M H_2SO_4 cases as it can be seen from the low cathodic peak

current during the negative scan. The second cathodic wave current shrink and is shifted to the right in 3M H_2SO_4 which indicates that the amount of MnOOH is less on the working electrode as the acid concentration increases.

- **1M Mn+1M Ti+3M H_2SO_4 after cyclic voltammetry experiment on a graphite rod working electrode**

From Figure 51(a), a black solid material was observed in 1M Mn+1M Ti+3M H_2SO_4 solution at the bottom of the cell after the cyclic voltammetry. The electrolyte color was changed to dark purple color after the cyclic voltammetry. When the solution is stirred, the black shadow material at the bottom of the vial is disappeared and mix with the solution as shown in Figure 51(b). When a 3 ml of the tested electrolyte after the cyclic voltammetry is mixed with a 3 ml of DI water in a separate vial, a brown solid material is observed to precipitate within approximately 2min and the dark purple color disappeared as shown in Figure 51(c)

(a) (b) (c)

Figure 51. 1M Mn-3M H_2SO_4 solution after the cyclic voltammetry experiment on graphite rod working electrode, (a) before stirring, (b) after stirring, and (c) after mixing with DI water.

The dark purple color and the dark black solid in 1M Mn+1M Ti+3M H_2SO_4 solution after the cyclic voltammetry are believed to be Mn(III) aqueous species in equilibrium with MnOOH resulted after the anodic peak current. This hypothesis may be supported by Figure 51(c) that after increasing the pH of the electrolyte by diluting the electrolyte with DI water, Mn(III) species formed MnO_2 solid precipitate which has a brown color by the disproportionation reaction as shown in Eq3.44 and Eq3.46.

$$(\gamma)\mathrm{MnOOH} + \mathrm{Mn^{3+}} \leftrightarrow \mathrm{Mn^{2+}} + \mathrm{H^{+}} + (\alpha)\mathrm{MnO_2}, \quad \mathrm{K=1.3\ E+7} \qquad \text{Eq3.44}$$

$$(\alpha)\mathrm{MnOOH} + \mathrm{Mn^{3+}} \leftrightarrow \mathrm{Mn^{2+}} + \mathrm{H^{+}} + (\gamma)\mathrm{MnO_2}, \mathrm{K=2.5E+7} \qquad \text{Eq3.46}$$

- **Observation of the graphite working electrode after the cyclic voltammetry of 1M Mn+3M H_2SO_4 solution**

A black solid deposit was found on the graphite rod working electrode surface after the cyclic voltammetry test in 1M Mn+3M H_2SO_4. This black material may due to the reduction of MnO_2 solid in Eq3.38 to form MnOOH that is less electrochemically active as shown in Figure 52.

Figure 52. Graphite working electrode after the cyclic voltammetry of 1M Mn-3M H_2SO_4 solution

- **Comparison of the cyclic voltammetry of $MnSO_4$ in 1M H_2SO_4 with and without $TiOSO_4$ addition**

The Mn^{2+} concentration is four times less, and the H^+ concentration is three times less when Ti is added to the solution than the one without the addition of Ti based on Table 8 and Table 14**.** Eq3.31 reduction potential is expected to be positively shifted according to the Nernst equation with the decrease of Mn^{2+}. The equilibrium reaction in Eq3.14 and Eq3.15 is expected to be favored toward the hydrolysis of Mn^{3+} as the H^+ decreases based on Le Châtelet's principle. Since the overall chemical reaction of Eq3.14 and Eq3.15 is second-order depended on the H^+ , the overall anodic process of lowering the concentration of Mn^{2+} and H+ with the addition of Ti in 1M Mn+1M H_2SO_4 solution is dominated by the decrease of H^+ concentrations. Therefore, the overall oxidation reaction is controlled by the hydrolysis of Mn^{3+} species in Eq3.14 and Eq3.15 to form $Mn(OH)_2^+$ that undergoes an oxidation reaction to form $Mn(OH)_2^{2+}$ as described in Eq3.36. Thus, 1M Mn+1M Ti+1M H_2SO_4 is expected to form more MnO_2 deposit during the positive scan compared to the solution without the addition of Ti, as the equilibrium reactions of Eq3.13 and Eq3.14 are shifted toward the products with the low acid concentration of 1M Mn+1M Ti+1M H_2SO_4.

This hypothesis can be supported from Figure 53 where the anodic peak current and the first cathodic peak current of 1M Mn+1M Ti+1M H_2SO_4 are higher than anodic peak current and the first cathodic peak current of 1M Mn+1M H_2SO_4 which indicates that more MnO_2 is formed during the anodic scan in 1M Mn+1M Ti+1M H_2SO_4.

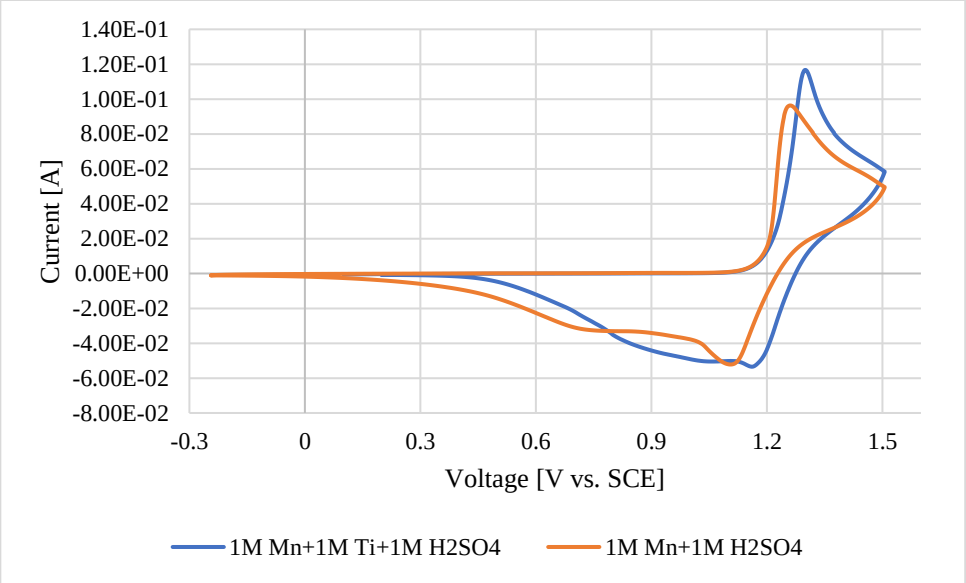

Figure 53. Third cyclic voltammetry scan of 1M $MnSO_4$ with and without 1M $TiOSO_4$ in 1M H_2SO_4 on carbon felt working electrode with 2mV/s scan rate

- **Comparison of the cyclic voltammetry of $MnSO_4$ in 3M H_2SO_4 with and without $TiOSO_4$ addition**

The resulted cyclic voltammetry of 1M Mn+3M H_2SO_4 solution with and without Ti on a carbon felt working electrode shown in Figure 54 matches the one obtained by SEI in terms of the high anodic peak current of the Ti-free solution and the positive shift of the first cathodic peak current when Ti is added. [16] The Mn^{2+} and H^+ concentrations when Ti is added to the 1M Mn+3M H_2SO_4 solution are about half that of the one without the addition of Ti based on Table 8 and Table 14**.** Eq3.31 reduction potential is expected to be positively shifted according to the Nernst equation with the decrease of Mn^{2+}. The equilibrium reaction in Eq3.14 and Eq3.15 is expected to be favored toward the hydrolysis of Mn^{3+} as the H^+ concentration decreases based on Le Châtelet's principle. However, the H^+ concentration in 1M Mn+1M Ti+3M H_2SO_4 is near 1.77M which is high compared to the Mn^{2+} concentration which is about 0.056 M. Therefore, it is assumed that the overall anodic process of lowering the concentration of Mn^{2+} and H^+ with the addition of Ti in 1M Mn+3M H_2SO_4 solution is dominated by the decrease of Mn^{2+} concentration

such that that the overall oxidation reaction is controlled by the oxidation of Mn^{2+} to Mn^{3+} species until it is limited by the diffusion of Mn^{2+} from the bulk to the electrode surface. With less formation of Mn^{3+} in 1M Mn+1M Ti+3M H_2SO_4 solution, the reactions in Eq3.14 and Eq3.15 are expected to form less $Mn(OH)_2^{+}$ that undergoes the oxidation reaction to form $Mn(OH)_2^{2+}$ as described in Eq3.36. Thus, 1M Mn+1M Ti+3M H_2SO_4 is expected to form less MnO_2 deposit during the positive scan compared to the solution without the addition of Ti as the equilibrium reactions of Eq3.13 and Eq3.14 are shifted toward the reactant with the low Mn^{3+} concentration of 1M Mn+1M Ti+3M H_2SO_4.

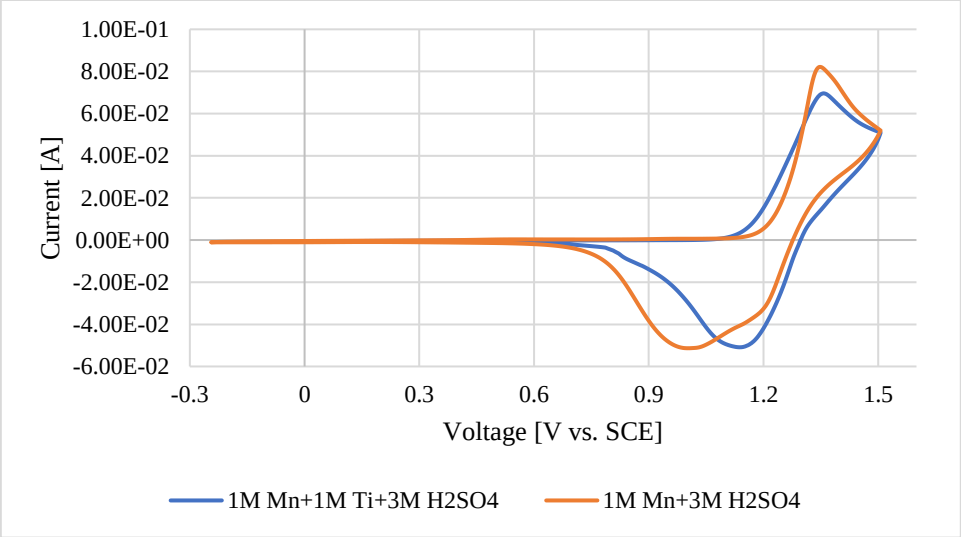

Figure 54. Third cyclic voltammetry scan of 1M $MnSO_4$ with and without 1M $TiOSO_4$ in 3M H_2SO_4 on carbon felt working electrode with 2mV/s scan rate

This hypothesis can be supported from Figure 54 where the anodic peak current of 1M Mn+1M Ti+3M H_2SO_4 is lower than anodic peak current of 1M Mn+3M H_2SO_4 which indicates that less MnO_2 is formed during the anodic scan of 1M Mn+1M Ti+3M H_2SO_4. Regarding the cathodic peak current of 1M Mn+1M Ti+3M H_2SO_4, it is believed that the broad single cathodic peak contains the first and the second cathodic peak currents, and the single cathodic peak becomes broader without the addition of Ti in the solution. Further investigation of the cathodic behavior of 1M Mn+1M Ti+3M H_2SO_4 and 1M Mn+3M H_2SO_4 solutions is shown in the next section.

4.3.2. Anodic Voltage Hold of Mn Electrolyte and the cathodic Linear Voltage Sweep Results

4.3.2.1. Investigating the Nature of Mn Anodic Products in 1M Mn-3M H_2SO_4 Solution with and without the Addition of 1M $TiOSO_4$

The anodic current response with respect to time resulted from holding the voltage at 0.6V vs. SCE for 5min followed by stepping the voltage up to 1.5V vs. SCE for 15min starting at zero time for 1M Mn+3M H_2SO_4 with and without Ti in the solution on a graphite rod working electrodes is shown in Figure 55.

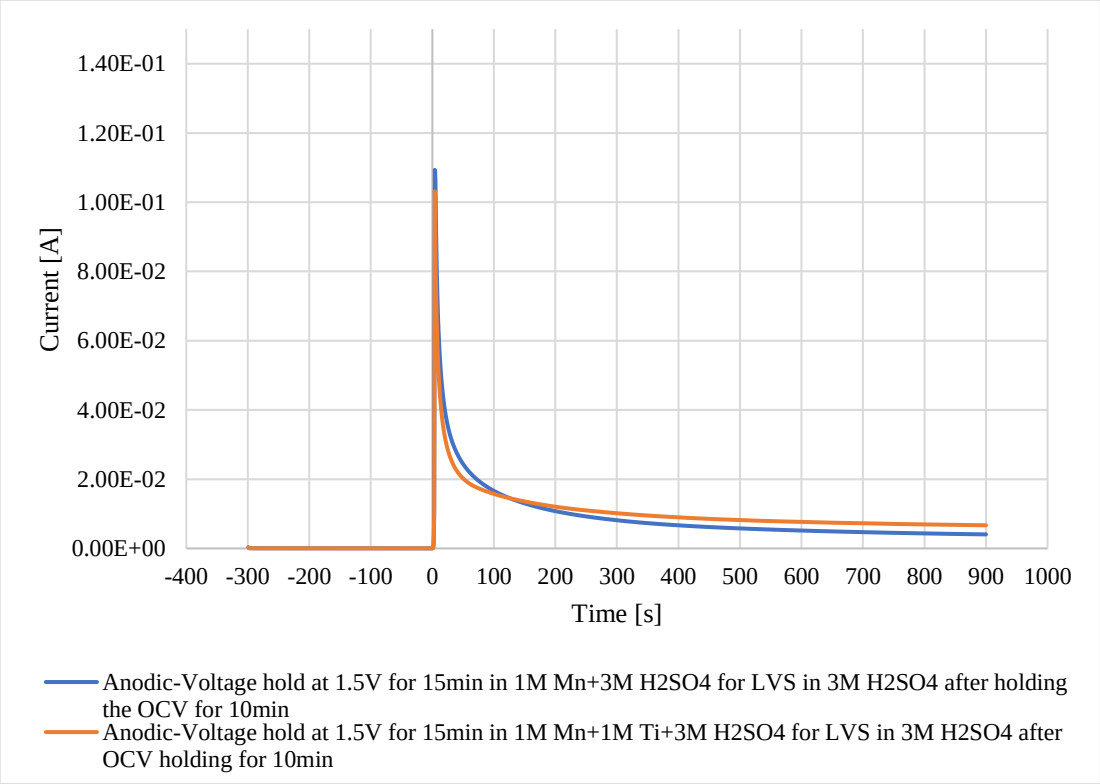

Figure 55. Anodic voltage hold at 1.5V vs. SCE for 15min in 1M Mn-3M H_2SO_4 with and without the addition of Ti in the solution on a graphite rod working electrode

Before the scan, no faradic current is measured because the applied voltage at 0.6V is lower than the minimum voltage requires to oxidize Mn^{2+}. At zero time, a faradic current is measured due to the oxidation reaction of Mn^{2+} as described by Eq2.2, and the anodic current peaks in the two tested Mn solutions due to the large MnO_2 deposit on the electrode surface. After 100s, a limited

anodic current is measured that may be attributed to the oxidation reaction of Mn^{2+} to Mn^{3+} as shown in Eq 3.31. The high anodic limited current in 1M Mn+1M Ti +3M H_2SO_4 indicates that less MnO_2 was deposited on the graphite rod than the solution without Ti. Furthermore, the high limiting anodic current in the Mn+Ti electrolyte may indicate that the Mn^{2+} oxidation reaction to Mn^{3+} in Eq3.31 was enhanced by the hydrolysis of Mn^{3+} to MnOOH in the electrolyte solution in Eq. 3.14, Eq 3.15, Eq.3.17, and Eq.3.18. However, the difference of the two limiting anodic currents are within 2 mA. The amount of the anodic charges resulted from the anodic voltage hold of 1M Mn+3M H_2SO_4 is 8.5C, and the amount of the anodic charges is 9.711C when 1M Ti is added to the solution.

- **Observation of the graphite rod working electrode after the anodic voltage experiment**

A clear solid deposit covering the full surface area of the electrode is observed after the anodic voltage experiment in the two Mn tested solutions as shown in Figure 56 (a) and (b). This deposit is believed to be a mixture of MnO_2 and MnOOH resulted from the oxidation reaction of Mn^{2+} on the working electrode. The solid deposit in Figure 56 (a) has a dark brown color; while, in Figure 56 (b) it is a dark black solid. This may indicate that the solid deposit resulted from Ti-free Mn electrolyte has more MnOOH mixed with the MnO_2 than with Ti.

(a) (b)

Figure 56. Pictures of the surface of the graphite rod working electrode after the anodic voltage hold experiment, (a) in 1M Mn-3M H_2SO_4, (b) in 1M Mn-1M Ti-3M H_2SO_4

The OCV was measured for the tested electrolyte after the anodic voltage hold experiment by using a new clean graphite rod working electrode after the working electrode used for the anodic voltage hold experiment was removed from the solution and the solution was stirred for 2min prior the OCV measurement. The measured OCV of the tested electrolyte shown in Figure 57 describes the equilibrium of the redox couple of Mn^{3+}/Mn^{2+} in the solution based on the Nernst equation of Eq3.31 in Eq4.1.

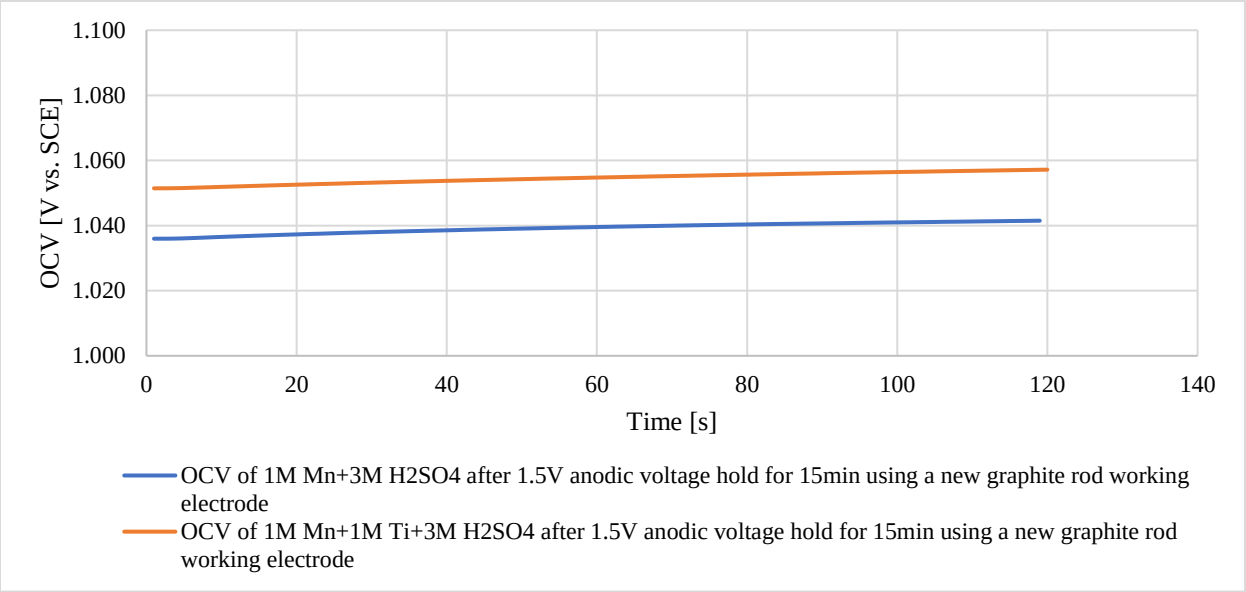

Figure 57. Measured Open Circuit Voltage (OCV) after the anodic voltage hold at 1.5V vs. SCE for 15min in 1M Mn-3M H_2SO_4 with and without the addition of Ti in the solution using a new graphite rod working electrode

The Mn^{3+} concentration can be calculated from Eq4.1 by using the measured OCV and the estimated concentration of Mn^{2+} in 3M H_2SO_4 with and without the addition of Ti in Tables 8 and 14. Based on the estimated Mn^{3+} concentration, the estimated anodic charges generated in the form of Mn^{3+} in the solution is calculated from Eq3.63, and the results are shown in Table 24.

$$Mn^{2+} \leftrightarrow Mn^{3+} + e^- \qquad E^0 = 1.26\ \text{V vs SCE} \qquad \text{Eq3.31}$$

$$C_{Mn^{3+}} = C_{Mn^{2+}}\, e^{\frac{F\left(E_{OCV} - E^0_{\left(\frac{Mn^{3+}}{Mn^{2+}}\right)}\right)}{RT}} \qquad \text{Eq4.1}$$

$$Q_{Mn^{3+}} = C_{Mn^{3+}} V nF \quad \text{Eq3.63}$$

From Table 24, the measured OCV indicates that the concentration of Mn^{3+} in Mn+Ti electrolyte is slightly higher than the one in Mn electrolyte. The estimated anodic charges used to generate Mn^{3+} is significantly low compared to the total anodic charges from the anodic voltage hold of Mn and Mn+Ti electrolyte.

Table 24. Results of the anodic charges in the form of Mn^{3+}in 1M Mn-3M H_2SO_4 with and without the addition of Ti.

Solution	**OCV [V vs. SCE]**	**$C_{Mn^{2+}}$ [Mole/L]**	**$C_{Mn^{3+}}$ [Mole/L]**	**Q_{Mn3+} [C]**
1M Mn+3M H_2SO_4	1.04	0.1099	2.09E-5	0.2
1M Mn+1M Ti+3M H_2SO_4	1.06	0.056	2.32E-5	0.22

The OCV measurements of the two deposited solid on the graphite rod working electrode in a new 3M H_2SO_4 solution show the same values which indicates that the same deposit material was generated during the anodic voltage hold experiment in Mn electrolyte and Mn+Ti electrolyte as shown in Figure 58.

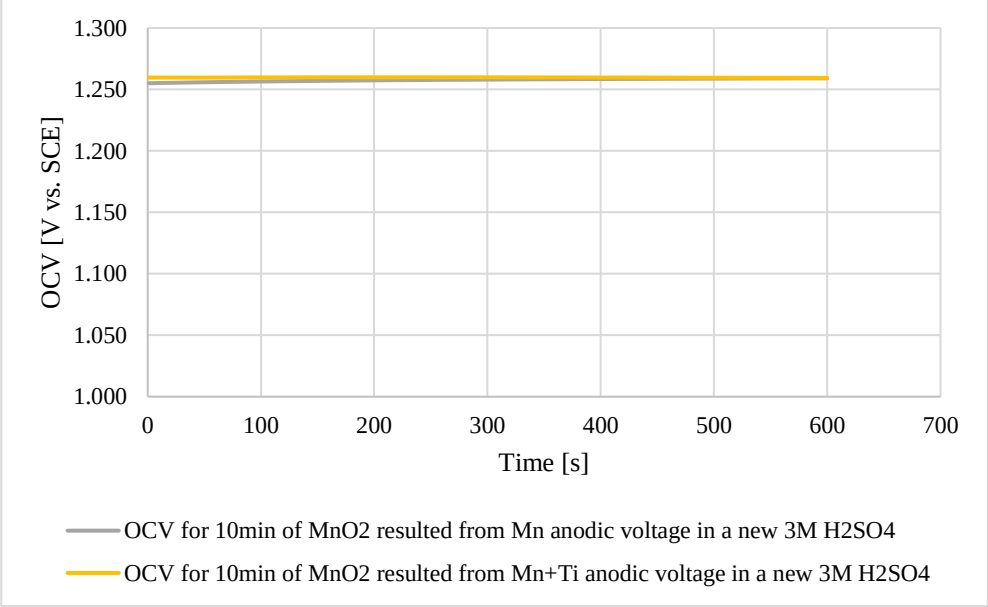

Figure 58. Measured Open Circuit Voltage (OCV) after the anodic voltage hold at 1.5V vs. SCE for 15min in a new 3M H_2SO_4 using the graphite rod working electrode that was used for the anodic voltage hold

From Figure 58, The measured OCV of the deposited solid on the working electrode after the anodic voltage hold experiment describes the equilibrium of the redox couple of MnO_2/MnOOH based on the Nernst equation of Eq3.38. The measured OCV is higher than the reduction potential of Eq 3.38. It is believed that the measured OCV represents the equilibrium potential of the redox reaction of the substrate layer attached on the surface of the working electrode, and based on the proposed mechanism of the oxidation of Mn electrolyte, the deposit layer is dominantly contained MnO_2 solid. Therefore, the measured OCV indicates the high activity of the MnO_2 solid substrate compared to MnOOH.

From Figure 59, the cathodic voltage scan started from the measured OCV for the two tested graphite rods in a new 3M H_2SO_4 solution.

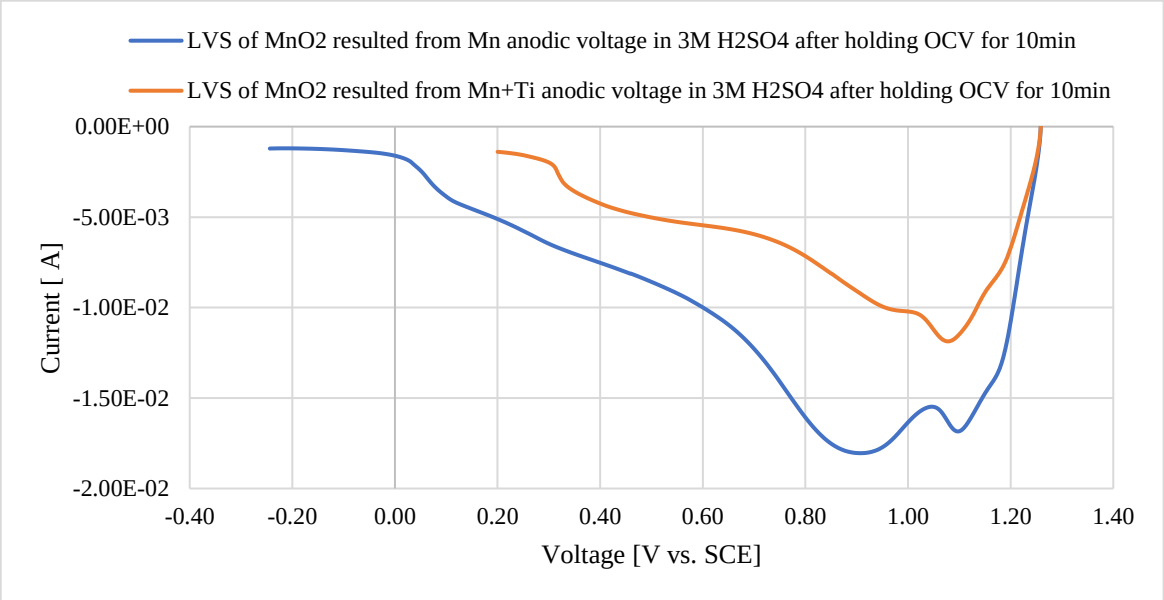

Figure 59. Cathodic linear voltage sweep of MnO_2 substrate resulted from the anodic voltage of Mn electrolyte and Mn-Ti electrolyte in new 3M H_2SO_4 solution at 2mV/s scan rate.

The first cathodic wave current before the cathodic peak current at 1.1V is attributed to the reduction reaction of MnO_2 to MnOOH as described by Eq3.38. The limited cathodic current at 1.1V is believed to result from the negligible availability of MnO_2 substrate on the graphite rod and the large formation of MnOOH. The first cathodic peak current is higher for the substrate

resulted from Mn electrolyte than the substrate resulted from Mn+Ti electrolyte which indicates that large amount of MnO_2 is resulted from the anodic voltage hold of Mn electrolyte due to the high Mn^{2+}concetration.

Regarding the irregular profile of the first cathodic wave current and the second cathodic peak current in Figure 59, it is suggested that the reduction reaction in Eq.3.38 may be affected by the interaction of MnOOH with H^+ during the first cathodic wave. This can be seen from the sudden slope change during the first cathodic wave before reaching the first cathodic peak current. Based on previous studies on the reduction of MnO_2 in sulfuric acid media, the reaction in Eq4.2 was suggested to interfere with the overall reduction of MnO_2 to MnOOH. [23, 45]

$$2MnOOH + 2H^+ \leftrightarrow Mn^{2+} + MnO_2 + 2H_2O \qquad \text{Eq4.2}$$

It is proposed that Eq4.2 is the sum of Eq4.3.a and Eq4.4.a:

$$3H^+ + MnOOH \leftrightarrow Mn^{3+} + 2H_2O \qquad \text{Eq4.3.a}$$

$$Mn^{3+} + MnOOH \leftrightarrow MnO_2 + Mn^{2+} + H^+ \qquad \text{Eq4.4.a}$$

Eq4.3.a may interfere with the reduction reaction of MnO_2 to MnOOH during the first cathodic wave and Eq4.4.a may start after the first cathodic peak current in which the H^+ concentration inside the solid is low. Eq.4.4.a may form more MnO_2 and H^+ inside the solid, so that the reduction reaction of MnO_2 may still proceed after the first cathodic peak as shown in Eq3.38 and a second peak is reached which may indicate the low availability of Mn^{3+} for Eq4.4.a. To confirm this hypothesis, the anodic voltage experiment was repeated in the Mn electrolyte to produce the same amount of the anodic charges generated in Figure 55 and the time of soaking the deposited graphite rod in 3M H_2SO_4 was varied from 5s, 10min, to 1.92hrs before the cathodic

linear voltage sweep experiment. The resulted cathodic voltage sweep of each holding OCV time is shown in Figure 60.

From Figure 60, with more soaking time, MnOOH may dissolve and form Mn^{3+} inside lattice structure of MnO_2, and once the reduction scan is applied, the reduction of MnO_2 to MnOOH is more affected by Eq4.3.a and Eq4.4.a. This can be seen from the intensity of the first cathodic peak current where MnO_2 with 5s OCV holding time is reduced with less interferences from Eq4.3.

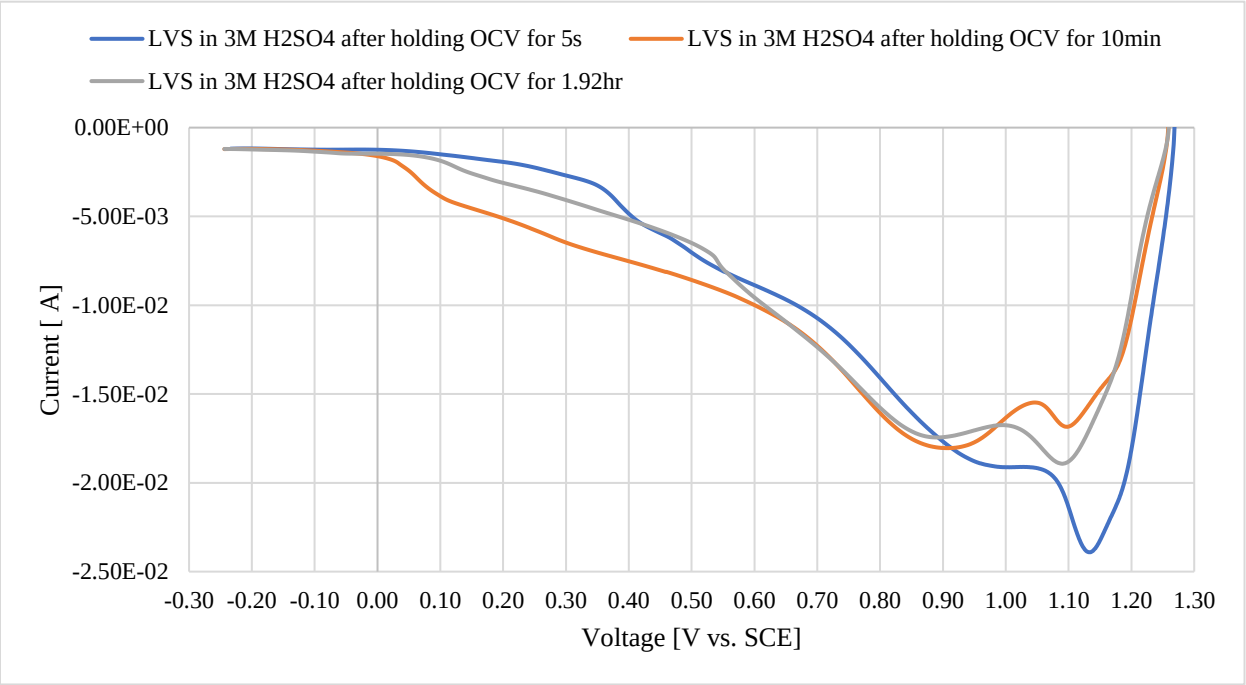

Figure 60. Cathodic linear voltage sweep of MnO_2 substrate resulted from the anodic voltage of Mn electrolyte in new 3M H_2SO_4 solution at 2mV/s scan rate with different OCV holding time.

With 10 min OCV holding time, the first cathodic peak current becomes less due to the high MnOOH interaction with H^+. As the OCV holding time extended to 1.92 hr, MnOOH is dissolved to Mn^{3+} according to Eq4.3, and as the time is extended, Mn^{3+} may react with the MnOOH according to Eq4.4 to generate more MnO_2. This can be seen from the large intensity of the first cathodic peak in the case of holding the OCV for 1.92 hr compared to the 10 min OCV holding time.

Going back to Figure 59, the second cathodic peak current is higher from the MnO_2 deposit resulted from Mn electrode due to the large amount of MnOOH solid formed within the solid of MnO_2 during the anodic voltage hold experiment compared to the Mn+Ti electrolyte anodic voltage hold. Solids fallen from the working electrode was observed below 0.8 V region during the cathodic linear voltage sweep of the two deposited working electrodes as shown in Figure 61.

From Figure 61, below 0.8V applied voltage the reduction of Mn^{3+} to Mn^{2+} may proceed in which it may be controlled by Eq4.3.a Below 0.8 V applied voltage, the amount of MnO_2 is less and more MnOOH is available on the electrode surface. In this case, the reduction of MnOOH can be described based on reaction Eq4.3.a and reaction Eq3.31.

$$3H^+ + MnOOH \leftrightarrow Mn^{3+} + 2H_2O \qquad \text{Eq4.3.a}$$

$$Mn^{3+} + e^- \leftrightarrow Mn^{2+} \qquad E^0 = 1.26\ \text{V vs SCE} \qquad \text{Eq3.31}$$

Figure 61. Fallen solids observed during the LVS in 3M H_2SO_4 for MnO_2 resulted from Mn electrolyte anodic voltage experiment

The falling solids at low applied voltage may due to the MnOOH sparingly dissolution and the fast reduction reaction of Mn^{3+} to Mn^{2+} which may cause the detachment of the solids from the working electrode surface. The recovered anodic charges are estimated by integrating the area of the cathodic current of Figure 59 with time. The percentages of the cathodic charges from Figure 59 to the anodic charges generated during the anodic voltage in Figure 55 are 79% for MnO_2

deposit resulted from Mn electrolyte and 35% for MnO_2 deposit resulted from Mn+Ti electrolyte. It is believed that negligible anodic charges were generated in the form of Mn^{3+} in the solution after the anodic voltage hold. The remaining anodic charges may be in the form of MnOOH solid that fell into and was therefore inaccessible for reaction at the working electrode.

4.3.2.2. Linear Voltage Sweep Results of Mn Anodic Products in Different Solutions on a Graphite Rod Working Electrode

Figure 62 shows the anodic current response with respect to time resulted from holding the voltage at 0.6V vs. SCE for 5min followed by stepping the voltage up to 1.5V vs. SCE and holding it for 15min starting at zero time for 1M Mn+3M H_2SO_4 solution on a graphite rod working electrode. The generated anodic charges in the form of solid deposit on the working electrode are planned to be investigated by cathodic linear voltage sweep in a new in 3M H_2SO_4 solution.

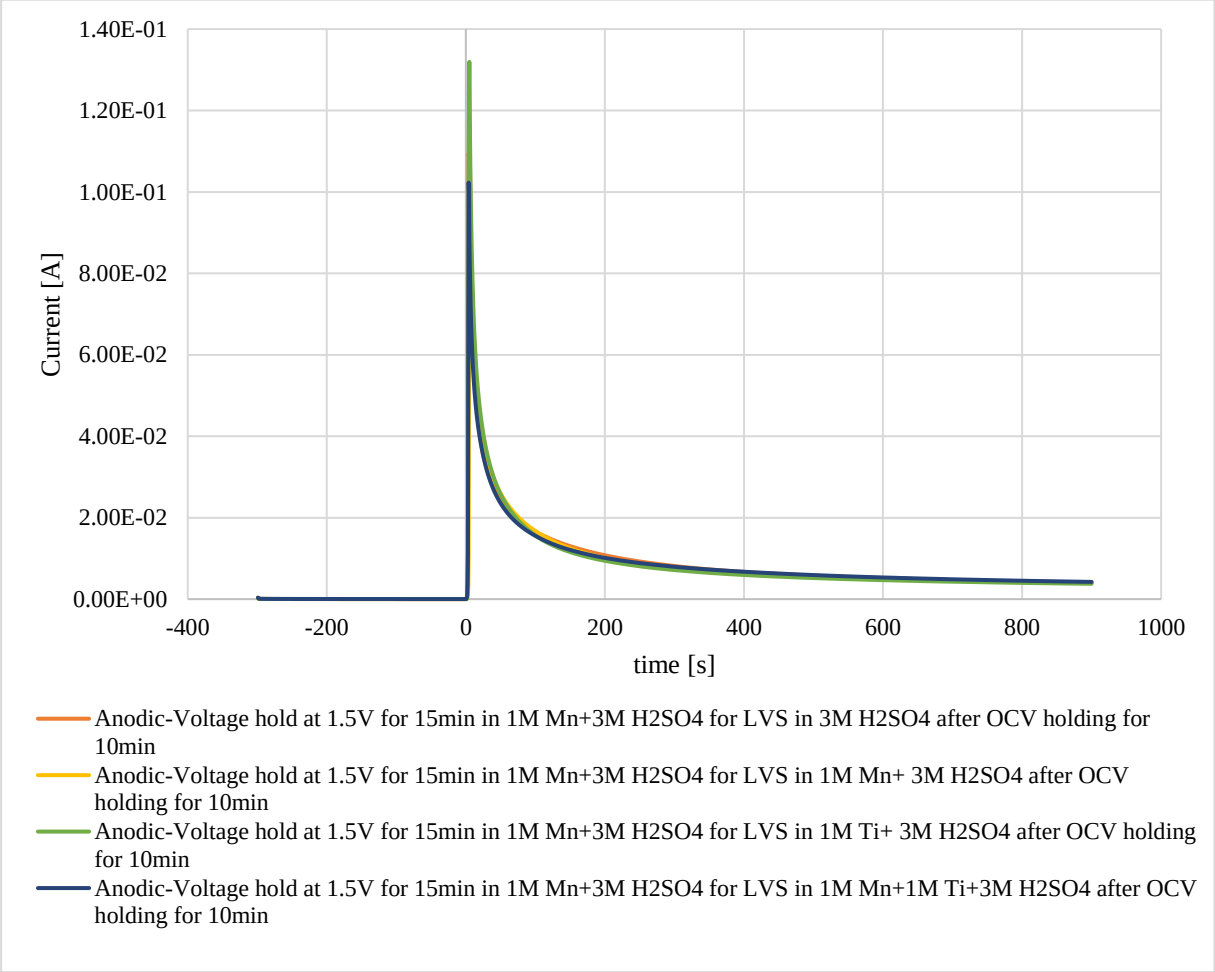

Figure 62. Anodic voltage hold at 1.5V vs. SCE for 15min in 1M Mn-3M H_2SO_4 on a graphite rod working electrode planned to be investigated by cathodic linear voltage in 1M Mn-3M H_2SO_4, 1M Ti-3M H_2SO_4,1M Mn-1M Ti-3M H_2SO_4, and in 3M H_2SO_4 solutions.

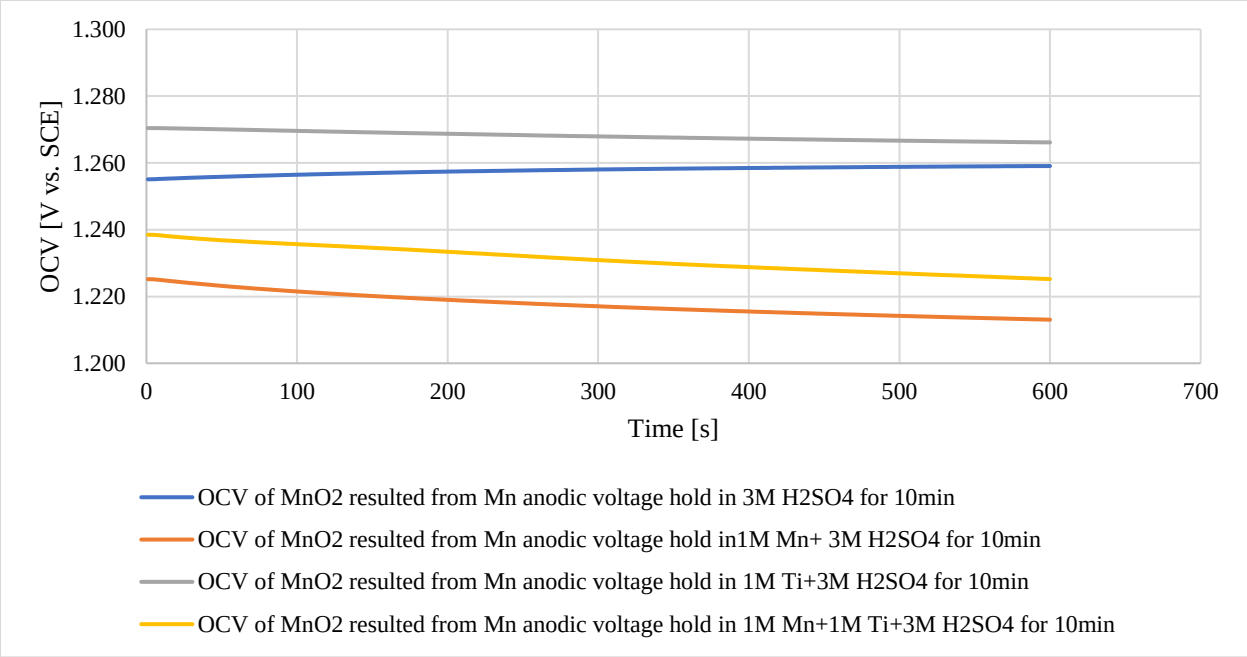

Figure 63. Measured Open Circuit Voltage (OCV) of the solid deposit on the graphite rod working electrode resulted from the anodic voltage hold of Mn electrolyte in a new 1M Mn-3M H_2SO_4, 1M Ti-3M H_2SO_4,1M Mn-1M Ti-3M H_2SO_4, and in 3M H_2SO_4 solutions.

From the Figure 63, the OCV of the substrate on the graphite rod working electrode is the highest in 1M Ti+3M H_2SO_4 and 3M H_2SO_4 solutions and the lowest in 1M Mn+3M H_2SO_4 and 1M Mn+1M Ti+3M H_2SO_4 solutions. The measured OCV of the deposited solid on the working electrode after the anodic voltage hold experiment describes the equilibrium of the redox couple of MnO_2/MnOOH based on the Nernst equation of Eq3.38. The low value of the OCV in 1M Mn+3M H_2SO_4 and 1M Mn+1M Ti+3M H_2SO_4 solutions is because of the comproportionation reaction of Mn^{2+} and MnO_2 substrate as shown in Eq4.4.b that forms Mn^{3+} and MnOOH on the substrate.

$$MnO_2 + Mn^{2+} + H^+ \leftrightarrow Mn^{3+} + MnOOH \qquad \text{Eq4.4.b}$$

Photographs were taking of the graphite rod during the OCV measurement in 3M H_2SO_4, 1M Mn+3M H_2SO_4 and 1M Mn+1M Ti+3M H_2SO_4 solutions, and they are shown in Figure 64.

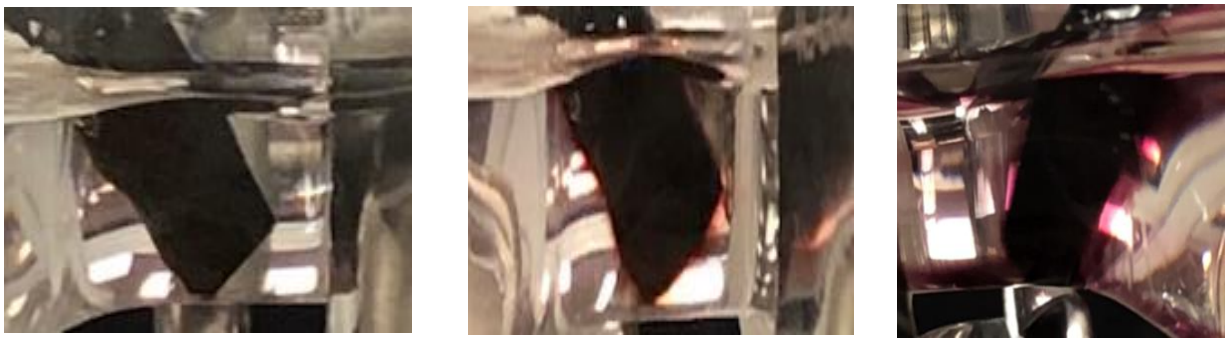

(a) (b) (c)

Figure 64. Photographs of the surface of the graphite rod working electrode after the anodic voltage hold during OCV measurement in (a) 3M H_2SO_4, (b) in 1M Mn-3M H_2SO_4, and (c) 1M Mn-1M Ti-3M H_2SO_4

From Figure 64, in (a), no change in solution color is observed, in (b), the observed color next to the working electrode is turned into red brown surrounding the surface, and in (c), the observed color next to the working electrode is turned into purple mixed with black region near the surface with accumulation of black materials at the bottom of the solution. Based on the observations in Figure 64, comproportionation reaction may form aqueous Mn^{3+} species, and the Mn^{3+} species may be in equilibrium with the Mn^{2+} and MnO_2 in Eq4.4.b due to the high H^+ concentration in 1M Mn+3M H_2SO_4; while, comproportionation reaction of Mn^{2+} in 1M Mn+Ti+3M H_2SO_4 may form aqueous Mn^{3+} species, and the resulted Mn^{3+} species may undergo a significant hydrolysis based on Eq4.3.b to form MnOOH in the solution due to the low H^+.

$$Mn^{3+} + 2H_2O \leftrightarrow 3H^+ + MnOOH \qquad \text{Eq4.3.b}$$

Precipitation of MnOOH in the solution in the case of 1M Mn+Ti+3M H_2SO_4 may sustain Eq4.4.b and may result in losing the anodic charges in the solution in the form of MnOOH solid.

From Figure 65, the cathodic voltage scan starts from the measured OCV for the deposited graphite rod in a new 1M Mn+3M H_2SO_4, 1M Ti+3M H_2SO_4, 1M Mn+1M Ti+3M H_2SO_4, and 3M H_2SO_4 solutions. The first cathodic wave current before the cathodic peak current at 1.1-1.15V is attributed to the reduction reaction of MnO_2 to MnOOH as described by Eq3.38. The limited

cathodic current at 1.1-1.15V is believed to result from the negligible availability of MnO_2 substrate on the graphite rod and the large formation of MnOOH.

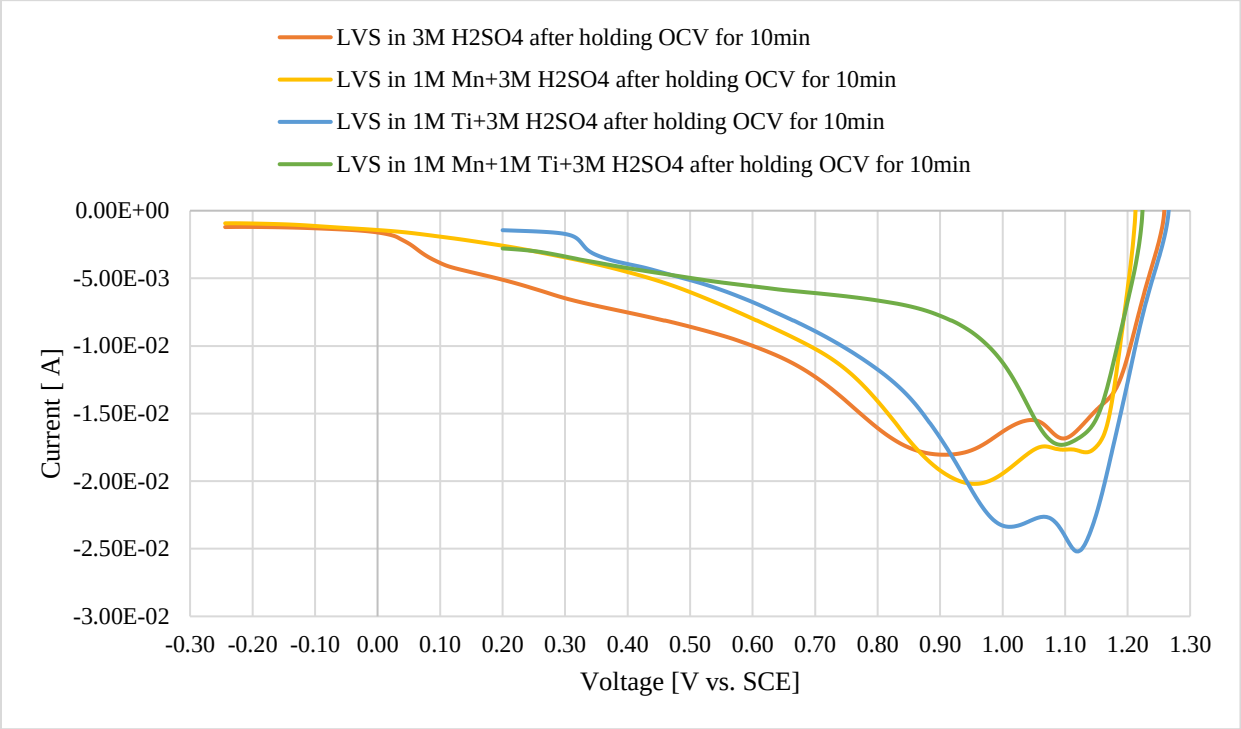

Figure 65. Cathodic linear voltage sweep of MnO_2 substrate resulted from the anodic voltage hold of Mn electrolyte in a new 1M Mn-3M H_2SO_4, 1M Ti-3M H_2SO_4, 1M Mn-1M Ti+3M H_2SO_4, and 3M H_2SO_4 solutions at 2mV/s scan rate.

The intensity of the first cathodic peak current is the highest when the MnO_2 substrate is reduced in 1M Ti+3M H_2SO_4, and the lowest when the MnO_2 substrate is reduced in 1M Mn+1M Ti+3M H_2SO_4, or 3M H_2SO_4. Based on Table 13, the H^+ concentration in 1M Ti+3M H_2SO_4 is lower than 1M Mn+3M H_2SO_4, and 3M H_2SO_4 solutions. Therefore, the interference of Eq4.3.a on the reduction reaction of MnO_2 to MnOOH in Eq3.38 is suppressed, so the first cathodic wave current is enhanced. However, the small observed limited cathodic current after the first cathodic peak indicates that a negligible amount of Mn^{3+} is formed inside the solid structures and a small amount of MnO_2 is formed by Eq4.4.a.

When the cathodic voltage scan of MnO_2 substrate takes place in 1M Mn+1M Ti+3M H_2SO_4 solution, the H^+ concentration in this solution is close to the solution without the addition of Mn^{2+}. Therefore, the interference of Eq4.3.a on the reduction reaction of MnO_2 to MnOOH in Eq3.38 is expected to be suppressed. However, the comproportionation reaction of Mn^{2+} in low H^+ concentration consumes some of the MnO_2 substrate and leads to a low cathodic peak current compared to the cathodic voltage scan of 1M Ti+3M H_2SO_4 solution. The second cathodic peak during the cathodic scan of 1M Mn+1M Ti+3M H_2SO_4 disappears which indicates the low possibility of forming a stable aqueous Mn^{3+} species inside the solid substrate by Eq4.3.a.

Regarding the cathodic voltage scan in the free-Ti solution, the high H^+ of 3M H_2SO_4 solution leads to a significant interference of Eq4.3.a on the reduction reaction of MnO_2 to MnOOH, and that leads to a low cathodic peak current of MnO_2 reduction. In 1M Mn+3M H_2SO_4 solution, the H^+ concentration is slightly less than the H+ concentration in 3M H_2SO_4 solution. Therefore, the interference of Eq4.3.a on the reduction reaction of MnO_2 to MnOOH in Eq3.38 is expected to be less. In addition to H^+, with the presence of Mn^{2+} species in contact with the MnO_2 substrate, the comproportionation reaction of Mn^{2+} in Eq4.4.b generates Mn^{3+} aqueous species, and with the high H^+ concentration, the hydrolysis of Mn^{3+} to MnOOH in Eq4.3.b is suppressed, so that the Mn^{3+} is at equilibrium in Eq4.4.b. The generated Mn^{3+} aqueous species is consumed by Eq4.4.a on the MnOOH substrate to form more MnO_2 solid on the working electrode, followed by the reduction reaction of MnO_2 during the second cathodic peak. The second cathodic peak current is high in 1M Mn+3M H_2SO_4 compared to the 3M H_2SO_4 solution because of the high concentration of Mn^{3+} species resulted from the comproportionation reaction in Eq4.4.b.

The estimated percentage of the cathodic charges of MnO_2 substrate resulted from Mn electrolyte anodic voltage hold during the cathodic linear voltage scan in the four new solutions relative to the generated anodic charges is shown in Table 25.

Table 25. Estimated percentage of the cathodic charges of MnO_2 substrate resulted from Mn electrolyte anodic voltage hold during the cathodic linear voltage scan in different solutions relative to the generated anodic charges.

Solution	Anodic charges [C]	Cathodic charges [C]	%Cathodic charges/anodic charges
CLVS in 1M Mn+3M H_2SO_4	8.340 C	-5.868 C	70.359%
CLVS in 3M H_2SO_4	8.501 C	-6.716 C	79.002%
CLVS in 1M Ti+3M H_2SO_4	8.216 C	-5.788 C	70.448%
CLVS in 1M Mn+1M Ti+3M H_2SO_4	8.284 C	-3.755 C	45.328%

From Table 25, more of the MnO_2 substrate resulted from the anodic voltage hold of Mn electrolyte is recovered during the cathodic linear voltage sweep in 3M H_2SO_4, by almost 79% due to the high dissolution of MnOOH in Eq4.3.a. In 1M Mn+3M H_2SO_4 the recovery of the cathodic charges of the MnO_2 substrate is about 70% which is less than 3M H2SO4 because of the Mn^{2+} comproportionation reaction that may remove some of the MnO_2 substrate. However, the overall recovery of the MnO_2 substrate in 1M Mn +3M H_2SO_4 solution is believed to be not significantly affected by the comproportionation reaction due to the possibility of forming aqueous Mn^{3+} that is in equilibrium with the MnO_2 substrate near the solution side.

The recovery of the cathodic charges of the MnO_2 substrate in 1M Ti+3M H_2SO_4 solution is almost the same of the recovery in 1 M Mn+3M H_2SO_4. The reduction reaction of MnO_2 to MnOOH is observed to be enhanced based on the intensity of the first cathodic peak current in Figure 65; however, it is believed that the low recovery of the cathodic charges in 1M Ti+3M H_2SO_4 compared to the 3M H_2SO_4 is due to the low dissolution reaction of MnOOH in Eq4.3.a because of the low H^+ and the substrate falling from the working electrode at low applied voltage. The recovery of the cathodic charges of the MnO_2 substrate in 1M Mn+1M Ti +3M H_2SO_4 solution

is highly affected by the comproportionation reaction in Eq4.4.b due to the low H^+ concentration that allows the Mn^{3+} to precipitate to MnOOH as shown in Eq4.3.b. As a result, MnO_2 cathodic charges is believed to be lost in the solution in the form of MnOOH falling off the working electrode.

4.3.2.3. Linear Voltage Sweep Results of Mn-Ti Anodic Products in Different Solutions on a Graphite Rod Working Electrode

The anodic current response with respect to time resulted from holding the voltage at 0.6V vs. SCE for 5min followed by stepping the voltage up to 1.5V vs. SCE and holding it for 15min starting at zero time for 1M Mn+1M Ti+3M H_2SO_4 solution on a graphite rod working electrode is shown in Figure 66.

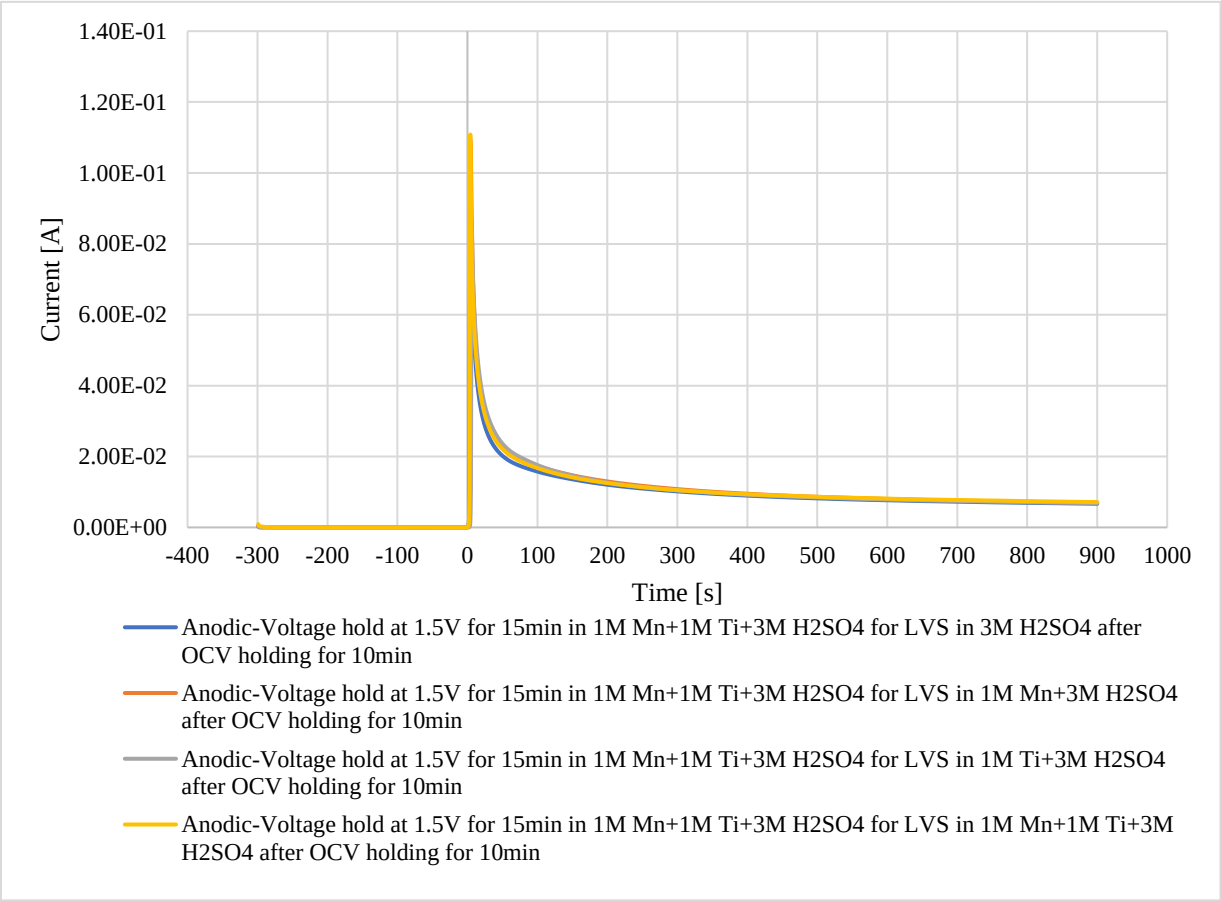

Figure 66. Anodic voltage hold at 1.5V vs. SCE for 15min in 1M Mn-1M Ti+3M H_2SO_4 on a graphite rod working electrode planned to be investigated by cathodic linear voltage in 1M Mn-3M H_2SO_4, 1M Ti-3M H_2SO_4,1M Mn-1M Ti-3M H_2SO_4, and in 3M H_2SO_4 solutions.

The average amount of the anodic charges resulted from the four anodic voltage hold of 1M Mn+3M H_2SO_4 experiments is 10.17C. The generated anodic charges in the form of solid deposit on the working electrode are planned to be investigated by cathodic linear voltage sweep in a new 1M Mn+3M H_2SO_4, 1M Ti+3M H_2SO_4, 1M Mn+1M Ti+3M H_2SO_4, and 3M H_2SO_4 solutions.

From Figure 67, the OCV of the substrate on the graphite rod working electrode is the highest in 1M Ti+3M H_2SO_4 and 3M H_2SO_4 solutions and the lowest in 1M Mn+3M H_2SO_4 and 1M Mn+1M Ti+3M H_2SO_4 solutions. The measured OCV of the deposited solid on the working electrode after the anodic voltage hold experiment describes the equilibrium of the redox couple of MnO_2/MnOOH based on the Nernst equation of Eq3.38. The low value of the OCV in 1M Mn+3M H_2SO_4 and 1M Mn+1M Ti+3M H_2SO_4 solutions is because of the comproportionation reaction of Mn^{2+} and MnO_2 substrate as shown in Eq4.4.b that forms Mn^{3+} and MnOOH on the substrate.

$$MnO_2 + Mn^{2+} + H^+ \leftrightarrow Mn^{3+} + MnOOH \qquad \text{Eq4.4.b}$$

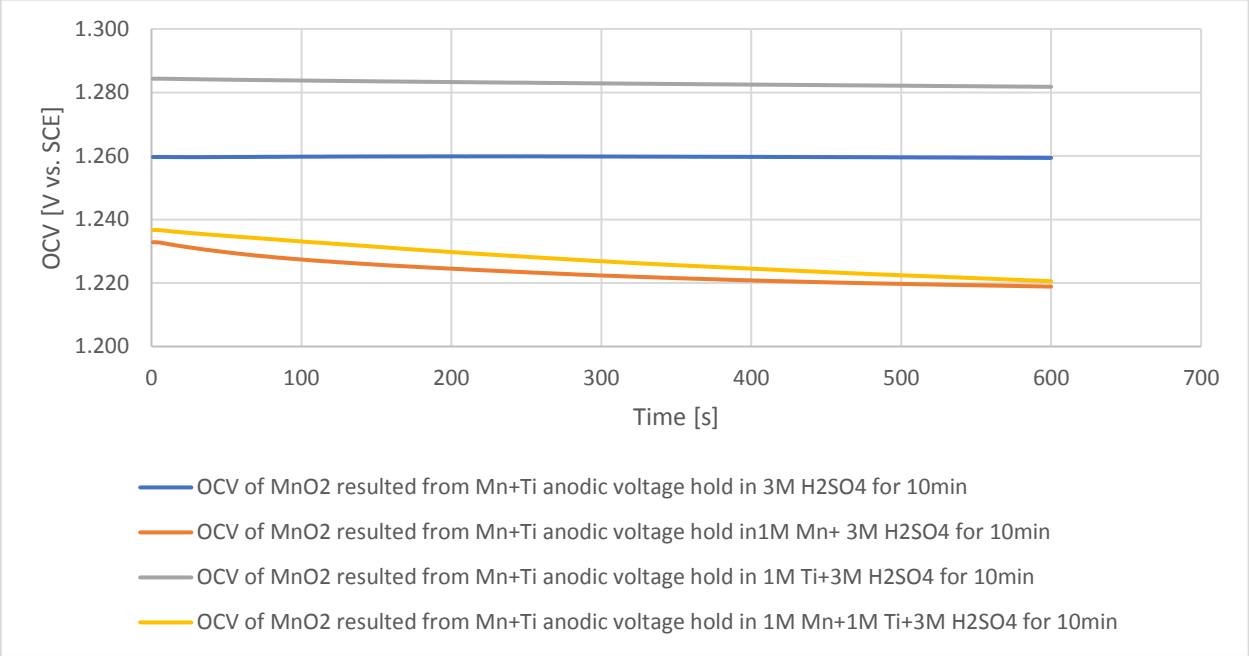

Figure 67. Measured Open Circuit Voltage (OCV) of the solid deposit on the graphite rod working electrode resulted from the anodic voltage hold of Mn-Ti electrolyte in a new 1M Mn-3M H_2SO_4, 1M Ti-3M H_2SO_4,1M Mn-1M Ti-3M H_2SO_4, and in 3M H_2SO_4 solutions.

All the measured OCV of the MnO_2 substrate resulted from Mn+Ti electrolyte in Figure 67 are shifted to a more positive voltages compared to the measured OCV values of the MnO_2 substrate resulted from Mn electrolyte anodic voltage in Figure 63. The higher OCV value indicates that the anodic products on the graphite rod working electrode resulted from Mn+Ti has

less MnOOH compared to the anodic products on the graphite rod working electrode resulted from Mn electrolyte.

Figure 68 shows the cathodic voltage scan started from the measured OCV for the deposited graphite rod in a new 1M Mn+3M H_2SO_4, 1M Ti+3M H_2SO_4, 1M Mn+1M Ti+3M H_2SO_4, and 3M H_2SO_4 solutions. The first cathodic wave current before the cathodic peak current at 1.1-1.15V is attributed to the reduction reaction of MnO_2 to MnOOH as described by Eq3.38. The limited cathodic current at 1.1-1.15V is believed to result from the negligible availability of MnO_2 substrate on the graphite rod and the large formation of MnOOH.

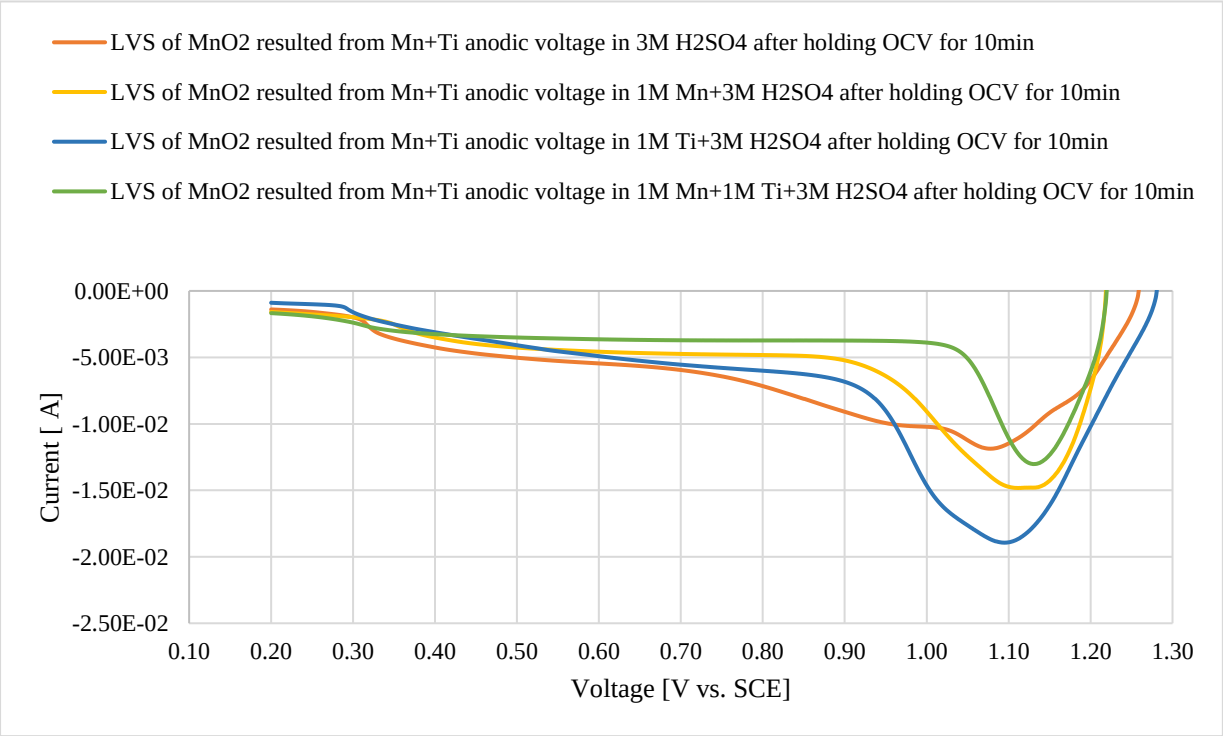

Figure 68. Cathodic linear voltage sweep of MnO_2 substrate resulted from the anodic voltage of Mn+TI electrolyte in a new 1M Mn-3M H_2SO_4, 1M Ti-3M H_2SO_4,1M Mn-1M Ti-3M H_2SO_4, and in 3M H_2SO_4 solutions at 2mV/s scan rate.

Figure 68 shows a similar trend to the one observed in Figure 65 in term of the intensity of the first cathodic peak current in different solutions. The highest first cathodic peak is when the MnO_2 substrate is reduced in 1M Ti+3M H_2SO_4, and the lowest when the MnO_2 substrate is

reduced in 3M H_2SO_4. However, the second cathodic peak current in 1M Mn+3M H_2SO_4 and 3M H_2SO_4 solutions is less compared to the second cathodic peak current of the substrate resulted from Mn electrolyte in Figure 65. This may indicate that less MnOOH may form on the graphite rod working electrode during the anodic voltage hold of Mn+Ti electrolyte. The estimated percentage of the reduced cathodic charges of MnO_2 substrate resulted from Mn+Ti electrolyte anodic voltage hold during the cathodic linear voltage scan in the four new solutions relative to the generated anodic charges is given on Table 26.

Table 26. Estimated percentage of the reduced cathodic charges of MnO_2 substrate resulted from Mn-Ti electrolyte anodic voltage hold during the cathodic linear voltage scan in different solutions relative to the generated anodic charges.

Solution	Anodic charges [C]	Cathodic charges [C]	%Cathodic charges/anodic charges
CLVS in 1M Mn+3M H_2SO_4	10.49 C	-3.004 C	28.6%
CLVS in 3M H_2SO_4	9.711C	-3.383 C	34.8%
CLVS in 1M Ti+3M H_2SO_4	10.19 C	-3.805 C	37.3%
CLVS in 1M Mn+1M Ti+3M H_2SO_4	10.29 C	-2.230 C	21.7%

From Table 26, the MnO_2 substrate resulted from the anodic voltage hold of Mn+Ti electrolyte is recovered during the cathodic linear voltage sweep in 1M Ti+3M H_2SO_4 by almost 37% due to the low H^+ concentration that helps to minimize the interference of MnOOH dissolution reaction in Eq4.3.a. In 1M Mn+3M H_2SO_4 the recovery of the cathodic charges of the MnO_2 substrate is about 28.6% which is less than 3M H_2SO_4 because of the Mn^{2+} comproportionation reaction that may consume some of the MnO_2 substrate. However, the overall recovery of the MnO_2 substrate in 1M Mn+3M H_2SO_4 solution is believed to be not significantly affected by the comproportionation reaction due to the possibility of forming aqueous Mn^{3+} that is in equilibrium with the MnO_2 substrate near the solution side.

The recovery of the cathodic charges of the MnO_2 substrate in 1M Mn+1M Ti+3M H_2SO_4 solution is highly affected by the comproportionation reaction in Eq4.4.b due to the low H^+

concentration that allows the Mn^{3+} to precipitate to MnOOH as shown in Eq4.3.b. As a result, MnO_2 cathodic charges is believed to be lost in the solution in the form of MnOOH falling off the working electrode.

Overall, the low recovery in Table 26 of the anodic substrate resulted from Mn+Ti electrolyte anodic voltage hold compared to the recovery in Table 25 of the anodic substrate resulted from Mn electrolyte anodic voltage is due to the high precipitation rate of MnOOH in the Mn+Ti electrolyte that is caused by the comproportionation reaction in Eq4.4.b. Therefore, less MnO_2 is available on the electrode during the linear voltage in a new solution and less estimated percentage recovery ratio of charges is found.

4.3.2.4. Linear Voltage Sweep Results of Mn and Mn-Ti Anodic Products in 3M H_2SO_4 Solution with and without Convection on a Graphite Rod Working Electrode

The anodic current response with respect to time resulted from holding the voltage at 0.6V vs. SCE for 5min followed by stepping the voltage up to 1.5V vs. SCE and holding it or 15min starting at zero time for 1M Mn+3M H_2SO_4 with and without Ti in the solution on a graphite rod working electrode and with and without convection is shown in Figure 69.

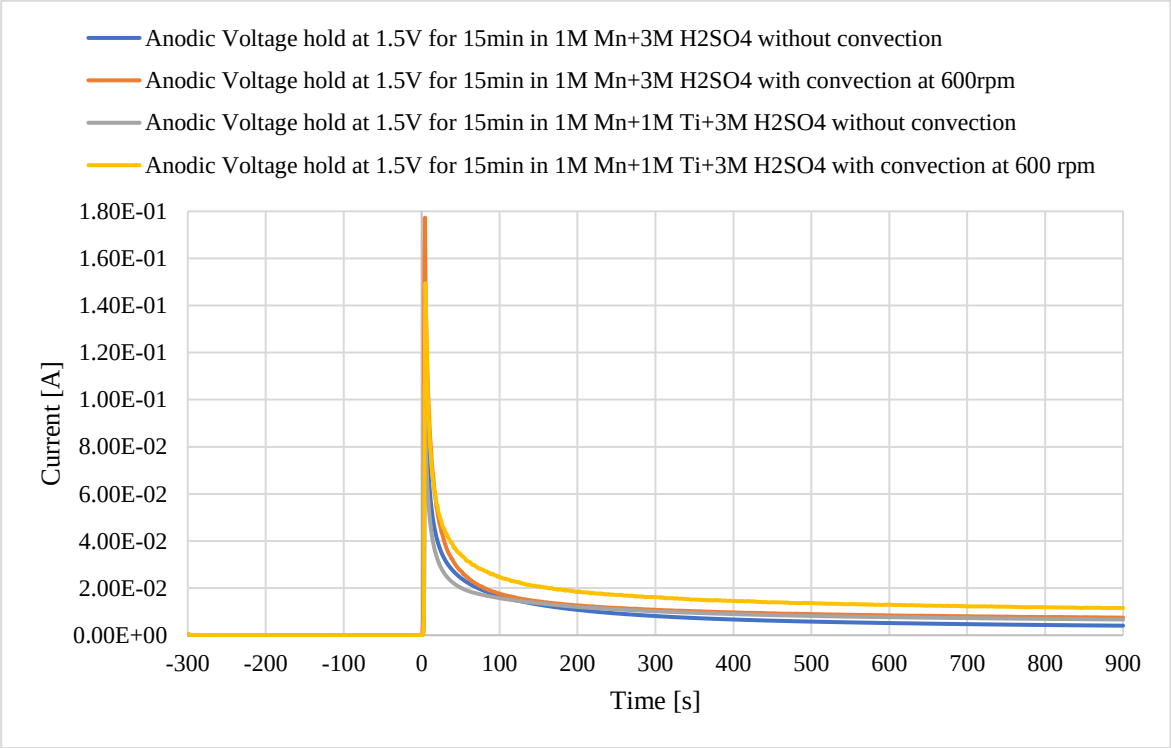

Figure 69. Anodic voltage hold at 1.5V vs. SCE for 15min in 1M M-3M H_2SO_4 and in 1M Mn-3M H_2SO_4 on a graphite rod working electrode with and without convection planned to be investigated by cathodic linear voltage in 3M H_2SO_4 solution

Before scanning, no faradic current is measured because the applied voltage at 0.6V is lower than the minimum voltage requires to oxidize Mn^{2+}. At zero time when the voltage is raised to 1.5V vs. SCE, a faradic current is measured due to the oxidation reaction of Mn^{2+} as described by Eq2.2, and the anodic current is peaked in the two tested Mn solutions due to the large MnO_2 deposit on the electrode surface. After 100s, a limited anodic current is measured that may be attributed to

the oxidation reaction of Mn^{2+} to Mn^{3+} as shown in Eq 3.31. The high anodic limited current in 1M Mn+1M Ti +3M H2SO4 indicates that less MnO_2 was deposited on the graphite rod than the solution without Ti. In addition, the high limited anodic current in Mn+Ti electrolyte may indicate to that Mn^{2+} oxidation reaction to Mn^{3+} in Eq3.31 was enhanced by the hydrolysis of Mn^{3+} to MnOOH in the electrolyte solution in Eq. 3.14, Eq 3.15, Eq.3.17, and Eq.3.18. When convection is applied during the anodic voltage hold experiment for both Mn electrolyte and Mn+Ti electrolyte, the anodic limited current slightly increases. The low measured effect on the anodic limited current may due to the large MnO_2 deposit on the small graphite rod working electrode.

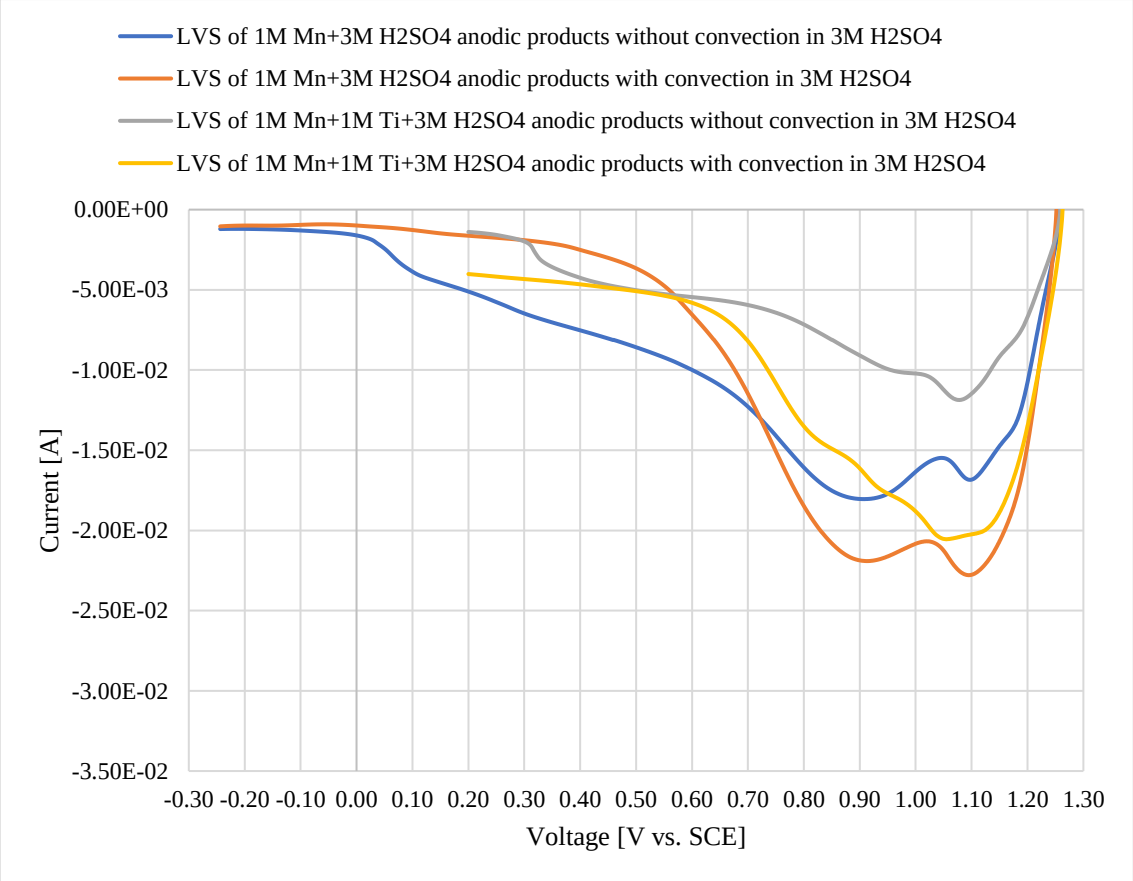

Figure 70. Cathodic linear voltage sweep of MnO_2 substrate on graphite rod working electrode resulted from the anodic voltage of Mn electrolyte and Mn-Ti electrolyte with and without convection in a new 3M H_2SO_4 solutions at 2mV/s scan rate after holding the OCV for 10min.

From Figure 70, the cathodic voltage scan is started from the measured OCV for the four tested graphite rods in a new 3M H_2SO_4 solution. The first cathodic wave current before the

cathodic peak current at 1.1V is attributed to the reduction reaction of MnO_2 to MnOOH as described by Eq3.38. The limited cathodic current at 1.1V is believed to result from the negligible availability of MnO_2 substrate on the graphite rod and the large formation of MnOOH. The first cathodic peak current is higher for the substrate resulted from Mn electrolyte than the substrate resulted from Mn+Ti electrolyte which indicates that large amount of MnO_2 is resulted from the anodic voltage hold of Mn electrolyte due to its high Mn^{2+}concetration.The first cathodic peak current of the MnO_2 substrate resulted from the anodic voltage hold of Mn electrolyte and Mn+Ti electrolyte with convection increases which indicates that more MnO_2 is formed on the working electrode during the anodic voltage hold with convection in both electrolytes due to the increase of the transport of Mn^{2+} species from the bulk to the electrode surface which may increase the rate of the oxidation reaction in Eq 3.31.

The percentage of the reduced cathodic charges of MnO_2 substrate resulted from Mn electrolyte and Mn+Ti electrolyte anodic voltage hold with and without convection during the cathodic linear voltage scan in a new 3M H_2SO_4 solution relative to the generated anodic charges is given in Table 27. The percentage recovery of the MnO_2 substrate resulted from the anodic voltage hold of Mn+Ti electrolyte without convection is almost the same to the percentage recovery of the MnO_2 substrate resulted from the anodic voltage hold of Mn+Ti electrolyte with convection. However, the percentage recovery of the MnO_2 substrate resulted from the anodic voltage hold of Mn electrolyte with convection is 30% less than without convection because of the removal of MnOOH substrate from the working electrode in the case of convection.

Table 27. Estimated percentage of the reduced cathodic charges of MnO_2 substrate resulted from Mn electrolyte and Mn-Ti electrolyte anodic voltage hold with and without convection during the cathodic linear voltage scan in 3M H_2SO_4 relative to the generated anodic charges.

Solution	Anodic charges [C]	Cathodic charges [C]	%Cathodic charges/anodic charges
CLVS of Mn anodic products in 3M H_2SO_4 with no convection	8.5 C	-6.7 C	79%
CLVS of Mn anodic products in 3M H_2SO_4 with convection	11.6 C	-6.4 C	55.2%
CLVS of Mn+Ti anodic products in 3M H_2SO_4 with no convection	9.7 C	-3.34 C	34.4%
CLVS of Mn+Ti anodic products in 3M H_2SO_4 with convection	15.8 C	-5.6 C	35.4%

4.3.2.5. Linear Voltage Sweep Results of Mn and Mn-Ti Anodic Products in 3M H_2SO_4 Solution with and without Convection on a Carbon Felt Working Electrode

The anodic current response with respect to time resulted from holding the voltage at 0.6V vs. SCE for 5min followed by stepping the voltage up to 1.5V vs. SCE for 15min starting at zero time for 1M Mn+3M H_2SO_4 with and without Ti in the solution on a carbon felt working electrode with and without convection is shown in Figure 71 .

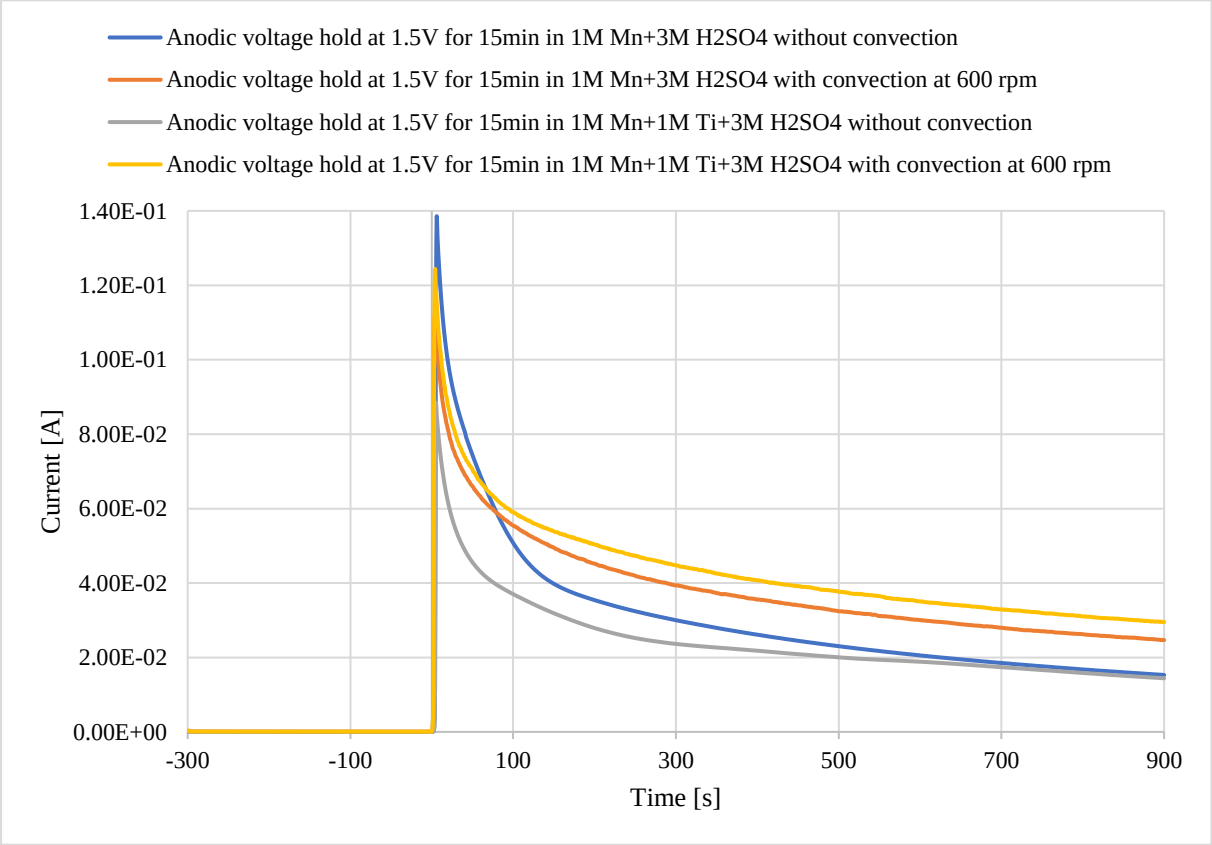

Figure 71. Anodic voltage hold at 1.5V vs. SCE for 15min in 1M M-3M H_2SO_4 and in 1M M-3M H_2SO_4 on a carbon felt working electrode with and without convection planned to be investigated by cathodic linear voltage in 3M H_2SO_4 solution

Before scanning, no faradic current is measured because the applied voltage at 0.6V is lower than the minimum voltage requires to oxidize Mn^{2+}. At zero time when the voltage is raised to 1.5V vs SCE, a faradic current is measured due to the oxidation reaction of Mn^{2+} as described by Eq2.2, and the anodic current is limited in the two tested Mn solutions due to Mn^{2+} transport. After 100s,

a limited anodic current is measured that may be attributed to the oxidation reaction of Mn^{2+} to Mn^{3+} as shown in Eq 3.31. The high anodic limited current in 1M Mn+3M H_2SO_4 is believed to be due to the high concentration of Mn^{2+} species compared to 1M Mn+1M Ti+3M H_2SO_4. Note that the reactions in this case are limited by the electrode surface area because a porous carbon felt is used. When convection is applied during the anodic voltage hold experiment for both Mn electrolyte and Mn+Ti electrolyte, the anodic limited current is significantly increased due to the high transport of Mn^{2+} species from the bulk solution to the surface of the working electrode. Although Mn^{2+} concentration in the bulk of 1M Mn+1M Ti+3M H_2SO_4 is less than the one in the bulk of 1M Mn+3M H_2SO_4, the fast hydrolysis of Mn^{3+} to $Mn(OH)^{+}_2$ in Eq3.14 and Eq3.15 because of the low H^+ concentration in 1M Mn+1M Ti+3M H_2SO_4 electrolyte compared to the 1M Mn+3M H_2SO_4 electrolyte, so that more $Mn(OH)^{+}_2$ is available on the working electrode to undergo the oxidation reaction in Eq3.36 and high anodic limited current is measured.

After the anodic voltage hold experiment, Mn+Ti electrolyte solution color turns into a non-transparent dark black, and Mn electrolyte solution color turns into a semi-transparent red black as shown in Figure 72.

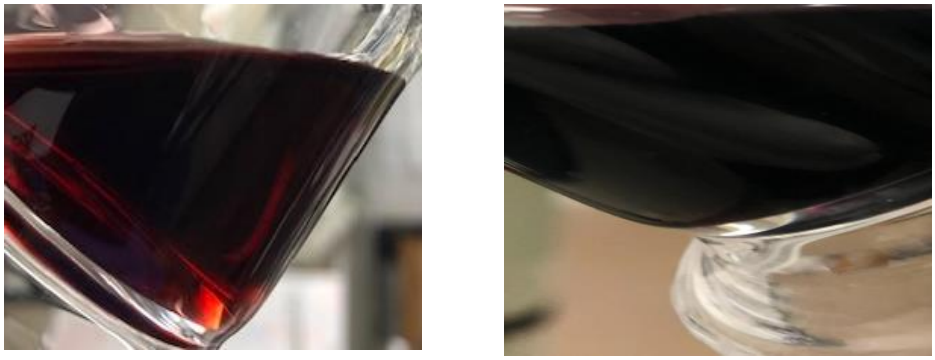

(a) (b)

Figure 72. 1M Mn-3M H_2SO_4 solution after the anodic voltage hold experiment on a carbon felt working electrode with convection, (a) without the addition of 1M Ti, (b) with the addition of 1M Ti.

The black color is believed to be MnOOH resulted from Mn^{3+} hydrolysis reaction in Eq4.3b where it is expected to be more in Mn+Ti electrolyte than Mn electrolyte due to the low H^+ concentration in Mn+Ti electrolyte. The semi-transparent red black in Mn electrolyte indicates that Mn^{3+} species is more in Mn electrolyte than Mn+Ti electrolyte due to the high acid concentration of Mn electrolyte. To confirm this findings, OCV measurements are conducted for the two tested electrolyte solutions using a clean graphite rod working electrode for 2 min as shown in Figure 73.

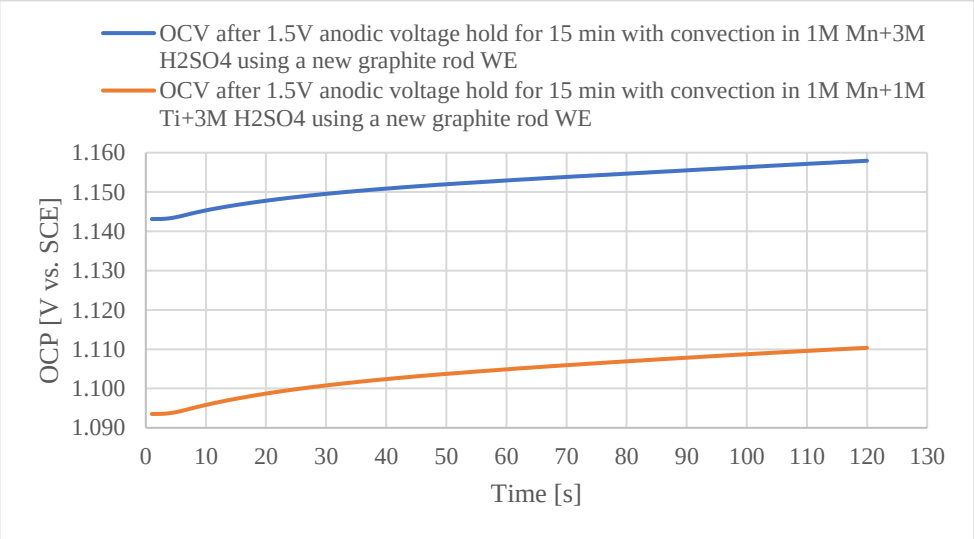

Figure 73. Measured Open Circuit Voltage (OCV) after the anodic voltage hold on a carbon felt working electrode with convection at 1.5V vs. SCE for 2 min in 1M Mn-3M H_2SO_4 with and without the addition of Ti in the solution using a new graphite rod working electrode

From Figure 73, the measured OCV of the Mn electrolyte is higher than the OCV of Mn+Ti electrolyte after the anodic voltage hold experiment on a carbon felt working electrode with convection which indicates that more Mn^{3+} cation species is formed in Mn electrolyte compared to Mn+Ti electrolyte. However, the increase of the measured OCV with time indicates that MnO_2 is forming on the electrode while measuring the OCV of the two tested electrolytes because of the disproportionation reaction of Mn^{3+} and MnOOH on the working electrode surface as shown in Eq4.4.a. Generally, the dominant form of Mn(III) species in the solution after the anodic voltage hold is in the form of MnOOH solid colloids and it is not electrochemically active unless it is on

the working electrode surface, so it can be reduced at very low voltage (less than 500mV) to Mn^{3+} by dissolution first into Mn^{3+}.

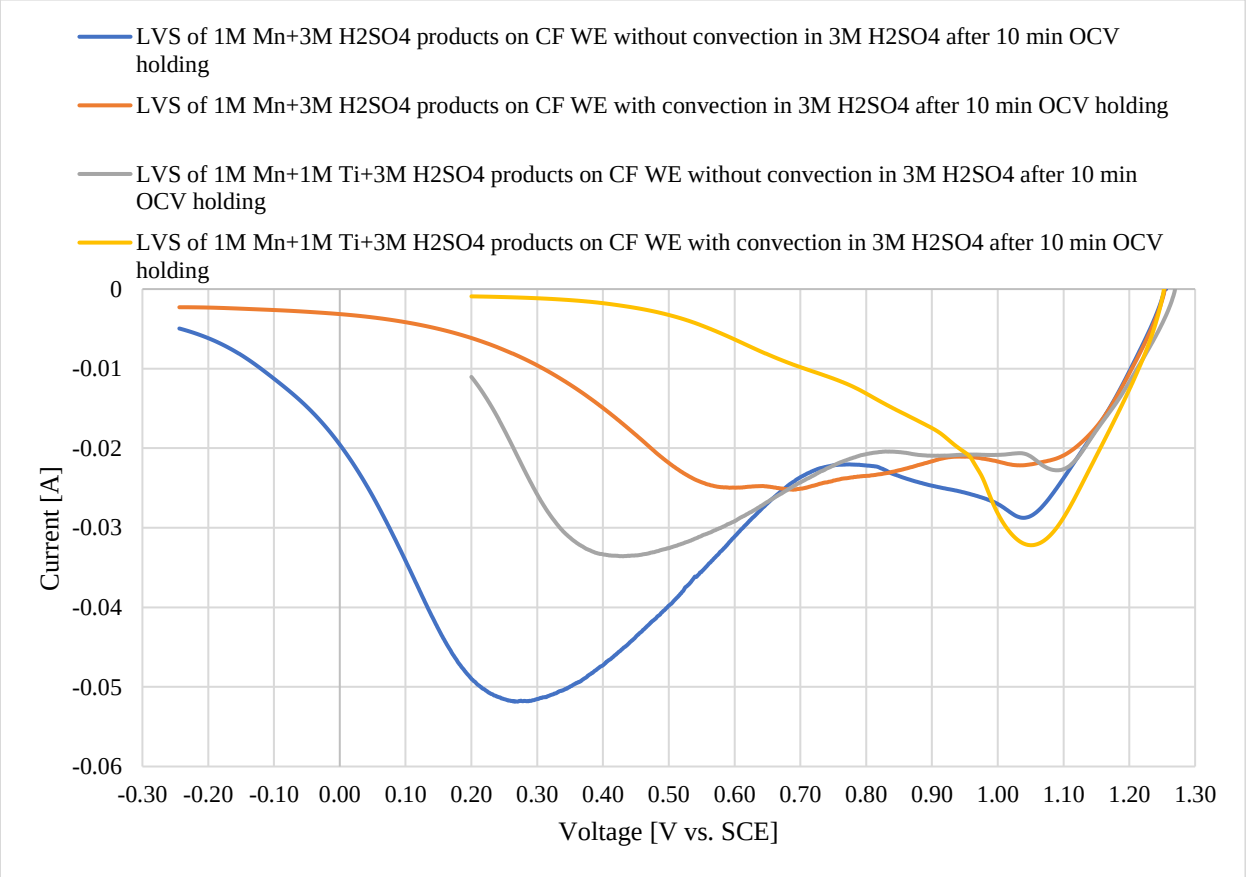

Figure 74. Cathodic linear voltage sweep of MnO_2 substrate on carbon felt working electrode resulted from the anodic voltage of Mn electrolyte and Mn-Ti electrolyte with and without convection in a new 3M H_2SO_4 solutions at 2mV/s scan rate after holding the OCV for 10min.

From Figure 74, the cathodic voltage scan starts from the measured OCV for the four tested carbon felt working electrodes in a new 3M H_2SO_4 solution. The first cathodic wave current before the cathodic peak current at 1V is attributed to the reduction reaction of MnO_2 to MnOOH as described by Eq3.38. The limited cathodic current at 1.1V is believed to result from the negligible availability of MnO_2 substrate on the carbon felt and the large formation of MnOOH. For the cathodic scan of the anodic products resulted without convection on the carbon felt, the first cathodic peak current is higher for the substrate resulted from Mn electrolyte than the substrate resulted from Mn+Ti electrolyte which indicates that large amount of MnO_2 is resulted from the

anodic voltage hold of Mn electrolyte due to the high Mn^{2+}concetration, and that the comproportionation reaction of Eq4.4b is less destructive to the deposit in 1M Mn+3M H_2SO_4 solution.

During the cathodic scan below 0.8V vs. SCE, a second cathodic peak current is observed where it peaks at 0.4V for the MnO_2 substrate resulted from Mn+Ti electrolyte, and at 0.25V for the MnO_2 substrate resulted from Mn electrolyte. The second cathodic peak of the MnO_2 substrate resulted from Mn electrolyte is higher than the one resulted from Mn+Ti electrolyte due to the high Mn^{2+} concentration in Mn electrolyte during the anodic voltage hold. This cathodic current wave is believed to be attributed to the reduction reaction of MnOOH to form Mn^{2+} based on Eq3.17, Eq3.18, Eq3.15, Eq3.14, and Eq3.31.

$$(\gamma)\mathrm{MnOOH} + \mathrm{H^+} \leftrightarrow \mathrm{Mn(OH)_2}^+ \qquad \text{K=1.1} \qquad \text{Eq3.17}$$

$$(\alpha)\mathrm{MnOOH} + \mathrm{H^+} \leftrightarrow \mathrm{Mn(OH)_2}^+ \qquad \text{K=2.14} \qquad \text{Eq3.18}$$

$$\mathrm{Mn(OH)_2^+ + H^+ \leftrightarrow\ Mn(OH)^{2+} + H_2O,} \qquad \text{K=2} \qquad \text{Eq3.15}$$

$$\mathrm{Mn(OH)^{2+} + H^+ \leftrightarrow Mn^{3+} + H_2O,} \qquad \text{K=0} \qquad \text{Eq3.14}$$

$$\mathrm{Mn^{3+} + e^- \leftrightarrow Mn^{2+}} \qquad \mathrm{E^0 = 1.26\ V\ vs\ SCE} \qquad \text{Eq3.31}$$

Regarding the anodic substrate resulted from the anodic voltage hold with convection on the carbon felt, the first cathodic peak current is higher for the substrate resulted from Mn+Ti electrolyte than the substrate resulted from Mn electrolyte which indicates that large amount of MnO_2 is resulted from the anodic voltage hold of Mn+Ti electrolyte. The large formation of MnO_2 is due to the fast hydrolysis of Mn^{3+} to $Mn(OH)^+_2$ in Eq3.14 and Eq3.15 because of the low H^+ concentration in Mn+Ti electrolyte compared to the Mn electrolyte. Therefore, more $Mn(OH)^+_2$ is

available on the working electrode to undergo the oxidation reaction in Eq3.36 and form MnO_2 on the working electrode.

As the H^+ concentration is high in Mn electrolyte, the applied convection on the working electrode during the anodic voltage hold scan helps minimizing the formation of MnO_2 on the working electrode by removing the Mn(III) species from the electrode surface and allowing it to precipitate in the solution in the form of MnOOH. Therefore, the first cathodic peak current of the MnO_2 substrate resulted from Mn electrode with convection is less than on without convection. However, the low H^+ concentration in the Mn+Ti electrolyte during the anodic voltage hold increases the formation of MnO_2 on the working electrode compared to the anodic voltage hold of Mn+Ti electrolyte without convection as it can be seen from the high intensity of the first cathodic peak current.

The formed MnOOH substrate on the carbon felt is believed to be resulted from the hydrolysis of Mn^{3+} species in Eq4.3.b and not from the MnOOH that is resulted from the reduction reaction of MnO_2 during the first cathodic wave current. This can be supported by the cathodic voltage scan of the MnO_2 substrate resulted from anodic voltage hold of Mn and Mn+Ti electrolytes with convection where the second cathodic peak current disappears. Therefore, two MnOOH solid phases are formed during the anodic voltage hold of Mn electrolyte, and Mn+Ti electrolyte. It is proposed that the phase of MnOOH formed by Mn(III) hydrolysis is $(\gamma)MnOOH$,and the phase of MnOOH resulted from the reduction reaction of MnO_2 substrate is $(\alpha)MnOOH$. It was confirmed that the resulted morphology of electrochemically generated MnO_2 in sulfuric acid media is in the form of $(\gamma)MnO_2$, so the reduction reaction of $(\gamma)MnO_2$ is suggested to form $(\alpha)MnOOH$. [23, 68]

The second cathodic peak current that is clearly observed in Figure 74, was less observed in Figure 70 because the large surface area of the carbon felt may increase the rate of the oxidation reaction of Mn^{2+} in Eq3.31 relative to the oxidation reaction of $Mn(OH)^{+}$ in Eq3.36, so that the overall anodic process is not limited by the MnO_2 substrate on the working electrode. In this case, more MnOOH is formed by Mn^{3+} hydrolysis as described in Eq4.3.b, and with the porosity of the carbon felt, if MnOOH is fallen from the working electrode, it may assumed to be trapped within the porous structure of the carbon felt working electrode.

The percentage of the reduced cathodic charges of MnO_2 substrate resulted from Mn and Mn+Ti electrolyte anodic voltage hold with and without convection on a carbon felt working electrode during the cathodic voltage scan in a new 3M H_2SO_4 solution relative to the generated anodic charges is given in Table 28.

Table 28. Estimated percentage of the reduced cathodic charges of MnO_2 substrate resulted from Mn electrolyte and Mn-Ti electrolyte anodic voltage hold with and without convection during the cathodic linear voltage scan in 3M H_2SO_4 relative to the generated anodic charges.

Solution	Anodic charges [C]	Cathodic charges [C]	%Cathodic charges/anodic charges
CLVS of Mn anodic products in 3M H_2SO_4 with no convection	27.5	-21.05	76.7
CLVS of Mn anodic products in 3M H_2SO_4 with convection	34.4	-10.60	30.8
CLVS of Mn+Ti anodic products in 3M H_2SO_4 with no convection	21.8	-12.36	56.9
CLVS of Mn+Ti anodic products in 3M H_2SO_4 with convection	38.9	-6.063	15.7

4.3.3. Comparing the Mn Cyclic Voltammetry Results to Previous Reported Results

The shape of the cyclic voltammetry of the Mn electrolyte with and without the addition of Ti obtained by SE in Figure 19 differs from the one obtained in Figure 54 because of the different experimental setup. In Figure 54, the cyclic voltammetry was conducted in a static cell where the working electrode was immersed in a large availability of the Mn electrolyte, so that not all the Mn electro-active species in the electrolyte was consumed during the cyclic voltammetry scan. SE conducted the cyclic voltammetry in a flow cell where the tested electrolyte was kept still in the working electrode, so that the Mn electro-active species was fully consumed during the cyclic voltammetry.

From SE cyclic voltammetry result in a Ti-free Mn electrolyte, it is believed that during the anodic scan, Mn^{2+} was oxidized to MnO_2 in a simultaneous two electron transfer reactions where Mn^{2+} is oxidized to Mn^{3+} which is further oxidized to form a solid MnO_2 layer on the working electrode. Then, the oxidation reaction of Mn^{2+} may proceed on the solid MnO_2 layer to form only Mn^{3+}, and due to the low stability of Mn^{3+} in the solution toward the hydrolysis, Mn^{3+} may form MnOOH and precipitate on the working electrode. The anodic peak current may be due to the low availability of Mn^{2+} on the working electrode where the anodic current significantly decreases after the anodic peak current. During the negative scan, although two reduction peak current was reported, in light of the findings from this thesis, it was assumed that the reduction reaction of γ-MnO_2 to α-MnOOH to proceed first followed by the reduction reaction of γ-MnOOH, formed from Mn(III) during the anodic scan, and α-MnOOH to Mn^{2+} where the dissolution of MnOOH proceed before the electron transfer reaction to Mn^{2+} within the broad reduction peak from 1.4V to 0.7V vs. Ag/AgCl. The proposed reduction mechanism of the anodic products is shown below:

$$H^+ + (\gamma)MnO_2 + e^- \leftrightarrow (\alpha)MnOOH \ , \ E^0 = 0.788 \text{ V vs SCE} \qquad \text{Eq3.38}$$

$$(\alpha)\mathrm{MnOOH} + \mathrm{H}^{+} \leftrightarrow \mathrm{Mn(OH)_2}^{+} \qquad \mathrm{K}=2.14 \qquad \text{Eq3.18}$$

$$(\gamma)\mathrm{MnOOH} + \mathrm{H}^{+} \leftrightarrow \mathrm{Mn(OH)_2}^{+} \qquad \mathrm{K}=1.1 \qquad \text{Eq3.17}$$

$$\mathrm{Mn(OH)_2^{+}} + \mathrm{H}^{+} \leftrightarrow \mathrm{Mn(OH)^{2+}} + \mathrm{H_2O}, \qquad \mathrm{K}=2 \qquad \text{Eq3.15}$$

$$\mathrm{Mn(OH)^{2+}} + \mathrm{H}^{+} \leftrightarrow \mathrm{Mn^{3+}} + \mathrm{H_2O}, \qquad \mathrm{K}=0.4 \qquad \text{Eq3.14}$$

$$\mathrm{Mn^{3+}} + \mathrm{e^{-}} \leftrightarrow \mathrm{Mn^{2+}} \qquad \mathrm{E^0} = 1.26\ \mathrm{V\ vs\ SCE} \qquad \text{Eq3.31}$$

With the addition of Ti to the system, the concentration of Mn^{2+} decreases due to the low H^{+} concertation from the addition of SO_4^{2-}, and this results in a lower oxidation peak current here than the one in Ti-free Mn electrolyte. This may result in less γ-MnO_2 and γ-MnOOH formed on the working electrode. During the negative scan, the same reduction reactions mentioned in Ti-free solution may still procced which are the reduction reaction of γ-MnO_2 to α-MnOOH to be proceeded first followed by the reduction reaction of γ-MnOOH and α-MnOOH to Mn^{2+}. The cause of the shifting of the reduction peak in Mn/Ti electrolyte to a higher voltage mainly due to the anodic solid mixture ratio of MnO_2/MnOOH on the working electrode. The formed mixture of MnO_2/MnOOH in Mn/Ti electrolyte is believed to have a high content of MnO_2 to MnOOH on the working electrode than the anodic content in Mn electrolyte. As a result, the reduction potential of MnO_2/MnOOH redox couple in Mn/Ti electrolyte is higher than the one in Mn electrolyte during the cathodic scan.

4.4. Ti Electrolyte Characterization Results

4.4.1. Cyclic Voltammetry of Ti Electrolyte Results

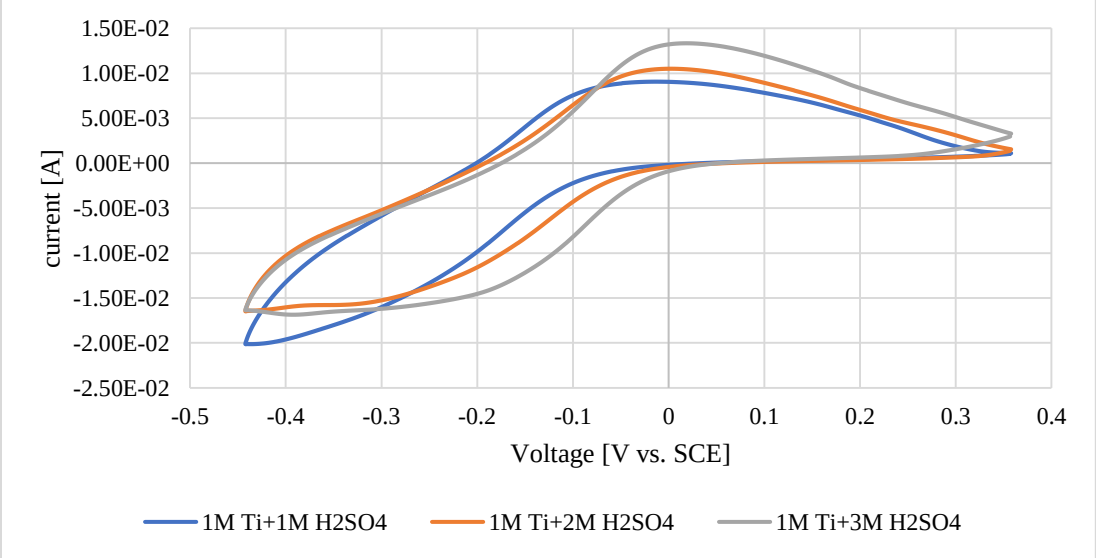

Figure 75. Third cyclic voltammetry scan of 1M $TiOSO_4$ in 1M H_2SO_4, 2M H_2SO_4, and 3M H_2SO_4 on graphite rod working electrode with 2mV/s scan rate

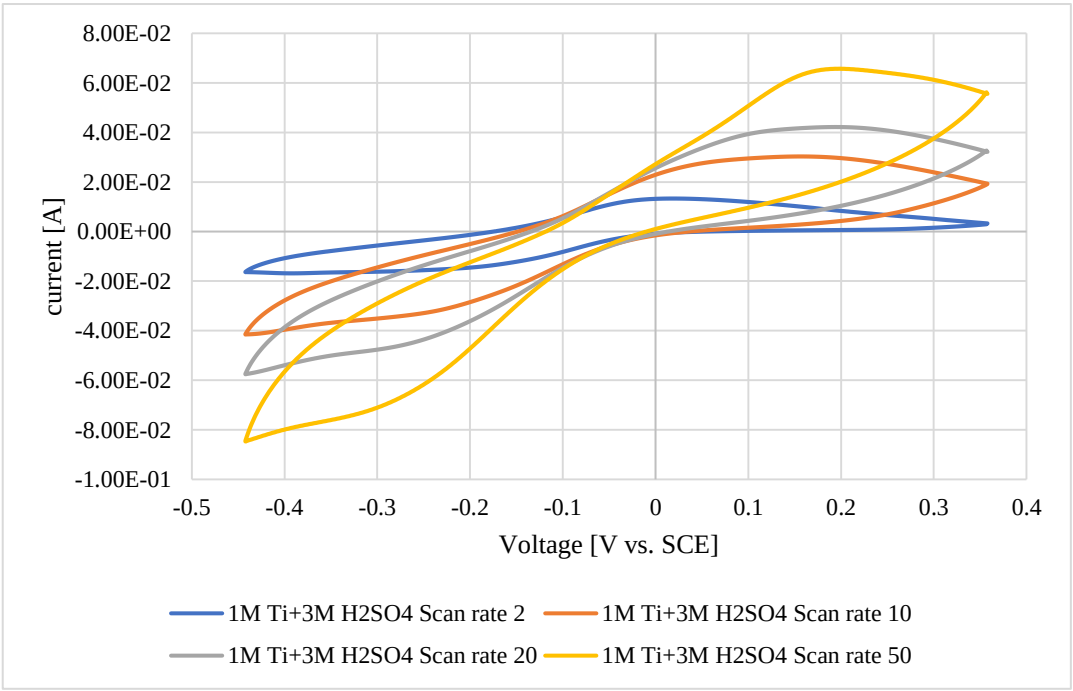

Figure 76. Third cyclic voltammetry scan of 1M $TiOSO_4$ in 3M H_2SO_4 on graphite rod working electrode with 2mV/s, 10mV/s, 20mV/s, and 50mV/s scan rate

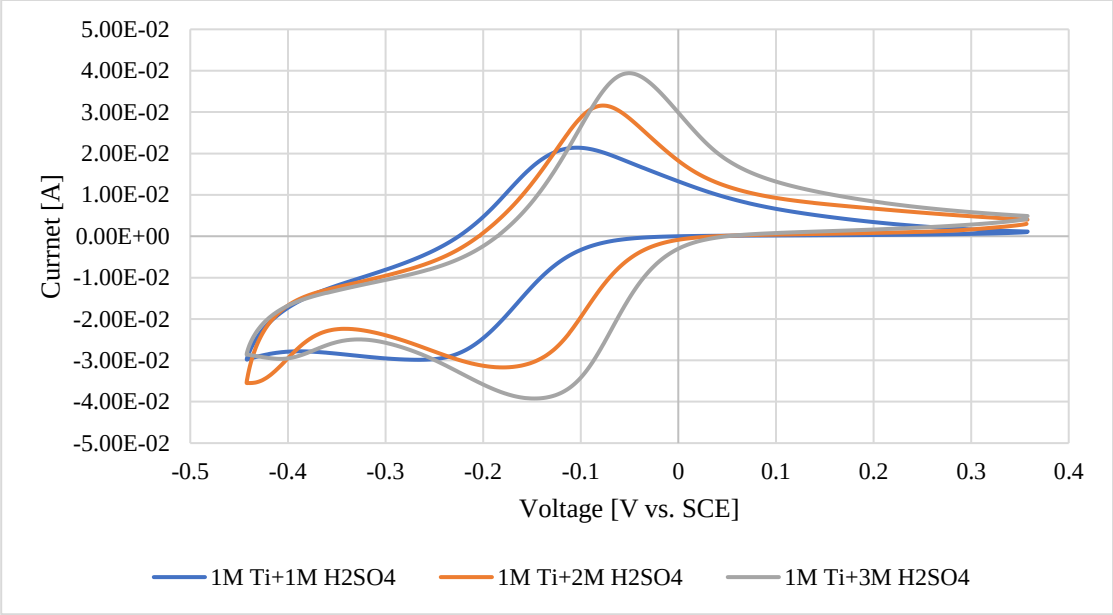

Figure 77. Third cyclic voltammetry scan of 1M $TiOSO_4$ in 1M H_2SO_4, 2M H_2SO_4, and 3M H_2SO_4 on carbon felt working electrode with 2mV/s scan rate

- **Observations from Figures 75, 76, and 77:**

  1) Figure 75 shows the third cyclic voltammetry scan of 1M Ti in 1-3M H_2SO_4 on graphite rod working electrode at 2mV/s voltage scan rate. One oxidation current peak and one reduction current peak are observed during the cyclic voltammetry scan of Ti in H_2SO_4. During the cathodic scan, the cathodic current wave shifts to more positive value as the sulfuric acid concentration increases in the electrolyte solution. A limited cathodic current is not observed during the cathodic scan in the case 1M Ti+1M H_2SO_4. Instead, the cathodic current builds up during the whole cathodic scan course and achieve a limited value near the end of the cathodic scan. For the case of 1M Ti+2M H_2SO_4 and 1M Ti+3M H_2SO_4 during the cathodic scan, a limited cathodic current is observed where the limited current is achieved earlier for the case of 1M Ti+3M H_2SO_4. During the anodic scan, the anodic current wave shifts to more positive value with a high anodic current peak as the sulfuric acid concentration increases in the electrolyte solution.

2) Figure 76 shows the third cyclic voltammetry scan of 1M Ti in 3M H_2SO_4 on graphite rod working electrode at a different voltage scan rate (2, 10, 20, and 50 mV/s). As the scan rate increases, the intensity of the anodic and the cathodic current increases due to the large availability of the electro-active species when a high overpotential is applied more quickly while the electro-active species is readily available. In addition to the faradic process, a non-faradic current is increased as the voltage scan rate increases. The cathodic peak current shifts to more negative voltage as the voltage scan rate increase. The anodic peak current shifts to more positive value as the scan rate increase.
3) Figure 77 shows the third cyclic voltammetry scan of 1M Ti in 1-3M H_2SO_4 on carbon felt working electrode at 2mV/s voltage scan rate. Similar to Figure 75, one oxidation current peak and one reduction current peak are observed during the cyclic voltammetry scan of Ti in H_2SO_4 where the anodic and the cathodic peaks current shift to more positive voltage when the sulfuric acid concentration of the electrolyte solution increases. However, instead of the getting unlimited cathodic current for the case 1M Ti+1M H_2SO_4, a limited cathodic current is observed when using a carbon felt working electrode. Also, a clear cathodic peak current can be seen for the case of 1M Ti+2M H_2SO_4 and 1M Ti+3M H_2SO_4 where the cathodic peak current is high when the sulfuric acid concentration is high. At low applied negative voltage (< -300mV vs. SCE) a second cathodic current wave is observed for the case of 1M Ti+2M H_2SO_4 and 1M Ti+3M H_2SO_4. The ratio of the cathodic peak current to the anodic peak current is almost unity in the case of 1M Ti+2M H_2SO_4 and 1M Ti+3M H_2SO_4; while, it is 0.6 for the 1M Ti+1M H_2SO_4. The voltage peak separation between the anodic peak

voltage to the cathodic peak voltage is almost 59 mV for the case of 1M Ti+3M H_2SO_4 and higher than 59mV in the cases of 1M Ti+1M H2SO4 and 1M Ti+2M H_2SO_4.

- **Possible redox reaction pathway of $TiOSO_4$ electrolyte in H_2SO_4**

During the cathodic scan, the cathodic current is attributed to the reduction of Ti(IV) electro-active species to Ti(III) species. The cathodic peak current and the anodic peak current do not reflect the mass transport limited current due to the increase of the viscosity of the electrolyte solution with the increase of sulfuric acid concentration. Rather, the behavior of the peak current as the acid concentration increases may be attributed to the availability of the electro-active species and the rate of the chemical reactions associated with the supply of the electro-active species that undergo the electron transfer rection. When one compare the cathodic behavior on graphite rod working electrode of 1M Ti+1M H_2SO_4 and 1M Ti+3M H_2SO_4, the electro-active species in 1M Ti+1M H_2SO_4 is reduced at low applied potential with unlimited cathodic current; while, the oxidized electro-active species in 1M Ti+3M H_2SO_4 is reduced at high voltage with an low limited cathodic current. This observation may reveal that there are two electro-active species that are coupled by a chemical reaction, and they undergo a reduction reaction in which one of these two electro-active species is sufficiently present at high acid concentration and it has a higher reduction potential compared to the second electro-active species. So, it may be reduced first. This hypothesis can be supported by the result from Figure 76 where in the case 1M Ti +3M H_2SO_4, the faster scan rate would allow the reduction of the second electro-active species that has a low reduction potential.

Based on the speciation study of Ti(IV) species, the possible two electro-active species that undergo a reduction reaction during the cathodic scan are Ti^{4+} and $TiSO_4^{2+}$ where the standard reduction potential of $TiSO_4^{2+}$ is higher than Ti^{4+}. According to the equilibrium concentration

calculation in Table 13 of the Ti(IV) species in 1M H_2SO_4, $TiSO_4^{2+}$ is present in a relatively negligible concentration, in the order of tens µmol, compared to Ti^{4+}. Therefore, Ti^{4+} may be the dominant electro-active species that is reduced in 1M Ti+1M H_2SO_4 solution; while, in 1M Ti+3M H_2SO_4, where $TiSO_4^{2+}$ concentration is increased, $TiSO_4^{2+}$ may be the main electro-active species that is reduced during the negative scan.

Another feature that needs to be considered in describing the cathodic scan is the chemical reactions of species associated with electro-active species during the reduction reaction. Ti(IV) presents mostly in the form of $Ti(OH)_2^{2+}$ in sulfuric acid solution. As the electro-active species concentration decreases, other Ti(IV) complexes can generate more electro-active species by the chemical reaction routes. For instances, the chemical reaction route to form more Ti^{4+} and $TiSO_4^{2+}$ depends on the H^+, SO_4^{-2}, and other Ti(IV) complexes forms that are couple with Ti^{4+} and $TiSO_4^{2+}$ reduction reactions. In addition, the chemical reactions associated with the reduced species may also alter the electron transfer reaction.

- **Possible mechanism for the redox reaction of Ti(IV)/Ti(III) couple in sulfuric acid solution**

$Ti(OH)_2^{2+} + H^+ \leftrightarrow Ti(OH)^{3+} + H_2O$	K=0.083	Eq3.48
$Ti(OH)^{3+} + H^+ \leftrightarrow Ti^{4+} + H_2O$	K=0.49	Eq3.49
$Ti^{4+} + SO_4^{-2} \leftrightarrow Ti(SO_4)^{+2}$	K=0.4065	Eq3.50
$Ti(SO_4)^{+2} + e^- \leftrightarrow Ti(SO_4)^+$	$E^0 = 0.065$ V vs SCE	Eq3.58
$Ti^{4+} + e^- \leftrightarrow Ti^{3+}$	$E^0 = -0.042$ V vs SCE	Eq.2.14
$Ti^{3+} + SO_4^{-2} \leftrightarrow Ti(SO_4)^+$	K=24.3	Eq3.57
$Ti^{3+} + H_2O \leftrightarrow Ti(OH)^{2+} + H^+$	K=0.072	Eq3.55

For the case of 1M Ti+1M H_2SO_4, the supply of Ti^{4+} depends on the amount of $Ti(OH)^{3+}$, $Ti(OH)_2^{2+}$, and the H^+ concentration based on Eq3.48, and Eq3.49. In addition to the chemical reactions associated with oxidized species, Ti^{3+} may couple with the sulfate as in E3.57 and may hydrolyze to generate more H^+ as in Eq3.55. Based on the shape of the cathodic wave and the ratio of the anodic/cathodic current peaks between the case of the graphite rod working electrode and the carbon felt working electrode, as Ti^{4+} concentration decreases, $Ti(OH)_2^{2+}$ and H^+ would generate more Ti^{4+} via the chemical reaction route. In the case of graphite working electrode, after the Ti^{4+} is reduced to Ti^{3+}, the small electrode area decreases the formation rate of Ti^{4+} via the chemical path and increase the hydrolysis of Ti^{3+} to form more H^+ that would eventually delay the limited current to the low applied voltage region. When using a carbon felt working electrode, the electron transfer reaction area increases and the consumption of Ti^{4+} increases. So, the supply of Ti^{4+} via the chemical path would be faster than the hydrolysis of Ti^{3+}. In this case a limited cathodic current is achieved due to the lack of H^+ concentration.

For the case of 1M Ti+3M H_2SO_4 and 1M Ti+2M H_2SO_4, the supply of $TiSO_4^{2+}$ depends on the amount of $Ti(OH)^{3+}$, $Ti(OH)_2^{2+}$, Ti^{4+}, SO_4^{-2} and the H^+ concentration as described by Eq3.48, and Eq3.49, and Eq3.50. In addition to the chemical reactions associated with oxidized species, Ti^{3+} may couple with the sulfate and hydrolyze to generate more H^+. Based on the equilibrium concentration in Table 13 of the Ti(IV) species in 3M H_2SO_4 and 2M H_2SO_4, SO_4^{-2} concentration is less than Ti^{4+}concentation, so the reduction reaction is more likely to be limited by the low SO_4^{-2} concentration. However, the reduced species $TiSO_4^+$ may decompose into Ti^{3+} and SO_4^{-2}. The generated SO_4^{-2} via the reduced species helps the formation of $TiSO_4^{2+}$ via reacting with Ti^{4+}. This process may be slow in the case of graphite working electrode due to small available area, so the reduction reaction is limited by the lack of SO_4^{-2} supply; while, the supply of SO_4^{-2} species is faster

in carbon felt working electrode cases. So, a peak current is clearly observed during the cathodic scan which indicates the low Ti^{4+} concentration. However, at a very low applied voltage, the rate of consumption of SO_4^{-2} may increase as opposed to the rate of SO_4^{-2} generation, and the Ti^{4+} reduction reaction may proceed instead of $TiSO_4^{2+}$. Thus, the second cathodic peak is attributed to the Ti^{4+} reduction reaction instead of $TiSO_4^{2+}$ where the cathodic wave is higher for the case of 3M H_2SO_4 due to the high H^+ concentration that supply $TiSO_4^{2+}$ via the chemical path.

4.4.2. Cyclic Voltammetry of Ti-Mn Electrolyte Results

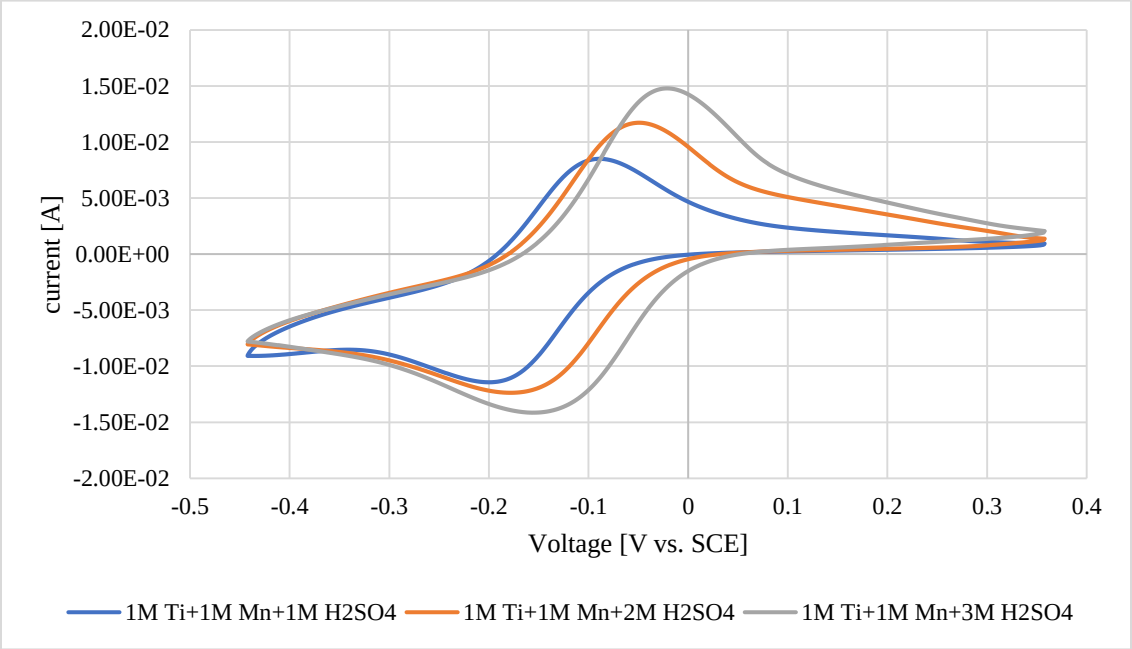

Figure 78. Third cyclic voltammetry scan of 1M $TiOSO_4$-1M $MnSO_4$ in 1M H_2SO_4, 2M H_2SO_4, and 3M H_2SO_4 on graphite rod working electrode with 2mV/s scan rate

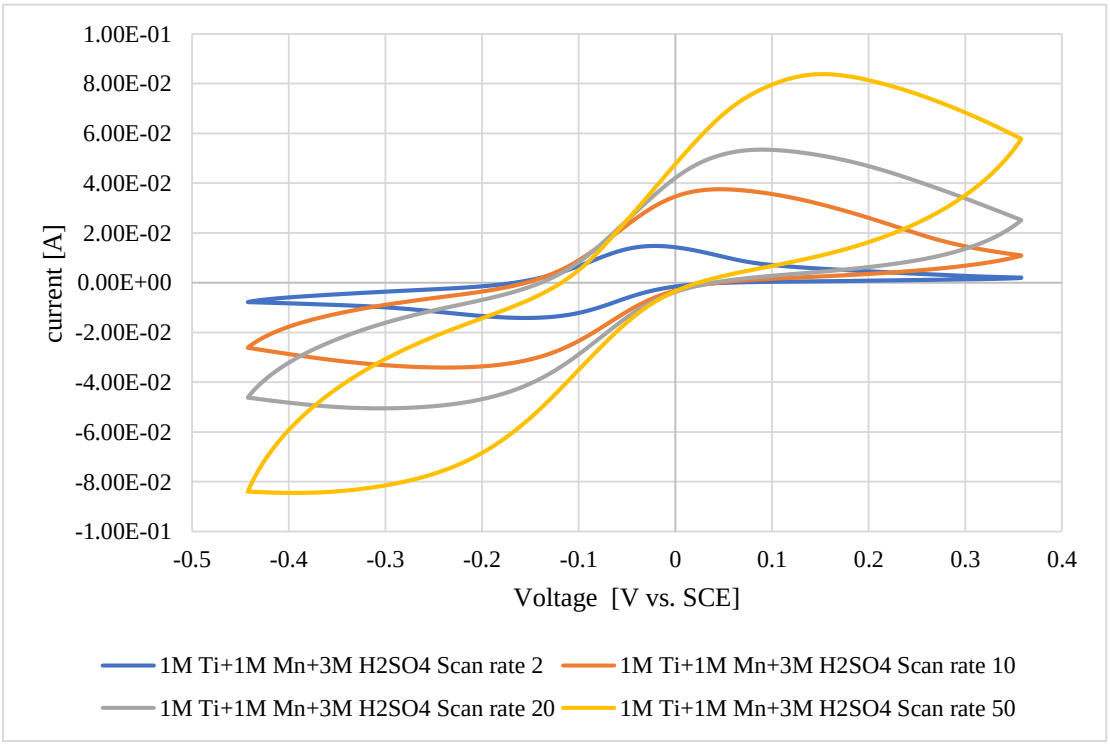

Figure 79. Third cyclic voltammetry scan of 1M $TiOSO_4$-1M $MnSO_4$ in 1M H_2SO_4, 2M H_2SO_4, and 3M H_2SO_4 on graphite rod working electrode with 2mV/s, 10mV/s, 20mV/s, and 50mV/s scan rate

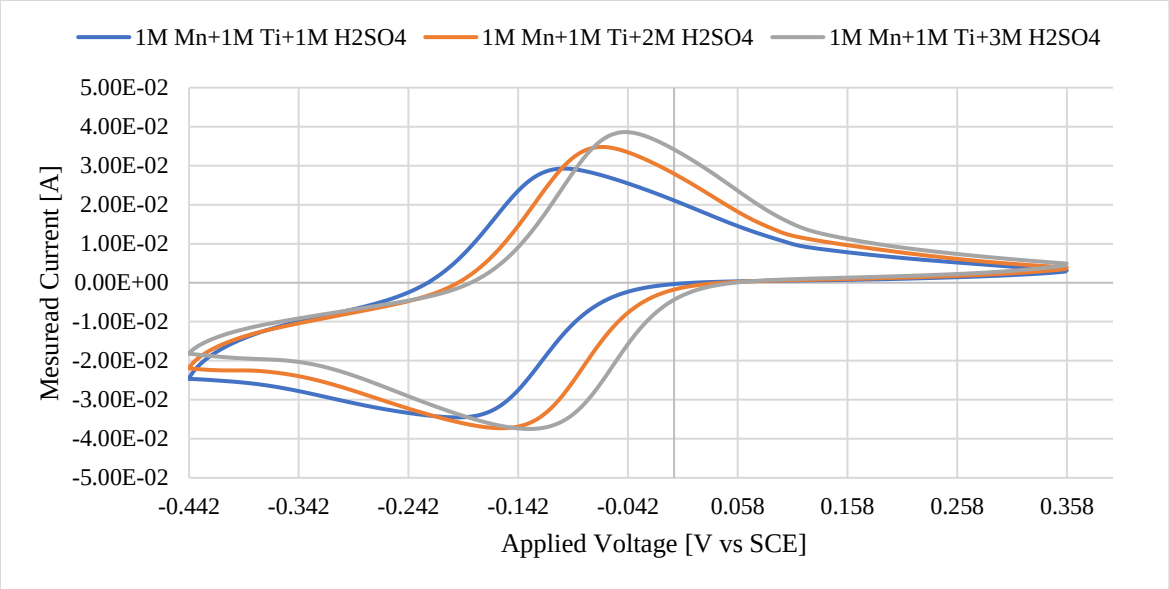

Figure 80. Third cyclic voltammetry scan of 1M $TiOSO_4$-1M $MnSO_4$ in 1M H_2SO_4, 2M H_2SO_4, and 3M H_2SO_4 on carbon felt working electrode with 2mV/s scan rate

- **Observations from Figures 78, 79, and 80:**

1) Figure 78 shows the third cyclic voltammetry scan of 1M Ti+1M Mn in 1-3M H_2SO_4 on graphite rod working electrode at 2mV/s voltage scan rate. One oxidation current peak and one reduction current peak are observed during the cyclic voltammetry scan of Ti+Mn in H_2SO_4. During the cathodic scan, the cathodic current wave shifts to more positive value as the sulfuric acid concentration increases in the electrolyte solution. A peak cathodic current is observed during the cathodic scan in the case 1M Ti+1M Mn+1M H_2SO_4 instead of unlimited current that was observed in the case without the addition of Mn. For the case of 1M Ti+1M Mn+2M $H_2SO_4$and 1M Ti+1M Mn+3M H_2SO_4 during the cathodic scan, a clear cathodic peak current is observed where the peak current is achieved earlier for the case of 1M Ti+1M Mn+3M H_2SO_4. During the anodic scan, the anodic current wave shifts to more positive value with a high anodic current peak as the sulfuric acid concentration increases in the electrolyte solution.

2) Figure 79 shows the third cyclic voltammetry scan of 1M Ti+1M Mn in 3M H_2SO_4 on graphite rod working electrode at a different voltage scan rate (2, 10, 20, and 50 mV/s). As the scan rate increases, the intensity of the anodic and the cathodic current increases due to the large availability of the electro-active species when a high overpotential is applied. In addition to the faradic process, a non-faradic current is increased as the voltage scan rate increases. The cathodic peak current shifts to more negative voltage as the voltage scan rate increase reaching a limited cathodic current. The anodic peak current shifts to more positive value as the scan rate increase.
3) Figure 80 shows the third cyclic voltammetry scan of 1M Ti in 1-3M H_2SO_4 on carbon felt working electrode at 2mV/s voltage scan rate. Similar to Figure 79, one oxidation current peak and one reduction current peak are observed during the cyclic voltammetry scan of Ti in H_2SO_4 where the anodic and the cathodic peaks current shift to more positive voltage when the sulfuric acid concentration of the electrolyte solution increases. The cathodic peak current intensity of 1M Ti+1M Mn+2M H_2SO_4 and 1M Ti+1M Mn+3M H_2SO_4 are almost the same; while the anodic peak current intensity of 1M Ti+1M Mn+3M H_2SO_4 is higher than the one for 1M Ti+1M Mn+2M H_2SO_4. The ratio of the cathodic peak current to the anodic peak current is almost unity in the case of 1M Ti+1M Mn+2M $H_2SO_4$and 1M Ti+1M Mn+3M H_2SO_4; while it is 0.75 for the 1M Ti+1M Mn+1M H_2SO_4. The voltage peak separation between the anodic peak voltage to the cathodic peak voltage is almost 59 mV for the case of 1M Ti+1M Mn+3M H_2SO_4 and it is higher than 59mV in the cases of 1M Ti+1M Mn+1M H_2SO_4 and 1M Ti+1M Mn+2M H_2SO_4.

- **Possible redox reaction pathway of $TiOSO_4$ +$MnSO_4$ electrolyte in H_2SO_4**

Similar to the analysis of the cyclic voltammetry scans without the addition of $MnSO_4$, when the Ti(IV) electro-active species concentration decrease, other Ti(IV) complexes can generate more electro-active species by the chemical reaction routes. For instances, the chemical reaction route to form more Ti^{4+} and $TiSO_4^{2+}$ depends on the H^+, SO_4^{-2}, and other Ti(IV) complexes forms that are coupled with the Ti^{4+} and $TiSO_4^{2+}$ reduction reactions. In addition, the chemical reactions associated with the reduced species may also alter the electron transfer reaction. However, the only difference from the cyclic voltammetry without $MnSO_4$ cases is that the high concentration of undissociated $MnSO_{4\ Aq}$ would help in providing unlimited SO_4^{-2} species, so that SO_4^{-2} is always available.

- **Possible mechanism for the redox reaction of Ti(IV)/Ti(III) couple in $MnSO_4$ and sulfuric acid solution**

$Ti(OH)_2^{2+} + H^+ \leftrightarrow Ti(OH)^{3+} + H_2O$	K=0.083	Eq3.48
$Ti(OH)^{3+} + H^+ \leftrightarrow Ti^{4+} + H_2O$	K=0.49	Eq3.49
$Ti^{4+} + SO_4^{-2} \leftrightarrow Ti(SO_4)^{+2}$	K=0.4065	Eq3.50
$Ti(SO_4)^{+2} + e^- \leftrightarrow Ti(SO_4)^+$	$E^0 = 0.065$ V vs SCE	Eq3.58
$Ti^{4+} + e^- \leftrightarrow Ti^{3+}$	$E^0 = -0.042$ V vs SCE	Eq.2.14
$Ti^{3+} + SO_4^{-2} \leftrightarrow Ti(SO_4)^+$	K=24.3	Eq3.57
$Ti^{3+} + H_2O \leftrightarrow Ti(OH)^{2+} + H^+$	K=0.072	Eq3.55
$MnSO_{4_{Aq}} \leftrightarrow Mn^{2+} + SO_4^{-2}$,	$K = 0.00158$	Eq3.11

For the case of 1M Ti+1M Mn+1M H_2SO_4, the supply of Ti^{4+} depends on the amount of $Ti(OH)^{3+}$, $Ti(OH)_2^{2+}$, and the H^+ concentration as described by Eq3.48 and Eq3.49. In addition to the chemical reactions associated with oxidized species, Ti^{3+} may couple with the sulfate and hydrolyze to generate more H^+ according the Eq3.57 and Eq3.55. Based on the shape of the cathodic wave and the ratio of the anodic/cathodic current peak between the case of graphite rod working electrode and the carbon felt working electrode, as Ti^{4+} concentration decreases, $Ti(OH)_2^{2+}$ and H^+ would generate more Ti^{4+} via the chemical reaction route. In the case of graphite working electrode, after the Ti^{4+} is reduced to Ti^{3+}, the small electrode area decreases the supply rate of Ti^{4+} via the chemical path and increase the hydrolysis of Ti^{3+} to form more H^+ that would eventually allow to shift the peak current to a low applied voltage region. However, the addition of MnSO4 may reduce the hydrolysis of Ti^{3+} by increasing the SO_4^{-2}, so that Ti^{3+} is complex with SO_4^{-2} and a cathodic peak current can be achieved due to the lack of H^+ concentration. When using a carbon felt working electrode, the electron transfer reaction area increases and the consumption of Ti^{4+} increases, so that the supply of Ti^{4+} via the chemical path would be faster than the hydrolysis of Ti^{3+} compared to the graphite working electrode case. In this case the cathodic current is achieved at higher applied voltage.

For the case of 1M Ti+1M Mn+3M H_2SO_4 and 1M Ti+1M Mn+2M H_2SO_4, the supply of $TiSO_4^{2+}$ depends on the amount of $Ti(OH)^{3+}$, $Ti(OH)_2^{2+}$, Ti^{4+}, SO_4^{-2} and the H^+ concentration based on Eq3.48, Eq3.49, and Eq3.50. In addition to the chemical reactions associated with oxidized species, Ti^{3+} may couple with the sulfate and hydrolyze to generate more H^+. Based on the equilibrium concentration in Table 14 of the Ti(IV) species in 3M H_2SO_4 and 2M H_2SO_4 in Table 14, SO_4^{-2} concentration is less than Ti^{4+}concentation, so the reduction reaction is more likely to be limited by the low SO_4^{-2} concentration. However, SO_4^{-2} may be always available from $TiSO_4^+$

decomposition into Ti^{3+} and SO_4^{-2} according to Eq3.57 and from $MnSO_4$ dissociation according to Eq3.11. The generated SO_4^{-2} helps the formation of $TiSO_4^{2+}$ via reacting with Ti^{4+} in Eq3.50 until Ti^{4+} become limited.

4.4.3. Summary of the Proposed Mechanism of Ti(IV)/Ti(III) Redox Couple in Sulfuric Acid Solution with and without $MnSO_4$

Four proposed possible mechanism of the electrochemical behavior of Ti(IV)/Ti(III) redox couple in sulfuric acid solution depending on the acid concentrations, the addition of $MnSO_4$, and the used working electrode.

- **Mechanism (1)**

This redox reaction route is proposed for the case of 1M Ti+1M H_2SO_4 on graphite rod working electrode:

$$Ti(OH)_2^{2+} + H^+ \leftrightarrow Ti(OH)^{3+} + H_2O \qquad K=0.083 \qquad \text{Eq3.48}$$

$$Ti(OH)^{3+} + H^+ \leftrightarrow Ti^{4+} + H_2O \qquad K=0.49 \qquad \text{Eq3.49}$$

$$Ti^{4+} + e^- \leftrightarrow Ti^{3+} \qquad E^0 = -0.042\ V \text{ vs SCE} \qquad \text{Eq.2.14}$$

$$Ti^{3+} + H_2O \leftrightarrow Ti(OH)^{2+} + H^+ \qquad K=0.072 \qquad \text{Eq3.55}$$

- **Mechanism (2)**

This redox reaction route is proposed for the following cases:

1) 1M Ti+1M H_2SO_4 on carbon felt working electrode,
2) 1M Ti+1M Mn+1M H_2SO_4 on graphite rod working electrode,
3) and 1M Ti+1M Mn+1M H_2SO_4 on carbon felt working electrode,

$$Ti(OH)_2^{2+} + H^+ \leftrightarrow Ti(OH)^{3+} + H_2O \qquad K=0.083 \qquad Eq3.48$$

$$Ti(OH)^{3+} + H^+ \leftrightarrow Ti^{4+} + H_2O \qquad K=0.49 \qquad Eq3.49$$

$$Ti^{4+} + e^- \leftrightarrow Ti^{3+} \qquad E^0 = -0.042 \text{ V vs SCE} \qquad Eq.2.14$$

$$Ti^{3+} + SO_4^{-2} \leftrightarrow Ti(SO_4)^+ \qquad K=24.3 \qquad Eq3.57$$

- **Mechanism (3)**

This redox reaction route is proposed for the following cases:

1) 1M Ti+2M H_2SO_4 on graphite rod working electrode
2) 1M Ti+3M H_2SO_4 on graphite rod working electrode

$$Ti(OH)_2^{2+} + H^+ \leftrightarrow Ti(OH)^{3+} + H_2O \qquad K=0.083 \qquad Eq3.48$$

$$Ti(OH)^{3+} + H^+ \leftrightarrow Ti^{4+} + H_2O \qquad K=0.49 \qquad Eq3.49$$

$$Ti^{4+} + SO_4^{-2} \leftrightarrow Ti(SO_4)^{+2} \qquad K=0.4065 \qquad Eq3.50$$

$$Ti(SO_4)^{+2} + e^- \leftrightarrow Ti(SO_4)^+ \qquad E^0 = 0.065 \text{ V vs SCE} \qquad Eq3.58$$

- **Mechanism (4)**

This redox reaction route is proposed for the following cases:

1) 1M Ti+2M H_2SO_4 on carbon felt working electrode
2) 1M Ti+3M H_2SO_4 on carbon felt working electrode
3) 1M Ti+1M Mn+2M H_2SO_4 on carbon felt working electrode
4) 1M Ti+1M Mn+3M H_2SO_4 on carbon felt working electrode
5) 1M Ti+1M Mn+2M H_2SO_4 on graphite rod working electrode
6) 1M Ti+1M Mn+3M H_2SO_4 on graphite rod working electrode

$$Ti(OH)_2^{2+} + H^+ \leftrightarrow Ti(OH)^{3+} + H_2O \qquad K=0.083 \qquad \text{Eq3.48}$$

$$Ti(OH)^{3+} + H^+ \leftrightarrow Ti^{4+} + H_2O \qquad K=0.49 \qquad \text{Eq3.49}$$

$$Ti^{4+} + SO_4^{-2} \leftrightarrow Ti(SO_4)^{+2} \qquad K=0.4065 \qquad \text{Eq3.50}$$

$$Ti(SO_4)^{+2} + e^- \leftrightarrow Ti(SO_4)^+ \qquad E^0 = 0.065 \text{ V vs SCE} \qquad \text{Eq3.58}$$

$$Ti^{3+} + SO_4^{-2} \leftrightarrow Ti(SO_4)^+ \qquad K=24.3 \qquad \text{Eq3.57}$$

$$Ti^{3+} + H_2O \leftrightarrow Ti(OH)^{2+} + H^+ \qquad K=0.072 \qquad \text{Eq3.55}$$

$$MnSO_{4_{Aq}} \leftrightarrow Mn^{2+} + SO_4^{-2}, \qquad K = 0.00158 \qquad \text{Eq3.11}$$

The observations from the cyclic voltammetry in 1M Ti+3M H_2SO_4 and in 1M Ti+1M Mn+3M H_2SO_4 on carbon felt working electrode at 2mV/s voltage scan rate indicate that these two system can be characterized as a quasi–reversible system based on the 59mV/s voltage peak separation at 2mV/s scan rate, the unity of the cathodic peak current to the anodic peak current ratio, and the large peak separation at high voltage scan rate. Thus, one may estimate the formal

potential, $E^{0\prime}_{Ti(IV)/Ti(III)}$, starting from the Nernst equation of the reduction reaction in Eq3.58 and coupling all the associated chemical reactions to the electro-active species in Eq3.58 to yield to Eq4.5.

$$E = 0.065 + \frac{RT}{F}\ln\left(6.82x10^{-4}\, C_{H^+}^{2+}\right) + \frac{RT}{F}\ln\left(\frac{C_{Ti(OH)_2^{2+}}}{C_{Ti^{3+}}}\right) \quad \text{Eq4.5}$$

The formal potential of the redox couple $Ti(OH)_2^{2+}/Ti^{3+}$, $E^{0\prime}_{Ti(OH)_2^{2+}/Ti^{3+}}$, is estimated for the case of 1M Ti+3M H_2SO_4 on carbon felt working electrode by substitution the estimated H^+ concentration in Table 13, to get Eq4.6.

$$E = -0.092 + \frac{RT}{F}\ln\left(\frac{C_{Ti(OH)_2^{2+}}}{C_{Ti^{3+}}}\right) \quad \text{Eq4.6}$$

The formal potential of the redox couple $Ti(OH)_2^{2+}/Ti^{3+}$, $E^{0\prime}_{Ti(OH)_2^{2+}/Ti^{3+}}$, is estimated for the case of 1M Ti +1M Mn+3M H_2SO_4 on carbon felt working electrode by substitution the estimated H^+ concentration in Table 14, to get Eq4.7.

$$E = -0.093 + \frac{RT}{F}\ln\left(\frac{C_{Ti(OH)_2^{2+}}}{C_{Ti^{3+}}}\right) \quad \text{Eq4.7}$$

The theoretical estimated formal potential, $E^{0\prime}_{Ti(OH)_2^{2+}/Ti^{3+}}$, in Eq4.6, and Eq4.7 are within 1% from the experimental half peak potential, $E_{1/2}$ as shown in Figure 81.

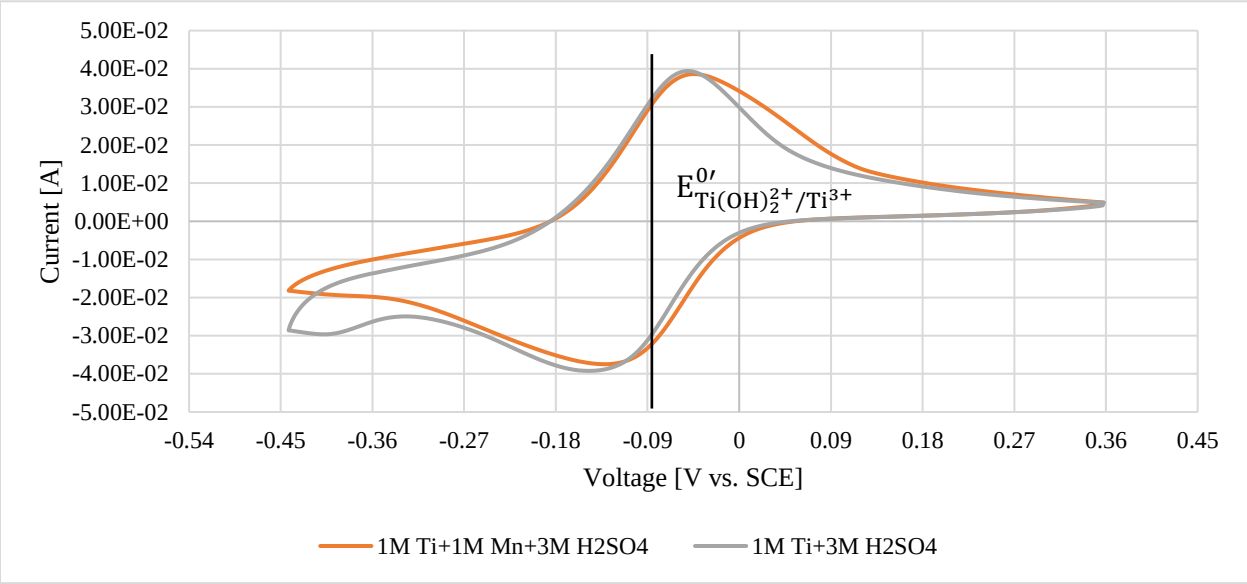

Figure 81. Third cyclic voltammetry scan of 1M $TiOSO_4$-1M $MnSO_4$ in 3M H_2SO_4 and 1M $TiOSO_4$ in 3M H_2SO_4 on a carbon felt working electrode with 2mV/s scan rate with the estimated formal potential.

4.4.4. Comparing the Ti Cyclic Voltammetry Results to Previous Reported Results

The shape of the cyclic voltammetry of the Ti electrolyte with and without the addition of Mn obtained by SE in Figure 28 differs from the one obtained in Figure 81 because of the different experimental setup. In Figure 81, the cyclic voltammetry was conducted in a static cell where the working electrode was immersed in a large availability of the Mn electrolyte, so that not all the Ti electro-active species in the electrolyte was consumed during the cyclic voltammetry scan. SE conducted the cyclic voltammetry in a flow cell where the tested electrolyte was kept still in the working electrode, so that the Ti electro-active species was fully consumed during the cyclic voltammetry and a zero current was achieved at the end of the cathodic scan. However, the anodic peak voltage and the cathodic peak voltage were the same to the one obtained by SE which

indicates that the same proposed mechanism for Ti(IV)/Ti(III) couple may still valid to describe the electrochemical behavior in the cyclic voltammetry.

Conclusions and Recommendations

An electrochemical characteristic evaluation of the Ti-Mn electrolyte system in sulfuric acid aqueous solution is studied in different acid concentrations with and without the mixing of $TiOSO_4$ and $MnSO_4$ electrolyte system.

First, solubility measurements are conducted to find the solubility of Ti and Mn electrolyte systems in different sulfuric acid concentrations at different temperatures. For Mn electrolyte, it is found that the solubility of $MnSO_4$ salt decreases as the concentration of H_2SO_4 in the solution increase, and the solubility of $MnSO_4$ negatively depends on the electrolyte temperature. For Ti electrolyte, the solubility of $TiOSO_4$ decreases as the concentration of H_2SO_4 in the solution increase. The solubility of $TiOSO_4$ positively depends on the electrolyte temperature.

A theoretical study on the Ti-Mn electrolytes is evaluated to study the speciation of Ti-Mn electrolyte in sulfuric acid solution, and possible the electro-active species in the electrolyte solution. For Mn electrolyte, the electro-active specie of Mn(II) is in the form of Mn^{2+} free cation. However, with the presence of SO_4^{2-} in sulfuric acidic media, Mn^{2+} forms undissociated aqueous $MnSO_4$ complex in the solution. For Ti electrolyte, two electro-active species are found to be electrochemically active within the studied voltage window which are Ti^{4+} and $TiSO_4^{2+}$. At low acid concentration (1M H_2SO_4), Ti^{4+} is found to be the dominant electro-active species, and at a high acid concentration (3M H_2SO_4), $TiSO_4^{2+}$ is found to be the dominant electro-active species. For Ti+Mn electrolyte, the addition of $TiOSO_4$ to the $MnSO_4$+H_2SO_4 solution is found to significantly reduce the H^+ concentration and the Mn^{2+} concentration in the electrolyte compared to Mn electrolyte without the addition of $TiOSO_4$.

The electron transfer reaction mechanism of Mn electrolyte is studied using the cyclic voltammetry and the anodic voltage hold techniques. Based on the theoretical study of the speciation of Mn electrolyte in sulfuric acid solution, a mechanism for the electron transfer reaction of Mn system is proposed and evaluated with the experimental observations from the electrochemical characterization results. It is concluded that the overall anodic behavior of Mn system can be described by the oxidation reaction of Mn^{2+} to MnO_2 where Mn^{3+} is an intermediate species. As the acid concentration increases, less MnO_2 is formed on the working electrode and more Mn^{3+} is formed in the solution; however, due to the instability of Mn^{3+} in an aqueous solution, Mn^{3+} undergoes a significant hydrolysis reaction to precipitate as MnOOH in the electrolyte solution. Mixing Ti with Mn electrolyte is found to lower the H^+ concentration which is believed to increase the amount of MnOOH in the solution and lower the aqueous Mn^{3+} concentration. In addition to the low H^+ concentration, the comproportionation reaction of Mn^{2+} in Mn+Ti electrolyte is found to have a negative effect on the generated MnO_2 where the comproportionation reaction results in forming MnOOH away from the working electrode. The formed MnOOH by the Mn^{3+} hydrolysis reaction is proven to be electrochemically active if it is deposited on the working electrode.

A summary of the findings from the electrochemical characteristic evaluation of the Mn electrolyte is listed as follow:

- Mn^{2+} is oxidized during the positive scan of the cyclic voltammetry on the working electrode to form Mn^{3+}species, and not directly to Mn(IV) species because Mn^{2+} must go through two elementary electron transfer reaction steps to form Mn(IV).
- The oxidation reaction of Mn(III) species to Mn(IV) species may be influenced by the Mn^{3+} hydrolysis reactions to form the electro-active Mn(III) species that undergoes the

oxidation reaction in which the its concentration decreases as the acid concentration increases The oxidized Mn(IV) species may undergo significant hydrolysis on the working electrode surface to form MnO_2 deposit on the electrode surface.

- As the MnO_2 covers the surface of the working electrode, Mn^{2+} may be oxidized on the MnO_2 substrate to form Mn^{3+}, and the formed Mn(III) may not be oxidized further to Mn(IV) species due to the low electronic conductivity of the substrate. Rather Mn^{3+} may diffuse away from the electrode or hydrolyze on the MnO_2 substrate to form MnOOH.
- When using a graphite rod working electrode, the MnO_2 coverage phenomenon may limit the overall anodic process due to the fast MnO_2 build up deposit on the working electrode.
- As the working electrode area increases when using a carbon felt working electrode, the limited anodic current may due to the diffusion limitation of Mn^{2+} species from the bulk to the electrode surface; however, the limited anodic current for the Mn electrolyte in 1M H_2SO_4 may still be due to the MnO_2 substrate due to the fast MnO_2 deposit build up on the working electrode.
- When using a carbon felt working electrode where the anodic process is not limited by the small area of the electrode, as the concentration of H^+ increases, less MnO_2 and less MnOOH are formed on the working electrode surface; however, more MnOOH is formed on the working electrode compared to the MnO_2
- The addition of $TiOSO_4$ to the $MnSO_4$+H_2SO_4 solution is suggested to significantly reduce the H^+ concentration and the Mn^{2+} concentration in the electrolyte compared to the Mn electrolyte without the addition of $TiOSO_4$, and the overall anodic process of

lowering the concentration of Mn^{2+} and H^{+} with the addition of Ti in 1M Mn+3M H_2SO_4 solution is dominated by the decrease of Mn^{2+} concentration. So, the overall oxidation reaction is controlled by the oxidation of Mn^{2+} to Mn^{3+} species until it is limited by the diffusion of Mn^{2+} from the bulk to the electrode surface, resulting in less formation of Mn^{3+} in 1M Mn+1M Ti+ 3M H_2SO_4 solution and less MnO_2 deposit is formed during the positive scan compared to the solution without the addition of Ti,

- From the anodic voltage hold of Mn electrolyte and Mn+Ti electrolyte on a graphite rod working electrode and the cathodic linear voltage sweep in 3M H_2SO_4 results, the estimated anodic charges of Mn^{3+} is significantly low compared to the overall anodic charges resulted from the anodic voltage hold of Mn and Mn+Ti electrolyte. The percentages of the recovered cathodic charges during the linear voltage sweep in 3M H_2SO_4 to the anodic charges generated during the anodic voltage are 79% for MnO_2 deposit resulted from Mn electrolyte and 35% for MnO_2 deposit resulted from Mn+Ti electrolyte.
- From the anodic voltage hold of Mn electrolyte on a graphite rod working electrode and the cathodic linear voltage sweep in 3M H_2SO_4 with varying the OCV holding time, it was confirmed that the dissolution of MnOOH to Mn^{3+} may interfere with the reduction reaction of MnO_2 to MnOOH, and the reduction reaction of MnO_2 may still proceed after the first cathodic peak at a limited current because Mn^{3+} may react with the MnOOH to generate more MnO_2 and H^{+}.
- From the anodic voltage hold of Mn electrolyte and Mn+Ti electrolyte on a graphite rod working electrode and the cathodic linear voltage sweep in 1M Mn+3M H_2SO_4 and 1M Mn+1M Ti+3M H_2SO_4, the comproportionation reaction of Mn^{2+} may form

aqueous Mn^{3+} species, and the Mn^{3+} species may be in equilibrium with the Mn^{2+} and MnO_2 due to the high H^+ concentration in 1M Mn+3M H_2SO_4. While, the comproportionation reaction of Mn^{2+} in 1M Mn+Ti+3M H_2SO_4 may form aqueous Mn^{3+} species, and the resulted Mn^{3+} species may undergo a significant hydrolysis to form MnOOH in the solution due to the low H^+. The overall recovery of the MnO_2 substrate in 1M Mn +3M H_2SO_4 solution is believed to be not significantly affected by the comproportionation reaction due to the possibility of forming aqueous Mn^{3+} that is in equilibrium with the MnO_2 substrate near the solution side. However, the recovery of the cathodic charges of the MnO_2 substrate in 1M Mn+1M Ti+3M H_2SO_4 solution is highly affected by the comproportionation reaction due to the low H^+ concentration that allows the Mn^{3+} to precipitate to MnOOH. Consequently, MnO_2 cathodic charges is believed to be lost in the solution in the form of MnOOH in the solution away from the working electrode.

- From the anodic voltage hold of Mn electrolyte and Mn+Ti electrolyte on a graphite rod working electrode and the cathodic linear voltage sweep in 1M Ti+3M H_2SO_4, the reduction reaction of MnO_2 to MnOOH is found to be enhanced due to the lower interference of the dissolution of MnOOH to Mn^{3+} on the reduction reaction of MnO_2 to MnOOH because of the low H^+ concentration in 1M Ti+3M H_2SO_4.
- From the linear voltage sweep results of Mn and Mn+Ti anodic products in 3M H_2SO_4 solution with and without convection on a graphite rod working electrode, more MnO_2 is formed on the working electrode during the anodic voltage with convection in both electrolytes due to the increase of the transport of Mn^{2+} species from the bulk to the electrode surface. The percentage of the recovery of the MnO_2 substrate resulted from

the anodic voltage hold of Mn+Ti electrolyte without convection is almost the same to the percentage recovery of the MnO_2 substrate resulted from the anodic voltage hold of Mn+Ti electrolyte with convection. However, the percentage recovery of the MnO_2 substrate resulted from the anodic voltage hold of Mn electrolyte with convection is 30% less than that of the MnO_2 substrate resulted from the anodic voltage hold of Mn electrolyte without convection because of the removal of MnOOH substrate from the working electrode in the case of convection. As a result, when convection is applied during the anodic voltage hold experiment for both Mn electrolyte and Mn+Ti electrolyte, the anodic limited current is slightly increased, and the low measured effect on the anodic limited current may due to the large MnO_2 deposit on the small graphite rod working electrode

- From the linear voltage sweep results of Mn and Mn+Ti anodic products in 3M H_2SO_4 solution with and without convection on a carbon felt working electrode, when convection is applied during the anodic voltage hold experiment for both Mn electrolyte and Mn+Ti electrolyte, the anodic limited current is significantly increased due to the high transport of Mn^{2+} species from the bulk solution to the surface of the working electrode. After the anodic voltage hold experiment, Mn+Ti electrolyte solution color turns into a non-transparent dark black, and Mn electrolyte solution color turns into a semi-transparent red-black where the black color is believed to be MnOOH resulted from Mn^{3+} hydrolysis reaction. More MnOOH is expected to be in Mn+Ti electrolyte than in Mn electrolyte due to the low H^+ concentration in Mn+Ti electrolyte, and the semi-transparent red-black color in Mn electrolyte indicates that there is more Mn^{3+} species in Mn electrolyte than in Mn+Ti electrolyte due to the high acid

concentration of the Mn electrolyte. The increase of the measured OCV with time after the anodic voltage hold experiment using a new clean graphite rod working electrode indicates that MnO_2 is forming on the electrode while measuring the OCV of the two tested electrolytes because of the disproportionation reaction of Mn^{3+} and MnOOH on the working electrode surface. From the cathodic voltage scan of the substrate on the carbon felt working electrode resulted from the anodic voltage hold under stagnant condition, large amount of MnO_2 and MnOOH are found from the anodic voltage hold of Mn electrolyte due to the high Mn^{2+}concentration, and that the comproportionation reaction has a lower effect on the deposit in Mn electrolyte compared to Mn+Ti electrolyte. The formed MnOOH substrate on the carbon felt is believed to be resulted from the hydrolysis of Mn^{3+} species, and not from the MnOOH that is resulted from the reduction reaction of MnO_2 during the first cathodic wave current. Therefore, two MnOOH solid phases are formed during the anodic voltage hold of Mn electrolyte and Mn+Ti electrolyte. It is proposed that the MnOOH phase formed by Mn(III) hydrolysis is $(\gamma)MnOOH$, and the phase of MnOOH resulted from the reduction reaction of MnO_2 substrate is $(\alpha)MnOOH$ which is electrochemically nonactive. From the cathodic voltage scan of the substrate on carbon felt working electrode resulted from the anodic voltage hold under convection condition, since the H^+ concentration is high in Mn electrolyte, the applied convection on the working electrode during the anodic voltage hold scan helps minimizing the formation of MnO_2 on the working electrode by removing the Mn(III) species from the electrode surface and allow it to precipitate in the solution in the form of MnOOH and aqueous Mn^{3+}. Therefore, the amount of MnO_2 substrate resulted from Mn electrode with convection is less than the one without

convection. However, the low H^+ concentration in the Mn+Ti electrolyte during the anodic voltage hold increases the formation of MnO_2 on the working electrode compared to the anodic voltage hold of Mn+Ti electrolyte without convection. Overall, the percentage of the reduced cathodic charges of MnO_2 substrate resulted from Mn electrolyte and Mn+Ti electrolyte anodic voltage hold is significantly less with convection.

It is recommended that further investigation for Mn/Ti electrolyte to be conducted using different anion media to prove or disprove weather the electrochemical behavior of Mn electrolyte with and without the addition of Ti was due to the interaction between Mn(III) and Ti(IV) in aqueous solution or due to the changing in the chemical equilibria of the electrolyte solution. If there is no clear evidence for the stabilization of Mn(III) by Ti cation, further study is highly recommended to discover a capable metal-complex ligand that can suppress the hydrolysis of Mn(III) species and limits the redox reaction to only Mn(III)/Mn(II) redox couple.

The electron reaction mechanism of Ti electrolyte is studied using the cyclic voltammetry technique. Based on the theoretical study of the speciation of Ti electrolyte in sulfuric acid solution, a mechanism for the electron transfer reaction of Ti system is proposed and evaluated with the experimental observations from the electrochemical characterization results. It is concluded that two electro-active species are electrochemically active within the studied voltage window which are Ti^{4+} and $TiSO_4^{2+}$. At low acid concentration (1M H_2SO_4), Ti^{4+} is found to be the dominant electro-active species, and at a high acid concentration (3M H_2SO_4), $TiSO_4^{2+}$ is found to be the dominant electro-active species. For Ti+Mn electrolyte, the addition of 1M $MnSO_4$ to the 1M $TiOSO_4$+3M H_2SO_4 solution results in a high concentration of undissociated $MnSO_4$, and it found that the dissociation of $MnSO_4$ to SO_4^{2-} improve the activity of the redox reaction of

Ti(IV)/Ti(III). With the increase of H_2SO_4 and the addition of $MnSO_4$ in the Ti electrolyte, the electrochemical behavior of the Ti(IV)/Ti(III) redox couple tends toward the reversibility.

A summary of the findings from the electrochemical characteristic evaluation of the Ti electrolyte is listed as follow:

- From the cyclic voltammetry of 1M Ti in 1M H_2SO_4 solution, after the Ti^{4+} is reduced to Ti^{3+} during the negative scan, the small electrode area decreases the supply rate of Ti^{4+} via the chemical path and increase the hydrolysis of Ti^{3+} to form more H^+ that would eventually allow to delay the limited current to a low applied voltage region. When using a carbon felt working electrode, the electron transfer reaction area increases and the consumption of Ti^{4+} increases, so that the supply of Ti^{4+} via the chemical path would be faster than the hydrolysis of Ti^{3+}. In this case a limited cathodic current is achieved due to the lack of H^+ concentration.
- From the cyclic voltammetry of 1M Ti in 2-3M H_2SO_4 solution, the supply of $TiSO_4^{2+}$ depends on the amount of $Ti(OH)^{3+}$, $Ti(OH)_2^{2+}$, Ti^{4+}, SO_4^{-2} and the H^+ concentration. In addition to the chemical reactions associated with oxidized species, Ti^{3+} may couple with the sulfate and hydrolyze to generate more H^+. Based on the speciation study of Ti(IV) in 2-3M H_2SO_4, the SO_4^{-2} concentration is less than the Ti^{4+}concentation, so the reduction reaction is more likely to be limited by the low SO_4^{-2} concentration. However, the reduced species $TiSO_4^+$ may decompose into Ti^{3+} and SO_4^{-2}. The generated SO_4^{-2} via the reduced species helps the formation of $TiSO_4^{2+}$ via reacting with Ti^{4+}. This process may be slow in the case of graphite working electrode due to small available area, so the reduction reaction is limited by the lack of SO_4^{-2} supply. The supply of SO_4^{-2} species is faster in carbon felt working electrode case, so a clear peak current is

observed during the cathodic scan which indicate the low Ti^{4+} concentration. However, at a very low applied voltage, the rate of consumption of SO_4^{-2} may increase as opposed to the rate of SO_4^{-2} generation and Ti^{4+} reduction reaction may proceed instead of $TiSO_4^{2+}$. Thus, the second cathodic peak is attributed to the Ti^{4+} reduction reaction instead of $TiSO_4^{2+}$ where the cathodic wave is higher for the case of 3M H_2SO_4 due to the high H^+ concentration that supply $TiSO_4^{2+}$ via the chemical path.

- From the cyclic voltammetry of 1M Ti+1M Mn in 2-3M H_2SO_4 solution, the supply of $TiSO_4^{2+}$ depends on the amount of $Ti(OH)^{3+}$, $Ti(OH)_2^{2+}$, Ti^{4+}, SO_4^{-2} and the H^+ concentration. In addition to the chemical reactions associated with oxidized species, Ti^{3+} may couple with the sulfate and hydrolyze to generate more H^+. Based on the equilibrium concentration of the Ti(IV) species in 2-3M H_2SO_4, the SO_4^{-2} concentration is less than the Ti^{4+}concentation, so the reduction reaction more likely to be limited by the low SO_4^{-2} concentration. However, SO_4^{-2} may be always available from $TiSO_4^+$ decomposition into Ti^{3+} and SO_4^{-2} and from the $MnSO_4$ dissociation. The generated SO_4^{-2} helps the formation of $TiSO_4^{2+}$ via reacting with Ti^{4+} until Ti^{4+} become limited.
- The formal potential of the redox couple $Ti(OH)_2^{2+}/Ti^{3+}$, $E^{0\prime}_{Ti(OH)_2^{2+}/Ti^{3+}}$, is estimated for the cyclic voltammetry of 1M Ti+3M H_2SO_4 on a carbon felt working electrode:

$$E = -0.092 + \frac{RT}{F}\ln\left(\frac{C_{Ti(OH)_2^{2+}}}{C_{Ti^{3+}}}\right) \qquad \text{Eq4.6}$$

- The formal potential of the redox couple $Ti(OH)_2^{2+}/Ti^{3+}$, $E^{0\prime}_{Ti(OH)_2^{2+}/Ti^{3+}}$, is estimated for the cyclic voltammetry of 1M Ti+1M Mn+3M H_2SO_4 on a carbon felt working:
    - $E = -0.093 + \frac{RT}{F}\ln\left(\frac{C_{Ti(OH)_2^{2+}}}{C_{Ti^{3+}}}\right)$ Eq4.7

Due to the improvement on the electrochemical behavior of the Ti(IV)/Ti(III) redox couple with the increasing of H_2SO_4 and the addition of $MnSO_4$ in the Ti electrolyte, further study is highly recommended to discover other salts with a sulfate anion that is soluble, but not fully dissociated.

References

[1] "BP Statistical Review of World Energy 68th Edition," The British Petroleum Company plc and BP Amoco plc, London, 2019.

[2] IEA, "Electricity demand by sector and scenario, 2018-2040," IEA, 19 11 2019. [Online]. Available: https://www.iea.org/data-and-statistics/charts/electricity-demand-by-sector-and-scenario-2018-2040. [Accessed 15 5 2020].

[3] IEA, "IEA, Electricity generation by fuel and scenario, 2018-2040," 21 11 2019. [Online]. Available: https://www.iea.org/data-and-statistics/charts/electricity-generation-by-fuel-and-scenario-2018-2040. [Accessed 16 5 2020].

[4] Haisheng Chen, Thang Ngoc Cong, Wei Yang, Chunqing Tan, Yongliang Li and Yulong Ding, "Progress in electrical energy storage system: A critical review," *Progress in Natural Science,* vol. 19, no. 3, pp. 291-312, 2009.

[5] S. V. d. Linden, "Bulk energy storage potential in the USA, current developments and future prospects," *ENERGY,* vol. 31, p. 3446–3457, 2006.

[6] G. Karmiris and Tomas Tengné, "Peak Shaving Control Method for Energy Storage," ABB AB, Corporate Research Center, Västerås, Sweden, 2016.

[7] Xing Luo, Jihong Wang, Mark Dooner and Jonathan Clarke, "Overview of current development in electrical energy storage technologies and the application potential in power system operation," *Applied Energy,* vol. 137, no. 1, pp. 511-536, 2015.

[8] Trung Nguyen and Robert F. Savinell, "Flow Batteries," *The Electrochemical Society Interface,* vol. 19, no. 3, 2010.

[9] Dapeng Zhang, Qinghua Liu and Yongdan Li, "Chapter 3 - Design of flow battery," in *Reactor and Process Design in Sustainable Energy Technology*, Elsevier, 2014, pp. 61-97.

[10] M. Skyllas-Kazacos, M. Rychcik, R. G. Robins, A. G. Fane and M. A. Green, "New All-Vanadium Redox Flow Cell," *Journal of The Electrochemical Society,* vol. 133, no. 5, pp. 1057-1058, 1986.

[11] M. Skyllas-Kazacos, "Novel vanadium chloride/polyhalide redox flow battery," *Journal of Power Sources,* vol. 124, no. 1, pp. 299-302, 2003.

[12] M. Lopez-Atalaya, G. Codina, J.R. Perez, J.L. Vazquez and A. Aldaz, "Optimization studies on a Fe/Cr redox flow battery," *Journal of Power Sources,* vol. 39, no. 2, pp. 147-154, 1992.

[13] V. Livshits, A. Ulus and E. Peled, "High-power H2/Br2 fuel cell," *Electrochemistry Communications,* vol. 8, no. 8, pp. 1358-1362, 2006.

[14] Yan Huang, Shuang Gu, Yushan Yan and Sam Fong Yau Li, "Nonaqueous redox-flow batteries: features, challenges, and prospects," *Current Opinion in Chemical Engineering*, vol. 8, pp. 105-113, 2015.

[15] 2019. [Online]. Available: https://www.vanadiumprice.com. [Accessed 2020].

[16] Dong, Y., H. Kaku, H. Miyawaki, R. Tatsumi, K. Moriuchi and T. Shigematsu, "Titanium-manganese electrolyte for redox flow battery," *SEI Technical Review,* vol. 84, pp. 35-40, 2017.

[17] Hirokazu Kaku, Yong-Rong Dong, Kei Hanafusa, Kiyoaki Moriuchi and Toshio Shigemats, "Effect of Ti(IV) Ion on Mn(III) Stability in Ti/Mn Electrolyte for Redox Flow Battery," *ECS Transactions,* vol. 27, no. 10, pp. 1-9, 2016.

[18] Bard A. J., Parsons R. and Jordan J., Standard Potentials in Aqueous Solution IUPAC, New York: Dekker, 1983.

[19] Colin J. Clarke, Gregory J. Browning and Scott W. Donne, "An RDE and RRDE study into the electrodeposition of manganese dioxide," *Electrochimica Acta,* vol. 51 , no. 1, p. 5773–5784, 2006.

[20] F. H. Fisher and D. F. Davis, "The Effect of Pressure on the dissociation of Manganese Sulfate Ion Pairs in Water," *The Journal of Physical Chemistry,* vol. 69, no. 8, pp. 2595-2598, 1965.

[21] J. D. Hem, "Manganese Complexes with Bicarbonate and Sulfate in Natural Water," *Journal of Chemical and Engineering Data,* vol. 8, no. 1, pp. 99-101, 1963.

[22] Paul L. Brown and Christian Ekberg, Hydrolysis of Metal Ions, Boschstr: John Wiley & Sons, 2016.

[23] S. Bodoardo, J. Brenet, M. Maja and P. Spinelli, "Electrochemical behaviour of MnO2 electrodes in sulphuric acid solutions," *Electrochimica Acta,* vol. 39, no. 13, pp. 1999-2004, 1994.

[24] Biedermann, Georg and Palombari, Roberto, "On the Hydrolysis of the Manganese(III) Ion," *Acta Chemica Scandinavica,* vol. 32, no. A, pp. 381-390, 1978.

[25] H. Kaku, Y. R. Dong, K. Hanafusa, K. Moriuchi and T. Shigematsu, "Effect of Ti(IV) Ion on Mn(III) Stability in Ti/Mn Electrolyte for Redox Flow Battery," *ECS Transactions*, vol. 72, no. 10, pp. 1-9, 2016.

[26] Sun, W., Kitchaev D. A., Kramer D. and Ceder G. , "Non-equilibrium crystallization pathways of manganese oxides in aqueous solution. Nature communications," *Nature communications*, vol. 10, no. 1, pp. 1-9, 2019.

[27] Claus Daniel and Jürgen O. Besenhard, Handbook of Battery Materials, Second Edition, Germany: Wiley, 2011.

[28] Paul Ruetschi and R. Giovanoli, "Cation Vacancies in Mn02 and Their Influence on Electrochemical Reactivity," *Journal of The Electrochemical Society*, vol. 135, no. 11, pp. 2663-2669, 1988.

[29] D. Landolt, Corrosion and surface chemistry of metals, Switzerland: EFPL Press, 2007.

[30] Kobylin P., Sippola H. and Taskinen P., " Thermodynamic Model for Acidic Metal Sulfate from Solubility Data," in *REWAS 2013: Enabling Materials Resource Sustainability*, SWITZERLAND, Springer, Cham, 2013, pp. 145-154.

[31] F. Albert Cotton, Geoffrey Wilkinson, Carlos A. Murillo and Manfred Bochmann, Advanced Inorganic Chemistry, 6th Edition, New Jersey : John Wiley and Sons, 1999.

[32] Kiyoshi Shimizu, Nori Tsuchihashi and Yoshihito Kondo, "Effect of pressure on dissociation of ion pairs : MnSO4, CuSO4 and ZnSO4," *The Review of Physical Chemistry of Japan*, vol. 47, no. 2, pp. 80-89, 1977.

[33] Biedermann, Georg and Palombari, Roberto, "On the Hydrolysis of the Manganese(III) Ion.," *Acta Chemica Scandinavica,* vol. 32a, pp. 381-390, 1978.

[34] Klewicki, J. Kenneth and Morgan, James J., "Kinetic Behavior of Mn(III) Complexes of Pyrophosphate, EDTA, and Citrate," *Environmental Science & Technology,* vol. 32, no. 19, pp. 2916-2922, 1988.

[35] Yamaguchi, Kenneth and Sawyer, Donald, "The Redox Chemistry of Manganese(III) and -(IV) Complexes," *Israel Journal of Chemistry,* vol. 25, no. 2, pp. 164-176, 1985.

[36] Javier Rubio-Garcia, Anthony Kucernak, Dong Zhao, Danlei Li, Kieran Fahy and Vladimir Yufit, "Hydrogen/manganese hybrid redox flow battery," *Journal of Physics: Energy,* vol. 1, no. 1, pp. 1-9, 2019.

[37] K. Nicholson, Manganese Mineralization: Geochemistry And Mineralogy of Terrestrial And Marine Deposits, London: Geological Society of London, 1996.

[38] S. G. Bratsch, "Standard Electrode Potentials and Temperature Coefficients in Water at 298.15 K," *The Journal of Physical Chemistry,* vol. 18, no. 1, 1989.

[39] G. Ottonello, Principles of Geochemistry, New York City: Columbia University Press, 2000.

[40] Wenhao Sun, Daniil A. Kitchaev, Denis Kramer and Gerbrand Ceder, "Non-equilibrium crystallization pathways of manganese oxides in aqueous solution," *Nature Communications,* vol. 10, no. 573, 2019.

[41] Daniil A. Kitchaev, Stephen T. Dacek, Wenhao Sun and Gerbrand Ceder, "Thermodynamics of Phase Selection in MnO2 Framework Structures through Alkali Intercalation and Hydration," *American Chemical Society,* vol. 139, p. 2672−2681, 2017.

[42] Bjerrum, J., G. Schwarzenbach and L. G. Sillén, Stability Constants of Metal-Ion Complexes, with Solubility Products of Inorganic Substances, Part II: Inorganic Ligands, vol. 7, London: The Chemical Society, 1958, p. 131.

[43] W. Kao and V. J. Weibel, "Electrochemical oxidation of manganese(II) at aplatinum electrode," *Journal of Applied Electrochemistry,* vol. 22, no. 1, pp. 21-27, 1992.

[44] S. Bodoardo, J. Brenet, M. Maja and P. Spinelli, "Electrochemical behaviour of MnO2 electrodes in sulphuric acid solutions," *Electrochimica Acta,* vol. 39, no. 13, pp. 1999-2004, 1994.

[45] S. Nijjer, J. Thonstad and G.M. Haarberg, "Oxidation of manganese(II) and reduction of manganese dioxide in sulphuric acid," *Electrochimica Acta ,* vol. 46, no. 1, p. 395–399, 2000.

[46] Fang-Qin Xue, Yong-LiangWang, Wen-HongWang and Xin-DongWang, "Investigation on the electrode process of the Mn(II)/Mn(III) couple in redox flow battery," *Electrochimica Acta ,* vol. 53, no. 1, p. 6636–6642, 2008.

[47] P. Ruetschi, "Influence of Cation Vacancies on the Electrode Potential of Mn02," *Journal of the Electrochemical Society,* vol. 135, no. 11, pp. 2657-2663, 1988.

[48] Egon Wiberg, A. F. Holleman and Nils Wiberg, Inorganic Chemistry, Massachusetts: Academic Press, 2001.

[49] Fabien Baillon, Elise Provost and Walter Fürst, "Study of titanium(IV) speciation in sulphuric acid solutions by FT-Raman spectrometry," *Journal of Molecular Liquids,* pp. 8-12, 2008.

[50] Alexandre Pichavant, Elise Provost, Walter Fürst, and Jean-François Hochepied, "Determination of the temperature dependence of Titanium(IV) hydrolysis and complexation constants in aqueous sulfuric or chlorhydric solutions," *The Journal of Chemical Thermodynamics,* vol. 131, pp. 184-191, 2019.

[51] G. Biedermann, "The hydrolysis of some tripositive ions," *Recueil des Travaux Chimiques des Pays-Bas,* vol. 75, no. 6, pp. 716-720, 1956.

[52] I. Cservenyák, G.H. Kelsall and W. Wang, "Reduction of Ti(IV) species in aqueous hydrochloric and sulfuric acids II. ECE Model the behaviour in sulfate media," *Electrochimica Acta,* pp. 573-582, 1996.

[53] Liberato ciavatta, Diego Ferri and Giuseppe Riccio, "On the hydrolysis of the titanium(IV) ion in chloride media," *Polyhedron,* vol. 4, no. 1, pp. 15-22, 1985.

[54] J. A. Dean, Lange's Handbook of Chemistry, 12th ed, 12th ed ed., New York: McGraw-Hill, 1979, pp. p 9-4–9-94.

[55] Yan Zhang, Zhibao Li and Edouard Asselin, "Determination and chemical modeling of the solubility of FeSO4 7H2O in the Ti(SO4)2 H2SO4 H2O system," *J. Chem. Thermodynamics,* p. 219–227, 2016.

[56] Malgorzata M. Lencka and Richard E. Riman, "Thermodynamics of the Hydrothermal Synthesis of Calcium Titanate with Reference to Other Alkaline-Earth Titanates," *Chem. Mater.,* pp. 18-25, 1995.

[57] E. V. Shkol'nikov, "Thermodynamics of the Dissolution of Amorphous and Polymorphic TiO2 Modifications in Acid and Alkaline Media," *Russian Journal of Physical Chemistry A,* p. 567–571, 2016.

[58] D. R. Lide, CRC Handbook of Chemistry and Physics, Cleveland, Ohio : CRC Press, 2004.

[59] J. Hall, Lab Manual for Zumdahl/Zumdahl's Chemistry, CA, United States: Cengage Learning, Inc, 2002.

[60] B.I. Nabivanets and V.V. Lukachina, " Hydroxo-complexes of titanium(IV)," *Ukr Khim Zhur,* vol. 30, no. 1, pp. 1123-1128, 1964.

[61] I. Cservenyák, G.H. Kelsall and W. Wang, "Reduction of Ti(IV) species in aqueous sulfuric and hydrochloric acids i. Titanium speciation," *Electrochimica Acta,* vol. 41, no. 4, pp. 563-572, 1996.

[62] I. Cservenyák, G.H. Kelsall and W. Wang, "Reduction of Ti IV species in aqueous hydrochloric and sulfuric acids II. ECE model of the behaviour in sulfate media," *Electrochimica Acta,* vol. 41, no. 4, pp. 573-582, 1996 .

[63] J. O. Bockris, Conway, Brian E. and White, Ralph E., Modern Aspects of Electrochemistry, New York, NY: Plenum Publishing Corp, 1982.

[64] G. Biedermann, "The hydrolysis of some tripositive ions," *Recueil des Travaux Chimiques des Pays-Bas,* vol. 75, no. 6, pp. 716-720, 1956.

[65] Noel, M. and Anantharaman, P.N., "Voltammetric studies on glassy carbon electrodes-111. A comparative study of electron-transfer kinetics of ti4+/ti3+ redox complexes on glassy carbon and mercury electrodes.," *Bulletin of Electrochemistry,* vol. 3, no. 4, pp. 349-357, 1987.

[66] P. Kiekens , J. Vandenbruwaene and E. Temmerman, "Voltammetric Behaviour of the Ti(IV)/Ti(III) Couple at Glassy Carbon in H2SO4 Solutions," *Bulletin des Sociétés Chimiques Belges,* vol. 90, no. 10, pp. 351-356, 1981.

[67] Elgrishi, Noémie, Rountree, Kelley J., McCarthy, Brian D., Rountree, Eric S., Eisenhart, Thomas T. and Dempsey, Jillian L., "A Practical Beginner's Guide to Cyclic Voltammetry," *Journal of Chemical Education,* vol. 95, no. 2, pp. 197-206, 2018.

[68] Allen J. Bard and Larry R. Faulkner, Electrochemical Methods: Fundamentals and Applications, 2nd Edition, New York: Wiley, 2001.

[69] Richard Guy Compton and Craig E Banks , Understanding Voltammetry (Third Edition), London: World Scientific Publishing Company, 2018.

[70] H.-H. Perkampus, UV-VIS Spectroscopy and Its Applications, Berlin Heidelberg: Springer , 2013.

[71] T. Scientific, "GENESYS™ 10S UV-Vis Spectrophotometer," Thermo Scientific, [Online]. Available: https://www.thermofisher.com/order/catalog/product/840-208100#/840-208100. [Accessed 30 6 2020].

[72] Renjini A and Dani Dileep, "Spectrophotometry and Spectrometry - Concept and Applications," *IJARIIE,* vol. 2, no. 4, pp. 2395-4396, 2017.

[73] J. Wang, Analytical electrochemistry 3rd ed, Hoboken, N.J: John Wiley & Sons, Inc., 2006.

Appendices

Appendix A. Sample Modeling Equations of the Equilibrium Concentration of Species in the Solution

For the equilibrium concentration of species in 1M $MnSO_4$+1M H_2SO_4, assume Eq.3.11, Eq.12, and Eq.3.30 take place in the solution where H_2SO_4 was assumed to be fully dissociate into HSO_4^- and H^+ based on Eq3.29. Assume x_1, x_2, and x_3 is the change of moles in each reaction.

$$HSO_4^- \leftrightarrow H^+ + SO_4^{2-} \qquad K=0.012 \qquad \text{Eq3.30}$$

$$MnSO_{4_{Aq}} \leftrightarrow Mn^{2+} + SO^{-2}, \qquad K = 0.00158 \qquad \text{Eq3.11}$$

$$Mn^{2+} + H_2O \leftrightarrow Mn(OH)^+ + H^+ \qquad K=2.725\ E\text{-}11 \qquad \text{Eq3.12}$$

Thus, the modeling equations for Eq.3.11, Eq.12, and Eq.3.30 are:

$$C_{HSO_4^-} = 1 - x_1 \qquad \text{Eq A.1}$$

$$C_{H^+} = 1 + x_1 + x_3 \qquad \text{Eq A.2}$$

$$C_{SO_4^{-2}} = x_1 + x_2 \qquad \text{Eq A.3}$$

$$C_{Mn^{2+}} = x_2 - x_3 \qquad \text{Eq A.4}$$

$$C_{MnSO_4} = 1 - x_2 \qquad \text{Eq A.5}$$

$$C_{Mn(OH)^+} = x_3 \qquad \text{Eq A.6}$$

$$0.012 = \frac{(1++x_1+x_3)(x_1+x_2)}{1-x_1} \qquad \text{Eq A.7}$$

$$0.00158 = \frac{(x_1+x_2)(x_2-x_3)}{1-x_2} \qquad \text{Eq A.8}$$

$$2.725\ E-11 = \frac{(1+x_1+x_3)X_3}{(x_2-x_3)} \qquad \text{Eq A.9}$$

Appendix B. Experimental Collected Data for the Solubility of Mn-Ti system

Raw data of $MnSO_4$ solubility from the UV-vis spectroscopy scan at 401.1nm at 25 ^oC

Table 29. Raw data of $MnSO_4$ solubility from the UV-vis spectroscopy scan at 401.1nm at 25 ^oC

At 20 ^oC	[M] H_2SO_4	Dilution	Intensity(1)	Intensity(2)	Intensity(3)	Intensity(Avg.)	Intensity (S.D)
	1.000	3.000	0.046	0.046	0.047	0.046	0.001
	2.000	3.000	0.034	0.034	0.034	0.034	0.000
	3.000	2.000	0.041	0.033	0.041	0.038	0.005
At 25 ^oC	[M] H_2SO_4	Dilution	Intensity(1)	Intensity(2)	Intensity(3)	Intensity(Avg)	Intensity (S.D)
	1.000	3.000	0.044	0.045	0.044	0.044	0.001
	2.000	3.000	0.036	0.032	0.032	0.033	0.002
	3.000	2.000	0.037	0.037	0.037	0.037	0.000
At 30 ^oC	[M] H_2SO_4	Dilution	Intensity(1)	Intensity(2)	Intensity(3)	Intensity()	Intensity (S.D)
	1.000	3.000	0.040	0.047	0.041	0.043	0.004
	2.000	3.000	0.029	0.032	0.034	0.032	0.003
	3.000	2.000	0.036	0.034	0.034	0.035	0.001
At 40 ^oC	[M] H_2SO_4	Dilution	Intensity(1)	Intensity(2)	Intensity(3)	Intensity(Avarage)	Intensity (S.D)
	1.000	3.000	0.041	0.042	0.034	0.039	0.004
	2.000	3.000	0.034	0.029	0.028	0.030	0.003
	3.000	2.000	0.030	0.033	0.030	0.031	0.002
At 45 ^oC	[M] H_2SO_4	Dilution	Intensity(1)	Intensity(2)	Intensity(3)	Intensity(Avarage)	Intensity (S.D)
	1.000	3.000	0.043	0.035	0.035	0.038	0.005
	2.000	3.000	0.038	0.026	0.024	0.029	0.008
	3.000	2.000	0.030	0.030	0.030	0.030	0.000

- Raw data of $TiOSO_4$ solubility of moles addition of $TiOSO_4$ salt before saturation

Table 30. Raw data of $TiOSO_4$ solubility of moles addition of $TiOSO_4$ salt until saturation

			Number of the addition of Ti until saturation is achieved				
	H_2SO_4[M]	$TiOSO_4$ concentration [M]	1	2	3	4	5
20 ºC	1	3.8	0.1	-	-	-	-
	2	2.7	0.1	-	-	-	-
	3	1.8	0.05	-	-	-	-
25 ºC	1	3.75	0.05	0.1	0.1	-	-
	2	2.65	0.05	0.05	0.05	-	-
	3	1.85	0.05	-	-	-	-
30 ºC	1	3.9	0.1	0.05	0.05	0.1	
	2	2.7	0.1	0.1	0.1	-	-
	3	1.85	0.05	0.05	-	-	-
40 ºC	1	4	0.1	0.1	0.05	0.1	0.1
	2	2.8	0.1	0.05	0.05	0.1	
	3	1.9	0.1	-	-	-	-
45 ºC	1	4.1	0.1	0.1	0.1	0.1	-
	2	2.8	0.1	0.1	0.1	0.1	-
	3	1.9	0.1	0.1	-	-	-

Appendix C. Additional Electrochemical Characterization Results

- OCV of fresh Mn electrolyte solutions before cyclic voltammetry

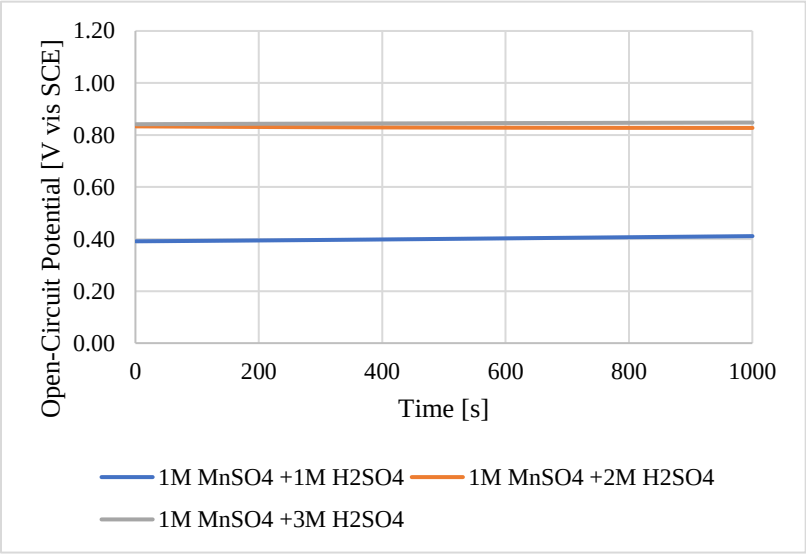

Figure 82. OCV of fresh Mn electrolyte solutions before cyclic voltammetry

- OCV of fresh Ti electrolyte solutions before cyclic voltammetry

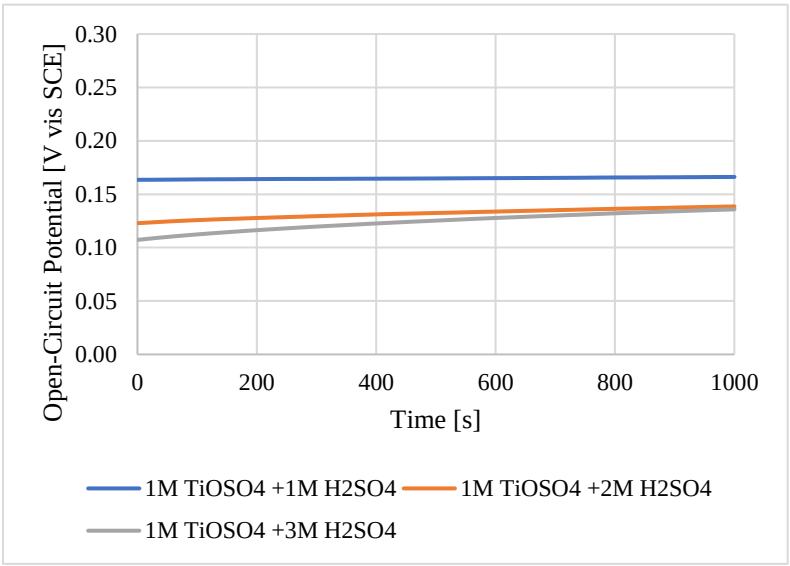

Figure 83. OCV of fresh Ti electrolyte solutions before cyclic voltammetry

- OCV of fresh Mn+Ti electrolyte solutions before cyclic voltammetry

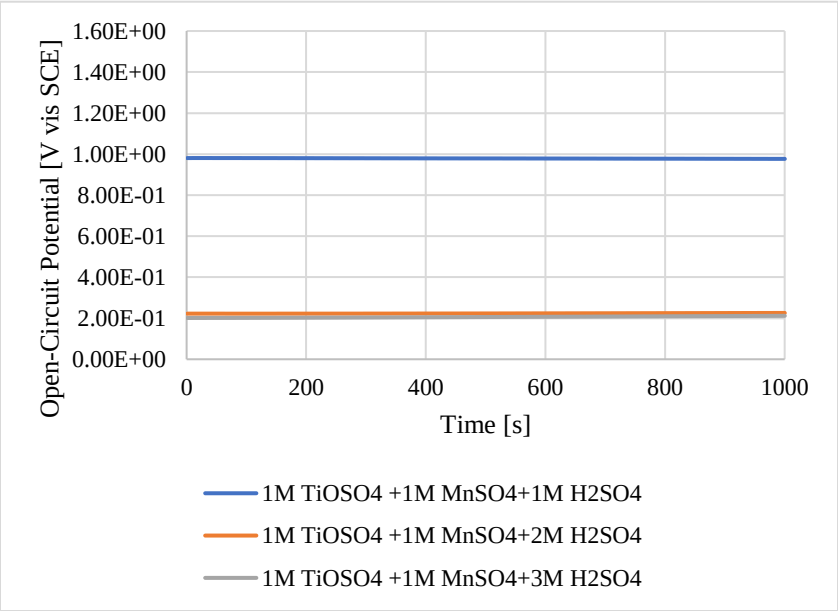

Figure 84. OCV of fresh Mn-Ti electrolyte solutions before cyclic voltammetry

- Ohmic resistance of Mn electrolyte using EIS spectroscopy

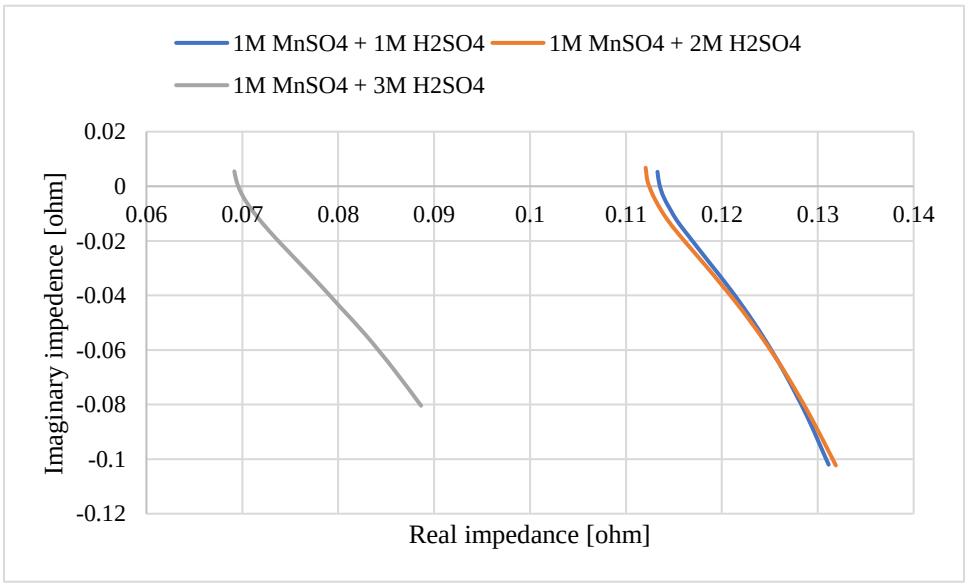

Figure 85. Ohmic resistance of Mn electrolyte using EIS spectroscopy

- Ohmic resistance of Ti electrolyte using EIS spectroscopy

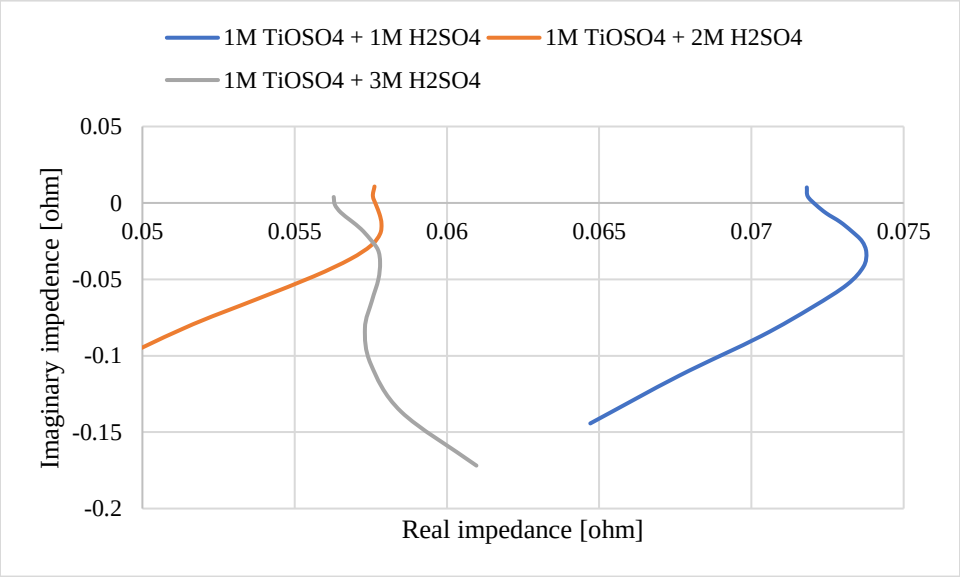

Figure 86. Ohmic resistance of Ti electrolyte using EIS spectroscopy

- Ohmic resistance of Mn+Ti electrolyte using EIS spectroscopy

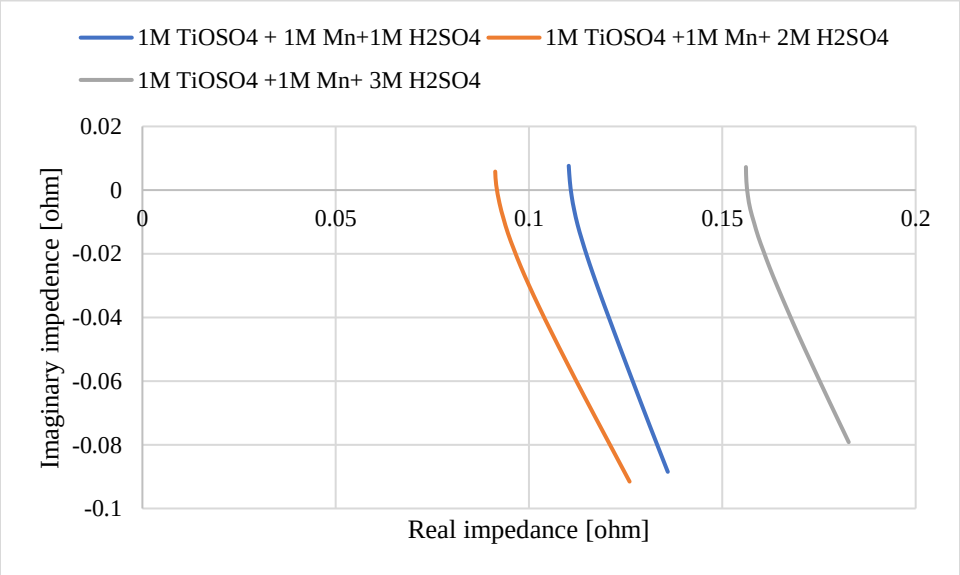

Figure 87. Ohmic resistance of Mn-Ti electrolyte using EIS spectroscopy

- First and second cyclic voltammetry scan of Mn electrolyte solutions on a graphite rod working electrode results.

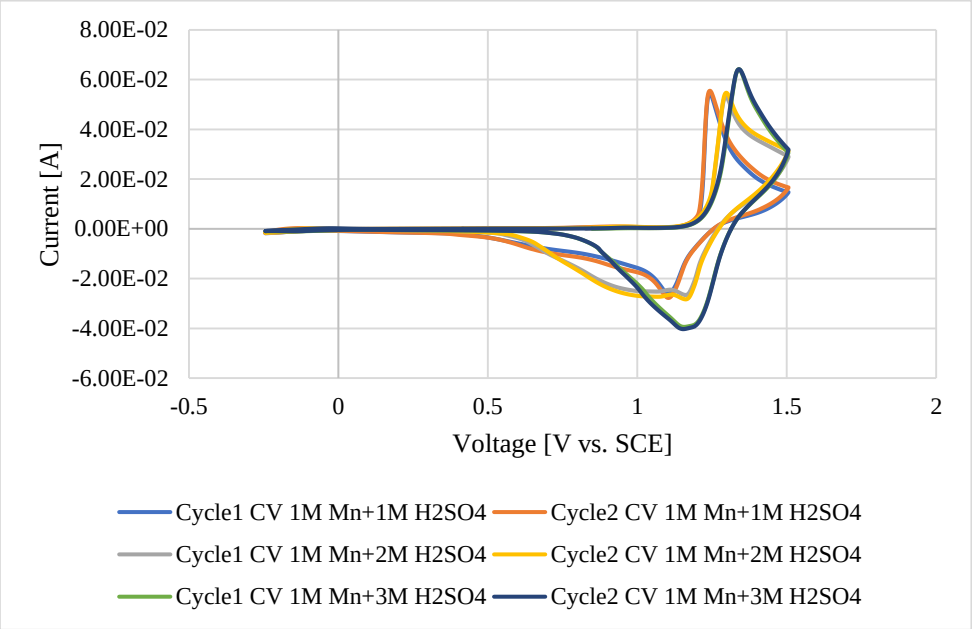

Figure 88. First and second cyclic voltammetry scan of Mn electrolyte solutions on a graphite rod working electrode results.

- First and second cyclic voltammetry scan of Mn electrolyte solutions on a carbon felt working electrode results.

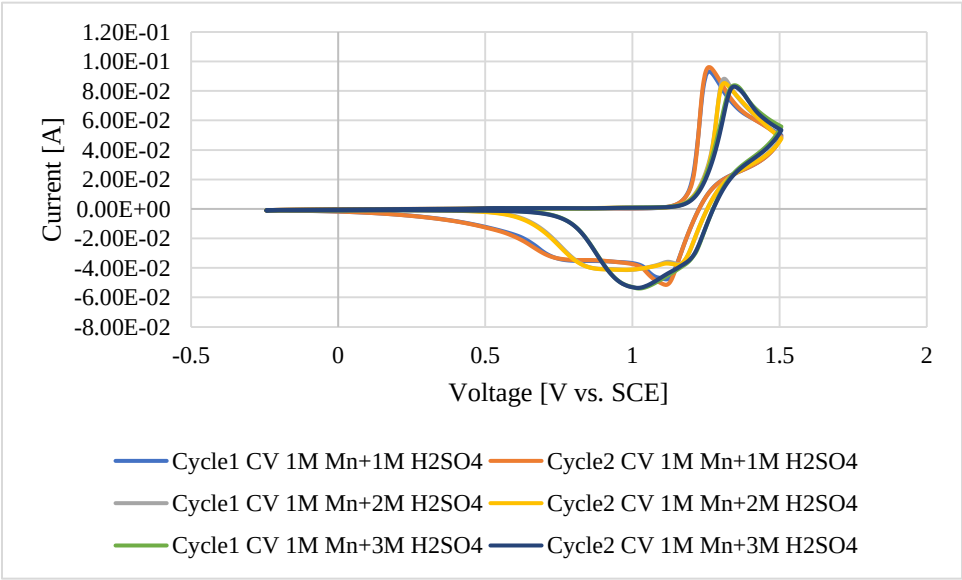

Figure 89. First and second cyclic voltammetry scan of Mn electrolyte solutions on a carbon felt working electrode results.

- First and second cyclic voltammetry scan of Ti electrolyte solutions on a graphite rod working electrode results.

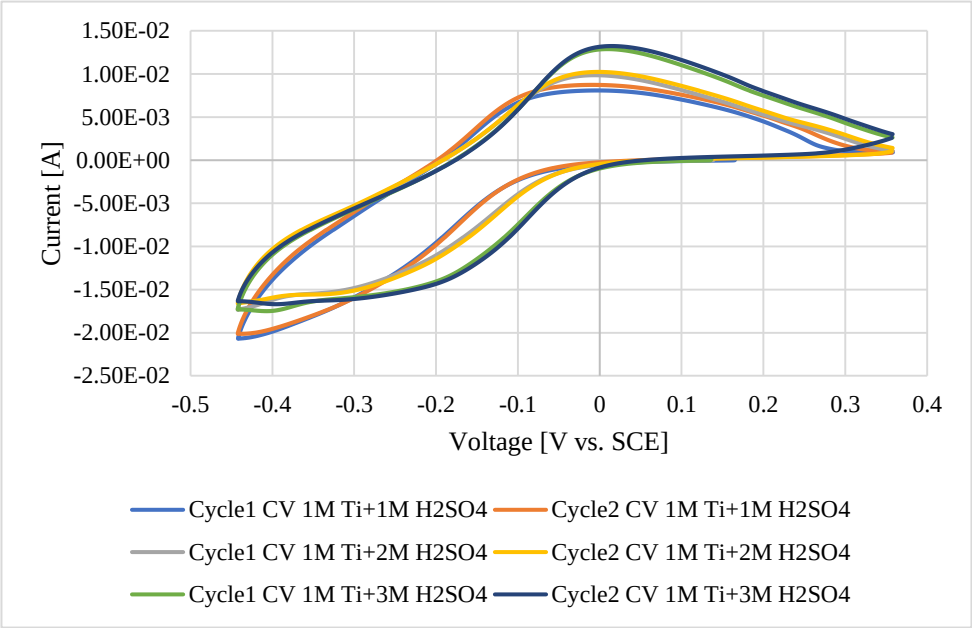

Figure 90. First and second cyclic voltammetry scan of Ti electrolyte solutions on a graphite rod working electrode results

- First and second cyclic voltammetry scan of Ti electrolyte solutions on a carbon felt working electrode results.

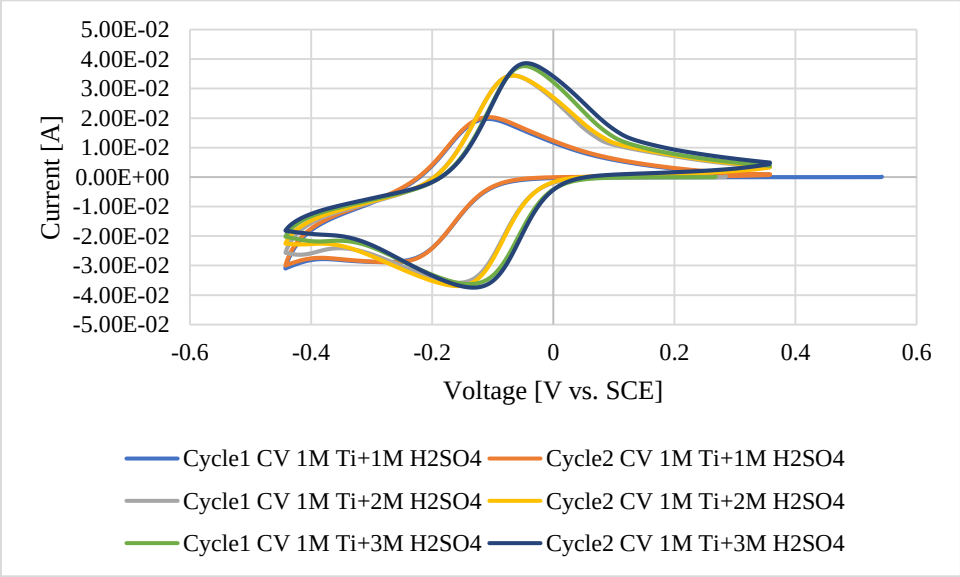

Figure 91. First and second cyclic voltammetry scan of Ti electrolyte solutions on a carbon felt working electrode results

- First and second cyclic voltammetry scan of Mn+Ti electrolyte solutions for Mn side on a graphite rod working electrode results.

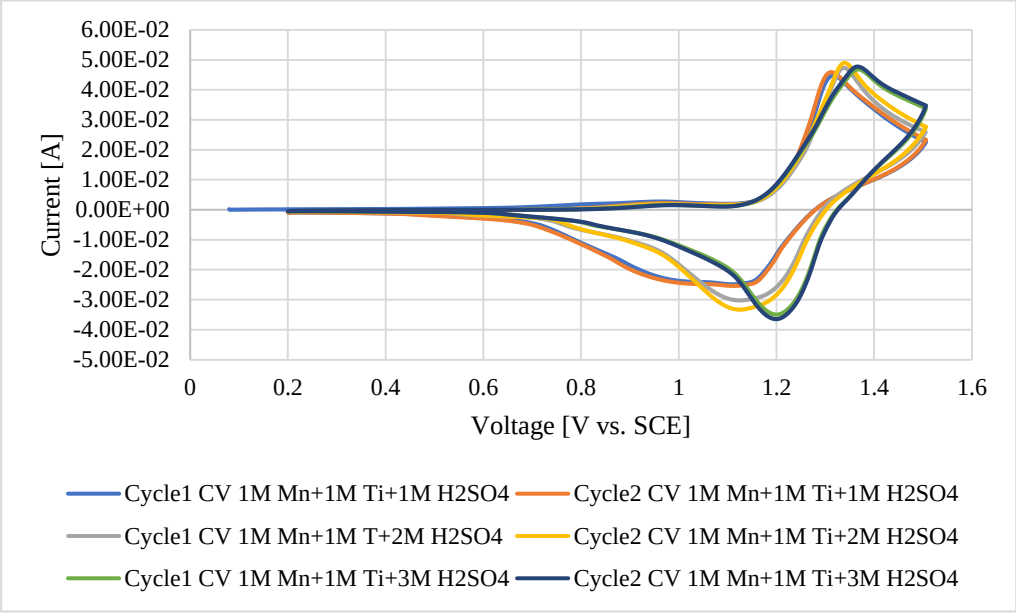

Figure 92. First and second cyclic voltammetry scan of Mn-Ti electrolyte solutions for Mn side on a graphite rod working electrode results.

- First and second cyclic voltammetry scan of Mn+Ti electrolyte solutions for Mn side on a carbon felt working electrode results

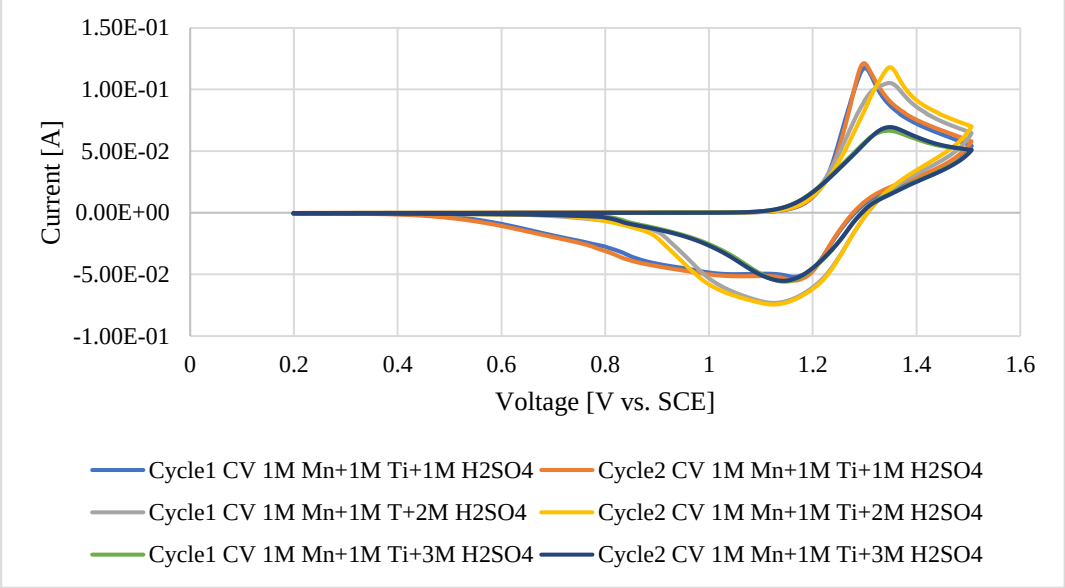

Figure 93. First and second cyclic voltammetry scan of Mn-Ti electrolyte solutions for Mn side on a carbon felt working electrode results

- First and second cyclic voltammetry scan of Mn+Ti electrolyte solutions for Ti side on a graphite rod working electrode results.

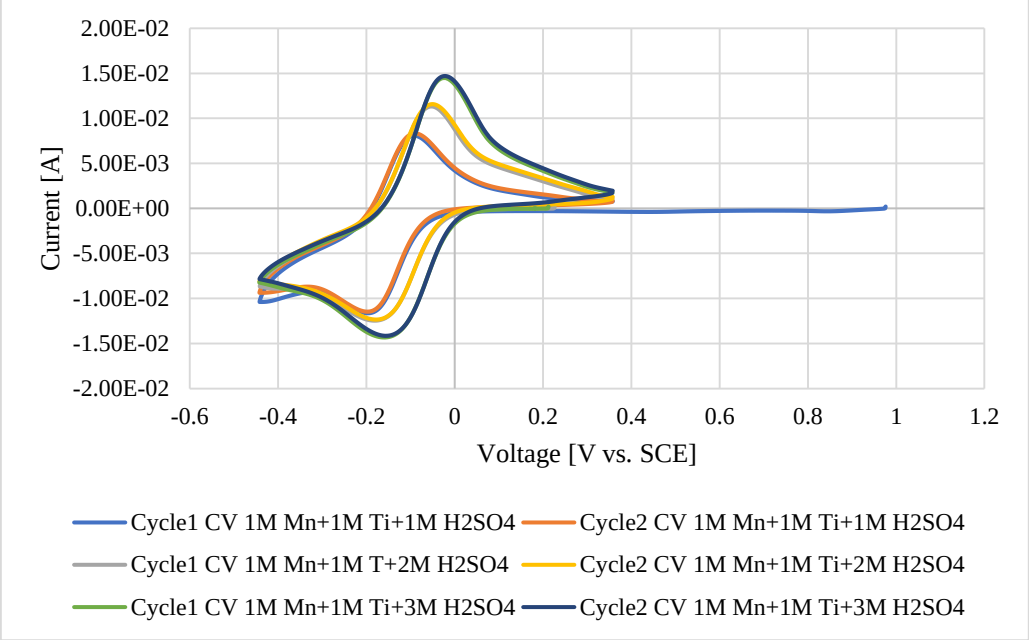

Figure 94. First and second cyclic voltammetry scan of Mn-Ti electrolyte solutions for Ti side on a graphite rod working electrode results.

- First and second cyclic voltammetry scan of Mn+Ti electrolyte solutions for Ti side on a carbon felt working electrode results.

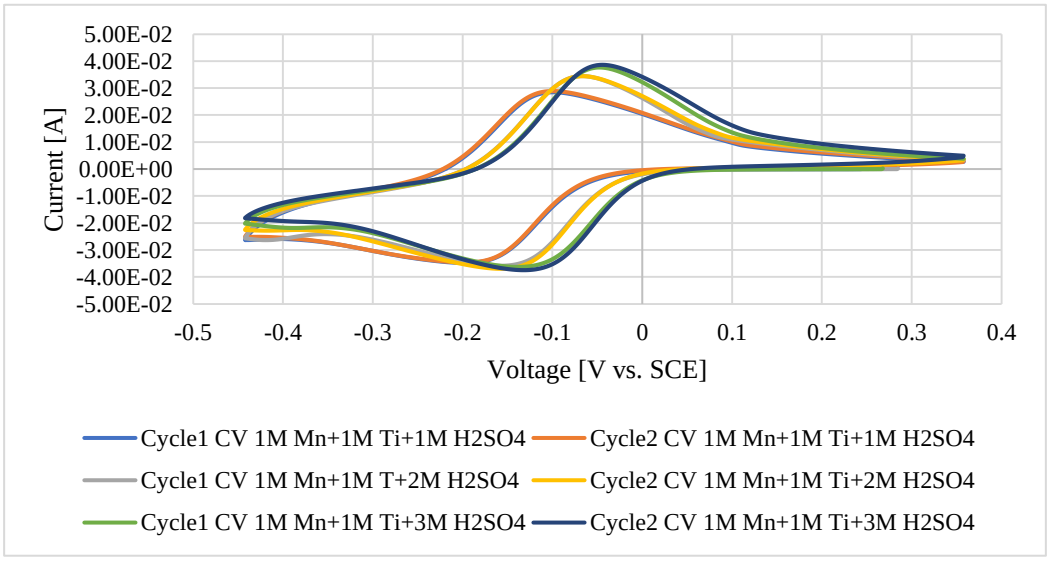

Figure 95. First and second cyclic voltammetry scan of Mn-Ti electrolyte solutions for Ti side on a carbon felt working electrode results